University of Alberta

Molecular Regulation and Function of the Protein Tyrosine Kinase Pyk2
in Cytotoxic T Lymphocytes

by

Samuel Cheung

A thesis submitted to the Faculty of Graduate Studies and Research
in partial fulfillment of the requirements for the degree of

Doctor of Philosophy

in

Immunology

Department of Medical Microbiology and Immunology

©Samuel Cheung
Fall 2013
Edmonton, Alberta

This PhD thesis is dedicated to my mother

ABSTRACT

Cytotoxic T lymphocytes (CTL) play a critical role in immune surveillance and elimination of virus-infected and malignant cells. CTL utilize two major cell-contact dependent mechanisms to kill antigen-bearing target cells. One mechanism involves the directional release of cytolytic molecules stored in granules. Another mechanism is through surface expression of Fas ligand (FasL), which bind Fas-expressing target cells to induce apoptosis. My research objectives are to dissect some of the molecular events and mechanisms that CTL employ to destroy infected and/or tumor cells, with a particular focus on elucidating the contribution of the proline-rich tyrosine kinase (Pyk2) to CTL-mediated cytotoxicity.

Pyk2 was initially identified as a calcium-dependent kinase but how Pyk2 activation is regulated by calcium in T cells had not been addressed. I found that calcium-mediated Pyk2 activation is regulated by reactive oxygen species (ROS). CTL stimulated with reagents that increase intracellular calcium concentration trigger the production of hydrogen peroxide (H_2O_2). Stimulation of CTL with H_2O_2 elicits Pyk2 activation and calcium-induced Pyk2 activation requires Erk and Src-family kinase. My data indicate that H_2O_2 also regulates Erk, which likely acts on Src-family kinase to mediate Pyk2 activity.

In my study of CTL function, I found that Pyk2 regulates CTL migration on ICAM-1. Inhibition or knockdown of Pyk2 results in defective CTL de-adhesion from an ICAM-1 coated surface. Deregulation of Pyk2 leads

to a significant reduction in overall CTL motility. My data indicate that Pyk2 is recruited to the site of integrin activation near the membrane and that Pyk2 phosphorylated on different tyrosines have distinct cellular localization in CTL. Inhibition of Pyk2 impairs intracellular LFA-1 distribution suggesting that Pyk2 regulates LFA-1 recycling. My results indicate that inhibition of Pyk2 impairs CTL degranulation. Upon CTL engagement of the target cell, there is reorientation of the microtubule organizing center (MTOC) towards the target cell which is thought to allow for directional release of the granules. Pyk2 contributes to MTOC reorientation in CTL towards the target cell. Taken together, my data show that Pyk2 regulates multiple aspects of CTL adhesion and function.

ACKNOWLEDGEMENTS

TABLE OF CONTENTS

CHAPTER 1: Introduction

CHAPTER 2: Materials and Methods

A. Materials

B. Methods

CHAPTER 3: Regulation of the tyrosine kinase Pyk2 by calcium is through production of reactive oxygen species in cytotoxic T lymphocytes

CHAPTER 4: Protein tyrosine kinase Pyk2 regulates ICAM-1 dependent adhesion and migration in CTL

CHAPTER 6: General discussion

A. Research Highlights

B. Model for the regulation and function of Pyk2 in CTL

CHAPTER 7: Bibliography

LIST OF TABLES

LIST OF FIGURES

LIST OF ABBREVIATIONS

ANOVA	Analysis of variance
APC	Antigen presenting cell
APC-	Allophycocyanin-conjugated
BAPTA-AM	1,2-Bis(2-aminophenoxy)ethane-N,N,N',N'-tetraacetic acid tetra(acetoxymethyl) Ester
BAK	Bcl-2 homologous antagonist/killer
BAX	Bcl-2-associated X protein
BCR	B cell antigen receptor
BID	BH_3 interacting domain death agonist
BLT	N-benzyloxycarbonyl-L-lysine thiobenzyl ester
BSA	Bovine serum albumin
Ca^{2+}	Calcium
CAKβ	Cell adhesion kinase-β
CAD	Caspase-activated deoxynuclease
CADTK	Calcium-dependent tyrosine kinase
CALDAG-GEF1	Ca^{2+} and DAG-regulated guanine nucleotide exchange factor 1
CaM kinase	Ca^{2+}/calmodulin-dependent protein kinase
Cbl	Casitas B-lineage
CD	Cluster of differentiation
CFSE	Carboxyfluorescein diacetate, succinimidyl ester
CMAC	7-Amino-4-Chloromethylcoumarin
CM-H_2DCFDA	5-(and-6)-chloromethyl-2',7'-dichlorodihydrofluorescein diacetate, acetyl ester
Csk	C-terminal Src kinase
cSMAC	Central supramolecular activation complex
cTEC	Cortex thymic epithelial cell
CTL	Cytotoxic T lymphocyte
CRAC	Ca^{2+} release-activated Ca^{2+} channels
DAG	Diacylglycerol
DC	Dendritic cell
DCFDA	Dichlorodihydrofluorescein diacetate
dCS	Defined calf serum
Dok1	Docking protein 1
Doux1/2	Dual oxidase 1 and Dual oxidase 2
D-PBS	Dulbecco's phosphate-buffered saline
DPI	Diphenyleneiodonium chloride
DTB	5'5-dithiobis(2-nitrobenzoic acid)
DMSO	Dimethyl sulfoxide
ECL	Enhanced chemiluminescence

EGF	Epidermal growth factor
EGTA	Ethylene glycol tetraacetic acid
EDTA	Ethylene diamine tetraacetic acid
ENDOG	Endonuclease G
ER	Endoplasmic reticulum
Erk	Extracellular signal-regulated kinase
E-Syt1	Extended Synaptotagmin-1
FA	Focal adhesion
FACS	Fluorescence-activated cell sorting
FAK	Focal adhesion kinase
FAK2	Focal adhesion kinase 2
FasL	Fas ligand
FAT	Focal adhesion targeting
FBS	Fetal bovine serum
FCS	Fetal calf serum
FERM	Four-point-one Ezrin Radixin Moesin
FITC	Fluorescein isothiocyanate
Fyn	Fibroblast Src/Yes novel gene
Gads	Grb2-related adaptor protein
Grb2	Growth factor receptor-bound protein 2
GST	Glutatione S-transferase
H_2O_2	Hydrogen peroxide
HEK	Human embryonic kidney
HRP	Horseradish peroxidase
IAP	Inhibitor of apoptosis proteins
ICAD	Inhibitor of caspases-activated deoxynuclease
ICAM-1	Intercellular adhesion molecule-1
IFN-α	Interferon-α
IFN-γ	Interferon-γ
IL	Interleukin
IP3	Inositol 1,4,5-trisphosphate
IS	Immune synapse
ITAMs	Immunoreceptor tyrosine-based activation motifs
ITK	Interleukin-2 tyrosine kinase
LAMP-1	Lysosomal-associated membrane protein-1
LAT	Linker for activation of T cell
Lck	Lymphocyte-specific cytoplasmic protein-tyrosine kinase
LCMV	Lymphocytic choriomeningitis virus
LD	Leucine-aspartic acid

LFA-1	Leukocyte function-associated antigen-1
MAPK	Mitogen-activated protein kinase
MEK	Map Erk Kinase
MHC	Major histocompatibility complex
MLR	Mixed lymphocyte reaction
MTOC	Microtubule organizing center
Munc	Mammalian uncoordinated protein
MYLK	Nonmuscle myosin light-chain kinase
MZB	Marginal zone B cell
NADPH	Nicotinamide adenine dinucleotide phosphate
NDUFS3	NADH dehydrogenase, ubiquinone, iron-sulfur protein 3
NFAT	Nuclear factor of activated T cells
NF-kB	Nuclear factor kappa B
NK	Natural killer
NOX	NADPH oxidase
NP	Nucleoprotein
NP40	Nonidet P-40
O_2^-	Superoxide anion
OVA	Ovalbumin
PB	Plate-bound
PBS	Phosphate-buffered saline
PF	PF431396
PIP2	Phosphatidylinositol-4,5-bisphosphate
PKA	Protein kinase A
PKC	Protein kinase C
PLCγ	Phospholipase C gamma
PMA	Phorbol myristate acetate
PRNK	Pyk2-related non-kinase
pSMAC	Peripheral supramolecular activation complex
PSGAP	PH- and SH3-domain-containing RhoGAP protein
PTP-PEST	proline-, glutamic acid-, serine-, threonine-rich family of protein tyrosine phosphatase
PVDF	Polyvinylidene fluoride
Pyk2	Proline-rich tyrosine kinase
RAFTK	Related adhesion focal tyrosine kinase
RAP1-GTPase	Ras-related protein-1 guanosine triphosphate
RAPL	Regulator of adhesion and cell polarization enriched in lymphoid tissues
RasGRP1	Ras guanyl nucleotide-releasing protein 1
RCF	Relative centrifugal force
ROS	Reactive oxygen species

RPM	Revolutions per minute
SDS-PAGE	Sodium dodecyl sulfate polyacrylamide gel electrophoresis
SERCA	sarco-ER-Ca^{2+}-ATPases
SFK	Src-family kinase
SH2	Src homology 2
siRNA	Short interfering ribonucleic acid
Slp2a	Synaptotagmin-like protein 2a
SLP-76	SH2 domain-containing leukocyte protein-76
SMAC	Second mitochondrial activator of caspases
SNARE	Soluble N-ethylmaleimide sensitive factor attachment protein receptor
SOS	Son of sevenless
STIM1	Stromal interaction molecule 1
TC	Target cell
TCR	T cell antigen receptor
T_H1	T helper type 1
T_H2	T helper type 2
TLR	Toll-like receptor
TNF	Tumor-necrosis factor
TRITC	Tetramethyl-rhodamine B isothiocyanate
TRPM2	Transient receptor potential cation channel subfamily M member 2
VAMP	Vesicle associated membrane protein
VAV1	Guanine nucleotide exchange factor VAV1 or GEF-VAV1
XL	Crosslinked or crosslinking
ZAP-70	Zeta (ζ) chain-associated 70 kDa tyrosine phospho-protein

CHAPTER 1

INTRODUCTION

Immune system

The immune system consists of an organized network of cells and organs that coordinate effective defense against foreign organisms. Each specialized cell of the immune system exerts its specific action in a spatial and temporal manner to ensure host protection. Environmental insults and pathogen invasion often challenge our immune system on a daily basis. The ability of the immune cells working together to distinguish self from non-self ensures our survival. Since survival of the host relies on the optimal performance of the immune system, it is fundamentally important to understand the mechanisms of immune cell regulation and function.

Innate immune cells

The function of innate immune cells is to mount a rapid and effective response against foreign invaders. Cells of the innate immune system predominantly consist of myeloid-lineage cells such as neutrophils, mast cells, basophils, eosinophils, monocytes, macrophages, dendritic cells (DC), and the lymphoid-derived natural killer (NK) cells. Neutrophils are phagocytic and are the most abundant granulocytes in circulation (1). Neutrophils recognize common molecules on pathogens through toll-like-receptors (TLR), among other receptors, expressed on cell surface. Neutrophil recognition of bacteria initiates receptor-mediated phagocytosis

that leads to breakdown of the microorganism. Upon encountering a larger pathogen, neutrophils release proteolytic enzymes stored in granules (1). Degranulation is a major effector mechanism also utilized by eosinophils, basophils, and mast cells. All of these cell types protect the host by releasing proteolytic enzymes upon pathogen encounter. These cells also provide inflammatory mediators from stored granules (2). However, degranulation by mast cells may also be problematic to the host due to its role in hypersensitivity reactions (3). Macrophages and dendritic cells both play an important role in innate immunity through phagocytosis and digestion of pathogens. They are also critical for initiation of adaptive immunity through antigen presentation and activation of lymphocytes (4). NK cells are specialized lymphocytes that recognize abnormal self-cells and exert killing functions by degranulation (5). All of the innate immune cells together form the first line of defense against immediate threats imposed by the invasion of pathogens.

Initiation of adaptive immunity

Although macrophages and DCs possess the ability for antigen uptake, processing and presentation, the DC is considered a key antigen presenting cell (APC) because of its ability to activate naïve T cells (6). DCs recognize and internalize pathogens through multiple mechanisms. The acquisition of antigen is mediated via conserved pathogen receptors, antibody receptors, complement receptors, or constitutive macropinocytosis (7). Once a DC has

ingested a pathogen at the site of infection, it becomes activated and migrates to the secondary lymphoid organs (8). Newly developed lymphocytes circulate between the blood and the lymphatic system until they encounter an antigen (9). Naïve lymphocytes are predominantly localized at the secondary lymphoid organs such as lymph nodes and spleen (10). Activated DC carry the antigens to the secondary lymphoid organs, where they process and present the antigen in the context of major histocompatibility complex (MHC) to naïve T lymphocytes (11). T cells express a broad repertoire of antigen receptors, and each receptor specifically recognizes a unique molecular epitope (12). Only lymphocytes that bind the epitopes derived from the pathogen in context of MHC are selected for activation.

Activation of naïve CD4$^+$ T lymphocytes by APC is a crucial step for initiation of adaptive immunity (13). This involves the interaction between specific T cell antigen receptors (TCR) on the T cell and the antigenic peptide presented on class II major histocompatibility complex (MHC II) expressed by the APC. Once a CD4$^+$ T cell is activated, it differentiates into a T helper cell that secretes cytokines. The nature of infection and the cytokine profile will dictate a particular immune response, which includes but is not limited to humoral and cell-mediated immunity (14).

Humoral and cell-mediated immunity

Humoral immunity refers to the production of antibody in response to a particular infection. This occurs as a result of B cell activation and

differentiation (15). It begins with the uptake of pathogen by DCs and the presentation of the antigens to naïve $CD4^+$ T cells. Meanwhile, naïve B lymphocytes expressing the B cell antigen receptor (BCR) that can bind the same pathogen also undergoes antigen processing and presentation (16). B cells presenting antigen in the context of MHC class II complex are recognized by the activated $CD4^+$ T helper cells (17). The cell-to-cell interactions between DCs, antigen-presenting B cells, and activated $CD4^+$ T helper cells lead to the formation of a germinal center, where B cell maturation, proliferation, and differentiation occur (18). Follicular T helper cells in the germinal center, produce T helper type 2 (T_H2) cytokines such as interleukin-4 (IL-4) to stimulate the antibody response of B cells (19). The resulting B cell activation and generation of memory B cells ensure long lasting antibody protection against the specific pathogen (15).

Cell-mediated immunity is governed by the presence of antigen-specific cytotoxic T lymphocytes (CTL) specific for the pathogen (20). The generation of CTL is a result of naïve CD8 T cell activation, which is facilitated by T helper type 1 (T_H1) cytokines produced by activated $CD4^+$ T helper cells (21). Since the focus of this thesis research is on the function of CTL, I will discuss in more detail T cell development, activation and effector function in the following sections.

T cell development and selection

T cell precursors originate from the bone marrow and are subjected to further development in the cortex of the thymus. T cells at their early developmental stage are called pro T cells. Pro T cells receive developmental signals through direct contact with cortex thymic epithelial cells (cTEC) and this signals the TCR β gene rearrangement to begin (22). Successful TCR β chain expression on the cell surface leads to formation of a preTCR-CD3 complex, which consists of a TCR β chain and a pre-Tα chain joined by a disulfide bond in addition to a CD3 complex. The signaling component of the CD3 complex consists of three subunits: the δ-ε chains, the γ-ε chains and the ζ-ζ chains (23). These subunits contain the immunoreceptor tyrosine-based activation motifs (ITAMs). The preTCR-CD3 complex is held together by electrostatic interactions within the trans-membrane domains. At this point, the pre-TCR-CD3 complex on the surface of pre T cells undergoes dimerization (24). Dimerization generates signals that lead to proliferation, induction of CD4 and CD8 expression, initiation of TCR α chain rearrangement, as well as inhibition of further β chain rearrangements. Furthermore, signals stemming from successful TCR β chain expression ensure thymocyte commitment to become an αβ T cell. This eliminates the potential for the thymocyte to become a γδ T cell, which typically only comprises ~ 1% of the total mature T cell population (25). Since the T cells used in the research presented in this thesis are αβ T cells, the development and function of γδ T cells will not be the focus of discussion here.

As the pre T cell differentiation program progresses, productive TCR α gene rearrangement leads to surface expression of TCR α chain, which replaces the pre-Tα chain to form a functional TCR $\alpha\beta$ heterodimer. At this point CD4/CD8 double positive immature T cells undergo positive and negative selection before exiting to the periphery (26). How T cells decide whether to become mature CD4 or CD8 T cells remains unclear but various signaling models have been proposed for T cell lineage commitment (27). Positive selection of T cells is primarily mediated by the thymic epithelial cell, which expresses both classes of MHC molecules with self-peptides. CD4$^+$ T cells are positively selected to bind MHC class II molecules, whereas CD8$^+$ T cells are positively selected to recognize MHC class I. Negative selection is partly mediated by DC and therefore may be spatially separate from positive selection. Negative selection ensures that TCR on T cells do not strongly bind self-peptides presented on self-MHC molecules. On average less than 5% of all T cell precursors will survive both selection processes to become part of the mature naïve T cell repertoire. Each newly developed mature CD4$^+$ or CD8$^+$ T cell will possess a unique TCR specificity and MHC restriction. Mature T cells exit the thymus and then circulate between blood and the lymphatic system, where they await activation by antigen presenting cells from the periphery.

Alloreactive T cells

T cells are positively selected in the context of self-MHC molecule, however this does not mean that they cannot recognize non-self MHC molecules and peptides. T cells that recognize non-self MHC are called alloreactive T cells (28). This phenomenon is commonly observed in transplantation where the donor graft with MHC mismatch is gradually infiltrated with recipient T cells responding to the graft as a result of strong cell-mediated immunity. It is estimated that 7% of the precursor T cells in a mouse model are alloreactive (29). The existence of alloreactive T cells present great challenges for organ transplants. Researchers make use of the high level of response by alloantigen to easily obtain sufficient cells for studies of lymphocyte function (30).

In vivo and *in vitro* activation of naïve CD8^{+} T Cells

As mentioned earlier, dendritic cells carry antigens to the lymph node for naïve T cell activation through antigen presentation. Activation of naïve CD8^{+} T cells requires three distinct but concurring stimulatory signals (Figure 1-1). The first signal stems from ligation of TCR with cognate peptide in the context of MHC. The interaction between TCR and peptide-MHC complex also enables the CD8 co-receptor to simultaneously bind the TCR-engaged MHC-I molecule. The second signal is derived from ligation of co-stimulatory molecules. One of the main co-stimulatory molecules for T cell activation is CD28, which binds CD80 or CD86 (B7-1 or B7-2) expressed on

DC. Ligation of CD28 activates signaling pathways that lead to CD8$^+$ T cell cytokine production and proliferation (31). The third signal comes from cytokines such as IL-12 and interferon-α (IFN-α) produced by DC and other cells. These cytokines are required for the differentiation of CD8$^+$ T cells into effector CTL and generation of memory (32).

Proliferation and differentiation of mouse naïve CD8$^+$ T cells to become CTL can be triggered *in vitro* as long as the three signals are provided. An example of *in vitro* activation of naïve CD8 T cells is the mixed lymphocyte reaction (MLR). In the MLR, two lymphocyte populations of different MHC background are cultured together. This triggers the activation of a naïve CD8 T cell population to respond to the other population with a different MHC allotype. The "stimulator population" provides the co-stimulatory signals and can be irradiated to prevent proliferation, so that the "responder population" can be activated and differentiate into effector CTL. The third signal likely comes from activated DC in these cultures. Recombinant IL-2 added to the culture provides survival signals. Through weekly re-stimulation by the same irradiated stimulator population, the responding effector CTL population will continue to expand and can be utilized for CTL functional studies. The advantage of using allo-reactive CTL is the ease of culturing and a generally robust cytotoxic response. A single clone of CTL can also be obtained by serial dilution. A disadvantage is that the identity of the antigenic peptide is usually unknown. This can be circumvented using a TCR transgenic system such as mouse expressing TCR

specific for the ovalbumin peptide (OT-1 mouse). With the transgenic mouse

model, addition of antigenic peptides and IL-2 to the splenic lymphocyte

culture is generally sufficient to stimulate naïve T cells to differentiate into

effector CTL in a few days.
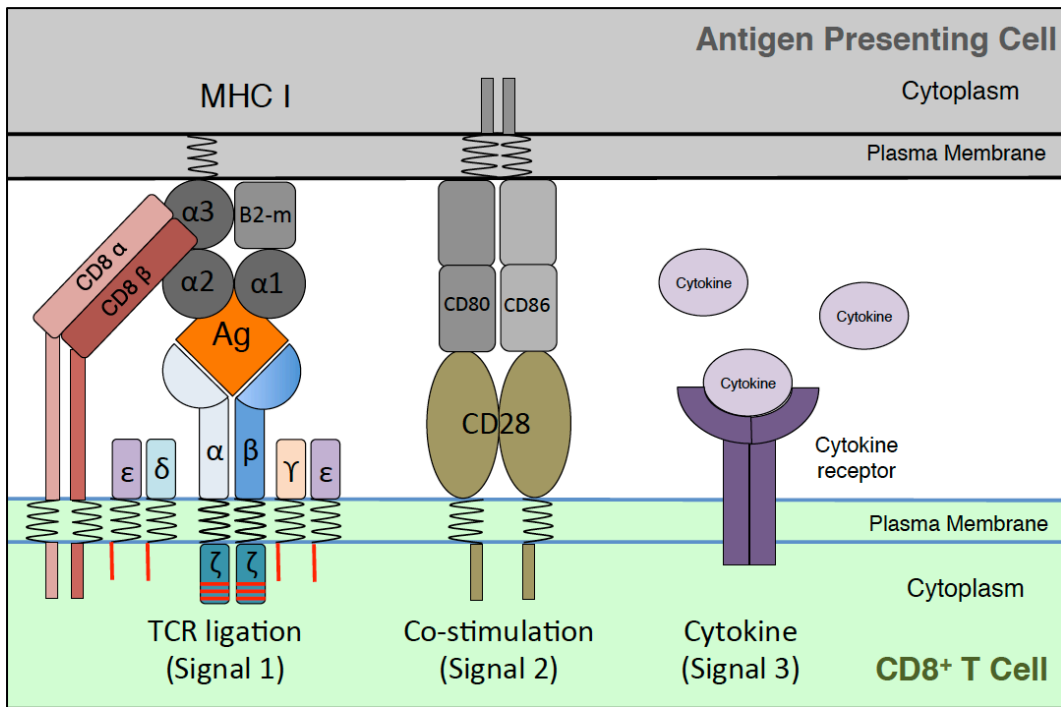
Figure 1-1. The three signals requirement for the activation of a naïve CD8+ T cell to proliferate and differentiate to become a cytotoxic T lymphocyte. Binding of TCR with peptide in the context of MHC constitutes signal 1 that confers antigen specificity. Signal 2 stems from ligation of co-stimulatory molecule, which leads to cytokine production and proliferation of T cell. Cytokine signaling is required for full differentiation and memory cell formation.   The combination of three signals ensures expansion and generation of both memory and effector CTL population against the specific antigen.

TCR proximal signaling upon T cell activation

Engagement of the TCR αβ heterodimer with antigenic peptide in complex with MHC class I (peptide-MHC) initiates the signal transduction events required for T cell activation. How the binding of peptide-MHC complex to the αβ-heterodimer of TCR itself triggers the first signaling event is not entirely clear but various mechanisms have been proposed (33). The first catalytic event in the cytoplasm is tyrosine phosphorylation of the ITAMs on CD3 chains by Src-family kinase (SFK). Although T cells predominantly express both lymphocyte-specific cytoplasmic protein-tyrosine kinase (Lck) and fibroblast Src/Yes novel gene (Fyn) among the known SFK members, the current model indicates that early TCR signaling is mainly regulated by Lck (34). In T cells, Lck is constitutively associated with the CD4 and CD8 co-receptors (35). A conventional TCR triggering model is that the interaction between CD8 and MHC-I will bring Lck in close proximity to CD3 for the phosphorylation of the ITAMs (33). However, since CD8 is not absolutely required for CTL activation (36), a different model suggested that the ITAM domains are hidden from Lck during resting state but become accessible due to conformation change upon peptide-MHC ligation. Another highly debated model is that TCR complexes are recruited to the Lck-enriched lipid raft after peptide-MHC complex ligation (33). Each proposed mechanism was derived from a distinct experimental approach but, physiologically, it is possible that all are involved and contribute to the optimal activation of TCR signaling pathways.

There are two main tyrosine phosphorylation sites on Lck that control its kinase activity. The general model is that auto-phosphorylation of Y394 leads to Lck activation whereas Y505 phosphorylation, which is mediated by C-terminal Src kinase (Csk), leads to auto-inhibition of Lck (34). It is speculated that differentially tyrosine phosphorylated Lck may simultaneously exist in an equilibrium state (34). In T cells, the transmembrane phosphatase CD45 preferentially dephosphorylates the inhibitory tyrosine (Y505) on Lck (37). Using a series of transgenic mice expressing different levels of CD45, it was demonstrated that there is an unequal level of Y394 and Y505 dephosphorylation as CD45 expression increases (38). Therefore, CD45 does not simply function to turn on Lck activity through dephosphorylation of Y505, but rather, the overall activity of Lck is also modulated by the factors that regulate CD45 expression and function as well. Interestingly, it has been shown that a major proportion of Lck in T cells is constitutively phosphorylated at Y394 prior to TCR ligation (39). This suggests that the cells are primed to propagate TCR signaling upon activation.

Lck phosphorylates ITAMs at the cytoplasmic CD3 ζ chain to create a binding site for selective Src homology-2 (SH2)-domain containing proteins (Figure 1-2). The double tyrosine-phosphorylated ITAMs bind the zeta (ζ) chain-associated 70 kDa tyrosine phospho-protein (ZAP-70) through the tandem SH2-domain on ZAP-70 (40). Currently, it is unclear how ZAP-70 is regulated at the plasma membrane. It is speculated that both direct

phosphorylation by Lck as well as trans-phosphorylation by ZAP-70 contributes to the overall activation of ZAP-70 (40). Activated ZAP-70 is important for the subsequent phosphorylation of a key molecule called the linker for activation of T cells (LAT) (40, 41). It was originally thought that membrane-associated LAT moves laterally to the activated TCR complex to allow phosphorylation by ZAP-70, but new evidence suggests that intracellular LAT pools are responsible for early TCR activation (42). Nonetheless, tyrosine phosphorylation of LAT is central to the assembly of a signaling complex that is critical for the activation of TCR-dependent pathways (43).
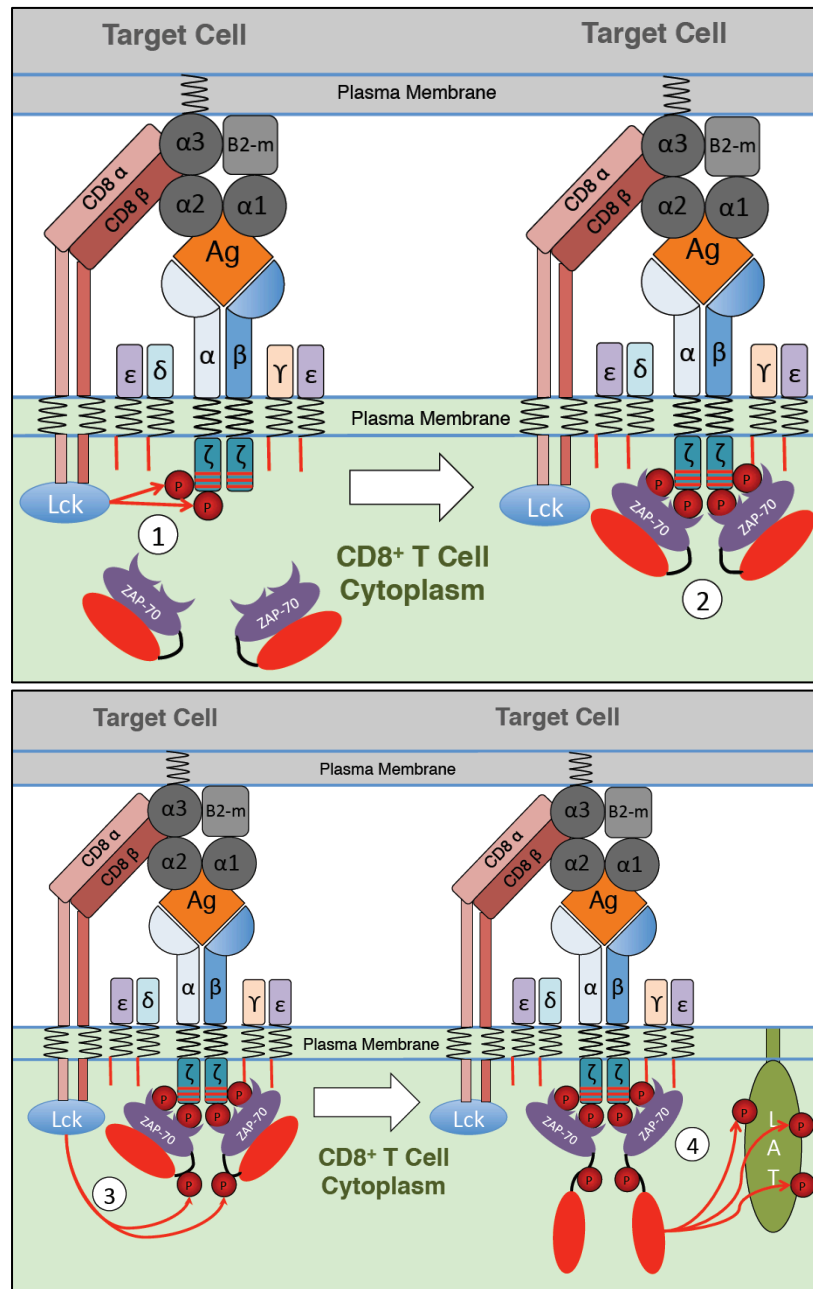
Figure 1-2. Mechanism of TCR-induced LAT activation. (1) Ligation of peptide-MHC to TCR recruits Lck to tyrosine phosphorylate ITAMs on CD3 ζ chain through the CD8 molecule. (2) The SH2 domains of ZAP-70 binds to tyrosine phosphorylated ITAMs. (3) ZAP-70 is activated by trans-phosphorylating itself or phosphorylation by Lck, or both. (4) Activated ZAP-70 phosphorylates LAT at multiple sites for subsequent signaling complex formation.

Tyrosine phosphorylation of LAT in close proximity to the TCR is followed by recruitment of various signaling molecules that participate in the formation of a signalosome (Figure 1-3). The key components of a TCR-induced signalosome and the detailed molecular interactions have been well described (43-45). Briefly, the phosphotyrosine residues on LAT serve as binding sites for SH2 domain containing proteins, which include growth factor receptor-bound protein 2 (Grb2), Grb2-related adaptor protein (Gads) and phospholipase C gamma (PLCγ) (46). The LAT-associated Grb2 utilizes its SH3 domain to recruit son of sevenless (SOS). SOS activates membrane-bound Ras, resulting in extracellular signal-regulated kinase (Erk) activation. Meanwhile LAT-associated Gads and PLCγ together bind SH2 domain-containing leukocyte protein-76 (SLP-76), which recruits interleukin-2 tyrosine kinase (ITK) to phosphorylate and activate PLCγ at the plasma membrane (47). Activated PLCγ near the membrane cleaves the phosphatidylinositol-4,5-bisphosphate (PIP2) to generate diacylglycerol (DAG) and inositol 1,4,5-trisphosphate (IP3). Membrane-bound DAG can bind Ras guanyl nucleotide-releasing protein 1 (RasGRP1) to subsequently trigger Erk activation as well as to induce activation of protein kinase C (PKC) family enzymes, which are important for the regulation of cytoskeletal rearrangements, cell adhesion, and gene expression (48, 49). How PLC activation modulates cell adhesion will be discussed in more detail later. IP3 binds its receptor on the endoplasmic reticulum (ER) resulting in increased

intracellular calcium (Ca^{2+}), which activates subsequent calcium-dependent

signaling pathways.
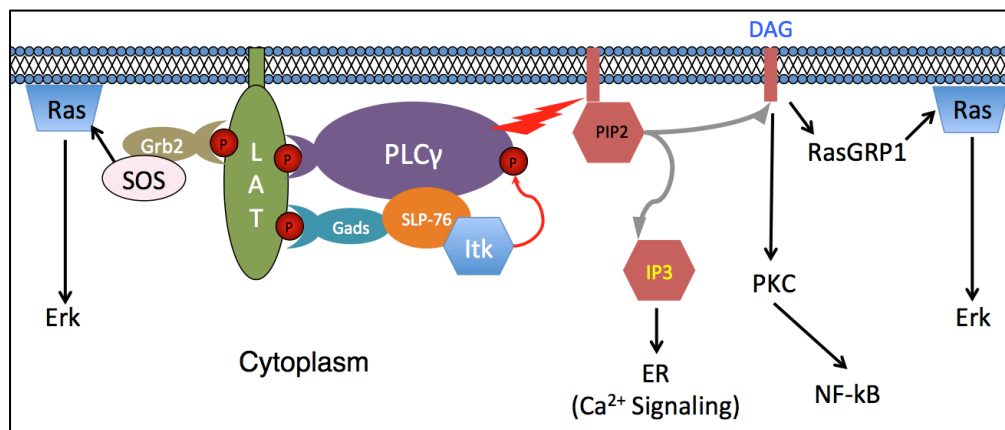
Figure 1-3. The LAT signalosome and TCR signaling pathways. Tyrosine phosphorylated LAT allows binding of PLCγ, Gads and Grb2 through their SH2 domains.   Grb2 recruits SOS to activate Ras, which leads to Erk activation. SLP-76 forms a complex with both PLCγ and Gads followed by binding of Itk, which phosphorylates and activates PLCγ.   Activated PLCγ cleaves PIP2 for generation of DAG and IP3. DAG activates PKC, which in turn activate NF-kB. DAG also binds to RasGRP1 to activate Erk through Ras. IP3 translocates to the ER to induce cytoplasmic increase of Ca^{2+}.

Mechanism of calcium signaling activation

TCR activation is followed by a rapid increase of intracellular Ca^{2+} concentration (50). This is mediated by the generation of IP3, which binds its receptor on the ER to trigger the release of ER-stored Ca^{2+}. Depletion of Ca^{2+} inside the ER leads to the activation of stromal interaction molecule 1 (STIM1). STIM1 is a trans-membrane ER Ca^{2+} sensor that contains an EF-hand motif that binds Ca^{2+} in its inactive state. Ca^{2+} depletion in the ER leads to activation-induced aggregation of STIM1 followed by its translocation to the plasma membrane to activate the Ca^{2+} release-activated Ca^{2+} channels (CRAC) (51). Activation of CRAC results in an influx of extracellular Ca^{2+} into the cytoplasm. The rapid increase in intracellular Ca^{2+} induces the activation of various Ca^{2+}-dependent signaling proteins including calcineurin and calmodulin (52). Consequently, transcription factors such as nuclear factor of activated T cells (NFAT) and nuclear factor kappa B (NF-kB) are activated to turn on genes that control cellular proliferation and cytokine production.

Experimentally, activation of Ca^{2+} signaling can be induced independent of TCR ligation using commercially available pharmaceutical reagents. Ionomycin is an ionophore that is highly specific for divalent cations such as Ca^{2+}. Stimulation of cells with ionomycin in Ca^{2+}-containing medium can artificially simulate the extracellular influx of Ca^{2+} across the plasma membrane into the cytoplasm. Another commonly used reagent that increases intracellular Ca^{2+} level is thapsigargin. Thapsigargin prevents the re-entry of the Ca^{2+} back into the ER by inhibition of the sarco-ER-Ca^{2+}-

ATPases (SERCA) pump (53). Stimulation with thapsigargin results in accumulation of Ca^{2+} in the cytoplasm. Both ionomycin and thapsigargin are widely used for stimulation of Ca^{2+}-dependent signaling. To study the loss of function in Ca^{2+}-dependent signaling, chelating reagents such as ethylene glycol tetraacetic acid (EGTA) and 1,2-Bis(2-aminophenoxy)ethane-N,N,N',N'-tetraacetic acid tetra(acetoxymethyl) ester (BAPTA-AM) can be used for inhibition of extracellular Ca^{2+} influx and ER-stored Ca^{2+} release, respectively.

TCR-induced generation of reactive oxygen species

Similar to Ca^{2+}, reactive oxygen species (ROS) can also serve as secondary messengers in multiple pathways. ROS are becoming recognized as signal regulators for normal cellular processes rather than merely harmful by-products of cellular metabolism (54). There are multiple sources for ROS generation in any given cell type, but a predominant source is derived from nicotinamide adenine dinucleotide phosphate (NADPH) oxidase family enzymes (55). Seven members of NADPH oxidase or NOX family enzymes have been identified. The regulation, expression and cellular distribution of NOX proteins depend on the cellular context (56). The two main ROS products generated by NADPH oxidase are superoxide anion (O_2^-) and hydrogen peroxide (H_2O_2). Ligation of TCR with anti-CD3 antibody induces the production of both O_2^- and H_2O_2 (57). Currently, it is unclear which NADPH oxidase is responsible for the majority of ROS production upon TCR signaling activation.

Unlike Ca^{2+}, ROS chemically modify substrates to exert its secondary messenger effect. For example, H_2O_2 selectively reacts with catalytic cysteine residues found in a specific group of phosphatases (54). The proposed function for H_2O_2 is to inactivate protein phosphatase activity through oxidation of the reactive cysteine residues, thereby permitting phosphorylation of downstream substrates to proceed. Several studies have demonstrated that H_2O_2-mediated phosphatase inactivation is a reversible process (58-60). Thereafter, H_2O_2 is removed and/or negatively regulated by specialized groups of antioxidant molecules including catalase, glutathione peroxidase and peroxiredoxins (61).

One commonly used method to study H_2O_2-mediated signaling pathways is to stimulate cells directly using H_2O_2. However, stimulation with exogenous H_2O_2 above physiological levels may induce cell death instead. An alternate method to study the molecular targets of H_2O_2 is to use an array of inhibitors and antioxidants to selectively inhibit and remove endogenous ROS, respectively. Both ROS inhibitors and scavengers are useful research tools for studying the loss-of-function in redox-sensitive signaling pathways. The production of ROS upon cell signaling activation can also be determined using specific redox sensitive probes. This enables qualitative estimation of endogenous ROS production in a given cell type.

CTL adhesion is mediated by integrins

CTL migration through tissue in search of target cells is dependent on adhesion molecules. T cell adhesion and migration are predominantly regulated by the leukocyte function-associated antigen-1 (LFA-1), which binds to its ubiquitously expressed ligand intercellular adhesion molecule-1, 2 or 3 (ICAM-1, ICAM-2 or ICAM-3) (62). LFA-1 is a transmembrane heterodimer consisting of an α and a β subunit. T cells express the $\alpha L\beta 2$ heterodimer (CD11a and CD18, respectively) that is critical for normal T cell activation, proliferation, adhesion and migration (63, 64). Through epitope mapping using conformation-specific antibodies derived against human LFA-1, it was proposed that LFA-1 could exist in three different molecular configurations with distinct ICAM-1 binding affinity (65). Low affinity LFA-1 is an inactive state where both α and β chains fold together to occlude the ICAM-1-binding site that is located on the αI domain of the α subunit. In the intermediate and high affinity LFA-1 states, both subunits are vertically extended to allow ICAM-1 binding. In contrast to the intermediate affinity conformation, the high affinity LFA-1 β subunit is stretched further away from the α subunit to fully expose the αI domain for enhanced ICAM-1 interaction (66). Although similar conformation-specific antibodies are not available for mouse integrin study, many aspects of LFA-1 regulation and activation are presumed to be identical in both systems.

LFA-1 regulates CTL migration

In vitro migration of T cells on an immobilized ICAM-1 substrate exhibits three distinctive zones: the leading edge, the central focal zone, and the trailing edge or 'uropod' (65). At the leading edge, LFA-1 is predominantly in its intermediate conformation, which allows transient but rapid scanning of surroundings for an antigen. The middle region or 'focal zone' of T cell contains high affinity LFA-1 that provides the firm extracellular adhesion to ICAM-1 and intracellular cytoskeletal support for migration stability. LFA-1 at the trailing edge is more perplexing since it appears to be in a high affinity conformation but no longer interacts with ICAM-1 (65). Currently, very little is known about how LFA-1 becomes inactivated or de-adhered from ICAM-1 at the trailing edge. Although a few candidate proteins have been shown to negatively regulate LFA-1 in various cell types, the molecular mechanism for T cell de-adhesion at the trailing edge remains undefined.

Adhesion-mediated activation of integrin

Ligation of LFA-1 with ICAM-1 triggers activation of high affinity LFA-1 expression. The self-induced affinity modulation by LFA-1 molecules is commonly known as 'outside-in' signaling (66). Both Lck and ZAP-70 are constitutively associated with LFA-1 inside the T cells (67). Binding of ICAM-1 to LFA-1 on the surface triggers Lck-dependent tyrosine phosphorylation of ZAP-70 that is essential for LFA-1 conformational switch from intermediate

to high affinity. ZAP-70 plays a key role by phosphorylating the guanine-nucleotide exchange factor (GEF) VAV1, resulting in its disassociation from talin (68). An *in vitro* study demonstrated that talin binding to the β-subunit of integrin is sufficient to induce the high affinity conformation (69). Therefore, a current model proposes that ZAP-70 phosphorylation of VAV1 relieves the inhibitory effect of VAV1 on talin, thereby allowing the LFA-1 affinity switch to occur (66). Other molecules such as regulator of adhesion and cell polarization enriched in lymphoid tissues (RAPL), Ras-related protein-1 guanosine triphosphate (RAP1-GTPase), and Kindlin-3 are associated with integrin during outside-in signaling but the mechanism of regulation is currently unknown (66). Ultimately, calpain-mediated proteolysis of talin is speculated to be the key event for LFA-1 inactivation (70). Although calpain cleavage of talin has not been directly demonstrated in T cells, inhibition of calpain impaired human T cell mobility on an ICAM-1 coated surface (71). In contrast to what is known about focal adhesion structure assembly and dissembly, the molecular mechanisms that control CTL de-adhesion is much less defined.

Receptor-mediated activation of integrin

When a CTL first encounters a potential target cell (TC) it binds the cell with very low avidity (Figure 1-4). If no antigen is encountered, the CTL releases the TC and quickly moves on to the next TC (65). Once the antigen presented on TC is engaged by the T-cell receptor, the transient, weak LFA-1-

dependent adhesion between CTL and TC becomes stable and tightens as a result of TCR signalling (72). Signalling receptor-mediated integrin activation is known as 'inside-out signalling'. The two most studied 'inside-out' signal inducers are chemokine and antigen receptors. Chemokine receptor induced LFA-1 activation is important for T cell migration into tissues during lymphocyte infiltration, whereas TCR-mediated LFA-1 activation is critical for tight adhesion and stable immune synapse formation (72). Various molecules have been shown to interact with the integrin cytoplasmic tails and are involved in 'inside-out' signaling. However, additional study is needed to elucidate the contribution of each molecule involved. A common theme is that PLC activation downstream of either chemokine or T cell receptor pathway is a critical event for inside-out signaling. This results in Ca^{2+} flux and production of DAG, which leads to Ca^{2+} and diacylglycerol-regulated guanine nucleotide exchange factor 1 (CALDAG-GEF1) mediated activation of RAP1-GTPase in human T cells (73). The exact intracelluar location for RAP1-GTPase activation remains controversial. RAP1-GTPase regulates the activity of RAPL, which is known to associate with the LFA-1 α subunit and plays a critical role during inside-out activation of integrin (66, 74).

As a result of inside-out integrin activation induced by TCR signaling, a CTL will adhere to the antigen expressing target cell with increased affinity. The interaction between CTL and its target leads to the formation of an immune synapse, which is characterized by a central TCR cluster surrounded

by adhesion molecules at the periphery (75). This is followed by translocation of the microtubule organizing center (MTOC) and the Golgi apparatus toward the target cell (76). The polarized MTOC close to the plasma membrane directs lytic granule exocytosis towards the target cell through the immune synapse (77). Consequently, the released contents of the CTL cytotoxic granules activates cell death pathways in the target cell.
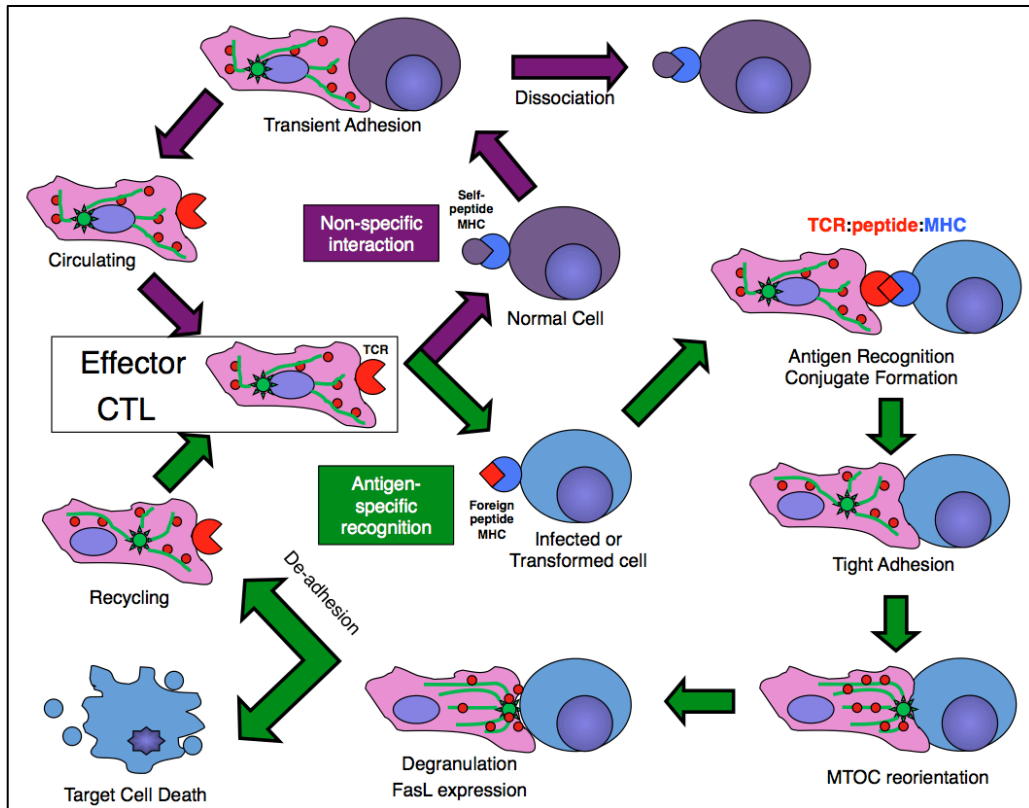
Figure 1-4. Cellular function of CTL. Migrating CTL briefly adhere to normal cells before finding their target at the infected site. The cell-to-cell interaction between CTL and by-stander cells is transient. Outside-in integrin activation plays a major role to ensure proper CTL migration. If there is no encounter with antigen (indicated by the path of purple arrow), CTL will detach from the by-stander cell and continue to search for an antigen-bearing target cell. Once an antigen is found in the context of MHC-I on target cells, TCR activation will trigger 'inside-out' signaling that leads to tight adhesion to the target cell. This is followed by CTL-mediated degranulation and induction of target cell death.

CTL-mediated cytotoxicity

CTL are differentiated CD8$^+$ T cells that work to destroy both infected and tumor cells. The importance of CTL in tumor control and surveillance can be seen in mice lacking cytotoxic T cell effector function: they were found to be more susceptible to tumors (78, 79). CTL utilize two major cell-contact dependent mechanisms to kill antigen-bearing TC. The first involves directional release of proteolytic enzymes stored in granules and the second is through surface expression of Fas ligand (FasL) which bind Fas on TC to induce apoptosis (80). It has been shown that CTL can undergo multiple cycles of target cell killing through sequential recognition and lysis of one TC after another (81).

The lysosomally-derived cytolytic granules (or secretory lysosomes) of CTL contain perforin and a series of serine proteases known as granzymes. Perforin was originally characterized as a pore-forming protein capable of triggering target cell lysis *in vitro* (82). Subsequent studies showed that perforin also facilitates the entry of granzymes into target cells (83, 84). Currently, five different functional granzymes have been identified in human and ten in mice (85). Most granzymes have a direct role in activation of programmed cell death pathways. However, there are subtle differences between each granzyme in regard to the cellular substrate and the apoptotic pathway induced. The most studied granzymes are granzyme A and granzyme B. It is well established that both perforin and granzymes work synergistically to induce target cell death (86, 87).

In addition to degranulation of cytolytic granules, CTL also utilize the expression of FasL to trigger Fas-induced target cell death. Our laboratory has shown that CTL express two distinct waves of FasL on the cell surface upon engagement of the target cell (88). The first wave of FasL is derived from pre-existing stores, whereas the latter wave requires new protein synthesis and a higher threshold of TCR activation (89). The cellular storage of FasL is spatially segregated from granzyme-containing vesicles (88). Both degranulation and early FasL expression appear to specifically kill antigen-bearing cells. In contrast, the late wave of FasL expression is capable of targeting any by-stander cell that expresses Fas (89). By-stander cell destruction may also be attributed to the production of cytotoxic cytokines such as interferon-γ (IFN-γ) and tumor-necrosis factor (TNF) (90). With multiple killing mechanisms in operation, active CTL ensure effective elimination of specific target cells to prevent the further spread of infection or tumor metastasis. This thesis research will specifically focus on degranulation of cytolytic molecules.

Mechanism of cytolytic granule delivery

The mechanism that regulates cytolytic granule delivery is gradually emerging. MTOC docking at the side of the cell where the immune synapse is located is necessary for granule exocytosis in mouse CTL (77). The MTOC in a migrating T cell is characteristically positioned at the trailing edge behind the nucleus (91). Once a CTL engages its target, TCR activation signals the

MTOC to translocate toward the target cell and this process depends on SFK. The MTOC in Fyn-deficient CTL was unable to reorientate around the nucleus, whereas Lck is required for recruitment and docking of MTOC at the immune synapse (92). Interestingly, detachment of MTOC from the nucleus is not a prerequisite for CTL-mediated target cell lysis (93). However, polarization and exocytosis of cytolytic granules must be triggered by signaling through high avidity TCR interaction with its peptide:MHC ligand (94).

In vitro stimulation of CTL using anti-CD3 antibodies demonstrated that signaling induced by strong directional TCR crosslinking is sufficient to trigger MTOC reorientation and degranulation (92, 95). CTL degranulation absolutely requires Ca^{2+} but Ca^{2+} is not required for MTOC reorientation (96). The sequential steps for degranulation are granule translocation, membrane docking, and fusion to the cell membrane. The signaling mechanisms that govern each step are currently under investigation. Studies on genetic diseases in humans that are linked to defective T cell cytotoxicity have led to the identification of key molecules in CTL degranulation (97). These molecules include mammalian uncoordinated 18-2 (Munc 18-2), Munc13-4, Syntaxin-11, and Rab27a. Early studies showed that CTL lytic granules from Rab27a-mutant mice translocate toward the immune synapse but failed to dock at the plasma membrane (98). Later studies suggested that Rab27a interacts with its effector Munc13-4 and synaptotagmin-like protein 2a (Slp2a) to regulate mast cell and CTL degranulation, respectively (99, 100).

Syntaxin-11 is a member of soluble N-ethylmaleimide sensitive factor attachment protein receptor (SNARE) family of proteins that regulate vesicle fusion. Natural killer cells obtained from patients with inherited Syntaxin-11 mutation exhibit severe defects in cytotoxicity (101, 102). A recent study using Syntaxin-11 deficient mice have confirmed similar defects in CTL degranulation (103). Munc 18-2 interacts with various SNARE family proteins that are important regulators of granule exocytosis (104). Although these proteins have been shown to play an essential role in CTL degranulation, none of them are directly regulated by Ca^{2+}. Therefore, Ca^{2+} likely controls CTL degranulation through unidentified Ca^{2+}-dependent effector molecules that regulate the function of the proteins that are essential for lytic granule exocytosis (105). Interestingly, MTOC reorientation does not automatically lead to degranulation under low avidity TCR activation (94). This suggests that MTOC reorientation and degranulation are differentially regulated by TCR signal strength.

Entry of cytotoxic molecules into target cell

After CTL degranulation occurs at the immune synapse, the granzymes in the cytolytic granule must enter the target cell cytoplasm to induce activation of cell death pathways. Several non-mutually exclusive mechanisms have been proposed to explain how granzymes, particularly granzyme B, may enter the target cell for activation of apoptosis (80). The first model states that granzyme B gains entry to the target cell through

membrane pores formed by perforin (80). The second model proposes that a perforin-induced membrane repair mechanism triggers an uptake of granzyme B through endocytosis (80). The third mechanism proposed that mannose-6-phosphate receptor functions as a granzyme B receptor (80).

While the first model created skepticism due to the limitation of insufficient perforin pore size, the latter two mechanisms lack a way for the granzymes to gain entry into the target cell cytoplasm. A potential explanation was provided by a recent study on how perforin may facilitate granzyme entry into the target cell. Thiery et. al. showed that perforins form various pore sizes through multimerization inside the target cell endosome (106). More importantly, they found that transfer of granzyme B to the cytosol, and subsequent endosome rupture, depends on perforin. Therefore, perforin likely regulates the entry of granzymes through a two-stage process: first on the cell surface to trigger endocytosis induced by membrane damage repair mechanism, followed by transport of granzymes into the cytosol inside endosomes within the target cell (106). Although it was not mentioned in the study, it has been established that the mannose-6-phosphate receptor is required for granule-mediated target cell death (107). Whether or not all three proposed mechanisms are involved in aspects of granzyme-mediated target cell killing is not clear.

Granzyme-mediated target cell death

In contrast to FasL, which specifically binds the death receptor Fas expressed on target cell surface to trigger apoptosis, granzyme B targets multiple cellular substrates to activate programmed cell death once it is transported into the cytosol of the target cell (80, 85). However, one study indicated that the substrate preference for granzyme B may depend on the species under study (108).

Two signaling pathways have been described for how granzyme B initiates target cell death (109). In the caspase-dependent pathway, granzyme B proteolytically activates caspase-3 by cleavage of pro-caspase-3. Activated caspase-3 removes the inhibitor of caspase-activated deoxynuclease (ICAD) from caspase-activated deoxynuclease (CAD), which is a DNA fragmentation factor. This results in a caspase-dependent, CAD-mediated, DNA fragmentation in the target cell to promote apoptosis (110). Granzyme B can target other cellular substrates to induce cell death in the presence of caspase inhibitor (111). This indicates a caspase-independent cell death pathway. However, the molecules cleaved by granzyme B in the caspase-independent pathway are actually downstream substrates of caspase-3 (109). In this pathway, granzyme B activates pro-apoptotic protein BH_3 interacting domain death agonist (BID) through proteolytic cleavage. Activated BID translocates to the mitochondrial membrane where it mediates oligomerization of Bcl-2-associated X protein (BAX) and/or Bcl-2 homologous antagonist/killer (BAK) proteins to trigger the release of second

mitochondrial activator of caspases (SMAC) and endonuclease G (ENDOG) (112, 113). The released SMAC from the mitochondria promotes full caspase-3 activation through inhibition of inhibitor of apoptosis proteins (IAP) (85, 114). In addition, ENDOG release as a result of BID activation induces DNA damage. Furthermore, granzyme B directly cleaves ICAD for the activation of CAD to induce DNA fragmentation (115). Therefore, granzyme B triggers target cell apoptosis through proteolytic processing of the downstream caspase substrates with or without caspase-3 activation.

Granzyme A (serine esterase) appears to target different cellular substrates and kills target cells through different programmed cell death pathways compared to granzyme B (85, 114). It also appears that purified granzyme A is less potent in causing target cell death compared to granzyme B alone (116). Evidence indicates that granzyme A induces cell death through cleavage of mitochondrial complex protein NADH dehydrogenase, ubiquinone, iron-sulfur protein 3 (NDUFS3) (117), resulting in ROS generation and subsequent cell death (85, 109). While the function and substrate specificity of other granzymes are being gradually deciphered, it is generally perceived that the combined action of different granzymes is essential to ensure target cell death (85, 114).

My research objectives are to dissect some of the molecular events and mechanisms that CTL employ to destroy target cells, with a particular focus on elucidating the contribution of the proline-rich tyrosine kinase (Pyk2) to CTL-mediated cytotoxicity at the molecular level.

Characterization and expression of proline-rich tyrosine kinase 2

Many research groups independently identified Pyk2 during the mid 90s and have given it various designations: Protein tyrosine kinase-2 (118), cell adhesion kinase-β (CAK-β) (119), related adhesion focal tyrosine kinase (RAFTK) (120), calcium-dependent protein-tyrosine kinase (CADTK) (121) and focal adhesion kinase 2 (FAK2) (122). Tissue analysis suggests that Pyk2 is abundantly expressed in various tissues including brain, lung, kidney, spleen and thymus in both humans (120) and in rats (119). Pyk2 is a non-receptor tyrosine kinase that shares 48% of amino acid sequence identity with the focal adhesion kinase (FAK) (120). Similar to FAK, Pyk2 has a central kinase domain, an N-terminal four-point-one Ezrin Radixin Moesin (FERM) domain and a C-terminal focal adhesion targeting (FAT) domain (Figure 1-5). There are also two proline-rich regions between the FAT domain and kinase domain that serve as binding sites for SH3 domain containing proteins such as Grb-2 (118).

Additional splice variants of Pyk2 have been reported since its initial identification. The original non-spliced form of Pyk2 obtained from brain tissue has a molecular mass of 110 kDa, whereas a shorter splice variant has a mass of 106 kDa and is predominantly expressed in cells of hematopoietic lineage (Pyk2-H) including B and T cells (123). Pyk2-H has a deletion of 42 amino acids between residues 739 and 780 (123, 124). Currently, it is unknown if the two splice variants have different functions, although it has been shown that each associates with distinct sets of proteins (123). Early

studies indicated that both Pyk2 and Pyk2-H are expressed simultaneously in certain cell types (123, 125). A recent study also suggested that each isoform is selectively expressed under certain conditions (126). A third splice variant is called Pyk2-related non-kinase (PRNK), which only contains the C-terminal portion of Pyk2 (127). The endogenous expression of PRNK protein has not been described in the literature, however message for PRNK has been detected (127). Interestingly, it was suggested that ectopic expression of PRNK could inhibit endogenous Pyk2 function (127-129). Our laboratory has previously shown that CTL predominantly express the Pyk2-H message (130).
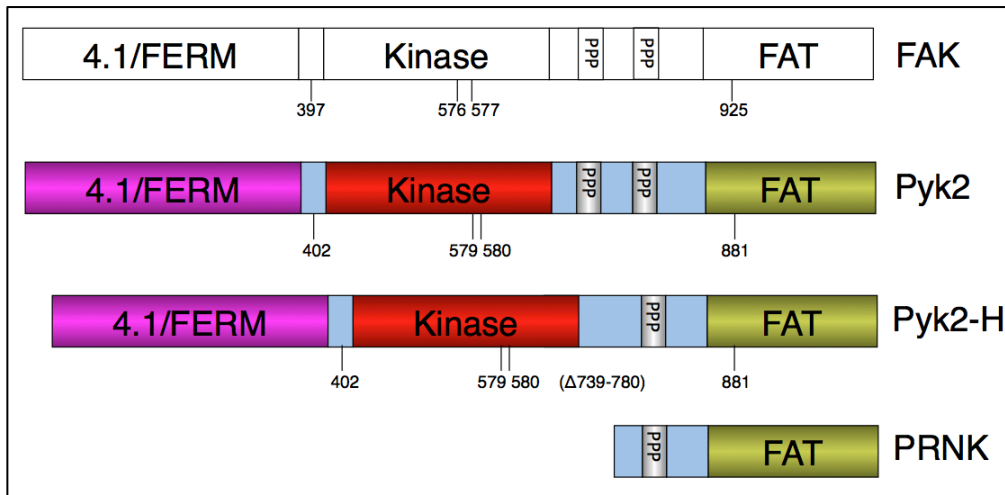
Figure 1-5. Structural features and splice variants of Pyk2. Pyk2 is structurally similar to FAK, which has a N-terminal 4.1/FERM domain, central kinase domain and a C-terminal FAT domain. It has two proline-rich (PPP) regions between the FAT and kinase domains, but one of the two was deleted in the Pyk2-H splice variant. It has 4 known characterized tyrosine phosphorylation sites (Y402, Y579, Y580 and Y881). PRNK protein expression has not been described in the literature except at the messenger RNA level.

Activation and regulation of Pyk2

In T cells, Pyk2 is tyrosine phosphorylated in response to stimulation through a variety of surface molecules including TCR (131-133), LFA-1 (134), CD44 (135), chemokine receptor (123, 136) and IL-2 receptor (137). The detailed mechanisms that lead to Pyk2 activation upon engagement of these surface molecules are still under investigation. Although Pyk2 was originally identified as a calcium dependent kinase (118, 121), how Ca^{2+} regulates Pyk2 phosphorylation remained unsolved for many years. Since Pyk2 does not contain a conventional Ca^{2+}-binding motif such as an EF-hand or C2 domain, it is likely that Ca^{2+} regulation of Pyk2 is through an indirect mechanism.

The mechanism of Pyk2 activation in T cells is not well understood, but a working model could be inferred based on various Pyk2 studies in different receptor systems in other cell types (Figure 1-6). Current literature indicates that TCR-mediated Pyk2 activation requires SFK activity (138). It was also shown that ZAP-70 played an important role in Pyk2 tyrosine phosphorylation upon anti-CD3 antibody stimulation (139). As described earlier, TCR proximal signaling leads to a subsequent increase in intracellular Ca^{2+} concentration. It has been reported that phosphorylation of Pyk2 is sensitive to Ca^{2+} inhibition in many cell types (140) suggesting that Pyk2 activation is regulated by Ca^{2+}.

In its inactive state, Pyk2 is presumed to adopt a similar auto-inhibitory conformation that has been described for FAK (141). The catalytic site of Pyk2 is blocked by the protein interaction between the FERM domain

and the kinase domain. In addition, in the auto-inhibited conformation the tyrosine residue 402 is predicted to be inaccessible to phosphorylation (Figure 1-6). TCR-mediated Ca^{2+} flux triggers the activation of Ca^{2+}-dependent effector molecules, which includes the binding of calmodulin (50). Ca^{2+}-bound calmodulin associates with two individual FERM domains of Pyk2, thereby bringing two Pyk2 molecules close together to form a tri-molecular complex (142). The interaction between calmodulin and Pyk2 FERM domains is speculated to induce a conformational shift to expose tyrosine residue 402, which allows initial trans-phosphorylation to occur (143). It is presumed that FERM domain binding to calmodulin is sufficient to release the kinase domain from an auto-inhibitory state. Once Pyk2 is tyrosine phosphorylated at Y402, it can associate with an inactive Pyk2 through a FERM-FERM domain interaction independent of calmodulin (144). This could explain how initial Pyk2 phosphorylation at Y402 can be potentiated in the absence of calmodulin association (144). The autoinhibitory mechanism is further supported by evidence that expression of a FERM domain alone inhibits oligomerization of Pyk2 (144). Pyk2 phosphorylation at Y402 (pY402) allows for association with SFK (143). SFK are not predicted to be required for Pyk2 Y402 phosphorylation in CTL, but it is likely required for subsequent Y579, Y580, and Y881 phosphorylation (138). Tyrosine phosphorylation at Y579 and Y580 is suggested to regulate the catalytic activity of Pyk2 (145). Y881 phosphorylation allows association with molecules such as Grb2, which contains a SH2 domain for specific

36

phospho-tyrosine binding (140). Although it has not been demonstrated in CTL, dephosphorylation of Pyk2 is likely mediated by the proline-, glutamic acid-, serine-, threonine-rich protein tyrosine phosphatase (PTP-PEST) (146).
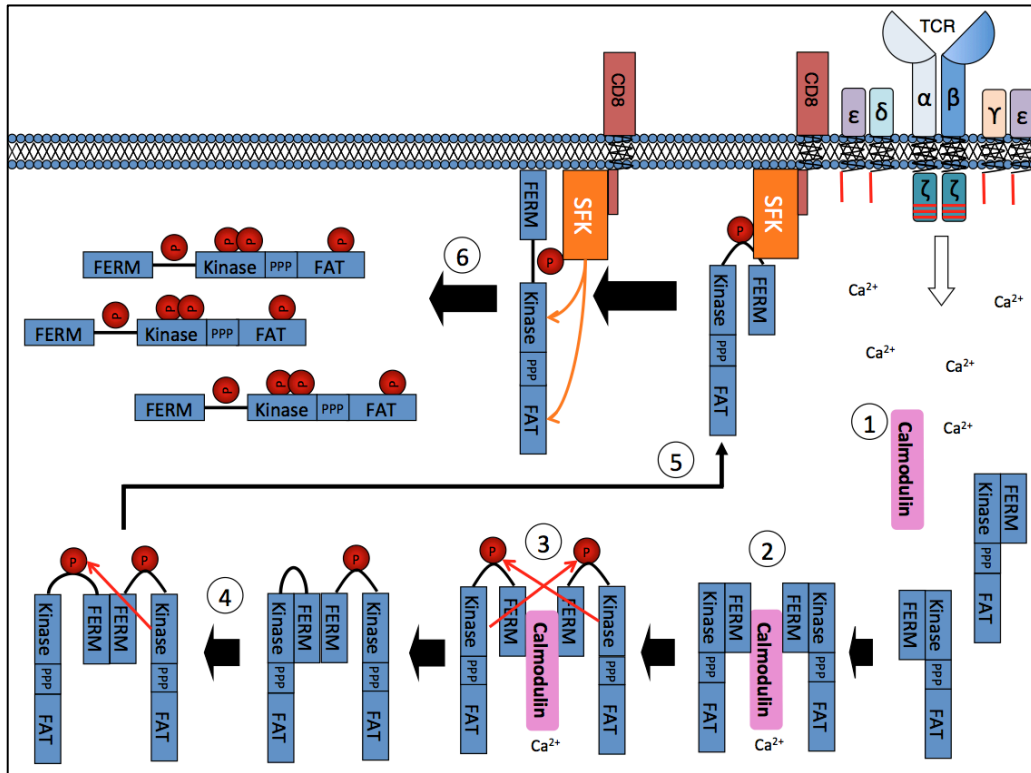
Figure 1-6. Proposed model for Pyk2 activation in T cells. (1) Ligation of TCR triggers the activation of signaling pathways that lead to Ca^{2+} mobilization, which activates Ca^{2+}-dependent effector molecules including calmodulin. (2) Activated calmodulin binds to Pyk2 FERM domains to form a trimer complex. (3) Molecular interaction between FERM domains and calmodulin induces conformational changes in Pyk2 that results in exposure and subsequent trans-phosphorylation of the tyrosine residue 402. (4) Activated Pyk2 oligomerizes through the FERM domains to amplify Pyk2 tyrosine phosphorylation at tyrosine 402. (5) Pyk2 with tyrosine 402 phosphorylation is recruited to SFK through an unknown mechanism that was speculated to involve the cytoskeleton (147). (6) SFK binds to Pyk2 through its SH2 domain and phosphorylates Pyk2 at Y579, Y580 and Y881 to promote full activation.

General function of Pyk2

While Pyk2 and FAK are structurally similar, they appear to have different molecular functions in certain cell types (138, 148). Since Pyk2 is related to FAK in amino acid sequence, many studies have focused on the potential role of Pyk2 in cell adhesion and spreading. Early studies showed that in Pyk2-negative breast cancer cells, heregulin-induced cell invasion was augmented by ectopic expression of Pyk2, but it was suppressed by expression of Pyk2 kinase-dead or tyrosine 402 phosphorylation mutants (149). Another study has shown that expression of PRNK can block epidermal growth factor (EGF) induced pheochromocytoma cell spreading and migration (129). Similar metastatic defects were also reported in other cancer cell lines (150). These studies, along with many others that showed a positive correlation between Pyk2 phosphorylation and cancer cell invasiveness, collectively implicated Pyk2 as an important regulator for cytoskeleton-dependent processes such as cell adhesion and migration.

Pyk2 can bind to and/or phosphorylate a number of protein substrates that regulate cytoskeletal reorganization. These proteins include PH- and SH3-domain-containing RhoGAP protein (PSGAP) (151), Casitas B-lineage (Cbl) (152, 153), VAV1 (154), integrin β3 subunit (155), Hic-5 (156), paxillin (132, 157), and others. The functional significance of the association with and/or phosphorylation by Pyk2 is not firmly established. Paxillin is probably the most well characterized substrate for Pyk2 that has a prominent role in the regulation of cytoskeleton (158). Paxillin directly

interacts with the Pyk2 FAT domain through its leucine-aspartic acid-4 (LD4) motif (159). The functional significance of Pyk2-paxillin association is currently unknown. Since both Pyk2 and paxillin are targeted to the MTOC, it is speculated that the interaction is important for mediating aspects of MTOC function (160, 161).

Molecular function of Pyk2 in hematopoietic cells

Pyk2 knockout mice have been generated for functional studies on a number of cell types. Unlike FAK deficient mice, which show extensive and abnormal embryonic development (162), Pyk2 deficient mice do not have a major aberrant developmental phenotype. The first Pyk2 knockout study described an absence of marginal zone B (MZB) cells in the spleen (163). The lack of MZB cells was attributed to a defect in the intrinsic ability of B cells to migrate in response to chemokine. In addition, humoral responses were slightly reduced in the absence of Pyk2 (163). The second study reported that migration of macrophages was severely impaired in Pyk2 knockout mice (164). The migration defect was attributed to a failure in cell polarization toward the chemotactic gradient. At the signaling level, chemokine-induced Ca^{2+} mobilization was severely compromised in the absence of Pyk2 (164). This observation is particularly intriguing since Pyk2 was characterized as a Ca^{2+}-dependent molecule rather than a mediator of Ca^{2+} release. The third report showed that Pyk2 is essential for osteoclasts to function in bone resorption (165). Pyk2-/- osteoclasts fail to form a podosome belt, which is a

microtubule-dependent structure, and are severely impaired in cell polarization (165). All of these studies collectively point to a defect in some aspects of cell polarization and motility in the absence of Pyk2.

Function of Pyk2 in T cells

Naïve CD8 T cells obtained from Pyk2 deficient mice were also defective in ICAM-1 dependent cell adhesion and polarization (166). This could explain why chemotaxis of CD8 T cells was significantly reduced in the absence of Pyk2. The development of various T cell subsets appeared normal in the Pyk2 deficient mice, but the short-lived effector CD8 T cell population was significantly reduced upon viral challenge (166). Interestingly, memory T cell development was not affected in the absence of Pyk2 (166). It remains unknown whether the Pyk2-deficient memory T cells are functional upon secondary challenge, but it is apparent that Pyk2 is involved in some aspects of cell adhesion and migration.

Evidence for a role of Pyk2 in killer cell mediated cytotoxicity

The earliest reports that implicate Pyk2 in cell-mediated cytotoxicity came from studies of NK cells. Although the mode of recognition and activation is very different between NK cells and CTL, both cell types utilize similar cytotoxic mechanisms to kill their target cells (167). One study showed that ectopic expression of either wild-type or kinase-dead Pyk2 moderately reduced target cell killing (168). The analysis showed that the

most significant impairment in target cell lysis was found in NK cells expressing the kinase-dead Pyk2 mutant (168). A separate study reported a similar observation, but showed that NK cells expressing either wild-type or kinase-dead Pyk2 have comparable reduction in target cell lysis (169). The slight difference between these two studies might be attributed to the level of Pyk2 protein expression in the NK cells. Interestingly, a recent study also showed that integrin-mediated degranulation is impaired in Pyk2-deficient neutrophils (170). These studies collectively point to a potential role of Pyk2 in regulating killer cell cytotoxicity and degranulation.

Pyk2 expression is up-regulated in certain cancers, and the expression level is quantitatively correlated to cancer progression (171, 172). Other studies have reported that over-expression of Pyk2 promotes tumor cell metastasis (150, 173). According to these studies, uncontrolled activity of Pyk2 may promote cancer cell migration. Pharmacological inhibition of Pyk2 and FAK has been suggested as a potential cancer therapy (174, 175). However, the functional consequence of inhibiting Pyk2 in CTL, which express very little FAK, remains unknown. If Pyk2 is required for CTL-mediated cytotxicity, then Pyk2 inhibition may limit the efficacy of CTL in the context of cancer and result in poorer prognosis for cancer patients than anticipated. From a therapeutic point of view it is important to understand the role of Pyk2 in the regulation of CTL function.

Hypothesis

Pyk2 regulates adhesion-dependent functions in cytotoxic T lymphocytes, which includes cell adhesion, migration and target cell conjugation. It plays an essential role in cytoskeleton-dependent processes such as cell polarity, MTOC translocation and lytic granule delivery.

Research objectives:

My research focus is two-fold. The first is to examine Pyk2 regulation by Ca^{2+} during T cell activation. The second focus is to determine if Pyk2 is required for CTL function. The following questions will be addressed in this research thesis.

1. What is the signaling mechanism for Pyk2 activation in CTL? Is Ca^{2+} absolutely required for Pyk2 tyrosine phosphorylation in CTL upon TCR activation?

2. Does Pyk2 contribute to CTL function?

3. What is the molecular basis of Pyk2 function in regulating CTL motility and killing?

The research progress in understanding the mechanism for CTL-mediated cytotoxicity is still in its infancy. The results from this research will contribute to our understanding of the regulation of CTL function. Pyk2 activation correlates with cancer growth and metastasis and is being explored as a treatment option using small molecule inhibitors. However, caution must be exercised in attempts to use inhibition of Pyk2 as a potential cancer treatment option since CTL contribute to cancer clearance and we do not know whether CTL function requires Pyk2.

CHAPTER 2

MATERIALS AND METHODS

A. Materials

Mice. C57BL/6 female mice were purchased from Charles River (Wilmington, MA). OT-1 (C57BL/6-Tg(TcraTcrb)1100Mjb/J) mice were a generous gift from Dr. Troy Baldwin and were generated as described previously (176, 177). B6.129ptprc[tm1Holm]/J mice were purchased from the Jackson Laboratory (Bar Harbor, Maine). CD45 knockout (CD45-/-) mice were generated from several backcrosses between B6.129ptprc[tm1Holm]/J and C57BL/6 mice. C57BL/6 mice were kept in a conventional housing facility while both OT-1 transgenic and CD45-/- mice were kept in a virus and antigen free facility. All mice were used after they were 6 to 8 weeks old.

Cells. The murine alloreactive CD8$^+$ T cell clone AB.1 and clone 11 are non-transformed antigen- and IL-2-dependent CTL that have specificity for MHC class-I H-2K^b (178, 179). CTL clone AB.1 was derived from BALB/c mice (H-2K^d) that were subjected to a mixed lymphocyte reaction to a C57BL/6 culture (H-2K^b) (178). CTL clone 11 was derived from peritoneal exudate cells of F1 mouse, which were a cross of B10.BR X B10.D2 mice, that was immunized with EL4 (H-2K^b) cells (179). Both CTL clone AB.1 and clone 11, which are specific for H-2K^b, were obtained through limited dilution from the original lymphocyte culture. CTL clone 3/4 was derived from C57BL/6 mice immunized with infectious A/PR/8/34 (H1N1) influenza virus (180). CTL

clone 3/4 is specific for the influenza nucleoprotein (NP) peptide with the single amino acid code ASNENMETM, which corresponds to the residues 366-374 expressed on MHC class I of the H-2K^b haplotype. All CTL clones were stimulated weekly with irradiated C57BL/6 splenocytes supplemented with 10 unit/ml of recombinant IL-2. To stimulate CTL clone 3/4, 1 X 10^8 C57BL/6 splenocytes (after lysis of red blood cells) were incubated with 80 µg ASNENMETM peptides in 400 µl of RPMI for 1 hour before used as stimulators. OT-1 specific CD8$^+$ T cells were derived from *ex vivo* stimulation of splenocytes from OT-1 transgenic mice with ovalbumin (OVA) peptide SIINFEKL for 3-4 days. After 3 days of CTL stimulation, cells were split 1 to 4 according to cell densities and additional IL-2 was added to the cultures. All CTL were used for experiments 4 to 6 days post stimulation. The target cells were derived from a murine lymphoma cell line (L1210) stably transfected with chimeric class I MHC H-2K^b/D^d (L1210$^{Kb/Dd}$). The parental L1210 cells were used as negative control in some experiments. EL4 is a lymphoma cell line derived from C57BL/6 mice.

Antibodies. Anti-phosphotyrosine (PY72.10.5) antibody was obtained from Dr. B. Sefton at The Salk Institute (La Jolla, CA). The hamster monoclonal antibody 145-2C11 (anti-mouse CD3) was obtained from ATCC (Burlington, Ontario). The polyclonal Pyk2-specific anti-sera F298 (against N-terminus Pyk2) and F245 (against C-terminus Pyk2) were generated by immunization of New Zealand White Rabbits with the Pyk2 amino acid sequence 2-12 alone

and Pyk2 amino acid sequence 720-862 fused with glutathione s-transferase (GST) protein, respectively (131). Rabbit anti-human α-tubulin antibody and anti-γ tubulin mouse monoclonal antibody were purchased from Abcam (Cambridge, MA). Pyk2/CAKβ-specific monoclonal antibody, anti-paxillin monoclonal antibody, anti-ZAP-70 antibody, fluorescein isothiocyanate (FITC)-conjugated anti-LFA-1 antibody, and FITC-conjugated rat anti-mouse CD107a (lysosomal-associated membrane protein 1 or LAMP-1) monoclonal antibody were purchased from BD Biosciences (Mississauga, ON). Anti-actin polyclonal antibody was purchased from Sigma (Mississauga, ON). Anti-Lck antibody was purchased from Santa Cruz Biotechnology Inc (Santa Cruz, CA). Phospho-Src family (p-Tyr416), phospho-Lck (p-Tyr505), phospho-p44/42 MAPK or phospho-Erk (Thr202/Tyr204) antibody, and phospho-ZAP-70 (Tyr 319) were purchased from Cell Signaling Technology (Boston, MA). Allophycocyanin (APC)-conjugated anti-LFA-1 (CD11a) antibody was purchased from eBioscience (San Diego, CA). Pyk2 phosphospecific antibody (pY402) was purchased from Biosource International (Camarillo, CA). Anti-calmodulin monoclonal antibody was purchased from Upstate (Lake Placid, NY). Horseradish peroxidase (HRP)-conjugated protein-A was purchased from Pierce (Rockford, IL). HRP-conjugated goat anti-mouse IgG, FITC-conjugated donkey anti-rabbit IgG, and goat anti-hamster IgG for crosslinking anti-CD3 antibody were purchased from Jackson ImmunoResearch Laboratories (West Grove, PA). Anti-Erk 1/2 (MAP kinase) monoclonal

antibody and Alexa-647-conjugated goat anti-mouse IgG antibody were purchased from Life Technologies (Burlington, ON).

Reagents. Fibronectin, Ionomycin, BAPTA-AM, KN-62, PP2, PP3, W7, W5, Ebselen, calpeptin, and N-benzyloxycarbonyl-L-lysine thiobenzyl ester (BLT) were purchased from EMD Millipore (Billerica, MA). PF431396 was purchased from Symansis (Auckland, New Zealand). Dimethyl sulfoxide (DMSO), U0126, thapsigargin, H_2O_2, diphenyleneiodonium chloride (DPI), Phorbol myristate acetate (PMA), EGTA, tetramethyl-rhodamine B isothiocyanate (TRITC)-conjugated Phalloidin, Histopaque-1077, and 5'5-dithiobis(2-nitrobenzoic acid) (DTB) were purchased from Sigma (Mississauga, ON). Mouse Ptk2b (Pyk2) specific short interfering ribonucleic acid (siRNA) with the target sequence GAACAUGGCUGAUCUCAUA was purchased from Dharmacon (Chicago, IL). Additional Ptk2b specific siRNA (with target sequence GGGAAGAACUUCAAGCUUGtt and GGACAAGUAUGAAUGUCUAtt), the negative control non-targeting siRNA, surfactant-free 5.2 μm sulfate latex beads, 5-(and-6)-chloromethyl-2',7'-dichlorodihydrofluorescein diacetate, acetyl ester (CM-H_2DCFDA), carboxyfluorescein diacetate succinimidyl ester (CFSE), CellTrace Violet, and CellTracker Blue 7-Amino-4-Chloromethylcoumarin (CellTracker Blue-CMAC) were purchased from Life Technologies (Burlington, ON). Recombinant mouse ICAM-1/CD54 Fc chimera and CXCL9/MIG were purchased from R&D Systems (Minneapolis, MN). Lab-Tek chambered

coverglasses of 1.5 mm thickness were purchased from Nunc (Rochester, NY). Transwell® 5.0 μm pore polycarbonate membrane inserts were purchased from Corning (Tewksbury, MA). Protein A-Sepharose was purchased from Amersham Biosciences (Piscataway, NJ). Lonza Nucleofector kits for mouse T cells were purchased from ESBE Scientific (Markham, ON). The NP peptide ASNENMETM and OVA peptide SIINFEKL were purchased from Sigma-Genosys (Canada) and GenScript (Piscataway, NJ), respectively. The plasmid pmCherry-α-tubulin was purchased from Addgene (Cambridge, MA). Enhanced chemiluminescence buffer (ECL) was purchased from PerkinElmer Life Science (Boston, MA).

B. Methods

Cloning of Pyk2 constructs. pBluescript SK plasmids encoding the hematopoietic form of Pyk2 (Pyk2-H) and the Pyk2 C-terminus (aa 678-1009) coupled to pEGFP-C1 (Clontech) were generated by Dr. T. Lysechko at the University of Alberta. The full length Pyk2 cDNA sequence (encoding amino acid 1-1009) was excised from the pBluescript plasmid using the restriction enzymes EcoR I and Sal I (Invitrogen), then subcloned into pEGFP-C1 plasmid (N-terminal GFP tag) and pEGFP-N3 plasmid (C-terminal GFP tag) separately. The cDNA sequence of the N-terminus FERM and Kinase domain of Pyk2 (correspond to amino acid sequence 1-717) was sub-cloned into pEGFP-N3 using the restriction enzymes EcoR I and Bam HI (Invitrogen). The kinase-dead Pyk2 (K457A) was generated by site-direct mutagenesis

using the primers 5'-GTGGCCGTCGCGACCTGTAAGAAAGACTGTACC-3' and 5'-CTTACAGGTCGCGACGGCCACATTAATTTTTTCC-3' on a Pyk2-pEGFP-N3 plasmid followed by applying PCR amplification protocol as described in Zheng et. al (181). All plasmids have been sequenced and individually verified.

CTL nucleofection. CTL nucleofection was performed using the Amaxa Mouse T Cell Nucleofector® kit according to the protocol with minor modification. After 3 days of CTL stimulation, CTL clones or *ex vivo* OT-1 CD8$^+$ T cells were resuspended in fresh medium and supplemented with IL-2 then diluted accordingly to avoid overgrowth. At day 4 post CTL stimulation, Histopaque-1077 was utilized for enrichment of live cells for nucleofection. Briefly, CTL were resuspended in 2 ml of RPMI containing 2% fetal calf serum (FCS). Histopaque-1077 was pre-warmed to room temperature and then gently added into the cell suspension from the bottom to push the CTL suspension upward. Separation was achieved through centrifugation at 2100 RPM (Beckman CS-15R centrifuge) at room temperature for 15 minutes. Live cells were harvested from the medium and Histopaque-1077 interface, then transferred to complete medium. All cell washing steps were performed on IEC clinical centrifuge with the dial set to 5, which roughly corresponds to 3000 revolutions per minute (RPM) on a Beckman CS-15R centrifuge. Cells were spun down and washed twice with Dulbecco's Phosphate-Buffered Saline (D-PBS) before the final spin at 100 relative centrifugal force (RCF) for

5 minutes (Eppendorf 5415D centrifuge). Approximately 1.5 X 10^6 million cells were used for each nucleofection. After electroporation (using the Amaxa nucleofector program setting X-01 according to manufacturer's specifications), cells from the electroporation cuvette were immediately transferred to 2 ml of pre-warmed complete medium (instead of the recovery medium) supplemented with IL-2 and component B. CTL nucleofected with fluorescent constructs were used at 24 hours post-nucleofection. The amount of plasmid(s) applied to each nucleofection varied between 0.5 μg to 2.0 μg. Samples nucleofected with siRNA were split 1:2 and supplemented with IL-2 after 24 hours, then utilized for experiments after 48 hours post-nucleofection. Pyk2 knockdown was achieved using a combined pool of siRNA purchased from Dharmacon (10 μg) and Ambion (15 μg of each siRNA from ID 94285 and ID 94190). A corresponding 40 μg of negative control siRNA was used for all experiments.

TCR-induced activation of CTL. CTL were washed 3 times in D-PBS containing 1 mg/L of Ca^{2+}/Mg^{2+} before stimulation with either soluble crosslinked anti-CD3 antibodies or immobilized anti-CD3 antibodies. Cross-linking of CD3 was performed as follows: 10 μg/ml anti-CD3 (145-2C11) antibodies were added to CTL and incubated on ice for 10 minutes. Cells were spun down briefly (2000 RPM for 30 seconds in Eppendorf 5415D centrifuge) and excess medium was removed, then resuspended in 5 μg/ml cross-linking antibody (goat anti-hamster IgG) for activation at 37°C. To stop

the activation, an equal volume of chilled 2.5% nonidet P-40 (NP40) lysis buffer containing 2 mM sodium orthovanadate and 4 mM EGTA was added to lyse the cells. Plate-bound anti-CD3 stimulation was performed by incubating CTL at 37°C on a non-tissue culture treated plate pre-coated with 10 µg/ml anti-CD3 antibody. Anti-CD3 antibody was reconstituted in PBS (without Ca^{2+}/Mg^{2+}) and incubated in culture plates overnight at 4°C. Coated plates were washed with three washes of PBS, then blocked with 2% bovine serum albumin (BSA) in PBS before being used for CTL activation. Equal volumes of chilled 2.5% NP40 lysis buffer containing sodium orthovanadate and EGTA were added to the CTL to stop the stimulation. Cell lysates were subjected to western blot analyses and/or immunoprecipitation as described below. Western blots of whole cell lysates were done with a cell volume that was equivalent to 3 X 10^5 CTL per lane. Western blots of immunoprecipitation products contained at least 10 million cell equivalents per lane. The experiments using inhibitor treatment will be described in the following section.

Ca^{2+}-induced activation of CTL. CTL clones were washed twice in D-PBS containing 1 mg/L of Ca^{2+}/Mg^{2+}, then treated with the indicated type of inhibitor (DMSO, DPI, Ebselen, W7, W5, or U0126) for 20 to 30 minutes at room temperature prior to stimulation. Stimulation with ionomycin and thapsigargin was performed using fresh thawed aliquots without a freezing and thawing cycle. Cells were activated at 37°C in the presence of inhibitor

for the duration of the experiment in D-PBS with 1 mg/L of Ca^{2+}/Mg^{2+}. At least 3 X 10^5 CTL were used for each test condition for experiments involving whole cell lysates and an equal volume of hot reducing sample buffer was added to stop the stimulation. For experiments that involved immunoprecipitation, at least 10 million cells were used for each test condition and an equal volume of chilled 2.5% NP40 lysis buffer containing sodium orthovanadate and EGTA was added to lyse the cells.

Stimulation of CTL with H_2O_2. CTL were washed 3 times and then resuspended in D-PBS containing 1 mg/L of Ca^{2+}/Mg^{2+} before stimulation with a fresh aliquot of H_2O_2. CTL were stimulated for the indicated time at 37°C before addition of hot reducing sample buffer to lyse cells for western blot analysis. Approximately 3 X 10^5 CTL were used in each test condition for western blot analysis.

Measurement of ROS production. CTL clone AB.1 cells were washed twice with D-PBS then resuspended at 4 X 10^6 cells per ml in D-PBS. For samples that utilized ebselen, CTL were pre-treated as described above. Cells were stimulated with anti-CD3, ionomycin or H_2O_2 at 37°C for 10 min. Immediately following stimulation, CM-H_2DCFDA was added at a final concentration of 0.5 μM for an additional 15 min at 37°C. Cells were washed twice at 4°C with PBS containing 1% fetal bovine serum (FBS) before data acquisition on a fluorescence-activated cell sorting (FACS) calibur.

Stimulation of thymocytes with thapsigargin. Thymi from CD45 wild-type and CD45 -/- mice were obtained and homogenized to a suspension of 2×10^7 cells per ml in D-PBS. Cells were treated with the indicated concentration of DPI or DMSO control at room temperature for 20 minutes, followed by stimulation with thapsigargin at 37°C for 10 minutes. At least 10 million cells were used for each immunoprecipitation and an equal volume of chilled 2.5% NP40 lysis buffer containing 2 mM sodium orthovanadate was added to stop the stimulation. All the immunoprecipitation procedures are described below.

Immunoprecipitation. For Pyk2 immunoprecipitation, treated CTL were lysed in 1% NP40 lysis buffer containing 1 mM sodium orthovanadate in D-PBS and 4 mM ethylene diamine tetraacetic acid (EDTA) for 30 minutes at 4°C. Cell lysates were spun down at maximum speed in an Eppendorf 5415D centrifuge for 10 minutes at 4°C. Post-nuclear lysates were subject to immunoprecipitation using 4 μl of Pyk2 antiserum (F245 or F298) then rotated for 1 hour at 4°C, followed by addition of protein A Sepharose bead and further rotation for an extra hour. The beads were centrifuged at 8000 RPM for 10 minutes at 4°C in an Eppendorf 5415D centrifuge, then washed three times with D-PBS before boiling in 70 μl of reducing sample buffer. To detect association with calmodulin, all CTL samples were lysed in 1% NP40 lysis buffer without EDTA. Calmodulin was immunoprecipitated with 5 μl of anti-calmodulin antibody overnight at 4°C with rotation.

Immunoblots. Sodium dodecyl sulfate polyacrylamide gel electrophoresis (SDS-PAGE) was performed with 8.5% polyacrylamide for all the western blot analyses except for the calmodulin experiments, which were performed at a 12.5% polyacrylamide concentration. Proteins were denatured by boiling in reducing sample buffer and separated on a 16 cm X 20 cm SDS-PAGE gel overnight. The separated proteins on the SDS-PAGE gel were transferred to a polyvinylidene fluoride (PVDF) membrane. Membranes were probed with the indicated primary antibody and HRP-coupled secondary antibody then visualized by enhanced chemiluminescence. When multiple immunoblots were performed on the same membrane, the membrane was stripped between each blot. Anti-phosphotyrosine blots were always performed first and loading controls were generally completed last.

Immobilized ICAM-1 and fibronectin induced CTL tyrosine phosphorylation. Recombinant ICAM-1 (10 μg/ml) or fibronectin (10 μg/ml) were incubated on a 96 well plate at 4°C overnight. The plate was washed 3X with PBS followed by blocking with 2% BSA in PBS for 1 hour at 37°C. Cells were pre-treated with either DMSO as control or PF431396 for at least 30 minutes at room temperature before stimulation. Approximately 3 X 10^5 CTL were resuspended in 30 μl of RPMI with 2% FCS for each condition. Cells were stimulated at 37°C for the indicated time followed by addition of

35 μl hot reducing sample buffer. All samples were boiled for 3 minutes and the cell lysates were used directly for western blot analysis.

ICAM-1 adhesion assay. Sulfate latex beads were coated with the indicated amount of recombinant ICAM-1 overnight at 4°C in PBS at a concentration of 10 million beads per ml. Beads were blocked with a 40% volume of 1% BSA for 1 hour at room temperature, then washed three times with RPMI containing 2% FCS before use. CTL clones were washed twice with RPMI containing 2% FCS before use. CTL were mixed with beads then immediately centrifuged at 700 RPM for 3 minutes at 4°C (in Beckman CS-15R centrifuge) to induce conjugate formation. This was followed by activation at 37°C for the indicated time before vortexing to disrupt loosely bound conjugates. In experiments involving inhibitor, CTL were incubated with the indicated amount of PF431396 or DMSO as a control for 45 minutes at room temperature before being used in conjugation assays. For experiments with Pyk2 knockdown cells, CTL were nucleofected with a pool of Pyk2 siRNA along with negative control siRNA for 48 hours, followed by three washes before use.

Cell migration assay. Lab-Tek chambered coverglasses were incubated with 3 μg/ml ICAM-1 in PBS for 2 days at 4°C before used. Coated coverglasses were washed gently three times with cold PBS before addition of CTL (1.5 X 10^5 cells resuspended in 300 μl of RPMI containing 2% FCS) for

imaging analysis. For cell migration assays, CTL resuspended in RPMI containing 2% FCS were first allowed to settle on coverglasses for a minimum of 40 minutes in the 37°C incubator before being transferred to a Olympus IX-81 microscope stage that is equipped with a live cell chamber. In experiments using nucleofected cells, Histopaque-1077 was used for live cell enrichment as described above. Cells were washed three times in RPMI containing 2% FCS before transferred onto the imaging slide.

Live cell imaging. Nucleofection and preparation of CTL on imaging slides was performed as described above. Acquisition of cell migration was performed at 37°C. The movement of cells was recorded for 15 minutes with 30 seconds intervals. No more than two separate acquisitions were obtained on a single imaging well at a random area to avoid phototoxicity. Acquisition was performed after 45 minutes of initial cell seeding. No live cell imaging acquisition was performed if the cells have been seeded on imaging slide for more than two hours. To visualize the distribution of GFP-coupled Pyk2 at the ICAM-1 contact zone, all images were acquired at room temperature instead of at 37°C in order to capture the fast-turnover adhesion complex. Image acquisition was performed inside a live cell chamber with 5% CO_2 and humidifier. For co-localization studies that involved GFP and mCherry-tubulin, separate wavelengths were acquired sequentially for each plane of a cell. The resulting image stacks were combined and shown in the figure.

Morphological analysis. The visual criteria to distinguish a normal CTL and a stretched CTL is as followed. A normal CTL has a single characteristic round trailing edge. It may extend, on average, no more than two cells diameter in length during migration. In contrast, a stretched CTL has one (or multiple) needle-like trailing edge. In most case it could extend over two cells diameter as it migrate. The visual criteria for determination of normal versus stretched phenotype are based on a combination of the trailing edge shape and the length of the cell.

Parameters for image acquisition. All images were acquired using the Olympus IX-81 microscope stage that is equipped with a live cell chamber. For cell migration analysis, images were acquired using 20X objective lens with emersion oil. Both bright field and emission signal from a 488 nm excitation wavelength were acquired for each interval. This is performed so that each cell can be tracked precisely if the GFP-positive cell happens to move out of focus. For each acquisition, a z-stack of 7-9 image layers was acquired using the contact point as the center. A space of 0.5 μm was provided between each Z-stack. Each bright field and GFP imaging signal was obtained from 50 and 200 ns duration, respectively. The laser intensity for 488 nm wavelength was adjusted accordingly between 10 to 15%. A series of time-lapse images were acquired using Metamorph software at 30 second intervals for 15 minutes duration or longer. To prevent photo-toxicity, a maximum of two sequential acquisitions were performed on a separate

region from each slide. An average of 6 acquisitions was obtained for each condition within a 2-hour limit. For a live-cell imaging at a single cell level, a 40X objective lens was used for imaging acquisition with an additional 1.6X magnification provided by the microscope stage. Whole cell z-stack images were acquired using 0.2 μm spaced between each image. The laser intensity and acquisition duration were adjusted according to the fluorochrome signal in order to obtain the best signal without immediate photo-toxicity to the cell.

Imaging analysis for cell migration assay. All acquired images were converted into single time-lapse video files using the 'create movie' function in Metamorph software. The video file was analyzed using the free-licensed ImageJ software (http://rsb.info.nih.gov/ij/). Each individual CTL movement was tracked manually using the "Manual Tracking" function under ImageJ plugins. Once tracking is finished, the program automatically generates a list of numerical parameters for the duration and distance of the selected cell movement from each imported video file. Manual tracking was performed only on cells that migrated within the imaging area. Cells that moved out of the frame during the 15 minute period of acquisition were not included as part of the analysis. A group of cells analyzed from a given condition were pooled together for data presentation as followed: the resulting numerical parameters obtained from a group of cells were pooled together on an Excel spreadsheet, which can be opened using the "Chemotaxis Tool" function

under ImageJ plugins. The average migration velocity was calculated manually using the parameter obtained and the migration profile was generated through the "Chemotaxis Tool" function.

Quantification of fluorescent intensity. To quantify fluorescence intensity, z-stack images were combined to form a single image. A rectangular profile was outlined around the cell and the intensity was analyzed using the ImageJ 'Plot profile' option under 'Analyze' function. A data list of numerical values for the intensity was obtained by choosing the 'List' function. The data were transferred to an Excel spreadsheet, then the cell fluorescence data was manually divided into three portions: leading edge, middle and trailing edge according to the cell length. The sum intensity for each portion was calculated using a spreadsheet, and the ratio of trailing edge over leading edge was obtained manually for each cell.

Transwell migration assay. Transwell® 5.0 μm pore polycarbonate membrane inserts were either pre-incubated with FCS or 3 μg/ml ICAM-1 for overnight at 4°C before use. The polycarbonate membrane was washed three times in D-PBS before use. CTL (5 X 10^5) were resuspended in 200 μl volume of RPMI containing 2% FCS followed by transferring onto the membrane insert to allow cell settling for 1 hour. The membrane insert was placed onto a 24-well culture plate containing the indicated amount of CXCL9 in 0.5 ml of

RPMI containing 2% FCS. The total number of migrated cells was counted after a 37°C incubation for the indicated period.

Immunostaining of extracellular LFA-1. CTL were treated with the inhibitor (calpeptin or PF431396) at room temperature for 40 minutes before transferring 1 X 10^5 cells onto an ICAM-1 coated imaging slide. This was followed by incubation at 37°C for 1 hour to allow cell adhesion, then cells were immediately fixed with 2% paraformaldehyde for 15 minutes. Cells were immunostained with FITC-conjugated anti-LFA-1 antibody for 1 hour in PBS containing 1% FCS, followed by three washes before image acquisition. For CTL that were nucleofected with Pyk2 constructs or siRNA, Histopaque-1077 was used for live cell enrichment as described above. GFP-expressing CTL were allowed to settle for at least 40 minutes before fixation and then were immunostained with APC-conjugated anti-LFA-1 antibody. The corresponding APC- and FITC-conjugated isotype antibody controls were used for each experiment.

Intracellular staining of Pyk2. CTL treatment and fixation were performed as described above. After paraformaldehyde fixation, cells were permeabilized with buffer containing 0.2% saponin in PBS with 4% defined Calf Serum (dCS). The samples were immunostained with 1 μl of F245 or F298 antibodies for 1 hour at room temperature. Samples were washed three times in PBS containing 1% dCS before addition of secondary antibody

61

(FITC-conjugated donkey anti-rabbit IgG) against Pyk2 anti-serum for 30 minutes. All samples were washed three times before image acquisition.

In vivo CD8 T cell migration. *Ex vivo* activation of OT-1 specific CD8 T cells and nucleofection have been described above. C57BL/6 splenocytes and nucleofected OT-1 CD8 T cells were labeled with 1 µM of Carboxyfluorescein diacetate, succinimidyl ester (CFSE) and CellTrace violet, respectively. Cells were labeled at 37°C for 20 minutes in D-PBS then washed once with RPMI containing 2% FCS. Labeled cells were resuspended in complete medium and incubated for an additional 5 minutes at 37°C. Cells were washed 2X with RPMI containing 2% FCS, then 1X with D-PBS before resuspension to a concentration of 2 X 10^7 cells per ml. A mixture of 1:1 CFSE-labeled splenocytes with CellTrace violet-labeled OT-1 CD8 T cells nucleofected with a control siRNA or Pyk2 siRNA, were intravenously injected into C57BL/6 mice of the same gender. A total of 5 million cells were used per injection. After 7 to 8 hours post injection, spleen and lymph nodes were obtained from each mouse and the number of CFSE and CellTrace violet positive cells were determined for each sample containing one million cells.

Bystander cell barrier assay. CTL clone AB.1 cells were first aliquoted onto V-bottom 96 plate then centrifuged at 1000 RPM for 5 minutes (in Beckman CS-6R centrifuge) at room temperature. Various numbers of by-stander cells (L1210) in the same volume were added carefully without disturbing the CTL

pellet. The plate was centrifuged again to compact by-stander cells above the CTL. The target cells (L1210$^{kb/Dd}$) were added last without the centrifugation step to allow settling. The experiment was conducted in RPMI containing 2% FCS in the presence of the indicated PF431396 concentration. Cell cultures were incubated at 37°C for 8 hours before harvesting supernatants to assay for serine esterase activity. A similar protocol was used for CTL transfected with siRNA.

Serine esterase (granzyme A) release assay. Both BLT and DTB (4.8 mg each) were dissolved in 50 ml of PBS followed by transfer of a 150 μl aliquot of the solution onto a 96-well flat-bottom microplate. Culture supernatants (25 μl) containing granzyme A from the CTL cell culture were added to the BLT/DTB solution and then incubated at room temperature until a color developed. The resulting color intensity was measured using a 405 nm filter in a kinetic microplate reader (179).

Target cell-induced CTL degranulation. CD107a expression was measured as a marker of target cell-induced CTL degranulation. Target cell-induced CD107a expression was performed using EL4 and L1210$^{kb/Dd}$ for CTL clone 3/4 and CTL clone AB.1, respectively. Target cells were labeled with 10 μM Cell Tracker Blue in plain RPMI for 20 minutes at 37°C, followed by a single wash in complete medium then resuspended in plain RPMI to allow excess dye release for 30 minutes at 37°C. After incubation the cells were washed

three times in RPMI with 2% FCS before use. EL4 cells were treated with the indicated amount of NP peptide ASNENMETM for 1 hour in plain RPMI at 37°C. EL4 cells were washed twice then resuspended in RPMI with 2% FCS, which also contained the corresponding amount of DMSO or PF431396, before mixing with CTL clone 3/4. CTL clone AB.1 was mixed with Cell Tracker Blue-labeled L1210$^{kb/Dd}$ or control L1210 cells. All CTL and the cognate target cells were pre-treated with the indicated amount of DMSO, PF431396 or EGTA at room temperature for at least 30 minutes before they were mixed together in the presence of 0.5 μg FITC-conjugated anti-CD107a antibody. Cell mixtures were kept on ice before centrifugation at 800 RPM for 3 minutes (in Beckman CS-15R centrifuge) to induce cell contact. CTL were activated by incubation of cell pellets in a 37°C waterbath for the indicated time. Termination of stimulation was performed by addition of cold 5 mM EDTA and mixing in a vortex mixer at high speed for 3 to 5 seconds. Samples were washed twice using D-PBS with 5 mM EDTA before analysis using a flow cytometer. The percentage of CD107a expressing cells were determined on the basis of gating on the Cell Tracker Blue negative population.

CTL conjugation assay. CTL clone AB.1 was labeled with 10 μM Cell Tracker Green, while L1210 and L1210$^{Kb/Dd}$ cells were labeled with 10 μM Cell Tracker Blue as described above. Both CTL and target cells were treated with either DMSO or PF431396 for 20 minutes at room temperature prior to

mixing in a 1:2 ratio. Cell conjugates were induced by brief centrifugation at 700 RCF for 3 minutes at 4°C in a Beckman CS-15R centrifuge. This was followed by incubation at 37°C for the indicated time, then vortexed to disrupt cell pellets. Cells were fixed with paraformaldehyde immediately after a brief vortexing and analyzed using FACSCanto. The percentage of conjugates was calculated based on the proportion of cells positive for both Cell Tracker Green and Cell Tracker Blue compared to the total number of CTL analyzed.

Target cell-induced MTOC reorientation. EL4 target cells were labeled with Cell Tracker Blue followed by treatment with 10 μM NP (ASNENMETM) and 10 μM OVA (SIINFEKL) peptides in plain RPMI and in pure FCS, respectively.   CTL and EL4 were mixed at the indicated ratio on ice. Conjugates were induced by brief centrifugation (100 RCF for 1 minute in Beckman CS-15R centrifuge) and incubated at 37°C for the indicated time. Induction of conjugation was necessary because Pyk2 is involved in regulating cell adhesion.   All cells were pretreated with the indicated concentration of PF431396 for 1 hour at room temperature and the experiment was performed in the presence of PF431396. After activation at 37°C, samples were subjected to brief vortexing and then transferred to poly-l-lysine coated imaging slides to settle for 10 minutes at room temperature. Cells were fixed with paraformaldehyde, then permeabilized and stained with an anti-tubulin antibody. The corresponding secondary antibodies were

used alone as a control for staining. For CTL that were transfected with GFP-coupled Pyk2 constructs, a similar procedure was used. GFP expressing CTL were analyzed immediately since GFP fluorescent signals gradually fade after paraformaldehyde fixation.

Statistical analysis. All statistical analysis was performed using the analyze function in Prism software.   The statistic analysis used for a specific experiment is indicated in the figure legend.

CHAPTER 3

REGULATION OF THE TYROSINE KINASE PYK2 BY CALCIUM IS THROUGH PRODUCTION OF REACTIVE OXYGEN SPECIES IN CYTOTOXIC T LYMPHOCYTES

A. Introduction

Pyk2 was initially identified as a calcium-dependent tyrosine kinase (CADTK) in neuronal and epithelial cell lines (118, 121). Early studies demonstrated that stimulation with A23187 or thapsigargin, which increase intracellular Ca^{2+} concentration, is sufficient to trigger Pyk2 tyrosine phosphorylation (118, 121). In contrast, treatment of cells with either BAPTA-AM or EGTA (chelator for the ER-stored or extracellular Ca^{2+}, respectively) leads to significant inhibition of receptor-mediated Pyk2 activation (118, 121). Various groups have found similar Ca^{2+}-dependent Pyk2 activation in many cell types including megakaryocytes (182), platelets (183), smooth muscle cells (184), and cardiomyocytes (185). Collectively, these studies suggest that Pyk2 tyrosine phosphorylation depends on intracellular Ca^{2+} concentration.

Although Pyk2 activation is thought to depend on Ca^{2+}, the molecular mechanism of regulation seems to differ depending on the cell type. Two early studies showed that Ca^{2+}-induced Pyk2 activation was mediated by Ca^{2+}/calmodulin-dependent protein kinase II (CaM kinase II) in vascular smooth muscle cells and rat brain cells (186, 187). Although these studies provide evidence that Ca^{2+}-mediated Pyk2 tyrosine phosphorylation is significantly reduced by CaM Kinase II inhibitors, they did not show a direct molecular association between CaM kinase II and Pyk2. Two other recent studies provided different mechanisms for Ca^{2+} regulation of Pyk2. One indicated that non-muscle myosin light-chain kinase (MYLK) is required for Pyk2 activation in neutrophils (188). They found that MYLK, a Ca^{2+}/calmodulin-dependent kinase, co-immunoprecipitates with Pyk2 and directly phosphorylates Pyk2 *in vitro*. Another group also identified a direct molecular association between calmodulin and Pyk2 in human embryonic kidney (HEK-293T) cells (142). It remains unknown whether these mechanisms operate in CTL or if there is a cell-context dependent mechanism.

Currently, there is no consensus on whether Pyk2 phosphorylation in T cells absolutely requires Ca^{2+} mobilization. One group showed that TCR-induced Pyk2 phosphorylation is only partially reduced after treatment with EGTA to chelate extracellular Ca^{2+} (132). Other research has found that TCR-induced Pyk2 phosphorylation is significantly impaired in Ca^{2+} free medium (139). In both cases, soluble crosslinking anti-CD3 antibody was used to

activate TCR on Jurkat T cells, but each study demonstrated differences in the requirement for cytosolic Ca^{2+} in Pyk2 activation. In contrast, a study reported that Pyk2 is not phosphorylated upon stimulation with ionomycin, a cell-permeable ionophore that elevates intracellular Ca^{2+} levels, and that there is no difference in TCR-induced Pyk2 phosphorylation with or without EGTA pre-treatment (133). Similar observations were made in T cells where TCR-induced Pyk2 phosphorylation does not require Ca^{2+} mobilization (189). Interestingly, all of these studies utilized the CD4+ Jurkat T cell line but the experimental outcomes varied from each other. The reason behind the differences is unknown.

Dr. Tara Lysechko used non-transformed CTL clones to study the requirement for Ca^{2+} in Pyk2 activation in T cells and the signaling mechanism involved. It was found that stimulation of CTL with ionomycin or thapsigargin induces Pyk2 phosphorylation (190). However, a similar response was not observed in all cell types tested. This indicates that the requirement for Ca^{2+} in Pyk2 activation depends on cellular context (190). Furthermore, the Ca^{2+} requirement for TCR-stimulated Pyk2 phosphorylation depends on the method of stimulation. CTL can be activated by either plate-bound (PB) anti-CD3 antibody coated on a solid surface, or by crosslinking (XL) of TCR using secondary antibody in suspension. Plate-bound anti-CD3 stimulation activates unidirectional signals that lead to CTL degranulation, whereas crosslinking of soluble anti-CD3 antibody triggers transient and relatively weak signals that do not lead to degranulation (95). Both

stimulation methods cause calcium mobilization and Pyk2 activation. TCR-induced Pyk2 activation does not require Ca^{2+} under plate-bound anti-CD3 stimulation, but Ca^{2+} is essential for activation by soluble crosslinking of TCR (190).

As mentioned in the introduction chapter, TCR engagement leads to SFK-dependent activation of Pyk2. Logically, Ca^{2+} would function downstream of SFK to regulate Pyk2 activation. However, Ca^{2+}-mediated Pyk2 activation requires SFK activity in CTL (190). This points to the existence of a signaling feedback loop driven by Ca^{2+} to mediate SFK-dependent Pyk2 activation. The data generated by Dr. Lysechko set the stage for me to identify the potential mechanism for Ca^{2+}-mediated Pyk2 activation in T cells.

B. Results

Calcium-induced Pyk2 phosphorylation does not involve calmodulin.

Since the requirement for Ca^{2+} in Pyk2 activation in T cells is variable and depends on the method of stimulation (190), I suspected the existence of a different or multiple mechanisms for regulation in T cells. To investigate the potential involvement of calmodulin in Pyk2 activation, I performed an immunoprecipitation experiment to examine the association between Pyk2 and calmodulin, which promotes dimerization and trans-phosphorylation of Pyk2 in the presence of Ca^{2+} in embryonic kidney cells (142). As shown in Figure 3-1A, thapsigargin induces Pyk2 tyrosine phosphorylation, but the Pyk2 immunoprecipitates did not show detectable association with calmodulin with or without stimulation. Notably, there was a small fraction of Pyk2 proteins associated with calmodulin immunoprecipitates, but the quantity did not increase upon thapsigargin stimulation. This suggests that the low level of association is not Ca^{2+}-dependent. Furthermore, treatment of CTL with W7, and a corresponding non-inhibitory analog W5, had no significant inhibition on thapsigargin-induced Pyk2 phosphorylation (Figure 3-1B). W7 is a calmodulin antagonist that interacts with the Ca^{2+} binding sites on calmodulin but does not lead to activation (191). W7 increases intracellular Ca^{2+} concentration in other cells through an unknown mechanism (192, 193). This might explain why W7 treatment leads to Pyk2 phosphorylation, as seen in Figure 3-1B. My data indicate that calmodulin is not required for Ca^{2+}-mediated Pyk2 phosphorylation in CTL.
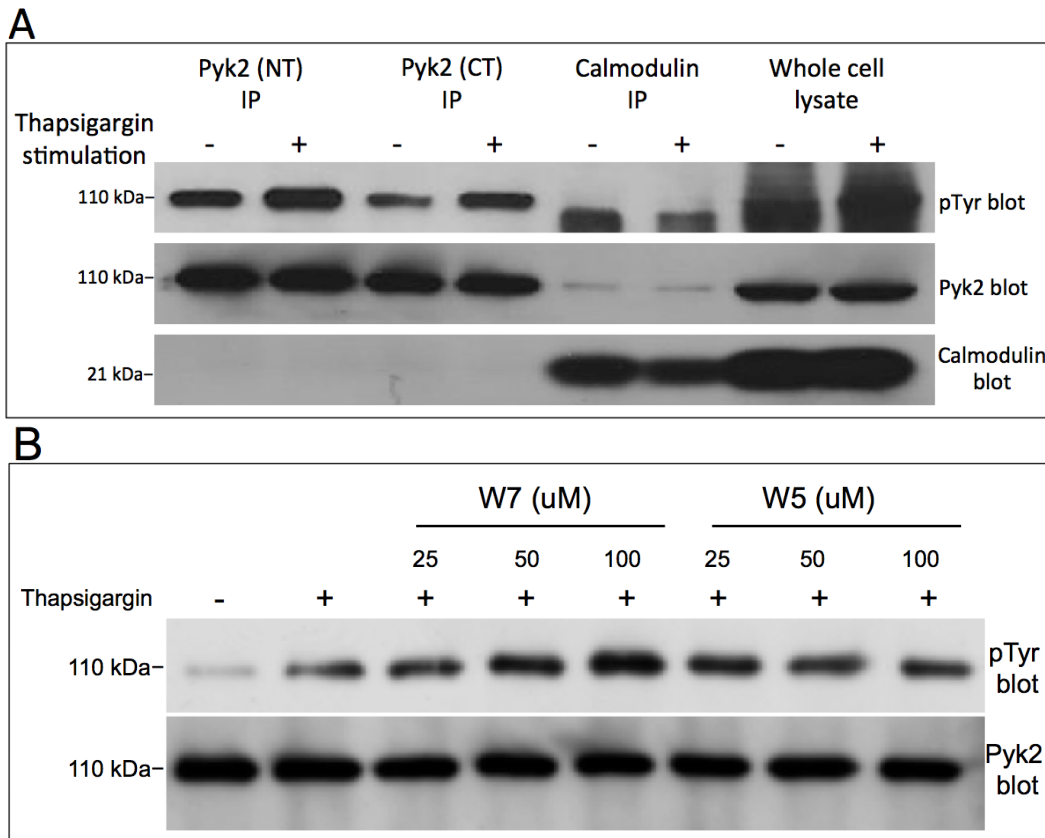
Figure 3-1. Calmodulin is not required for calcium-induced Pyk2 phosphorylation. (A) CTL clone AB.1 were stimulated with 1 µM thapsigargin for 10 min at 37°C followed by cell lysis in 2% NP40 buffer containing calcium without EGTA. Cell lysates were subjected to immunoprecipitation with specific antibody for the N terminus (NT - F298) or C terminus (CT - F245) of Pyk2, as well as anti-calmodulin antibody. The immunoblot was first probed with anti-phosphotyrosine antibody (PY72), then stripped and reprobed simultaneously for total Pyk2 (mAb) and calmodulin. (B) CTL clone AB.1 were pretreated with the indicated concentration of W7 and W5 for 20 minutes at room temperature, followed by stimulation with 0.5 µM thapsigargin for an additional 10 minutes at 37°C. Cell lysates were immunoprecipitated with F245 antibody and subjected to western blot analysis. The immunoblot was first probed with PY72 antibody then stripped and reprobed with F245 antibody for total Pyk2. Each condition used at least 10 million cells and all experiments were independently performed three times with the representative data shown.

Calcium-induced tyrosine phosphorylation in CTL is regulated by NADPH oxidase.

The finding that Ca^{2+}-mediated Pyk2 activation, which bypasses TCR signaling, requires SFK suggests the involvement of a signaling feedback loop (190). How an increase in intracellular Ca^{2+} concentration modulates SFK activity is even more perplexing. In B lymphocytes, B cell antigen-receptor activation induces a positive feedback loop between H_2O_2 production and Ca^{2+} mobilization (194). Although similar pathways have not been described in T cells, TCR activation induces rapid ROS production (57). Since ROS, particularly H_2O_2, can regulate phosphatase activity to affect the phosphorylation balance of the corresponding substrate, I speculated that Ca^{2+}-mobilization initiates ROS generation and in turn modulates Pyk2 activation in CTL.

How Ca^{2+} triggers ROS production remains unknown in the mouse model, but in humans it is through the activation of a Ca^{2+}-dependent NADPH oxidase 5 (Nox5) (195). Although a Nox5 ortholog is absent in rodents, TCR-mediated H_2O_2 production depends on an NADPH oxidase-like enzyme (57). I speculated that ROS plays a role in Ca^{2+}-induced Pyk2 tyrosine phosphorylation. Since TCR-induced ROS production is through NADPH oxidase (57), my first experiment was to test if inhibiting NADPH oxidase affects Ca^{2+}-induced CTL signaling. I treated CTL clone AB.1 with a commonly used NADPH oxidase inhibitor diphenyleneiodonium chloride (DPI) followed by stimulation with either ionomycin or thapsigargin for 10

minutes. As shown in Figure 3-2A, the control experiment without DPI demonstrated that either ionomycin or thapsigargin stimulation induced substantial tyrosine phosphorylation in CTL clone AB.1. Robust tyrosine phosphorylation can be observed in two distinct regions: one at proteins between 84 kDa and 116 kDa plus another protein(s) just below 48.5 kDa. With the same stimulation under DPI treatment, tyrosine phosphorylation of most proteins was significantly reduced except for the protein(s) just below 48.5 kDa. Interestingly, proteins where Pyk2 is expected to migrate near 110 kDa displayed the most significant reduction in tyrosine phosphorylation. The selective effect of NADPH oxidase inhibition on tyrosine phosphorylation of these proteins became more apparent in a thapsigargin and DPI titration experiment (Figure 3-2B). While ionomycin stimulation resulted in peak tyrosine phosphorylation on proteins around 110 kDa at 0.5 μM (Figure 3-2A), thapsigargin stimulated a linear tyrosine phosphorylation pattern (Figure 3-2B). Furthermore, there were no significant changes in tyrosine phosphorylation of the proteins below 48.5 kDa with or without DPI. This suggests that NADPH oxidase contributes to phosphorylation of substrates induced by Ca^{2+} signaling. My results indicate that NADPH oxidase activity plays a role in Ca^{2+}-induced signaling pathways in CTL.
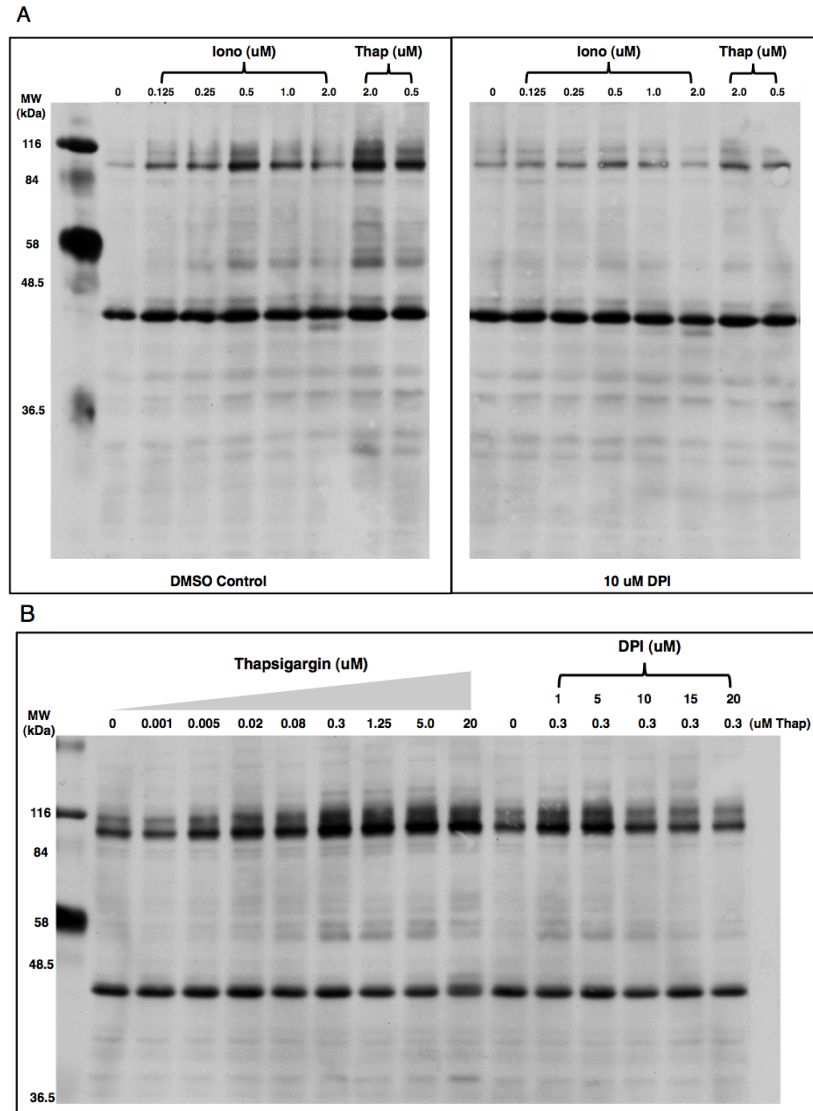
Figure 3-2. Inhibition of NADPH oxidase leads to substantial reduction in ionomycin- and thapsigargin-induced tyrosine phosphorylation in CTL. (A) CTL clone AB.1 were treated with either DMSO control or 10 μM DPI for 25 minutes at room temperature, then stimulated with either ionomycin (Iono) or thapsigargin (Thap) for 10 minutes at 37°C. (B) CTL clone AB.1 were pre-incubated with the indicated concentration of DMSO control or DPI for 20 minutes at room temperature followed by stimulation with thapsigargin for 10 minutes at 37°C. For both experiments, each lane contained 3×10^5 whole cell lysates and DPI was present throughout the experiment. Cells were lysed immediately after stimulation and the whole cell lysates were subjected to SDS-PAGE analysis. The PVDF membrane was probed with anti-phosphotyrosine antibody (PY72). All experiments were performed at least three times and representative data are shown.

Calcium-induced Pyk2 tyrosine phosphorylation is regulated by NADPH oxidase and ROS.

Since NADPH oxidase contributes to Ca^{2+}-induced tyrosine phosphorylation in CTL, I tested specifically whether NADPH oxidase and its ROS products play a role in Ca^{2+}-induced Pyk2 tyrosine phosphorylation. I performed Pyk2 immunoprecipitation after thapsigargin stimulation with and without DPI treatment. As seen in Figure 3-3A, Pyk2 was tyrosine phosphorylated upon thapsigargin stimulation and increased in response to increasing thapsigargin concentration. Thapsigargin-induced Pyk2 tyrosine phosphorylation was significantly inhibited by DPI treatment at a dose as low as 5 μM. At a 20 μM DPI concentration, Pyk2 phosphorylation was reduced to near background level. This result indicates that NADPH oxidase function is required for Ca^{2+}-mediated Pyk2 phosphorylation. To determine whether NADPH oxidase products are also required, I stimulated CTL with ionomycin in the presence of ebselen. Ebselen is an antioxidant that has similar functional characteristics as peroxiredoxin, which effectively enhances the breakdown of H_2O_2 by cellular reductase (196). Therefore, ebselen can be used as an effective H_2O_2 scavenger. As shown in Figure 3-3B, ionomycin induced Pyk2 activation is strongly inhibited by ebselen in a dose dependent manner. An additional observation from Figure 3-3B is that Pyk2 phosphorylation peaks at 0.5 μM ionomycin concentration. The reason for this is not understood. My results indicate that Ca^{2+}-induced Pyk2

phosphorylation requires NADPH oxidase and its ROS products, particularly

H_2O_2.
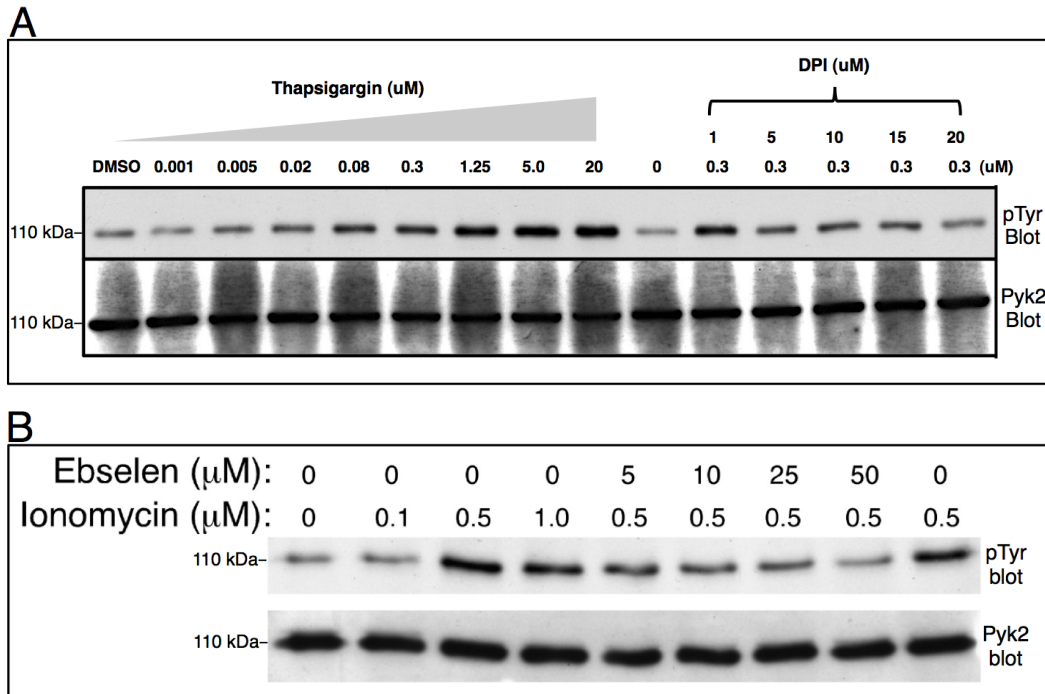
Figure 3-3. Calcium-mediated Pyk2 phosphorylation is regulated by NADPH oxidase and requires ROS. (A) CTL clone AB.1 were pre-treated with either DMSO control or the indicated concentration of DPI for 20 minutes at room temperature, followed by stimulation with the indicated amount of thapsigargin for 10 minutes at 37°C. (B) CTL clone AB.1 were pre-incubated with the indicated concentration of DMSO control or ebselen for 20 minutes at room temperature and then stimulated with ionomycin for 10 minutes at 37°C. In both experiments, at least 10 X 10^6 cells were used for each condition and lysed with 2% NP40 buffer. Either DPI or ebselen was present throughout the experiment. Post-nuclear lysates were immunoprecipitated for Pyk2 using F245 antisera. All immunoprecipitates were subjected to SDS-PAGE analysis. The PVDF membrane was first probed with PY72 anti-phosphotyrosine antibody, then stripped and reprobed with F245 antibody for total Pyk2. All experiments were performed at least three times.

Activation of Ca^{2+} signaling induces ROS production.

To determine if Ca^{2+} induces H$_2$O$_2$ production, I used a ROS-sensitive indicator 5-(and-6)-chloromethyl-2',7'-dichlorodihydrofluorescein diacetate, acetyl ester (CM-H$_2$DCFDA) to detect intracellular H$_2$O$_2$ production induced by ionomycin and thapsigargin stimulation. The cell-permeable indicator CM-H$_2$DCFDA has an additional chloromethyl (CM) group that can covalently bind to intracellular proteins upon catalysis by cellular esterase. Once it is bound intracellularly and oxidized by ROS, it generates fluorescence detectable by a standard fluorometric assay (197). CM-H$_2$DCFDA is derived from an older version of ROS indicator DCFDA. In T cells, DCFDA can be used as an effective and selective H$_2$O$_2$ sensor (198). I first determined the sensitivity of the dye by titrating H$_2$O$_2$ directly onto CTL. As seen in Figure 3-4A, CTL loaded with CM-H$_2$DCFDA produced fluorescent signals corresponding to the amount of H$_2$O$_2$ added. This showed that intracellular CM-H$_2$DCFDA is oxidized by exogenous H$_2$O$_2$ that diffused into the cell. To determine if endogenous H$_2$O$_2$ is produced upon CTL activation, I treated the CTL with anti-CD3 antibody followed by addition of a secondary crosslinking antibody. As shown in figure 3-4B, while anti-CD3 antibody alone did not increase CM-H$_2$DCFDA oxidation, addition of crosslinking antibody induced apparent CM-H$_2$DCFDA oxidation. These data suggest that this assay is useful for the qualitative measurement of endogenous H$_2$O$_2$ generation.

After establishing an assay to measure H$_2$O$_2$ production, I first examined if activation of Ca^{2+} signaling can trigger H$_2$O$_2$ production. I

stimulated CTL with ionomycin or thapsigargin followed by immediate measurement of CM-H_2DCFDA oxidation. As shown in Figure 3-4C and 3-4D, both ionomycin and thapsigargin caused H_2O_2 production in a dose-dependent manner. Ionomycin stimulation triggered maximal H_2O_2 generation between 0.5 and 1.0 µM with 2 µM showing reduced H_2O_2 generation. Interestingly, this peak in H_2O_2 generation corresponds to the peak in Pyk2 tyrosine phosphorylation noted in Figure 3-3B. Thapsigargin stimulation yielded a linear H_2O_2 production pattern. This pattern also matched the extent of Pyk2 tyrosine phosphorylation induced by Thapsigargin (Figure 3-3). Therefore, the quality of H_2O_2 production positively correlates to Pyk2 tyrosine phosphorylation under similar stimulatory conditions. My results here indicate that Ca^{2+}-mobilizing agents are effective inducers of H_2O_2 production in CTL.

I further examined if ionomycin-induced H_2O_2 production can be removed by ebselen. I pretreated CTL with or without ebselen followed by stimulation of CTL with ionomycin. As shown in Figure 3-4E, ebselen significantly decreased CM-H_2DCFDA oxidation induced by ionomycin. This demonstrates that ebselen is an effective antioxidant for scavenging H_2O_2 under our experimental conditions. Furthermore, oxidation of CM-H_2DCFDA induced by 0.5 µM ionomycin was only slightly lower than the oxidation induced by 0.5 mM H_2O_2 (Figure 3-4F). This suggests that 0.5 µM ionomycin induces H_2O_2 production at a quantity comparable to 0.5 mM exogenously

added H_2O_2. My results indicate that CTL generate high, but presumed transient, levels of H_2O_2 upon activation of Ca^{2+} signaling pathways.
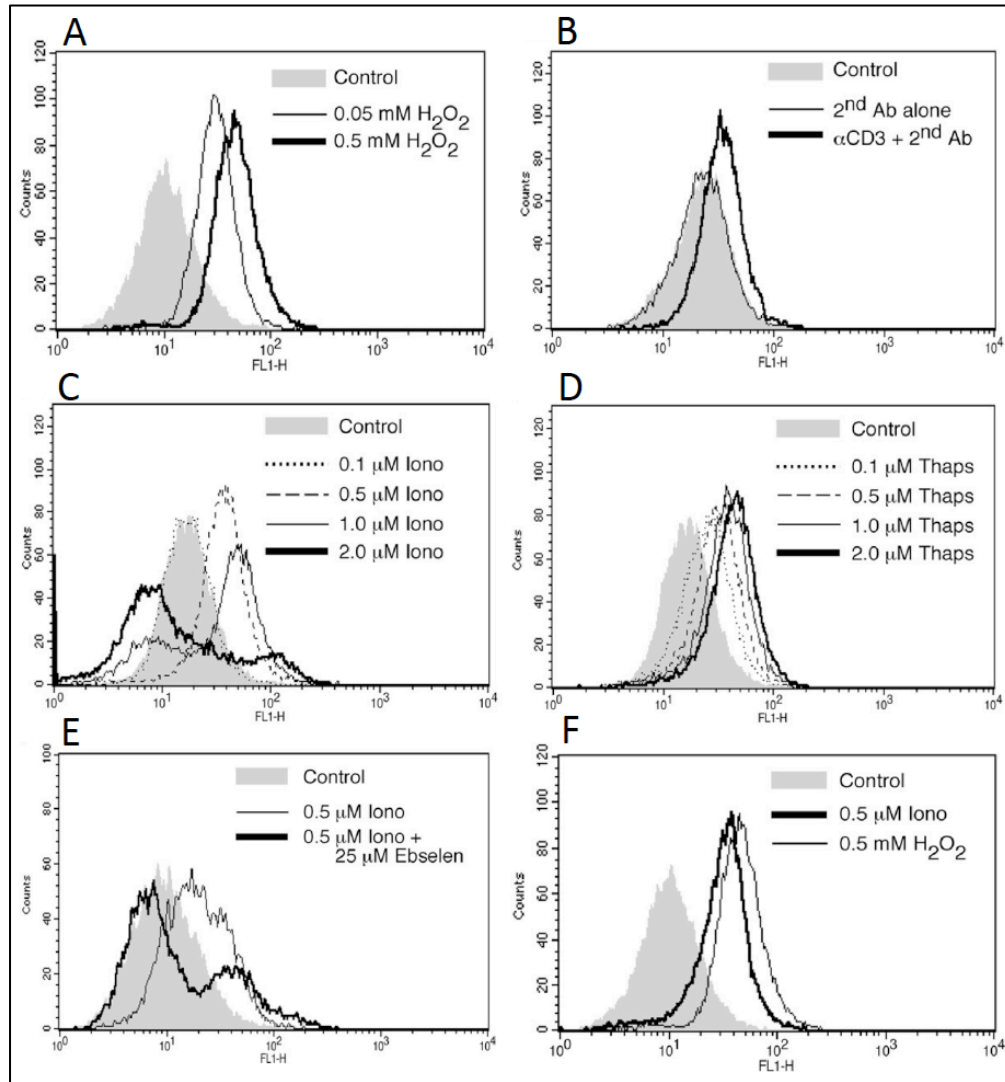
Figure 3-4. Calcium-induced H_2O_2 generation in CTL. (See description on next page)

Figure 3-4. Calcium-induced H_2O_2 generation in CTL. (A) CTL clone AB.1 were stimulated with the indicated concentration of H_2O_2 for 10 minutes at 37°C. (B) CTL clone AB.1 were either untreated, or incubated with 10 μg/ml anti-CD3 antibodies (145-2C11) for 5 minutes on ice. Cells were washed followed by addition of 5 μg/ml cross-linking antibody (rabbit anti-hamster IgG) and incubated for 10 minutes at 37°C. (C and D) CTL clone AB.1 were stimulated with the indicated amount of ionomycin or thapsigargin for 10 minutes at 37°C. (E) CTL clone AB.1 were pretreated with 25 μM ebselen at room temperature for 25 minutes, followed by stimulation with ionomycin for an additional 10 minutes at 37°C. (F) CTL clone AB.1 were stimulated with 0.5 μM ionomycin or 0.5 mM H_2O_2 for 10 minutes at 37°C. For all the experiments described above, stimulated cells were incubated with 0.5 μM of CM-H_2DCFDA for an additional 15 minutes. After CM-H_2DCFDA treatment, cells were resuspended in, and washed twice with PBS containing 1% FBS before using a FACS calibur to assay for CM-H_2DCFDA oxidation. All control conditions were loaded with CM-H_2DCFDA and either mock treated or containing equal volume of maximal DMSO used for the corresponding stimuli. For each experiment, all conditions were performed and acquired under similar durations of time to account for the spontaneous CM-H_2DCFDA oxidation. Approximately 5000 live cells were used for flow cytometry analysis in each condition. All experiments were performed at least three times and representative data are shown.

H_2O_2 induces Pyk2 tyrosine phosphorylation in CTL.

My results indicate that Pyk2 tyrosine phosphorylation requires H_2O_2 production triggered by Ca^{2+} signaling (Figure 3-3B). Although H_2O_2 activates Pyk2 tyrosine phosphorylation in other cell types (199-201), it is unclear whether a similar response can be found in CTL. As shown in Figure 3-5A, increasing amounts of H_2O_2 resulted in increased tyrosine phosphorylation of multiple proteins in a dose-dependent manner. An increase in global tyrosine phosphorylation was apparent at a concentration around 0.08 mM H_2O_2 stimulation. To demonstrate that Pyk2 is activated by H_2O_2, I performed a similar experiment and then used phospho-specific antibody raised against phosphorylated tyrosine 402 of Pyk2. As mentioned in the introduction chapter, tyrosine phosphorylation of Y402 is the first step of Pyk2 activation. Phosphorylation of Y402 results in association with Src family kinases, which is critical for activation of Pyk2. Figure 3-5B showed that Pyk2 Y402 is significantly phosphorylated with increasing H_2O_2 stimulation. My results indicate that H_2O_2, one of the prominent ROS species in cell signaling, elicits Pyk2 activation in CTL.
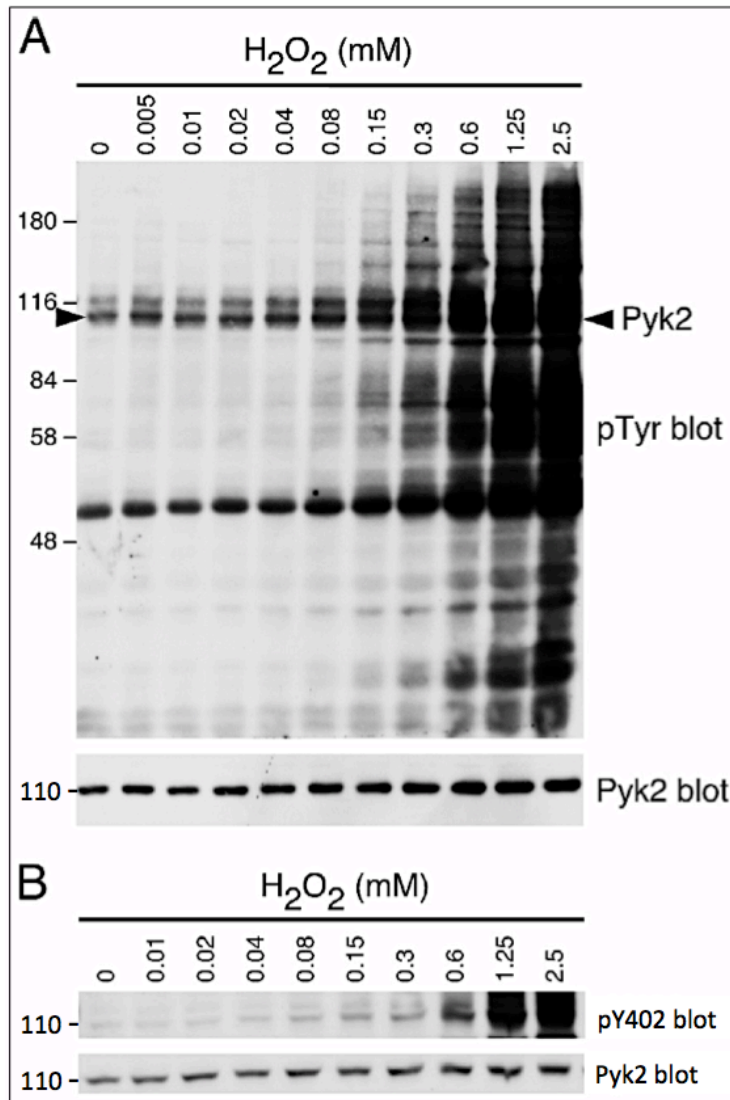
Figure 3-5. H₂O₂-induced tyrosine phosphorylation and Pyk2 activation in CTL. (A) CTL clone AB.1 were stimulated with the indicated amount of H₂O₂ for 10 minutes at 37°C. After stimulation the cells were lysed immediately and the whole cell lysates were probed with anti-phosphotyrosine antibody (PY72). The blot was stripped and reprobed for total Pyk2 as a loading control. (B) CTL clone AB.1 were stimulated as in part A. The whole cell lysates were first probed for phospho-specific antibody against Pyk2 Y402 (P-Tyr402), then stripped and reprobed for total Pyk2. At least 3 X 10⁵ cells were used for each lane. All the experiments were performed three times and representative data are shown.

CD45 phosphatase is not required for Ca^{2+}-mediated Pyk2 phosphorylation.

Data from our initial study showed that Ca^{2+}-induced Pyk2 activation requires SFK activity (190). PP2, a specific Lck and Fyn inhibitor (202), suppresses both ionomycin and thapsigargin induced Pyk2 phosphorylation (190). Lck activity is coordinated by phosphorylation of two key tyrosine residues. It is positively regulated by Y394 phosphorylation, while Y505 phosphorylation is generally inhibitory (203). Since Lck is dephosphorylated by CD45 (37), and CD45 phosphatase activity can be inactivated by H_2O_2 (204), I hypothesized that Ca^{2+}-mediated H_2O_2 production leads to the modulation of CD45 phosphatase activity. The production of H_2O_2 would therefore affect overall SFK activity and change the level of Pyk2 activation in the cell (Figure 3-6A). However, since CD45 is required for T cell development and differentiation, CD45-/- mice do not have CTL available for testing my hypothesis (205, 206). To overcome this obstacle, I obtained an immature T cell population from the CD45-/- mice to examine the involvement of CD45 in this pathway. I stimulated thymocytes harvested from CD45 wild-type and knockout mice with thapsigargin to determine the extent of Pyk2 phosphorylation. As shown in Figure 3-6B, thapsigargin-induced Pyk2 phosphorylation in thymocytes from CD45 wild-type mice was not affected by DPI treatment. This suggests that NADPH oxidase does not play a role in this signaling pathway in these cells. Although stimulation with thapsigargin increases Pyk2 phosphorylation in the absence of CD45, the

basal tyrosine phosphorylation is much lower in these cells. The reduction in Pyk2 tyrosine phosphorylation likely results from an increased level of Lck Y505 phosphorylation in the absence of CD45 (38). My data indicate that CD45 is not essential for signaling that regulates Ca^{2+}-dependent Pyk2 activation, but it is required for the optimal induction of Pyk2 tyrosine phosphorylation.
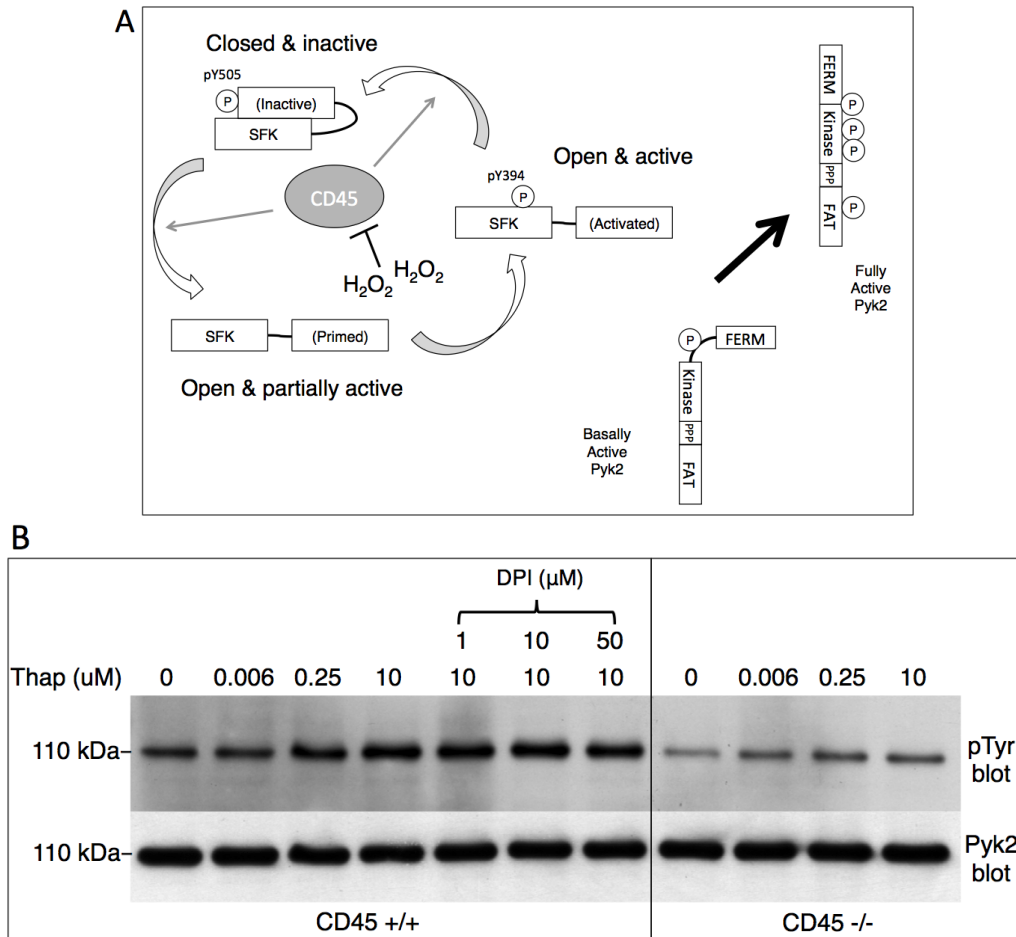
Figure 3-6. Calcium-induced Pyk2 tyrosine phosphorylation does not involve CD45. (A) General model for CD45 regulation of SFK activity. SFK can exist in equilibrium as several forms: closed and not active, open and active, and open but not fully active (34). Inhibition of CD45 phosphatase, which differentially dephosphorylates pY394 and pY505 (38), potentially affects Pyk2 tyrosine phosphorylation by changing overall SFK activity. (B) Thymocytes from CD45 WT mice were treated with the indicated concentration of DPI at room temperature for 20 minutes, followed by stimulation with thapsigargin at 37°C for 10 minutes. Similar thapsigargin stimulation was performed in thymocytes from CD45 knockout mice. At least 1×10^7 cells were used for each condition and Pyk2 was immunoprecipitated with F245 antibody followed by western blot analysis. The immunoblot was first probed with PY72 antibody, then stripped and reprobed with F245 antibody for total Pyk2. Three independent experiments were performed and representative data are shown.

Calcium induces electrophoretic mobility shift of Lck.

Among the known SFK members, T cells predominantly express Lck and Fyn (34). Data from an earlier study revealed that the AB.1 CTL clone expresses very little Fyn (130). This allowed me to focus on examining the phosphorylation status of Lck upon Ca^{2+}-stimulated Pyk2 activation. I stimulated CTL clones with ionomycin and thapsigargin to determine the extent of Lck activation, as evaluated by the degree of tyrosine phosphorylation on the two key residues Y384 and Y505. As shown in Figure 3-7A, there were no apparent differences in tyrosine phosphorylation on either residue upon ionomycin or thapsigargin stimulation. As a positive control, H_2O_2 stimulation triggers strong phosphorylation of both Y394 and Y505 residues, as anticipated (207). However, I did observe a mobility shift of Lck in total Lck immunoblot. The mobility shift has a positive correlation to serine phosphorylation of Lck, which affects overall kinase activity (208, 209). The apparent electrophoretic mobility shift of a small fraction of the total Lck was shown in Figure 3-7B. My data indicate that ionomycin or thapsigargin stimulation does not induce robust activation of Lck through tyrosine phosphorylation, but it may modulate Lck activity through serine phosphorylation.
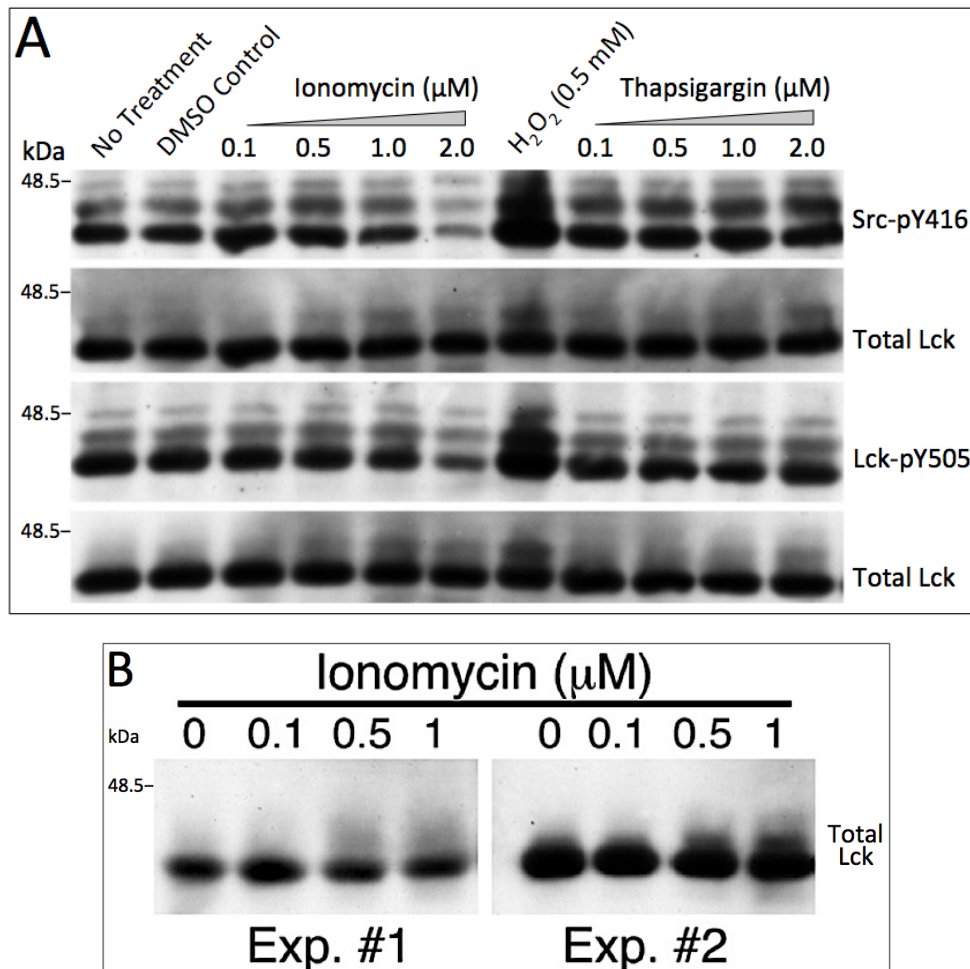
Figure 3-7. **Ionomycin and thapsigargin induce electrophoretic mobility shift of Lck.** (A) CTL clone AB.1 were stimulated with the indicated concentration of ionomycin and thapsigargin for 10 minutes at 37°C. H_2O_2 stimulation was used as a positive control. At least 3 X 10^5 cells were used for each condition and whole cell lysates were subjected to immunoblot analysis. Individual membranes were first probed with the indicated phospho-specific antibody (Src-pY416 or Lck-pY505), then stripped and reprobed with anti-Lck antibody. Anti-Src-pY416 antibody was used for detecting pY394 since the sequence is highly conserved among SFK family members. (B) CTL clone AB.1 were stimulated with ionomycin for 10 minutes at 37°C. Cell lysates were probed with anti-Lck antibody. All experiments were performed at least three times and representative data are shown. Two independent experiments are shown for part (B).

Calcium-induced Pyk2 phosphorylation requires Erk.

The evidence from my previous experiment suggested that activation of Ca^{2+} signaling triggers apparent serine phosphorylation of Lck. My next step was to identify a signaling molecule that is activated by Ca^{2+} signaling and uses Lck as a substrate. One candidate kinase is Erk, which serine phosphorylates Lck (208) and is activated by ionomycin stimulation in T cells (210). I first examined whether Ca^{2+}-induced Pyk2 phosphorylation requires Erk. I used the Map Erk Kinase (MEK) kinase inhibitor U0126 (211), which is upstream of Erk and inhibits it phosphorylation. As shown in Figure 3-8A, ionomycin-induced Pyk2 phosphorylation was significantly impaired in the presence of U0126. This indicates a requirement for Erk in Pyk2 activation downstream of Ca^{2+} signaling. In addition, Erk is phosphorylated upon stimulation with H_2O_2 in CTL (Figure 3-8B). These data suggest that Erk and H_2O_2 operate under the same signaling conditions that mediate Ca^{2+}-induced Pyk2 activation.
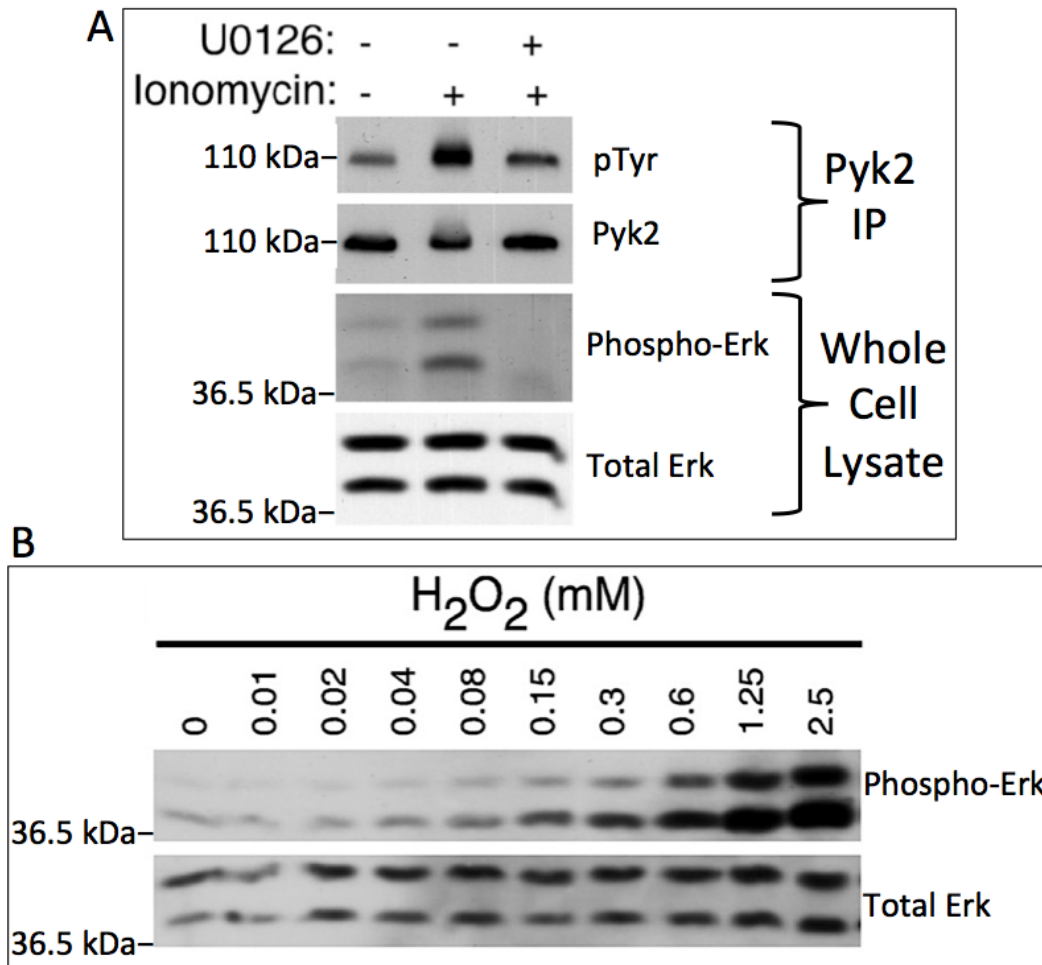
Figure 3-8. Ionomycin-induced Pyk2 phosphorylation requires Erk. (A) CTL clone AB.1 were treated with either DMSO as control or 10 μM U0126 for 30 minutes at room temperature, followed by stimulation with 0.5 μM ionomycin. At least 1×10^7 cells were used in each condition for immunoprecipitation of Pyk2. Pyk2 was immunoprecipitated with F245 antibody and a portion of the post-nuclear whole cell lysates were used for western blot analysis. The Pyk2 immunoprecipitates were first probed with phospho-tyrosine antibody (PY72) then stripped and reprobed with F245 antibody. The corresponding whole cell lysate immunoblots were first probed with phospho-Erk antibody, then stripped and reprobed for total Erk. (B) CTL clone AB.1 were stimulated with the indicated concentration of H_2O_2 for 10 minutes at 37°C. Cells were lysed and immediately subjected to immunoblot analysis. The immunoblot was first probed with phospho-Erk, then stripped and reprobed with Erk 1/2 antibody. All experiments were performed three times and representative data are shown.

H$_2$O$_2$ and Erk are required for Pyk2 phosphorylation induced by cross-linked anti-CD3 but not plate-bound anti-CD3.

Ca^{2+} is not required for TCR-induced Pyk2 activation under plate-bound anti-CD3 stimulation, but is essential for activation induced by soluble crosslinking of TCR (190). I wanted to determine if there is a differential requirement for H$_2$O$_2$ and Erk in Pyk2 phosphorylation using other TCR stimulation methods. To determine if H$_2$O$_2$ is required, I treated CTL with ebselen followed by activation of TCR using either method as described. As shown in Figure 3-9A, the presence of ebselen had no effect on Pyk2 tyrosine phosphorylation induced by plate-bound anti-CD3 stimulation. In contrast, Pyk2 activation appeared to be delayed in the presence of ebselen when CTL were activated by soluble crosslinking of TCR. This indicates a partial requirement for H$_2$O$_2$ in Pyk2 activation. Next, I used the MEK inhibitor U0126 and found that Pyk2 tyrosine phosphorylation was also dependent on Erk activity under soluble crosslinking but not in plate-bound anti-CD3 stimulation (Figure 3-9B). My data strongly suggest that under stimulatory conditions where Ca^{2+} is required for Pyk2 activation, H$_2$O$_2$ and Erk also play important roles in regulation of Pyk2 tyrosine phosphorylation.
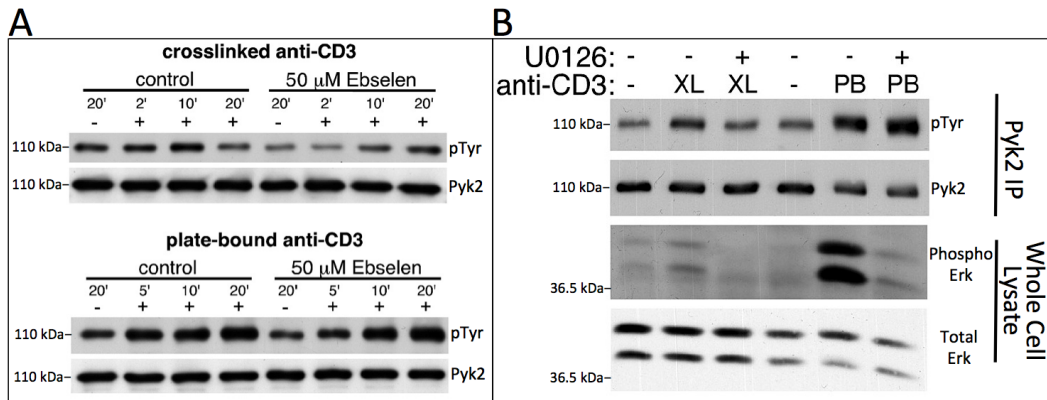
Figure 3-9. **H$_2$O$_2$ and Erk are required for Pyk2 phosphorylation induced by cross-linked anti-CD3 but not plate-bound anti-CD3.** (A) CTL clone AB.1 were treated with 50 μM ebselen at room temperature for 25 minutes, followed by TCR activation for the indicated period at 37°C. Cross-linking (XL) TCR was performed as follows: 10 μg/ml anti-CD3 antibodies were added to CTL on ice for 10 minutes, cells were washed and then resuspend in 5 μg/ml secondary antibody for cross-linking (see materials and methods for details) at 37°C for 10 minutes. Plate-bound (PB) anti-TCR stimulation was performed by incubating CTL for 20 minutes at 37°C on a 60 mm dish coated with 10 μg/ml anti-CD3 antibody. At least 1 X 10^7 cells were used for each condition. Pyk2 was immunoprecipitated with an F245 antibody. The immunoblot was first probed with anti-phosphotyrosine antibody (PY72), then stripped and reprobed with F245 antibody for total Pyk2. (B) CTL clone AB.1 were treated with U0126 for 30 minutes at room temperature, followed by similar TCR activation and immunoprecipitation as described in part (A). Pyk2 immunoprecipitates were subjected to immunoblot analysis. The immunoblots were first probed with phospho-tyrosine (PY72) then stripped and reprobed with F245 antibody. A portion of the cell lysates from Pyk2 immunoprecipitation were subjected to immunoblot analysis. The immunoblot was first probed with phospho-Erk, then stripped and reprobed with Erk 1/2 antibody. All experiments were performed three times and representative data are shown.

C. Discussion

In this chapter I identified a signaling mechanism that modulates Pyk2 tyrosine phosphorylation in response to Ca^{2+} mobilization. My data show that Ca^{2+}-mediated Pyk2 phosphorylation in CTL does not require calmodulin (Figure 3-1), but requires NADPH oxidase activity (Figure 3-3). My results indicate that H_2O_2 is produced upon TCR activation as well as ionomycin or thapsigargin stimulation (Figure 3-4). Furthermore, I have shown that direct H_2O_2 stimulation is sufficient to trigger Pyk2 phosphorylation (Figure 3-5). Since SFK is absolutely required for Pyk2 phosphorylation, I found that stimulation of CTL with ionomycin induces a shift in the electrophoretic mobility of Lck (Figure 3-7). I concluded that Lck activity is likely regulated by Erk, which can be activated by either Ca^{2+} mobilization or H_2O_2 stimulation (Figure 3-8). The proposed mechanism for Pyk2 regulation by Ca^{2+} is depicted in Figure 3-10.
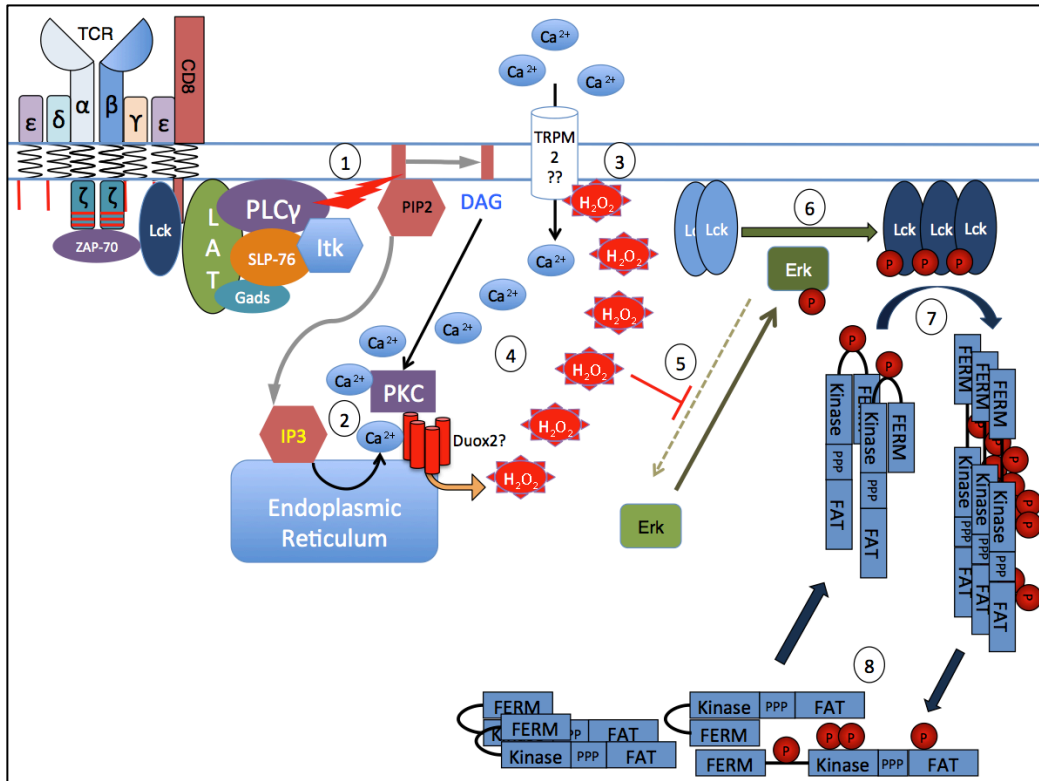
Figure 3-10. Proposed model for Ca²⁺-dependent Pyk2 phosphorylation in CTL. (1) TCR proximal signaling leads to the activation of PLCγ, which catalyzes the breakdown of PIP2 to generate DAG and IP3. (2) Initial IP3-mediated release of Ca^{2+} from the ER, in addition to DAG-mediated PKC activation, leads to theoretical Duox2-dependent H_2O_2 production. (3) H_2O_2 activates Ca^{2+}-influx through the speculated involvement of TRPM2, along with CRAC channel activation by STIM1 (not depicted), resulting in elevation of intracellular Ca^{2+} levels. (4) This triggers a positive feedback loop between TRPM2 and Duox2, which regulates Ca^{2+}-influx and H_2O_2 production, respectively. (5) The presence of H_2O_2 increases Erk phosphorylation through inactivation of effectors that de-phosphorylate Erk. (6) Activated Erk Ser/Thr phosphorylates Lck and stabilizes Lck activity. (7) The increased quantity of active Lck associates with active Pyk2, which is present initially at low levels in CTL, to amplify Pyk2 phosphorylation. (8) Additional Pyk2 phosphorylation enables self-oligomerization with inactive Pyk2 to further enhance overall Pyk2 levels.

We observed that the requirement for Ca^{2+} in Pyk2 activation depends on TCR signal strength (190). Strong, unidirectional TCR stimulation induced by immobilized anti-CD3 antibodies triggers Ca^{2+}-independent Pyk2 activation while transient, non-directional TCR stimulation induced by soluble anti-CD3 antibodies requires Ca^{2+} for Pyk2 tyrosine phosphorylation (190). Under our experimental conditions, 4 mM EGTA significantly inhibited soluble anti-CD3 antibody stimulated Pyk2 phosphorylation in CTL (190). This could explain why one study showed that anti-CD3-induced Pyk2 phosphorylation was inhibited by 4 mM EGTA treatment whereas another study showed no inhibition when 1 μM EGTA was used (132, 189). I found that 0.5 μM ionomycin stimulation resulted in peak Pyk2 phosphorylation (Figure 3-3B) while increasing ionomycin concentrations led to a decrease in Pyk2 phosphorylation. The reason for this is not understood, but this would explain why 1 μM ionomycin stimulation used in another study is not optimal for induction of Pyk2 phosphorylation (133). We are the first group to demonstrate that the requirement for Ca^{2+} in Pyk2 activation depends on the method of TCR stimulation. My results show that the requirement for Ca^{2+} in Pyk2 phosphorylation correlates with the requirement for H_2O_2 and Erk under soluble anti-CD3 stimulation (Figure 3-9). This indicates that Ca^{2+}, H_2O_2, and Erk are regulated through a common pathway to control Pyk2 phosphorylation triggered by soluble crosslinking of TCR.

I have identified a signaling mechanism for Ca^{2+}-mediated Pyk2 activation in CTL that has not been previously described in any cell type. The

mechanism does not involve calmodulin, since I found no significant association between Pyk2 and calmodulin upon thapsigargin stimulation (Figure 3-1A). However, I could not exclude the potential involvement of calmodulin in regulating some aspects of Pyk2 activation in other T cell subsets. It is not uncommon for T cells to utilize different signaling molecules throughout their developmental stages. For example, NADPH oxidase is not involved in Ca^{2+}-mediated Pyk2 activation in thymocytes (Figure 3-6B) but it is required for CTL (Figure 3-3A). Hence, it is possible that calmodulin plays a role in Pyk2 activation in thymocytes. Perhaps the difference in molecular requirements is also related to the signaling threshold in different cell types. This is supported by the observation that different methods of TCR stimulation have differential requirements for Ca^{2+} in mediating Pyk2 activation (190). Since the expression of NADPH oxidase is differentially regulated during T cell development (212), the signaling pathway that regulates Pyk2 activation differs among T cell subsets.

A mechanism for Ca^{2+}-mediated, NADPH oxidase-dependent H_2O_2 production in T cells has not been described in the literature. Among the seven known NADPH oxidase family members, only NADPH oxidase 5 (NOX5), Duox1 and Duox2 (Dual oxidases) contain the Ca^{2+}-binding EF-hand motifs (56). Kwon et. al. recently implicated Duox1 in TCR-induced Ca^{2+}-dependent ROS generation in CD4+ Jurkat T cells (213). However, in contrast to my results in Figure 3-4, Kwon et. al. did not observe ROS production upon stimulation with either thapsigargin or ionomycin (213). Based on this, I

hypothesize that CTL employ a different type of NADPH oxidase, possibly Duox2, distinct from the one used by CD4^{+} Jurkat T cells. Duox1 and Duox2 are differentially regulated by distinct protein kinases (PKA and PKC, respectively) in a reconstituted system (214). An early study indicated that expression of Duox1 and Duox2 is specifically induced by T_H2 and T_H1 cytokines, respectively, in human epithelial cells (215). Therefore, Duox2 is more relevant for the function of Th1-dependent cellular response that is mediated by CTL. I speculate that upon TCR ligation, activation of PKC leads to the phosphorylation of Duox2 (214), which is regulated by Ca^{2+} resulting in Ca^{2+}-dependent H_2O_2 production (Figure 3-10).

The identity of the NADPH oxidase responsible for TCR-mediated ROS generation is unknown. Although NOX5 was not found in rodents, other NOX family members (NOX1, 2 3 and 4) could be involved in Ca^{2+}-dependent ROS generation in T cells. Unlike Duox1 and Duox2, the NOX complexes require the assembly of multiple components (216). The existence of multi-subunit NADPH oxidase in T cells is supported by the evidence that gp91[phox]- or p47[phox]-deficient mice are defective in TCR-induced H_2O_2 generation in CD4^{+} T cells (57). The functional significance of NADPH oxidase, particularly NOX2, has only been recently described for CD4^{+} T cells (212). It is possible that Ca^{2+}-dependent phosphorylation of the p47[phox] subunit regulates the assembly of NOX2 complex to elicit ROS production in CTL (55). The mechanisms that ionomycin and thapsigargin initiate for direct induction of H_2O_2 generation in CTL remains to be established. Nonetheless, my data

show that DPI treatment inhibited Ca^{2+}-induced tyrosine phosphorylation (Figure 3-2). This indicates that NADPH oxidase is involved in Ca^{2+}-mediated signaling pathways in CTL.

The mechanism for H_2O_2-induced Pyk2 phosphorylation is currently unknown. In line with my speculation that Duox2 is involved, one group showed that PKC is required for H_2O_2-induced Pyk2 phosphorylation in epithelial cells (217). This suggests that H_2O_2 positively regulates signaling components that are upstream of PKC. Another group has recently shown in a monocyte cell line that H_2O_2 stimulation activates Ca^{2+} influx through transient receptor potential cation channel subfamily M member 2 (TRPM2), which is required for Pyk2 phosphorylation (218). These studies support a positive feedback relationship between ROS and Ca^{2+} in many cell types, which has already been observed in a B cell study (194). Perhaps the initial TCR-mediated Ca^{2+} release from the ER is sufficient to activate the oxidase, which initiates H_2O_2 production to subsequently amplify the Ca^{2+} and ROS response, and potentiate TCR signaling. The importance of ROS as a signal amplifier is affirmed by recent research on $CD4^+$ T cells that showed that Duox1 is essential for optimal TCR activation (213). Emerging evidence suggests that Ca^{2+} and ROS signaling crosstalk regulates T cell activation. According to my data, activation of Pyk2 in CTL requires both Ca^{2+} and H_2O_2 upon soluble TCR crosslinking. This supports a role for Pyk2 as a signal sensor downstream of TCR.

Regardless of the TCR stimulation methods, SFK is critical for mediating Pyk2 activation. I speculate that SFK, specifically Lck in CTL, is regulated by Erk to mediate Ca^{2+}-dependent activation of Pyk2. I showed that Ca^{2+}-mediated Pyk2 phosphorylation is dependent on Erk (Figure 3-8A) and H_2O_2 stimulation induces Erk phosphorylation (Figure 3-8B). Although it is well established that ROS induces Erk phosphorylation (219), the molecular mechanism behind this is still unknown. Nonetheless, ROS-induced Erk phosphorylation presumably occurs through H_2O_2 inactivation of tyrosine phosphatases, which normally keep the specific kinases under negative control, consequently allowing Erk phosphorylation to proceed (220). Once Erk is activated, it is able to phosphorylate and stabilize the activity of SFK (208), which directly associates with and phosphorylates Pyk2.

How Pyk2 can be activated independent of Ca^{2+} under immobilized anti-CD3 antibody stimulation is currently unknown. One major difference between immobilized and soluble anti-CD3 antibody mediated T cell activation is the involvement of the cytoskeleton (95). While immobilized anti-CD3 antibody stimulation requires intact cytoskeleton for TCR signaling activation, disruption of cytoskeleton assembly with cytochalasin D has no effect on soluble anti-CD3-mediated TCR activation (95). Perhaps cytoskeletal proteins promote association of Pyk2 with the constitutively active fraction of Lck at the membrane under immobilized anti-CD3 stimulation, thereby effectively by-passing the requirement for Ca^{2+} (39).

Many questions remain unanswered and require further research. For example, as a non-receptor tyrosine kinase, how is Pyk2 recruited to the plasma membrane to associate with Lck in CTL? Are there other molecules, such as paxillin, involved in sequestering inactive Pyk2 from the constitutively active pool of Lck? What is the mechanism for Ca^{2+}-mediated ROS generation in T cells? More insights should become available to address these questions as research continues.

CHAPTER 4

PROTEIN TYROSINE KINASE PYK2 REGULATES ICAM-1 DEPENDENT ADHESION AND MIGRATION IN CTL

A. Introduction

Pyk2 is structurally similar to the focal adhesion kinase (FAK) hence many studies have focused on the potential role of Pyk2 in regulating adhesion and migration (221). The importance of Pyk2 in cell adhesion and migration was characterized in Pyk2-deficient (Pyk2-/-) mouse studies. The first study showed that splenic marginal zone B cells are specifically absent in Pyk2-/- mice while other B cell subsets appeared normal (163). The absence of marginal zone B cells was attributed to the defective chemotactic response associated with Pyk2-/- B cells (163). A second study found a similar migratory defect in macrophages in the absence of Pyk2 (164). In addition, morphological analysis revealed that the polarization of Pyk2-/- macrophages was severely impaired and that the cells had reduced motility (164). Further study of Pyk2-/- mice showed that Pyk2 is required for normal polarization of osteoclasts as well as formation of an adhesion complex (165). A study using neutrophils further supports a critical role of Pyk2 in mediating cell adhesion and migration on a fibrinogen-coated surface (170). These studies give evidence that Pyk2 is an important regulator for aspects of cell polarization, adhesion, and migration in cells of hematopoietic lineage.

T cell adhesion is predominantly mediated by the integrin LFA-1, a transmembrane heterodimer consisting of an α_L and a β_2 subunit (66).

Genetic mutation or functional knockout of either subunit will cause severe defects in T cell activation, migration, and adhesion (63, 64). The integrin heterodimer is held together by ionic interactions through conserved residues at the cytoplasmic tails (74). The cytoplasmic tails of each subunit associate with a unique set of proteins for transmission of integrin signaling (222). Experimentally, LFA-1 is activated by crosslinking-antibodies, magnesium (Mg^{2+}) or manganese (Mn^{2+}) ions, and purified integrin ligands such as ICAM-1 (62). Crosslinking of the integrin $\alpha_L\beta_2$ with antibodies elicits Pyk2 tyrosine phosphorylation (223). Tyrosine phosphorylation of Pyk2 can be activated through ligation of $\alpha_v\beta_3$ with fibronectin or vitronectin (224). The molecular mechanism of integrin-induced Pyk2 activation is currently unknown, but an intact cytoskeleton and Ca^{2+} are required (223, 225). Both α_L-deficient and Pyk2-/- mice have similar defects in the CD8 T cell response during lymphocytic choriomeningitis virus (LCMV) challenge (166). This suggests that Pyk2 is one of the main functional effectors downstream of the LFA-1 signaling pathway. How Pyk2 modulates LFA-1 function is unknown.

In resting T cells, Pyk2 is expressed throughout the cytoplasm with apparent localization to the MTOC (223). Past studies suggested that Pyk2 is redistributed to a different cellular location upon integrin activation. One group showed that stimulation of T lymphoblasts with LFA-1 ligand ICAM-1 resulted in more restricted Pyk2 localization at the cell periphery and at the MTOC (225). Another study found that stimulation of NK cells with ICAM-1 coated beads causes an accumulation of tyrosine-phosphorylated Pyk2

(pY402) at the contact site (226). In CTL, tyrosine phosphorylated Pyk2 is also found at the cell contact region, but is undetectable at the MTOC after target cell stimulation (161). It is not known if Pyk2 is recruited to the plasma membrane or specifically targeted to the integrin cytoplasmic domain upon activation. In addition, it is unclear if there are differences in Pyk2 localization in response to integrin and TCR signaling. Nonetheless, the specific cellular localization of Pyk2 upon signaling activation is presumably important for Pyk2 to exert its particular function at the site.

Consistent with the Pyk2-/- studies in B cells and macrophages, naïve CD8 T cells also require Pyk2 for cell adhesion and polarization on an immobilized ICAM-1 surface (166). An *in vitro* transwell migration assay revealed that Pyk2 is critical for optimal ICAM-1 dependent chemotactic response in naïve CD8 T cell (166). The lack of normal cell adhesion and polarization explains why naïve CD8 T cells did not migrate efficiently toward the chemokine gradient. The defective adhesion phenotype in Pyk2-/- CD8 T cells is in contrast with the phenotype of macrophages and osteoclasts, which exhibit cell adhesion even with impaired polarization (166). Whether Pyk2 selectively regulates cell adhesion, polarization, and migration in different cellular contexts is undetermined. To investigate a role of Pyk2 in CTL adhesion and migration, I manipulated Pyk2 function through the use of a PF431396, knockdown of Pyk2 expression with siRNA, and expression of a dominant negative form of Pyk2.

B. Results

PF431396 inhibits Pyk2 and paxillin tyrosine phosphorylation but not ZAP-70.

The drug PF431396 is an ATP mimetic and a potent pyrimidine-based inhibitor against the recombinant Pyk2 enzyme (227, 228). *In vivo* studies demonstrated that daily treatment of PF431396 in rats causes a significant increase in bone density (227), which was phenotypically similar to Pyk2-/- mice (165). Analysis of crystal structure revealed that PF431396 binds to the catalytic pocket of Pyk2 once the kinase domain is conformationally active (229). This suggests that PF431396 suppresses Pyk2 trans-phosphorylation at tyrosine 402 as well as tyrosine phosphorylation of Pyk2 substrates. Although *in vitro* kinase assays indicate that PF431396 non-specifically inhibits a panel of purified kinases (229), potential off-target effects have not been directly demonstrated in a cell-based assay.

I first tested the ability of PF431396 to inhibit Pyk2 tyrosine phosphorylation in CTL initiated by both integrin- and TCR-mediated signaling activation. Although antibody-mediated crosslinking of LFA-1 induces Pyk2 phosphorylation in T lymphoblasts (223), the use of a natural ligand (ICAM-1) to elicit Pyk2 activation has not been reported in CTL. I examined the extent of Pyk2 tyrosine phosphorylation and inhibition by PF431396 upon stimulation with integrin ligand ICAM-1 as well as fibronectin, a known ligand that activates Pyk2 in CTL through β_3 integrin (230). As shown in Figure 4-1A, fibronectin stimulation resulted in weak

tyrosine phosphorylation of proteins where Pyk2 was predicted to migrate. In contrast, ICAM-1 stimulation in CTL generated more robust tyrosine phosphorylation. CTL treated with PF431396 showed significant inhibition in both fibronectin and ICAM-1 stimulated tyrosine phosphorylation of a protein migrating with Pyk2. Notably, the presence of PF431396 inhibited rather than delayed the tyrosine phosphorylation of proteins at 116 kDa throughout the length of the experiment. In contrast, TCR stimulation caused more robust Pyk2 tyrosine phosphorylation (Figure 4-1B). Significant Pyk2 inhibition by PF431396 can be seen at both 10 and 30 minute stimulation time points in a dose-dependent manner. However, the presence of PF431396 did not completely inhibit TCR-induced Pyk2 tyrosine phosphorylation even at a dose up to 10 μM. From these results I conclude that PF431396 inhibits Pyk2 tyrosine phosphorylation triggered by either integrin or TCR signaling activation.

My next step was to determine whether PF431396 treatment would affect the upstream signaling regulators as well as downstream substrates of Pyk2. I have shown in a previous chapter that ionomycin stimulation results in Pyk2 activation (Figure 3-3B). Since paxillin is a substrate for Pyk2 tyrosine phosphorylation (170) and it is regulated by serine/threonine (Ser/Thr) phosphorylation by MAP kinases (231), I stimulated CTL with reagents that prompt tyrosine and Ser/Thr phosphorylation of paxillin in the presence of PF431396. As shown in Figure 4-1C, ionomycin induced paxillin tyrosine phosphorylation was strongly inhibited in the presence of

PF431396 (lanes 1, 3 and 4). In contrast, PMA-induced Ser/Thr phosphorylation of paxillin, as indicated by the mobility shift in the total paxillin immunoblot, was unchanged in the presence of PF431396 (lanes 1, 5 and 6). Furthermore, PF431396 has no apparent effect on the upstream ZAP-70 tyrosine phosphorylation generated by immobilized anti-CD3 stimulation (Figure 4-1D). My results indicate that PF431396 treatment inhibits Pyk2-dependent paxillin tyrosine phosphorylation, but does not affect Ser/Thr phosphorylation of paxillin induced by PMA stimulation or TCR-mediated ZAP-70 phosphorylation.
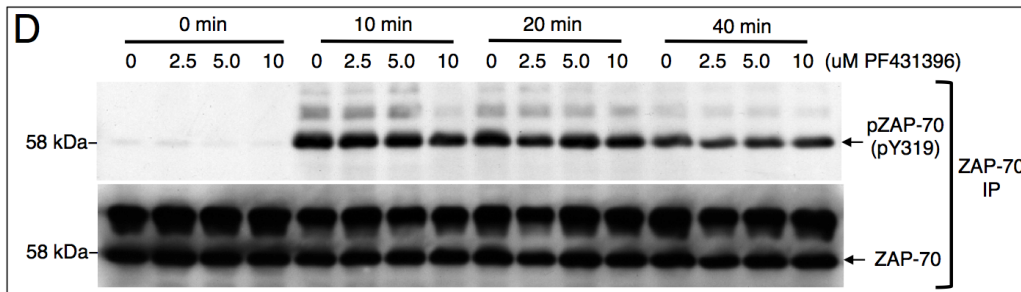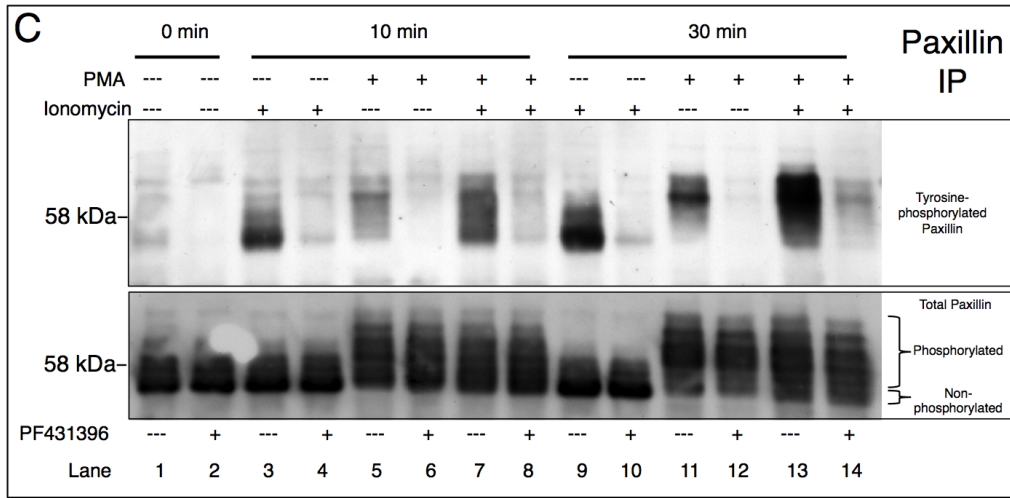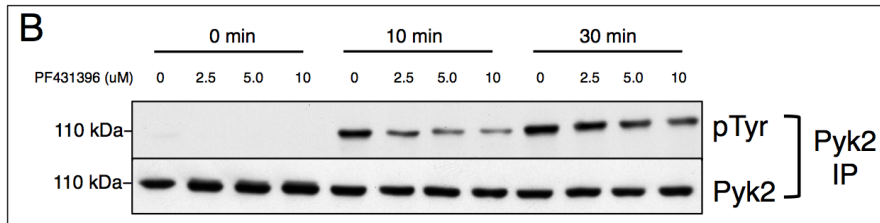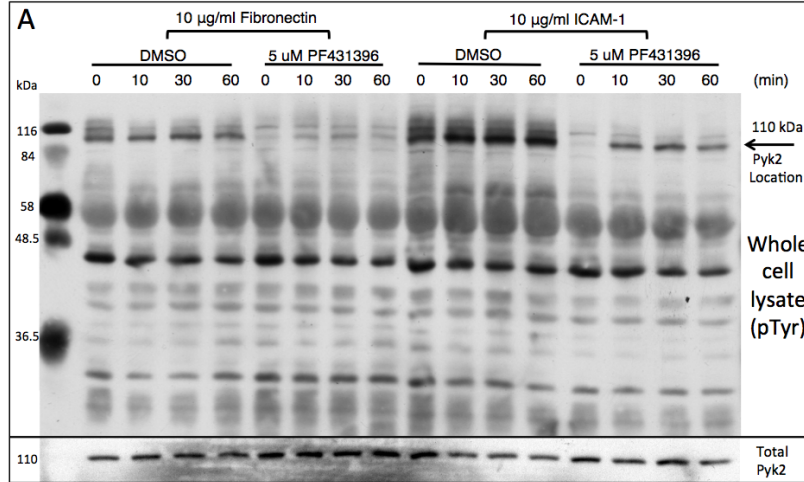
Figure 4-1. PF431396 inhibits Pyk2 and paxillin tyrosine phosphorylation but not ZAP-70. (A) CTL clone AB.1 were pre-treated with either DMSO as a control or 5 μM PF431396 for 1 hour followed by transferring 2.5 X 10^5 cells onto fibronectin or ICAM-1 coated plates for stimulation. Cells were lysed immediately after incubation at 37°C with 2 X reducing sample buffer at the indicated time followed by western blot analysis. The membrane was probed with anti-phospho-tyrosine antibody PY72 (top), then stripped and reprobed with anti-Pyk2 monoclonal antibody (bottom). The open arrow indicates the approximate location of Pyk2 protein. (B) CTL clone AB.1 were treated with the indicated concentration of inhibitor in suspension for 1 hour at room temperature. At least 1 X 10^7 cells were transferred to a culture dish coated with 10 μg/ml of anti-CD3 (145-2C11) antibody and incubated for the indicated period at 37°C. Cells were lysed with 2% NP40 buffer followed by immunoprecipitation for Pyk2 using F245 antibody. Immunoprecipitates were subjected to immunoblot analysis. The membrane was first blotted with anti-phospho-tyrosine antibody (PY72), then stripped and reprobed with F245 antibody. (C) CTL were stimulated with 2 μM ionomycin and/or 100 ng/ml PMA at 37°C for the indicated time, then lysed and immunoprecipitated with 1 μg of anti-paxillin antibody. Immunoblot was first probed with PY72 antibody, then stripped and reprobed with anti-paxillin antibody. (D) CTL were immunoprecipitated using 1 μg anti-ZAP-70 antibody. The membrane was first blotted with phospho-ZAP-70 (pY319) antibody, then stripped and reprobed with anti-ZAP-70 antibody. All experiments were performed three times and the representative data are shown. Experiment B was performed as a single trial.

Pyk2 is required for optimal CTL adhesion to ICAM-1 coated beads.

Naïve CD8$^+$ T cells from Pyk2-deficient mice are defective in adhesion and polarization on an ICAM-1 coated surface (166). This suggests that either the scaffolding or kinase activity of Pyk2 is required for T cell adhesion. To determine whether inhibition of Pyk2 kinase activity is sufficient to de-regulate CTL adhesion to an ICAM-1 coated surface, I pre-treated CTL with PF431396 followed by incubation with ICAM-1 coated beads to allow cell adhesion to occur. As shown in Figure 4-2A, there was a dose-dependent reduction in overall CTL adhesion to ICAM-1 coated beads when treated with increasing PF431396 concentrations. Although there were variations in the extent of adhesion from one experiment to another, a similar trend can still be observed (Figure 4-2B). My results indicate that inhibition of Pyk2 enzymatic activity using PF431396 is sufficient to de-regulate CTL adhesion to ICAM-1.

To determine if CTL absolutely require normal Pyk2 protein expression for ICAM-1 adhesion, I transfected various CTL clones with a combined pool of Pyk2 siRNA to achieve maximal knockdown in Pyk2 expression for an adhesion assay. As shown in figure 4-2C, transfection using Pyk2 siRNA substantially reduced the levels of Pyk2 proteins in two different CTL clones. After performing a similar ICAM-1 adhesion assay as described previously (Figure 4-2A & B), I found that CTL clone AB.1 exhibited a greater difference in ICAM-1 adhesion between the control siRNA and Pyk2 siRNA transfected samples in comparison to CTL clone 3/4 (Figure 4-2D). This

suggests that there are clonal differences in the level of adhesion to ICAM-1. However, the observed differences may be simply due to the extent of Pyk2 knockdown in each clone. I also observed a defect in background adhesion among the control samples with no ICAM-1. This phenotype was also observed in Pyk2-deficient naïve CD8 T cells (166). My results indicate that Pyk2 contributes to optimal CTL adhesion to ICAM-1.
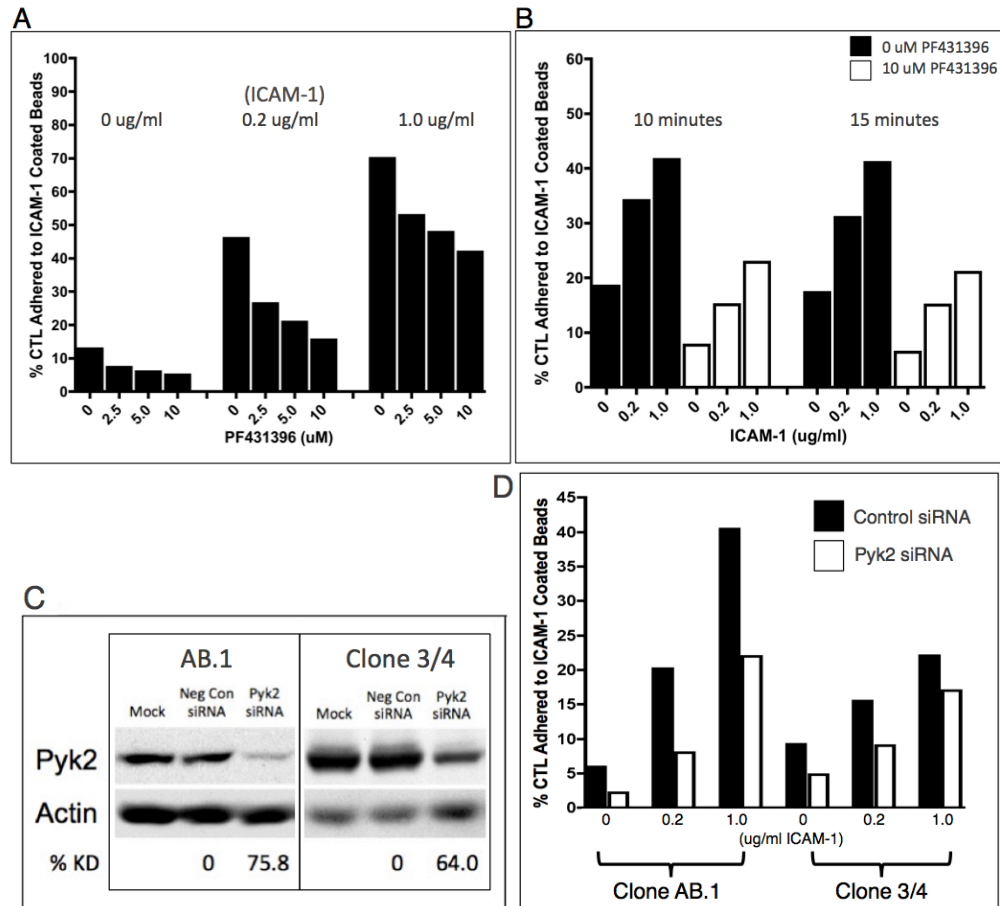
Figure 4-2. Pyk2 is required for optimal CTL binding to an ICAM-1 coated surface. (A) CTL clone AB.1 were pre-treated with the indicated concentration of PF431396 for 45 minutes followed by induced conjugation with ICAM-1 coated beads. CTL and bead conjugates were induced by brief centrifugation then incubated at 37°C for 15 minutes. Weakly bound conjugates were disrupted by vortexing briefly. The percentage of conjugates was determined on the basis of differences in distinctive forward and side scatter patterns using flow cytometer analysis. (B) A similar experiment was performed as in part A but using different time points and PF431396 concentration. (C) The extent of Pyk2 knockdown in various CTL after 48 hours of nucleofection with either negative control siRNA or Pyk2 siRNA. 3 X 10^5 cells were used per lane in the western blot to probe for total Pyk2, then stripped and re-blotted with anti-actin antibody as the loading control. The percentage of Pyk2 knockdown was calculated based on Pyk2 to actin ratio using negative control siRNA as the normalization standard. Relative intensity for each protein was quantified using ImageJ software. (D) Control or siRNA nucleofected CTL clone AB.1 and clone ¾ were incubated with ICAM-1 beads for 10 minutes followed by similar protocol as described in part A. The experiments involved PF431396 was performed three times and two representative results are shown. The experiments in (C) and (D) were performed three times and the representative data are shown.

Inhibition or knockdown of Pyk2 results in aberrant CTL spreading on ICAM-1.

Since inhibition or knockdown of Pyk2 did not completely block CTL adhesion to ICAM-1 after 15 minutes (Figure 4-2B), I tested whether CTL are able to restore adhesion on an ICAM-1 coated surface after one hour. I placed CTL on ICAM-1 coated coverslips in the absence or presence of PF431396 at 37°C for 1 hour followed by cell morphology analysis. Surprisingly, despite the reduced adhesion phenotype I had observed in the short-term assay (Figure 4-2A), CTL were able to spread and polarize on ICAM-1 in the presence of PF431396. I found that more CTL exhibited an elongated phenotype in the presence of PF431396 compared to the control (Figure 4-3A). Interestingly, a small fraction of cells even showed multiple membrane extensions (as indicated by the red arrow) in PF431396 treated conditions. Morphological analysis over a panel of images revealed that the percentage of aberrant cells significantly increased in the presence of PF431396 compared to the control group (Figure 4-3B). These images indicate that inhibition of Pyk2 kinase activity leads to an enhanced cell spreading, and presumably able to adhere, in spite of initial defects (Figure 4-2A&B).

To determine if Pyk2 protein expression is also crucial for normal CTL spreading and polarization on ICAM-1, I transfected CTL with Pyk2 siRNA to perform a similar morphological study. In order to visualize cells that were transfected with the siRNA, I performed co-transfection using a GFP expressing plasmid in this experiment. As shown in Figure 4-3C, CTL

transfected with Pyk2 siRNA, as visualized by expression of GFP, exhibited similar aberrant phenotypes as in CTL treated with PF431396. Morphological analysis of Pyk2 siRNA transfected CTL also revealed nearly identical results as in CTL treated with PF431396 (Figure 4-3B and 4-3D). My data suggest that either Pyk2 knockdown or kinase inhibition have no significant effect on the ability of CTL to bind ICAM-1 after an adhesion has been established. However, Pyk2 appears to be involved in some aspects of CTL interaction with ICAM-1 as indicated by the stretched phenotype.
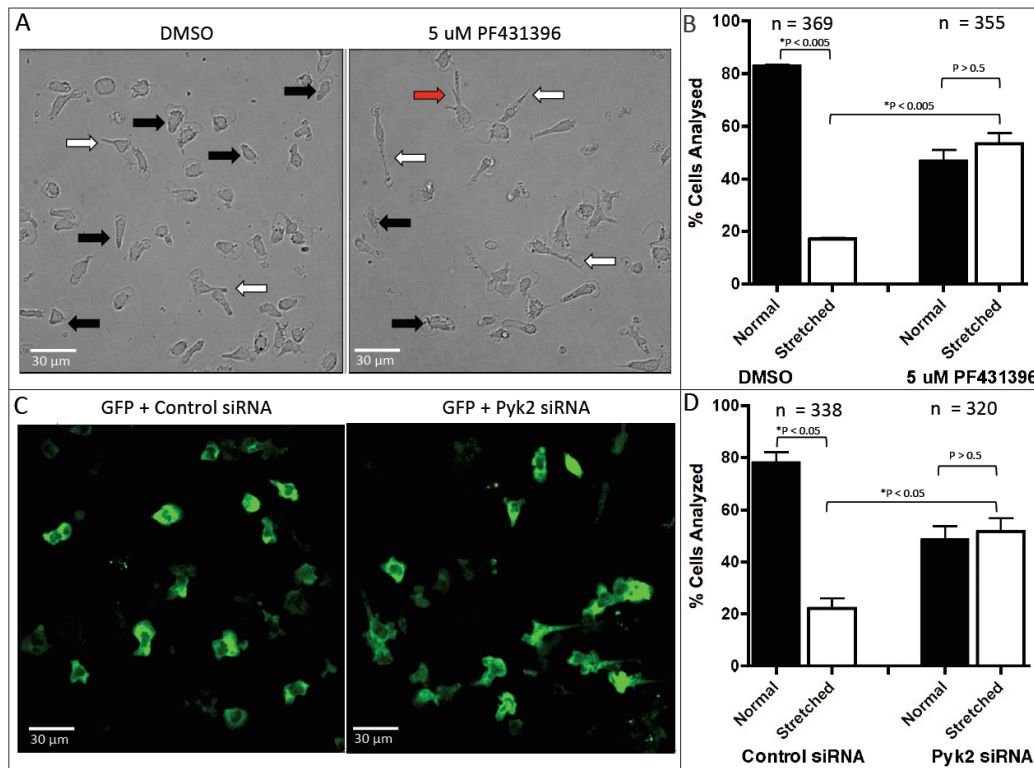
Figure 4-3. De-regulation of Pyk2 results in extensive CTL stretching on an ICAM-1 coated surface. (A) CTL clone AB.1 were treated with either DMSO or 5 μM PF431396 for 1 hour before transferring 2 X 10^5 cells to an imaging chamber coated with 3 μg/ml ICAM-1. CTL were incubated for an additional 1 hour at 37°C to allow adhesion to occur in the presence of PF431396. Images were acquired randomly throughout the imaging slide and cell morphology was individually scored for each group. Black and white arrows indicate normal and stretched phenotype, respectively, as described in materials and methods. (B) At least 5 images were acquired randomly from each condition and the cell morphology was visually categorized into either normal or stretched for each group of cells. Data represents combined results from 3 independent experiments and the total number of cells analyzed is shown (n). (C) CTL clone AB.1 were co-nucleofected with GFP and control siRNA or Pyk2 siRNA for 48 hours followed by the same treatment as described in (A). (D) Similar morphological analysis was performed in CTL clone 11 as described in part B. The figure shows the pooled results from 3 independent experiments. All images were acquired using spinning disk confocal microscope. All experiments were performed three times independently and the representative images from each condition are shown. Paired t-test was performed to compare difference in quantity between normal and stretched phenotype within the same condition. Unpaired t-test was used to compare similar phenotype between two different conditions. Asterisk indicates P-value with 95% confidence intervals. Error bar represents mean with standard deviation.

114

Pyk2 regulates CTL de-adhesion from ICAM-1.

To uncover how the aberrant phenotype developed, I placed CTL on ICAM-1 coated imaging chambers to perform live cell imaging in the presence or absence of the PF431396. Under my experimental conditions the control DMSO or PF431396 treated CTL were able to adhere on ICAM-1 coated imaging slides after 40 minutes of incubation. Following cell settlement, the majority of ICAM-1 bound CTL showed immediate random motility. I found that PF431396 has no detectable effect on CTL motility at the leading edge (Figure 4-4A, indicated by green arrows). Conversely, de-adhesion of the trailing edge was severely compromised (indicated by white arrows). The defective trailing edge seemed to anchor CTL at one position while the leading edge continued to move forward to form an extensively stretched phenotype. This explains what I had previously observed in CTL treated with PF431396 in Figure 4-3A (indicated by white arrows). The data suggest that PF431397 treatment led to a severe defect in CTL de-adhesion at the trailing edge.

To validate and complement the results observed with PF431396 treatment, I used a different approach to inhibit Pyk2 function in CTL. Previous studies suggested that PRNK, a splice variant only containing the C-terminal FAT domain of Pyk2 (Figure 1-5), potentially blocks the function of endogenous Pyk2 by acting as a dominant negative protein (127, 129, 232). I transfected CTL with the truncated form of Pyk2 containing only the sequence of PRNK to determine if a similar inhibitory phenotype could be

observed. As shown in Figure 4-4B, ectopic expression of the C-terminal domain of Pyk2 (GFP-FAT) produced similar morphological features compared to using the PF431396 (Figure 4-4A and 4-3A). The defective trailing edge was apparent, as indicated by white arrows, in CTL expressing the C-terminal domain of Pyk2. Some of the GFP-FAT expressing cells even exhibited multiple pseudopods (Figure 4-4B bottom) as seen in CTL treated with PF431396 (Figure 4-3A top). This evidence further supports a dominant negative effect of PRNK to inhibit endogenous Pyk2 function. I concluded that Pyk2 inhibition using PF431396 or expression of FAT domain leads to a severe defect in ICAM-1 dependent de-adhesion in migrating CTL.
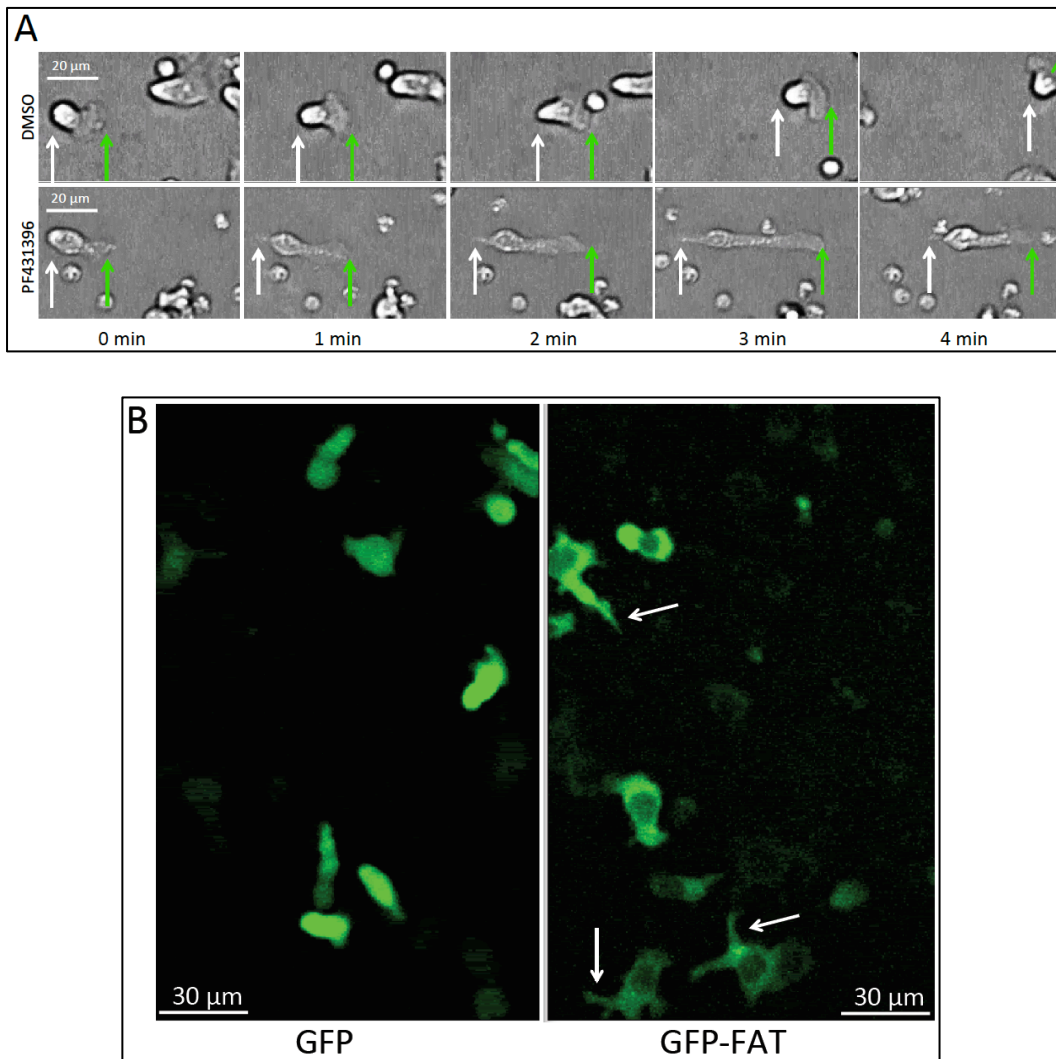
Figure 4-4. Pyk2 is required for normal CTL de-adhesion at the trailing edge. (A) CTL clone AB.1 were pre-treated with either DMSO control or 5 uM PF431396 for 1 hour in suspension, followed by incubation on imaging slides coated with 3 μg/ml ICAM-1 for an additional 1 hour to allow adhesion. Live-cell time-lapse images were acquired using the bright field function on the confocal microscope. (B) CTL clone AB.1 were nucleofected with either GFP vector or GFP-coupled to Pyk2 C-terminal FAT domain (GFP-FAT) for 24 hours then transferred to an ICAM-1 coated slide. Images were taken 1-hour post transfer using a confocal microscope with 20X objective lens. White arrows indicate the abnormal trailing edge. All experiments were performed more than three times and the representative images are shown.

Inhibition of Pyk2 severely impairs CTL motility.

Although Pyk2 inhibition led to defective de-adhesion at the trailing edge, the leading edge of PF431396 treated CTL seemed unaffected and appeared to protrude at a similar kinetic as the control CTL (Figure 4-4A). To determine if Pyk2 plays a role in non-directional CTL migration on ICAM-1, I followed a group of migrating CTL using live cell imaging and analyzed the movement of two different CTL clones using ImageJ software. As shown in Figure 4-5A, inhibition of Pyk2 with PF431396 resulted in a substantial reduction in CTL motility in both CTL clone AB.1 and clone 11 (Figures 4-5A and 4-5C). Computational analysis revealed that the overall velocity of movement was also significantly compromised in the presence of PF431396 (Figures 4-5B and 4-5D). Furthermore, a similar defect in migration can be seen in CTL transfected with either Pyk2 FAT domain or Pyk2 siRNA (Figures 4-6). My results indicate that Pyk2 is required for optimal CTL motility on the ICAM-1 surface and it may contribute to migration by regulating de-adhesion.

I extended my findings using *ex-vivo* activated CD8 T cells isolated from mice expressing a TCR specific for the ovalbumin peptide SIINFEKL (OT-1 mice). As shown in figure 4-7, OT-1 CD8 T cells exhibited a similar aberrant elongated phenotype in the presence of PF431396. I performed similar migration experiments and analysis using PF431396 treatment, transfection of Pyk2 FAT-domain, and transfection of Pyk2 siRNA in these cells. As shown in Figures 4-7 and 4-8, Pyk2 was also required for optimal

migration distance and velocity in the *ex-vivo* activated primary CD8 T cells.

My data indicate that Pyk2 is critical for CTL migration, and deregulation of

Pyk2 leads to severely impaired CTL motility on ICAM-1.
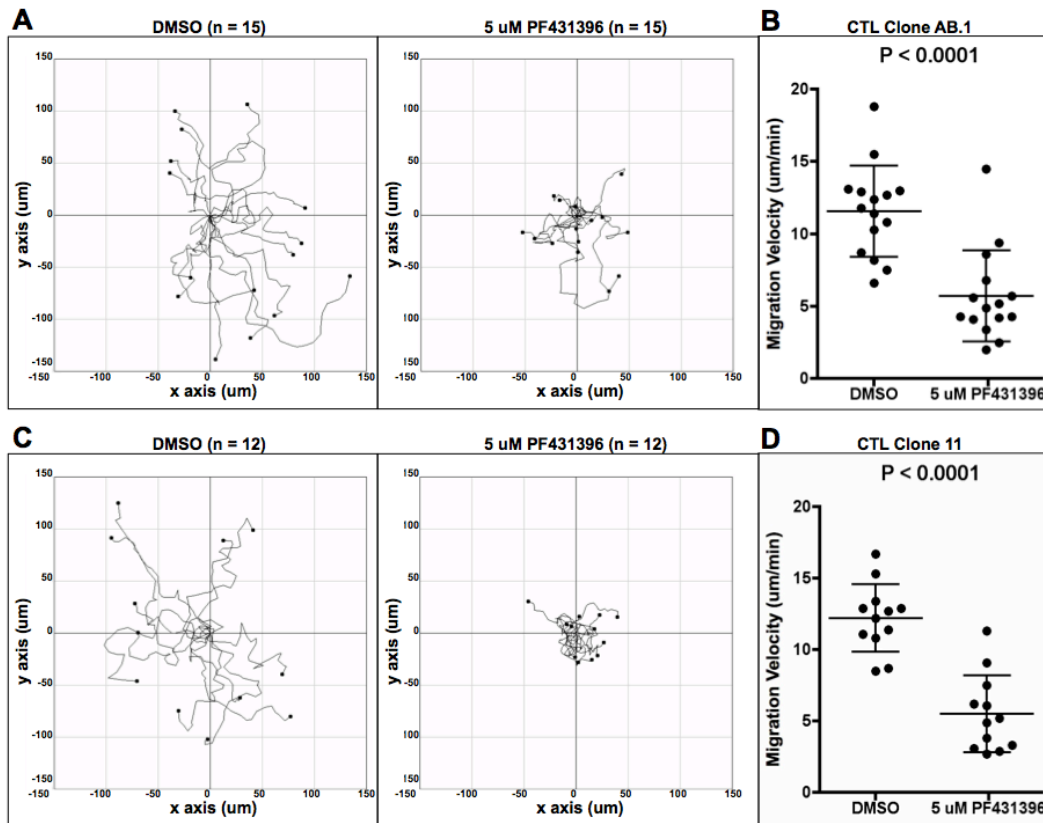
Figure 4-5. Inhibition of Pyk2 severely impairs CTL motility. (A) The migration distance and direction of CTL clone AB.1 on an ICAM-1 coated imaging chamber during a 15 minute period was determined. Cells were pre-treated with DMSO or 5 μM PF431396 for 1 hour, then transferred to the imaging chamber and allowed to settle and adhere for a minimum of 40 minutes. Time-lapsed cell movement was acquired using the bright field channel on the spinning disk confocal microscope. The acquired data were analyzed by ImageJ software using the manual tracking function as described in the materials and methods. (B) The numerical parameters obtained from the manual tracking function were converted into a velocity unit for each migrating CTL from part A. (C) & (D) The corresponding migration distance and velocity for CTL clone 11 in the presence and absence of PF431396. The sample size is indicated for each condition and each dot represents a single cell in the velocity graph. All experiments were performed three times and representative data are shown. The statistical analysis was performed using an unpaired t-test with 95% confidence intervals. Error bar represents mean with standard deviation.
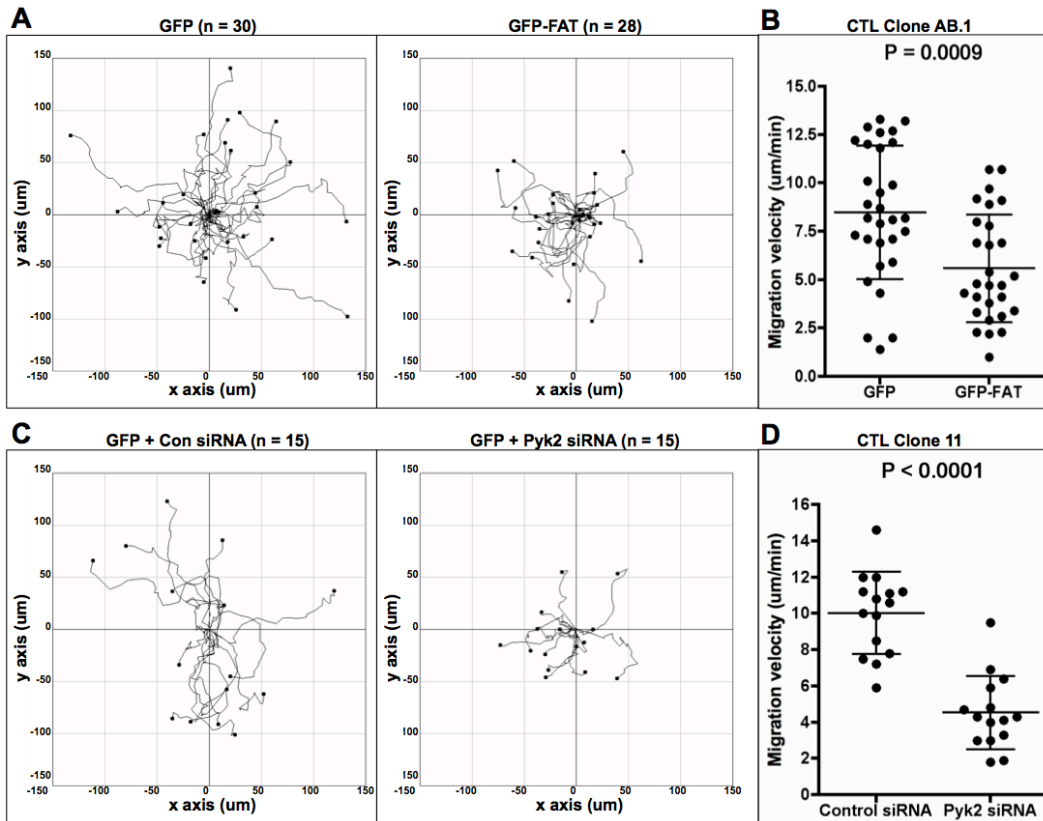
Figure 4-6. Pyk2 is required for optimal CTL migration on ICAM-1 coated surface. (A) & (B) The migration pattern and velocity of CTL clone AB.1 expressing either GFP or FAT-GFP during a 15 minute migration period on an ICAM-1 coated imaging chamber. CTL were analyzed after 24 hours post transfection. (C) & (D) The migration pattern and velocity of CTL clone 11 expressing GFP that were also co-transfected with either control siRNA or Pyk2 siRNA. SiRNA transfected cells were transferred to ICAM-1 imaging chamber at 48 hours post transfection. All transfected cells were washed before transferring to an ICAM-1 coated chamber. Cells were allowed to settle for a minimum of 40 minutes before image acquisition for a 15-minute period. The sample size is indicated for each condition and each dot represents a single cell in the velocity graph. Experiments using FAT-GFP expressing CTL were performed three times whereas experiments using siRNA-transfected cells were performed twice. All experiments were performed independently and the representative data are shown. The statistical analysis was performed using an unpaired t-test with 95% confidence intervals. Error bar represents mean with standard deviation.
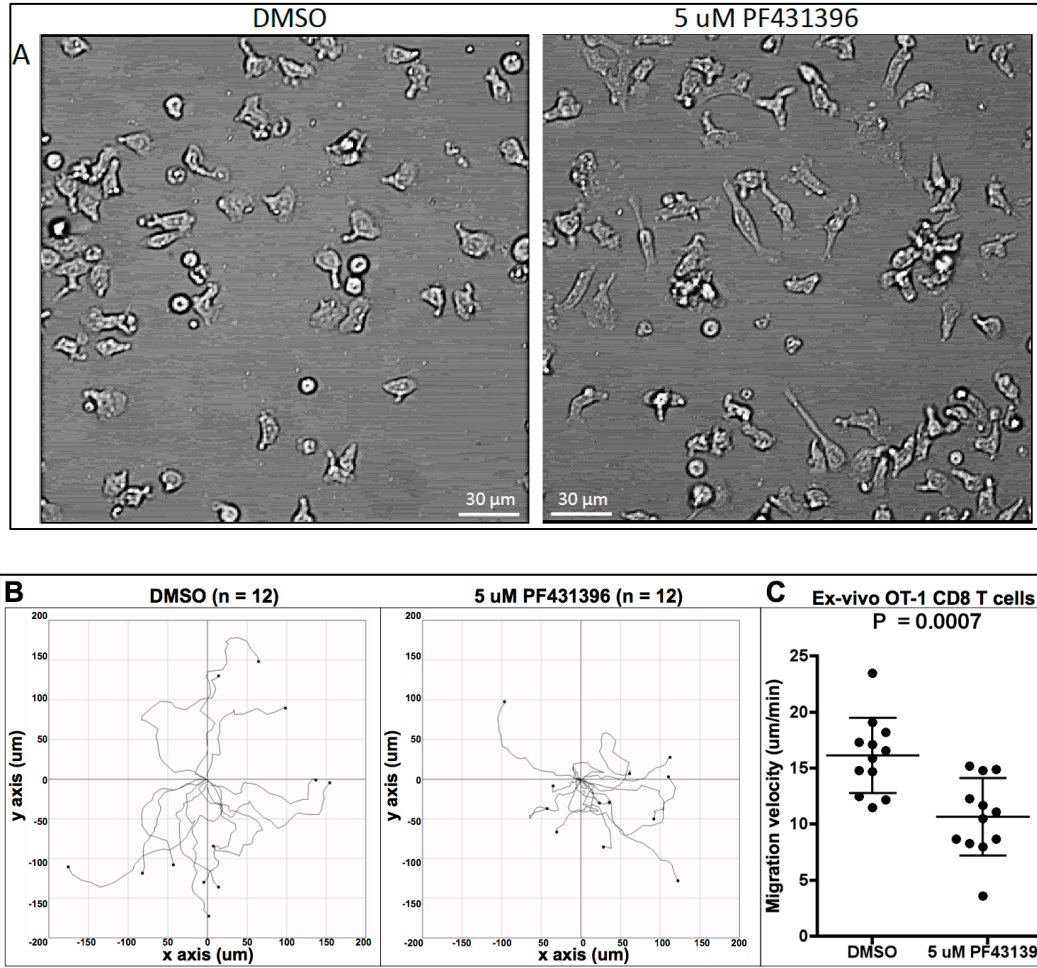
Figure 4-7. Inhibition of Pyk2 leads to migrational defects in primary CD8+ T cells on an ICAM-1 coated surface. (A) Splenocytes from OT-1 transgenic mice were *in vitro* stimulated with the OVA peptide SIINFEKL for 3 days followed by Histopaque enrichment for CD8+ T cells. The activated CD8+ T cells were treated with either DMSO or 5 μM PF431396 for 1 hour before transfer to the ICAM-1 coated imaging chamber. Bright field images were taken at 80 minutes after cell settling on ICAM-1 coated slide. (B) & (C) The effect of Pyk2 inhibition on migration distance and velocity in *ex vivo* OT-1 CD8+ T cells during a 15 minute period. The sample size is indicated for each condition and each dot represents a single cell in the velocity graph. All experiments were performed twice independently and the representative data are shown. The statistical analysis was performed using an unpaired t-test with 95% confidence intervals. Error bar represents mean with standard deviation.
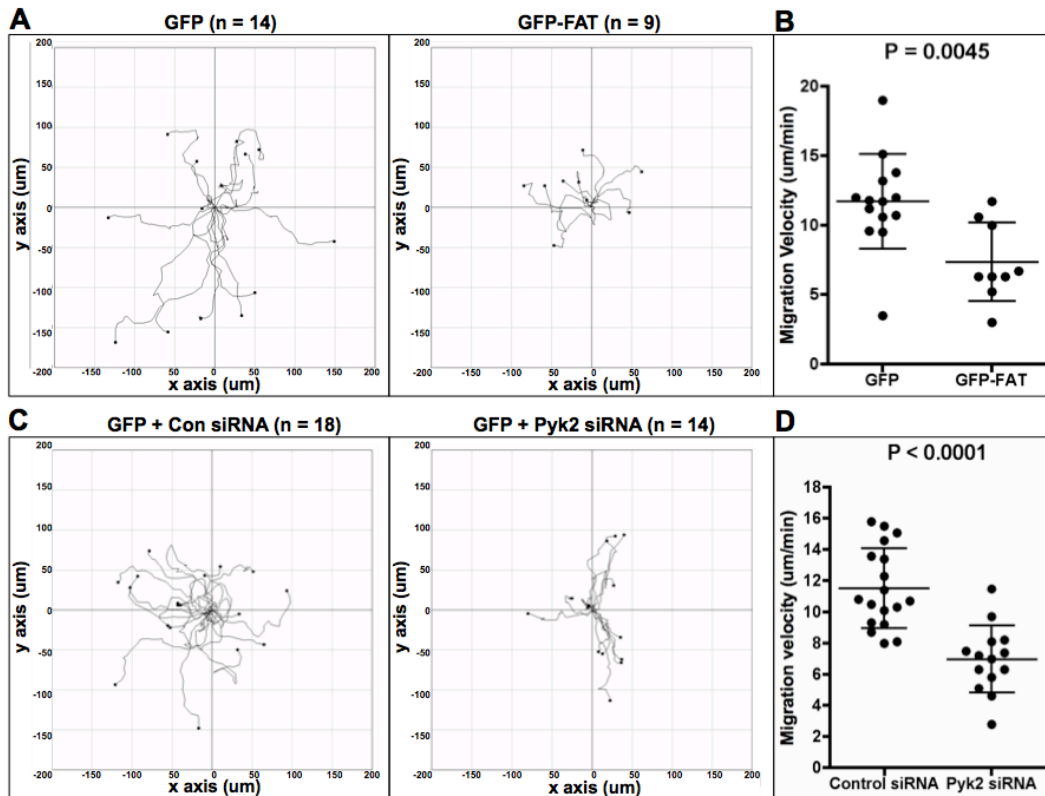
Figure 4-8. De-regulation of Pyk2 leads to migrational defects in primary CD8+ T cells on an ICAM-1 coated surface. (A) & (B) The migration distance and velocity of GFP or GFP-FAT expressing OT-1 CD8+ T cells on an ICAM-1 coated chamber after 24 hours post nucleofection. Transfected cells were incubated on imaging the imaging slide for at least 40 minutes prior to image acquisition. (C) & (D) The migration distance and velocity of GFP+ OT-1 CD8+ T cells on an CAM-1 coated imaging slide. Cells were co-nucleofected with GFP and either control siRNA or Pyk2 siRNA for 48 hours, then transferred to an ICAM-1 coated imaging slide for 45 minutes before imaging acquisition and analysis. The sample size is indicated for each condition and each dot represents a single cell in the velocity graph. All experiments were performed twice independently and the representative data are shown. The statistical analysis was performed using an unpaired t-test with 95% confidence intervals. Error bar represents mean with standard deviation.

CTL adhere to an ICAM-1 surface under Pyk2 inhibition but fail to migrate efficiently toward chemokine CXCL9.

My previous data highlight a vital role for Pyk2 in regulating the intrinsic and non-directional motility of CTL on an ICAM-1 coated surface (Figure 4-5 to Figure 4-8). Since Pyk2 is activated in response to chemokine stimulation (123, 136, 233), I performed experiments to determine if Pyk2 plays a role in chemokine-driven motility of CTL. First, I examined the responsiveness of CTL clone 11 to the chemokine CXCL9, which binds the receptor CXCR3 that is highly expressed on activated T cells (234). As shown in Table 4-1, CTL clone 11 migrated through the transwell membrane pores in response to CXCL9 in a dose dependent manner. At a concentration of 1 μg/ml CXCL9, nearly twice the number of CTL had migrated through the BSA blocked transwell membrane toward the chemokine during a 90-minute period compared to the control group.

To determine if Pyk2 plays a role in CTL chemotactic response toward CXCL9 on an ICAM-1 coated surface, I treated the CTL with PF431396 and performed the migration assay in the presence of additional PF431396. As shown in Figure 4-9A, CTL migrated more efficiently on an ICAM-1 coated surface with the same dose of CXCL9 compared to migration on a BSA coated surface (Table 4-1). In the presence of PF431396, the percentage of CTL that migrated through the transwell membrane was significantly reduced. This is consistent with a study using naïve CD8 T cells isolated from Pyk2 deficient mice (166). However, the actual mechanical link between an early defect in

adhesion and the subsequent reduction in chemotaxis was not addressed in this previous study (166). In my experiment, I found that the majority of CTL still adhered to the transwell membrane coated with ICAM-1 (Figure 4-9B). Increasing PF431396 concentrations resulted in more cells remaining on the upper transwell chamber rather than migrating in response to the chemokine. This strongly suggests that the reduction in overall CTL migration is due to a defect in CTL de-adhesion from ICAM-1 rather than a previously assumed inability to bind to ICAM-1 (166). From these results I conclude that Pyk2 inhibition leads to a severe impairment in CTL chemotactic response on an ICAM-1 coated surface.

CXCL9 (μg/ml)	0	0.2	1.0	2.4
Trial 1	19.0%	22.0%	33.5%	ND
Trial 2	17.4%	43.0%	47.5%	61.0%

Table 4-1. *In vitro* **migration of CTL in response to CXCL9.** CTL clone 11 cells were placed on the upper transwell filter blocked with 2% BSA in PBS and allowed to settle for 30 minutes at room temperature before transferring to a chemotaxis chamber containing the indicated concentration of CXCL9. After 90 minutes of incubation at 37°C, the absolute number of cells migrated to the bottom chemotaxis chamber was determined.
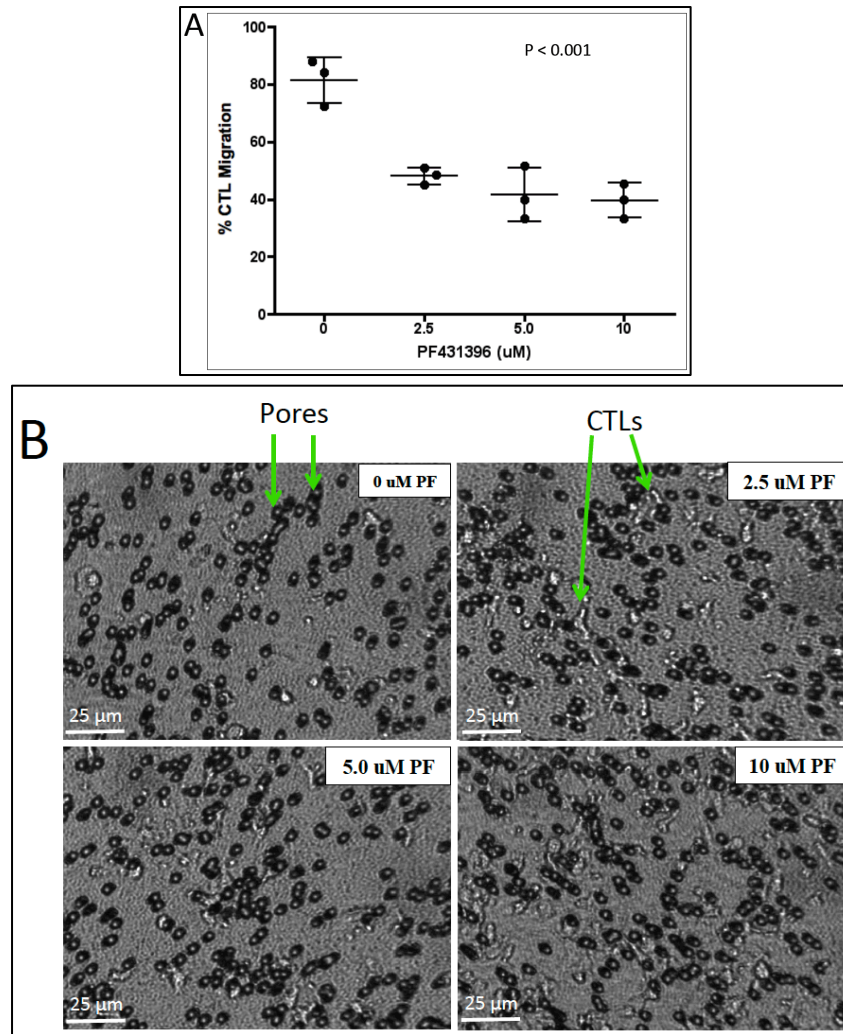
Figure 4-9. Pyk2 inhibition significantly reduces CTL migration on ICAM-1 in response to chemokine CXCL9 stimulation. (A) CTL clone 11 were pre-treated with the indicated PF431396 for 30 minutes in suspension, and then 2 X 10^5 cells were transferred to upper transwell filter pre-coated with 3 µg/ml ICAM-1. The cells were allowed to settle for 1 hour. After cell settling, the filter containing CTL was transferred to a chemotaxis chamber containing 1 µg/ml CXCL9 and incubated at 37°C for 2 hours. The absolute number of cells migrated through the filter were counted. The data represents the pooled results from three independent experiments. (B) The representative images of the upper transwell filter, which was coated with 3 µg/ml ICAM-1 2 hours after the CTL chemotaxis assay. PF indicates the corresponding concentration of PF431396 presence. Error bar represents the mean and standard deviation. A one-way analysis of variance (ANOVA) with Dunnett's multiple comparison test was performed using 0 ug/ml CXCL9 as the control group.

Pyk2 is targeted to the ICAM-1 contact zone and the C-terminal domain of Pyk2 is sufficient to de-regulate trailing edge de-adhesion.

I have shown that Pyk2 plays a critical role in ICAM-1-dependent CTL motility through three different methods of Pyk2 manipulation: inhibition of Pyk2, expression of a putative dominant-negative FAT domain, and knockdown of Pyk2 expression using siRNA (Figures 4-5 and 4-6). Each manipulation method interferes with a specific aspect of Pyk2 function, but all showed a significant reduction in cell migration distance and velocity. In gain insight on how Pyk2 structurally contributes to optimal CTL migration at the molecular level, I transfected CTL using various Pyk2 constructs to determine which domain regulates CTL migration. I focused on the contact sites, as depicted in Figure 4-10A, where CTL binds ICAM-1. I used live cell imaging to determine the relative Pyk2 distribution. As shown in Figure 4-10B, I found that all of the Pyk2 constructs localized throughout the contact zone during CTL migration. A small quantity of wild-type Pyk2 is found aggregated at the leading edge (as indicated by green arrows) while enrichment was clearly visible at the trailing edge (as indicated by white arrows). Similar localization patterns were found in CTL expressing the Pyk2-FAT domain or the kinase-dead mutant of Pyk2. Although the FERM/kinase domain of Pyk2 localized to the ICAM-1 contact sites, there was no detectable aggregation as was observed in CTL expressing the other Pyk2 constructs.

According to the imaging data, CTL transfected with the wild-type or kinase-dead Pyk2 showed similar trailing edge stretching morphology as CTL transfected with the FAT domain. Similar phenotypes were not observed in CTL transfected with the FERM/kinase domain. The imaging results suggest that ectopic expression of the FAT domain may be sufficient to block normal trailing edge de-adhesion, as observed in Figure 4-4B. After several attempt, the expression efficiency of full length Pyk2 constructs was too low for a migration study. Therefore, it remains unknown whether similar motility defects can be observed in CTL transfected with the wild-type Pyk2 or the kinase-dead Pyk2. My imaging results suggest that Pyk2 is targeted to the contact sites during ICAM-1 mediated migration. The FAT domain of Pyk2 alone appears to be sufficient to block normal CTL de-adhesion presumably through abnormal aggregation at the trailing edge.
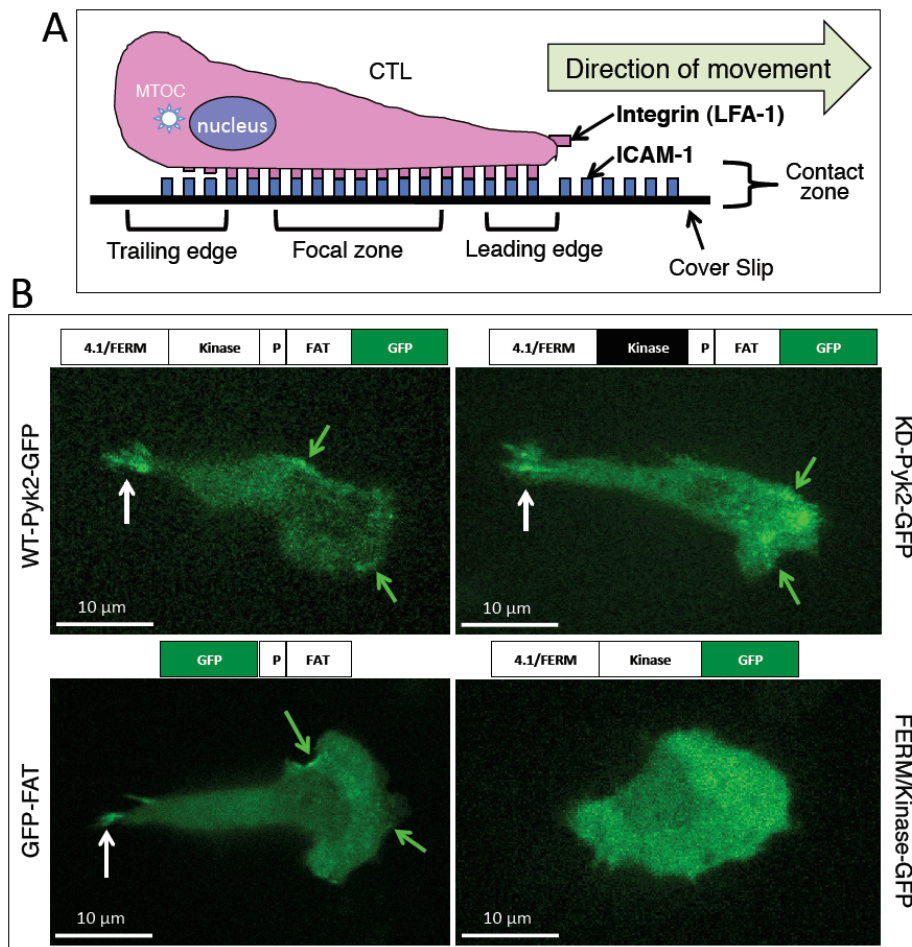
Figure 4-10. Pyk2 is targeted to the contact zone during CTL migration.
(A) Schematic diagram of migrating CTL (side view) on an ICAM-1 coated surface. The LFA-1 at the leading edge and focal zone bind ICAM-1 with intermediate and high affinity, respectively. The LFA-1 at the trailing edge has high affinity characteristics but it is no longer interacting with ICAM-1 for efficient de-adhesion. The diagram also depicts the "contact zone", which is a region where CTL contact the ICAM-1 coated surface. (B) CTL clone 11 was nucleofected with either full-length Pyk2, kinase-dead mutant of Pyk2 (K457A), N-terminus Pyk2 (contain both FERM and kinase domains) or Pyk2 C-terminal FAT domain for 24 hours. Nucleofected CTL were placed on ICAM-1 coated imaging slides for 1 hour to allow cell settling. Images of migrating CTL were acquired using confocal microscopy focusing specifically on the contact zone between the imaging slide and the CTL (top view). White arrows indicate aggregation at the trailing edge whereas green arrows indicate aggregation at the leading edge. Experiments were performed twice independently and at least 10 migrating cells were analyzed for each condition. The representative images are shown.

Pyk2 phosphorylated at specific sites preferentially associates with different contact regions in migrating CTL on ICAM-1.

To determine how endogenous Pyk2 contributes to CTL migration on ICAM-1, I examined the extent of Pyk2 tyrosine phosphorylation using specific phospho-tyrosine antibodies against pY402, pY579, pY580 and pY881 of Pyk2 on migrating CTL. In order to distinguish the leading edge from the trailing edge in polarized CTL, cells were also stained with anti-γ-tubulin antibodies to label the MTOC, which characteristically locates at the trailing edge of migrating T cells (91). As shown in Figure 4-11, tyrosine 402 phosphorylated Pyk2 (pY402) was found scattered throughout the contact region with modest aggregation near the trailing edge. In contrast, tyrosine 579/580 and 881 phosphorylated Pyk2 preferred to associate with the leading edge and trailing edge, respectively. The distribution pattern between pY579 and pY580 appeared similar with obvious preference for the leading edge and the cell periphery where initial integrin engagement occurs. In general, all four specific tyrosine phosphorylated Pyk2 fractions were associated with the MTOC when CTL were plated on ICAM-1. This is contradictory to the previous study from our lab that showed activated Pyk2 was undetectable at the MTOC upon target cell stimulation (161). From this new information, I determined that Pyk2 activated by integrin-mediated signaling is differentially distributed inside the CTL compared to Pyk2 activated by TCR-mediated signaling.

I used ImageJ software to quantify the relative amounts of Pyk2 fluorescence at the trailing edge and the leading edge, with particular focus at the contact sites where differential distribution of Pyk2 was evident (Figure 4-11 bottom). The analysis was performed for each individual cell focusing at the contact zone with a 1 μm thickness. Each cell image was arbitrarily, but equally divided into three sections: the leading edge, middle focal zone and the trailing edge. The total fluorescence intensity of the trailing edge (TE) was divided by the total fluorescence intensity of the leading edge (LE) to obtain a numerical ratio for comparison purpose. The results from my analysis indicate that while pY402 fractions of Pyk2 have no significant difference in distribution between the leading edge and the trailing edge compared to antibody that recognize total Pyk2, the antibodies that recognize pY579 and pY881 are significantly more localized at the leading edge and trailing edge, respectively. This suggests that as the CTL migrate on an ICAM-1 surface, Pyk2 is recruited to the site of LFA-1 activation and becomes phosphorylated at Y579 and Y580. As the cell crawls, Pyk2 becomes tyrosine phosphorylated at Y881 at the trailing edge. This implies that the four known tyrosine residues of Pyk2 are sequentially phosphorylated as the cell advances.
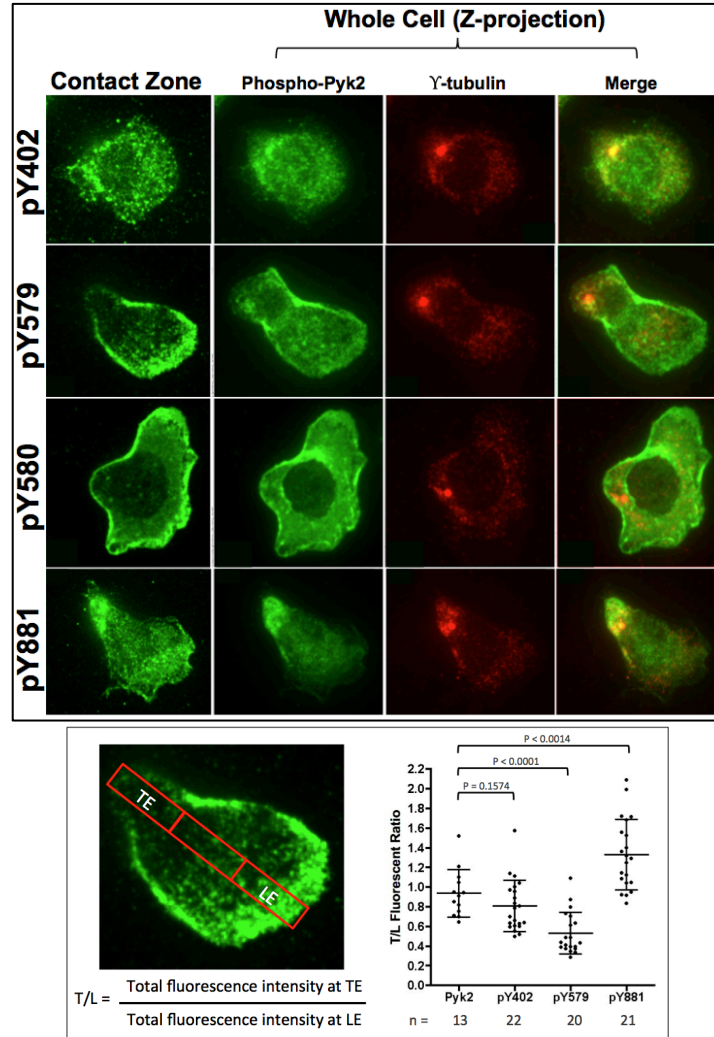
Figure 4-11. **Pyk2 phosphorylated at specific sites preferentially associates with different contact regions in migrating CTL on an ICAM-1 coated surface.** (Top) CTL clone 11 cells were incubated on ICAM-1 coated imaging slide for 1 hour followed by methanol fixation. Cells were stained with the indicated Pyk2 phospho-specific and anti-γ tubulin antibodies as described in the materials and methods. The images of contact zone represent 1 μm thickness at the ICAM-1 contact site. Images were acquired using a confocal microscope with 60X objective lens. (Bottom) Left: A representative image to show how the fluorescence intensity of trailing edge to leading edge ratio was determined for each individual cell. Right: Analysis of the trailing edge to leading edge fluorescence ratio at the contact zone between different tyrosine phosphorylated fractions of Pyk2. The number of cells analyzed from each condition is indicated. Total Pyk2 was derived from samples stained with anti-Pyk2 antibody. Experiments were independently performed three times and the representative images and analysis are shown. Error bar represents mean and standard deviation. P values were obtained using an unpaired t-test.

De-regulation of Pyk2 does not inhibit LFA-1 turnover.

Lymphocyte migration requires efficient formation and disassembly of the adhesion complex at the leading edge and trailing edge, respectively (66). Given the structural similarity between FAK and Pyk2 (Figure 1-5), in addition to my previous data that showed activated Pyk2 localizes to both leading edge and trailing edge (Figure 4-11), I hypothesized that Pyk2 is involved in some aspect of adhesion complex formation and/or disassembly in migrating CTL. Based on the compelling evidence that de-regulation of Pyk2 impairs normal trailing edge de-adhesion (Figure 4-4 to 4-8), I examined a possible role of Pyk2 in regulating adhesion complex disassembly at the trailing edge.

A recent study showed that inhibition of calpain leads to a significant reduction in human T cell migration distance and velocity (71). The authors found that calpain inhibition impaired LFA-1 turnover, and the migration analysis was strikingly similar to my CTL migration data in Figures 4-5 and 4-6 (71). Calpain is a cysteine protease that can cleave various focal adhesion associated proteins, including FAK and Pyk2, and it is essential in focal adhesion turnover and disassembly in adherent cells (235-237). A simplified model for calpain function is depicted in the top panel of Figure 4-12. The general function of calpain is considered to be a positive regulator of cell migration and cell spreading (236). Calpain cleaves FAK between residues 745 and 746 (235), but the corresponding sequence is absent in the hematopoietic Pyk2 expressed in CTL. Whether there are additional calpain

133

cleavage sites in hematopoietic Pyk2 is unknown. However, a recent study indicated that Pyk2 is cleaved by a calpain-dependent mechanism in other cell types (237). Alternatively, it has been proposed that FAK may serve as a scaffolding molecule to regulate calpain-mediated cleavage of talin to facilitate adhesion turnover (236). Calpain forms a complex with FAK through the proline residues that lie between amino acid 368 and 378 (238). Although these two proline residues are conserved in Pyk2 (NCBI Accession: NM_172498), an association between calpain and Pyk2 has not been described in the literature. Therefore, Pyk2 could serve as a direct calpain substrate and/or as a scaffold molecule to facilitate calpain cleavage of its substrates during CTL migration.
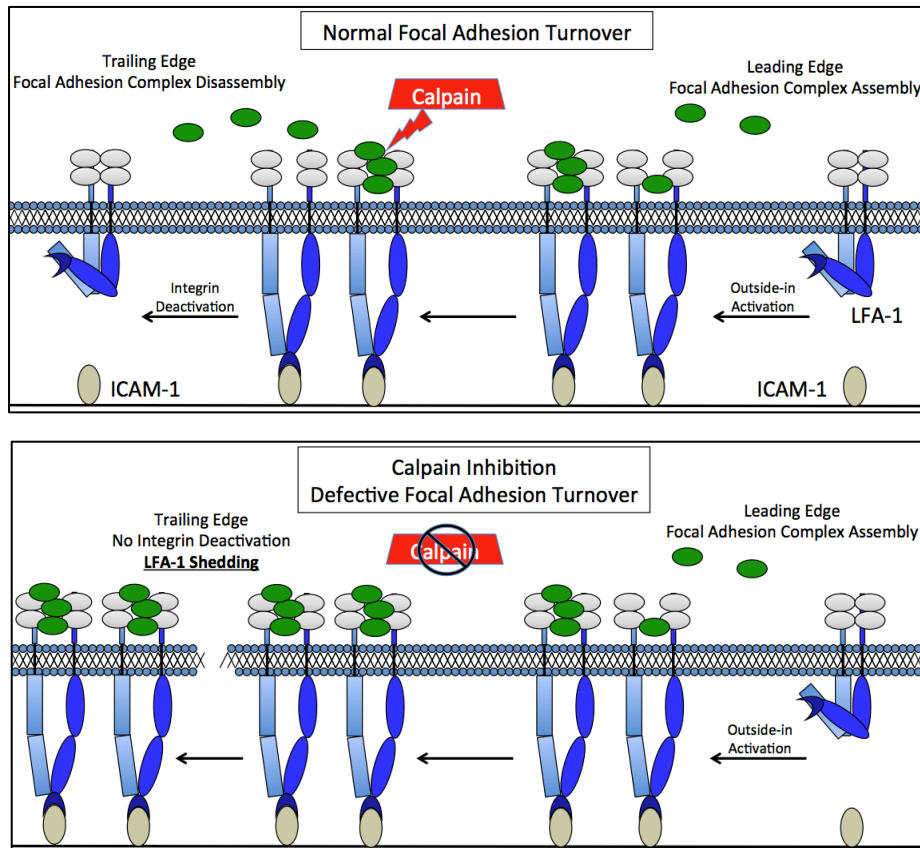
Figure 4-12. Model for calpain-dependent turnover of LFA-1 in T cell.
(Top) Upon ICAM-1 binding, outside-in signaling triggers assembly of focal adhesion (FA) complex at the leading edge. The green circles represent proteins that are essential for the formation of FA. As the cytoskeleton advances the cell forward, the FA complex lags behind at the trailing edge of the cell. LFA-1 deactivation requires FA disassembly, which is mediated by calpain. (Bottom) Inhibition of calpain blocks disassembly of FA, which leads to impaired integrin deactivation followed by subsequent LFA-1 shedding (71). Pyk2 either facilitates cleavage of FA substrates by calpain or serves as a calpain substrate itself for proper integrin deactivation and CTL de-adhesion.

To test if Pyk2 and calpain operate in the same pathway to regulate CTL migration, I performed experiments to determine if calpain inhibition would yield a similar defective phenotype in LFA-1 turnover as inhibition of Pyk2. The characteristic phenotype was described as having numerous long and extensive LFA-1 trails shed behind the migrating T cells under calpain inhibition (71). I treated CTL with either calpain inhibitor calpeptin or PF431396 followed by incubation of cells on ICAM-1 coated slides to allow migration to proceed. Cells were subsequently fixed and stained for surface LFA-1 to determine if LFA-1 trails were present behind the path of migrating CTL in the presence of inhibitor. As shown in Figure 4-13A, CTL treated with calpeptin showed a LFA-1 turnover defect as evidenced by LFA-1 shedding on the ICAM-1 coated surface. However, the level of LFA-1 shedding in CTL was not as robust as that observed in human T cells (71). Conversely, I found no obvious LFA-1 shedding in CTL treated with PF431396. In some instances, there were small amounts of LFA-1 found in the vicinity of CTL, but it lacked the trail-like characteristics. Upon examination of the images from each inhibitor treated sample, the trailing edge structure was visually distinct between calpeptin and PF431396 treated CTL (Figure 4-13B). While inhibition of calpain produced numerous thin and long membrane tails, Pyk2 inhibition led to multiple thick trailing edges. This indicates that although both inhibitors can reduce ICAM-1 dependent T cell migration, Pyk2 and calpain likely regulate different aspects of the cell de-adhesion process at the trailing edge.
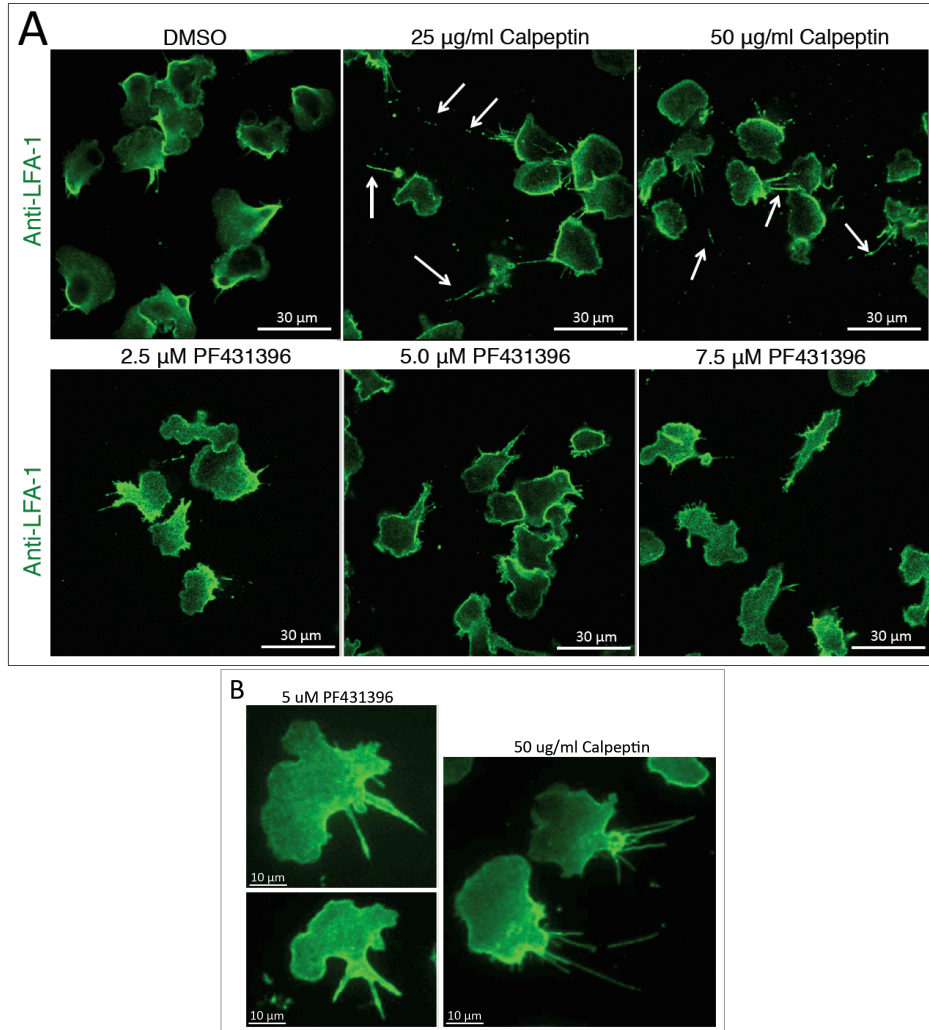
Figure 4-13. Morphological comparison between calpain and Pyk2 inhibition in CTL migration on ICAM-1 surface. (A) For conditions that used calpeptin, CTL clone 11 was plated on an ICAM-1 coated imaging slide for at least 40 minutes at 37°C, followed by addition of DMSO control or the indicated amount of calpeptin for an additional 40 minutes. For conditions that use PF431396, CTL clone 11 was pretreated with the indicated amount of PF431396 for 1 hour at room temperature, and then transferred to an ICAM-1 coated slide to incubate for at least 40 minutes at 37°C. Cells were fixed with paraformaldehyde and stained with FITC-conjugated anti-LFA-1 antibody. Images were acquired with a confocal microscope using 40X objective lens. White arrows indicate apparent LFA-1 shedding on ICAM-1 coated surface. All images are showing only the ICAM-1 contact zones. (B) Cells were treated as described above. Images were acquired using 60X objective lens and the whole z-projection is shown. Two different PF431396 treated and a pair of calpeptin treated CTL were shown. All experiments were performed at least three times and representative images are shown.

I also investigated whether CTL transfected with Pyk2 siRNA or Pyk2 FAT domain would lead to LFA-1 shedding at the trailing edge. As shown in figure 4-14, under either condition there was no apparent LFA-1 shedding found on the ICAM-1 coated surface. Similar to the previous data shown in figure 4-10B, Pyk2 FAT domain was aggregated throughout the CTL at the contact sites with particular preference at the cell periphery and trailing edge (Figure 4-14B). Although the FAT domain aggregated at the trailing edge and seemed to anchor the cell at one position, there was no detectable trail of LFA-1 left behind the FAT expressing cells. My results indicate that neither knockdown of Pyk2 expression or expression of the dominant negative FAT domain leads to LFA-1 shedding as observed in calpeptin treated cells.
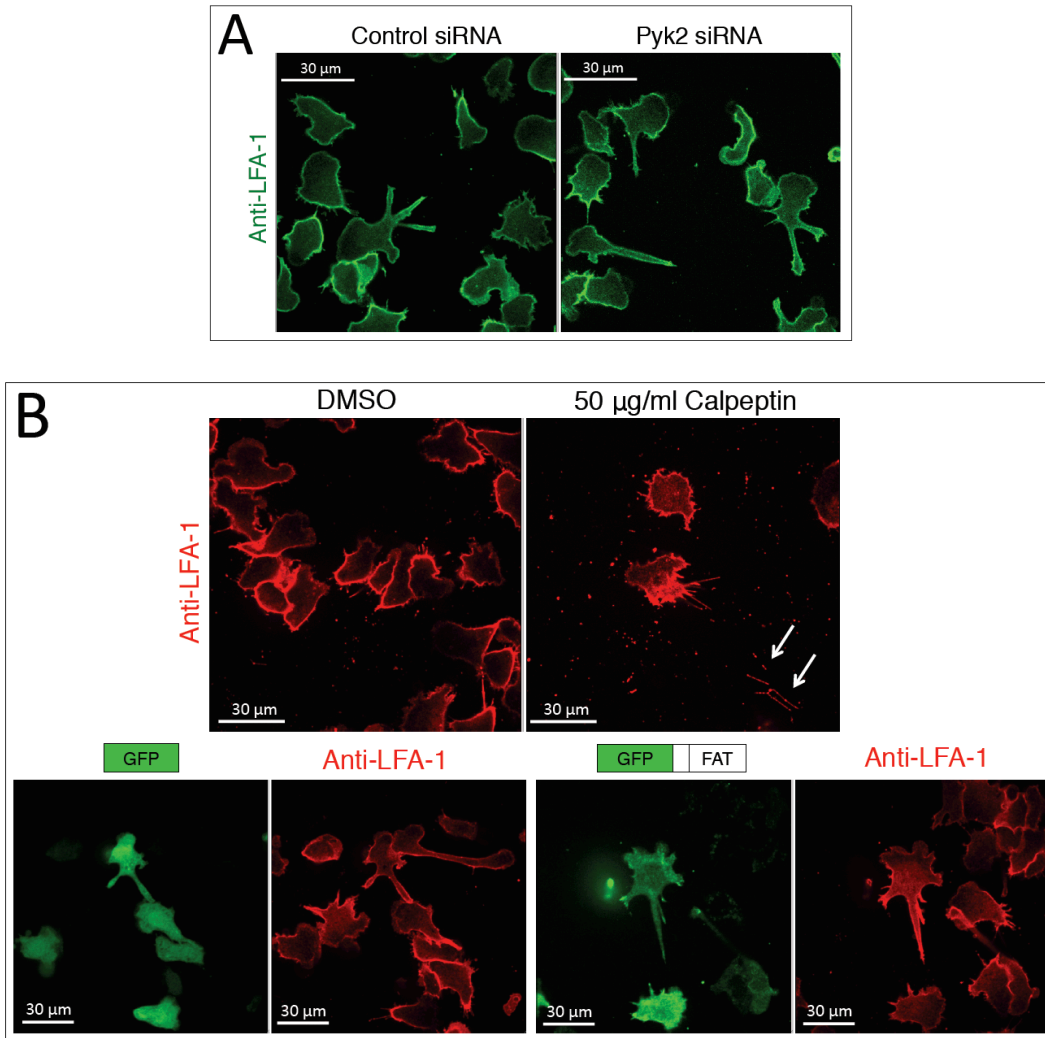
Figure 4-14. Pyk2 inhibition does not lead to LFA-1 shedding. (A) CTL clones were transfected with either control or Pyk2 siRNA for 48 hours, then transferred to an ICAM-1 coated slide to incubate for at least 40 minutes at 37°C. Cells were fixed and surface stained with FITC-conjugated anti-LFA-1 antibody. (B) In the top panel, the control experiment using calpeptin treatment was performed as described in Figure 4-12 except that cells were surface stained with APC-conjugated anti-LFA-1 antibody. White arrows indicate the long LFA-1 trail left behind calpeptin treated CTL. In the bottom panel, CTL clone 11 were transfected with either GFP or GFP-FAT for 24 hours. Cells were transferred to an ICAM-1 coated slide for an additional 1 hour before fixation and surface stained with APC conjugated anti-LFA-1 antibody. All experiments were performed twice independently and the representative data are shown. All images were focused only at the contact zone between CTL and ICAM-1 surface.

Inhibition of Pyk2 de-regulates total cellular LFA-1 distribution.

My data show that inhibition of Pyk2 results in a significant reduction in CTL migration velocity due to defects in de-adhesion on an ICAM-1 coated surface (Figures 4-5 and 4-6). The trailing edge stretching is particularly intriguing since there was no apparent shedding of LFA-1 during CTL migration under Pyk2 inhibition (Figure 4-13). I have shown that despite the trailing edge being anchored at one position under Pyk2 inhibition, the trailing edge can still eventually detach from ICAM-1 due to normal forward motion (Figure 4-4A). Integrin turnover at the trailing edge is through an endocytic pathway so that it can recycle back toward the cell front (239). Therefore, I investigated whether LFA-1 distribution is defective under Pyk2 inhibition, which could affect normal CTL migration.

I performed an experiment to determine if PF431396 has an effect on total LFA-1 distribution in CTL. LFA-1 is predominantly localized at the rear end of a migrating lymphocyte with the least amount at the leading edge (240). Quantitatively, the trailing edge should have a higher amount of LFA-1 compared to the leading edge. I assessed the total cellular LFA-1 to determine if there is any difference between the control and PF431396 treated CTL. Visually I found that both control DMSO and PF431396 treated CTL have similar patterns of LFA-1 distribution with the majority of fluorescence polarized to the trailing edge (Figure 4-15A). Computational analysis revealed that the total fluorescence ratio of trailing edge over the leading edge was significantly different between DMSO and PF431396

treated CTL (Figure 4-15B). In the CTL group that was treated with the PF431396, the fluorescence ratio of trailing edge over leading edge was noticeably reduced compared to the control DMSO treated group regardless of the cell morphology. It is unknown whether the altered ratio of LFA-1 distribution stems from changes at the leading edge or the trailing edge, or both. My data suggest that the total intracellular LFA-1 distribution in CTL is altered under Pyk2 inhibition. Based on this finding, Pyk2 inhibition could have an effect on integrin trafficking and/or recycling.
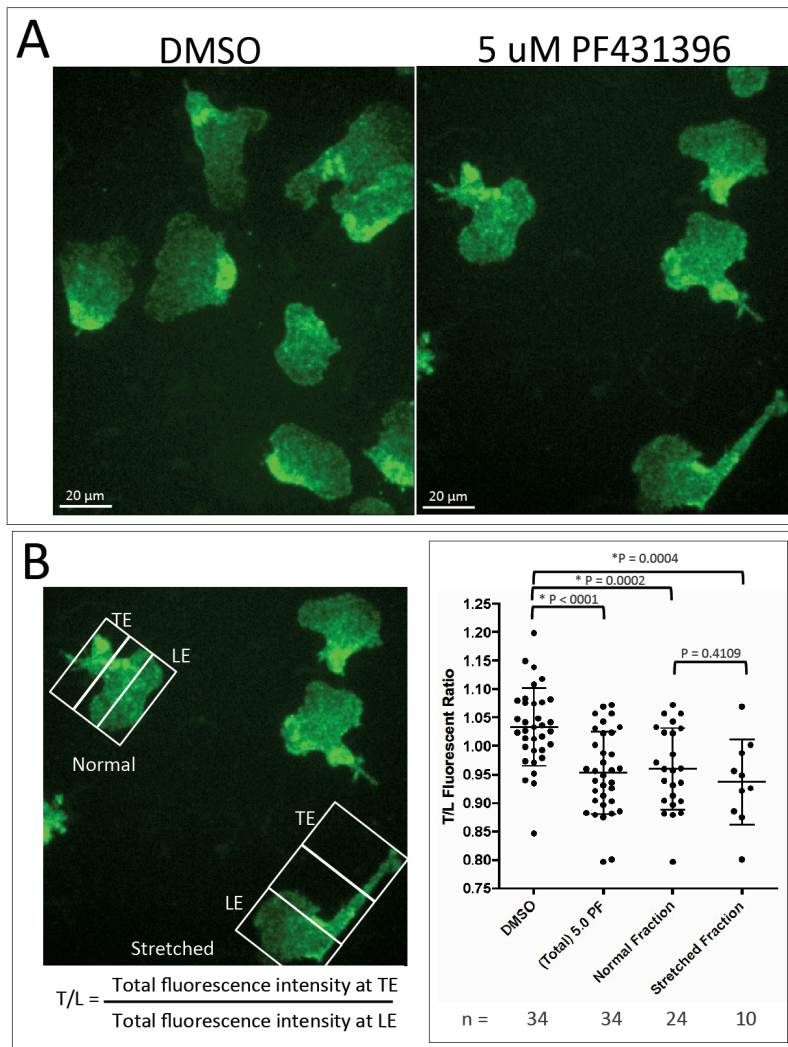
Figure 4-15. Inhibition of Pyk2 altered LFA-1 distribution. (A) Clone 11 CTL were treated with either DMSO or PF431396 for 1 hour at room temperature before transfer to an ICAM-1 coated plate. Cells were incubated at 37°C for 1 hour to allow adhesion and migration followed by fixation with methanol. Cells were stained with FITC-conjugated anti-LFA-1 and images were acquired using a confocal microscope equipped with 40X objective lens. Images were shown as z-stack of the whole cell. (B) An example of how cells were subdivided into leading edge and trailing edge for analysis is shown. Each cell from a z-stack image was equally divided into three sections. The total fluorescence intensity of trailing edge (TE) was divided by the total fluorescence intensity of leading edge (LE). The calculated T/L value from each cell was plotted as a single dot represented in the figure. The population of cells treated with 5.0 μM PF431396 was visually grouped into normal and stretched fraction to indicate that inhibition of Pyk2 altered LFA-1 distribution despite difference in cell morphology. All of the experiments and analysis were performed three times independently and the representative results are shown. Error bar represents mean with standard deviation. P values were obtained using an unpaired t-test.

Knockdown of Pyk2 expression has no significant effect on CD8 T cell trafficking *in-vivo*.

All my previous data indicated that Pyk2 is essential for optimal CTL migration *in vitro*. To evaluate the physiological significance of Pyk2 in CTL migration, I performed an *in vivo* migration experiment to determine whether CTL trafficking to secondary lymphoid organs is also impaired when Pyk2 expression is reduced. The experiment design is outlined in Figure 4-16 top panel. Briefly, Pyk2 siRNA-transfected CD8 T cells were adoptively transferred to a C57BL/6 host through intravenous injection. Using labeled splenocytes as an internal migration control, I measured the number of siRNA transfected CD8 T cells that migrated to spleen and lymph nodes relative to the number of control cells in the same host. After a few attempts I was unable to obtain statistically significant differences between control siRNA and Pyk2 siRNA transfected samples (Figure 4-16 bottom panel). However, a closer look at the data suggested that migration of Pyk2 siRNA transfected CD8 T cells was either equivalent or lower, but never substantially higher than the control siRNA transfected samples. Notably, the overall migration difference between the control and Pyk2 siRNA treated groups was greater in the spleen than in lymph nodes. This may not be surprising since activated CD8 T cell express chemokine receptors such as CXCR3 that direct migration into the periphery (234). The extent of Pyk2 knockdown in these OT-1 CD8$^+$ T cells was similar to the level of Pyk2 knockdown observed in CTL clones AB.1 (Figure 4-2C). Additional western

blot analysis indicated that there was no obvious difference in the level of Pyk2 expression before and after the adoptive transfer. The lack of statistically significant differences in the results may simply be due to a small sample size. My results suggest that Pyk2 may contribute to optimal CTL trafficking to the spleen and lymph nodes *in vivo,* but it is not required under the experimental conditions used for these studies.
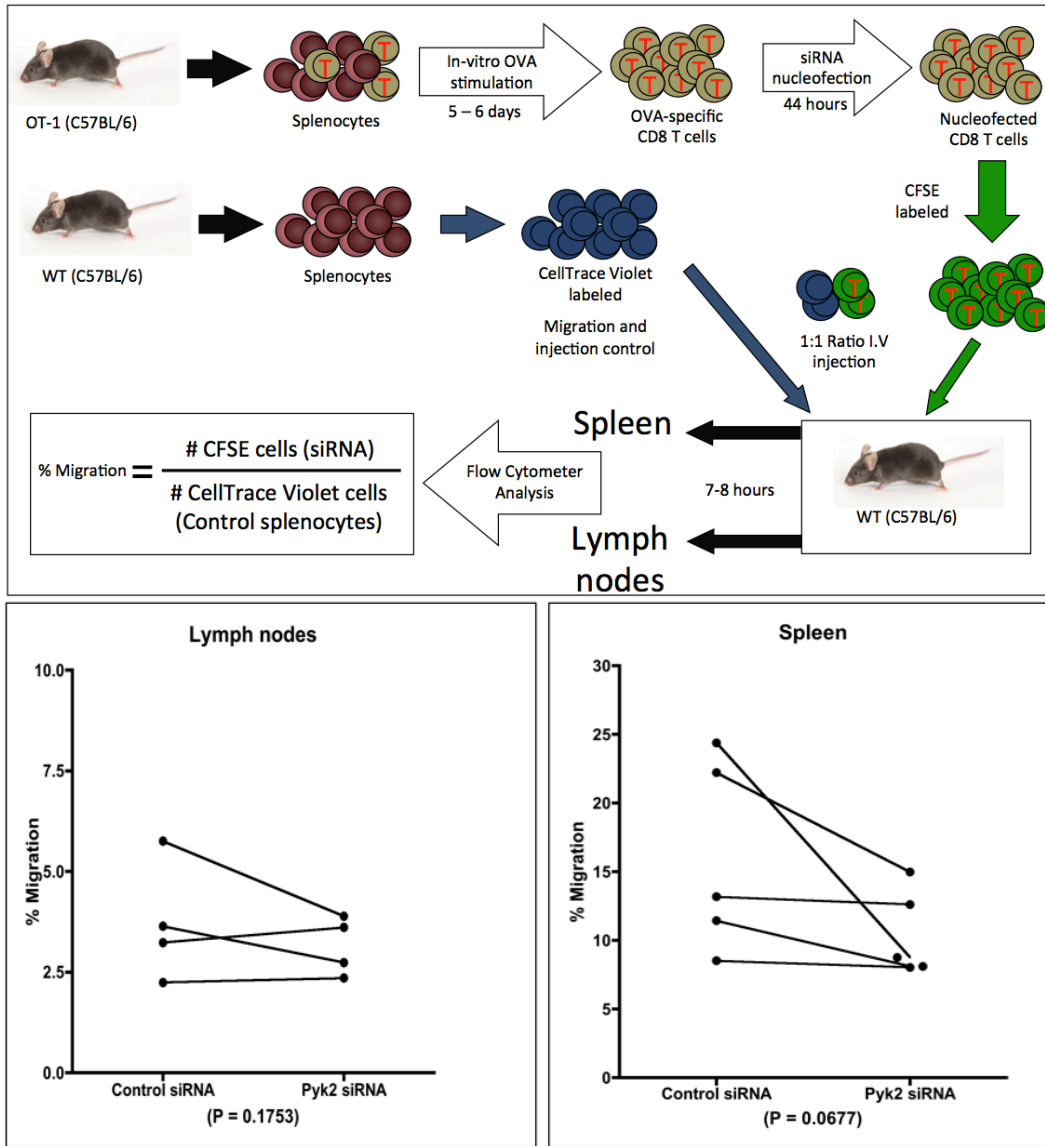
Figure 4-16. *In vivo* **migration of CD8 T cells nucleofected with Pyk2 siRNA.** (Top) The experimental set up for the preparation of CD8 T cells and adoptive transfer assay. Detailed experimental procedures are provided in the materials and methods chapter. (Bottom) The pooled results obtained from all trials and each independent experiment was indicated by a line connection. The percentage of migration was calculated using the indicated equation, as determined per each million of total cells from either spleen or lymph nodes. The experiments were performed independently at least 5 times and the pooled results are shown. P values were obtained using a paired t-test.

Pyk2 regulates cell contact dependent migration of CTL.

To determine if Pyk2 regulates CTL migration through tissues, I developed an *in vitro* assay to examine the contribution of Pyk2 to CTL migration through a by-stander cell layer (Figure 4-17A). In this *in vitro* migration assay, I anticipated that under Pyk2 knockdown or inhibition conditions, CTL would migrate slower than control samples through a layer of by-stander cells that do not have the antigen recognized by the CTL before reaching the antigen-bearing target cells. I assessed the extent of CTL degranulation, as measured by granzyme A release, as an indicator that CTL had reached the target cells. I established that knockdown of Pyk2 has no significant effect on CTL degranulation upon direct stimulation with target cells (Figure 4-17B).

As seen in Figure 4-17C, CTL degranulation from the control siRNA transfected group was successively lower as the amount of by-stander cells increased. Similar trend was observed in Pyk2 siRNA transfected CTL group. This indicates that the CTL require more time to reach the target cells as the number of by-stander cells increases. There was no significant different in degranulation between the control and Pyk2 siRNA transfected CTL when no bystander cells is involved (P value = 0.4913). In the presence of bystander cells, the degranulation of CTL transfected with Pyk2 siRNA was significantly reduced when comparing to the corresponding control group. This indicates that the ability for CTL to migrate through a bystander cell layer is impaired when Pyk2 expression is reduced.
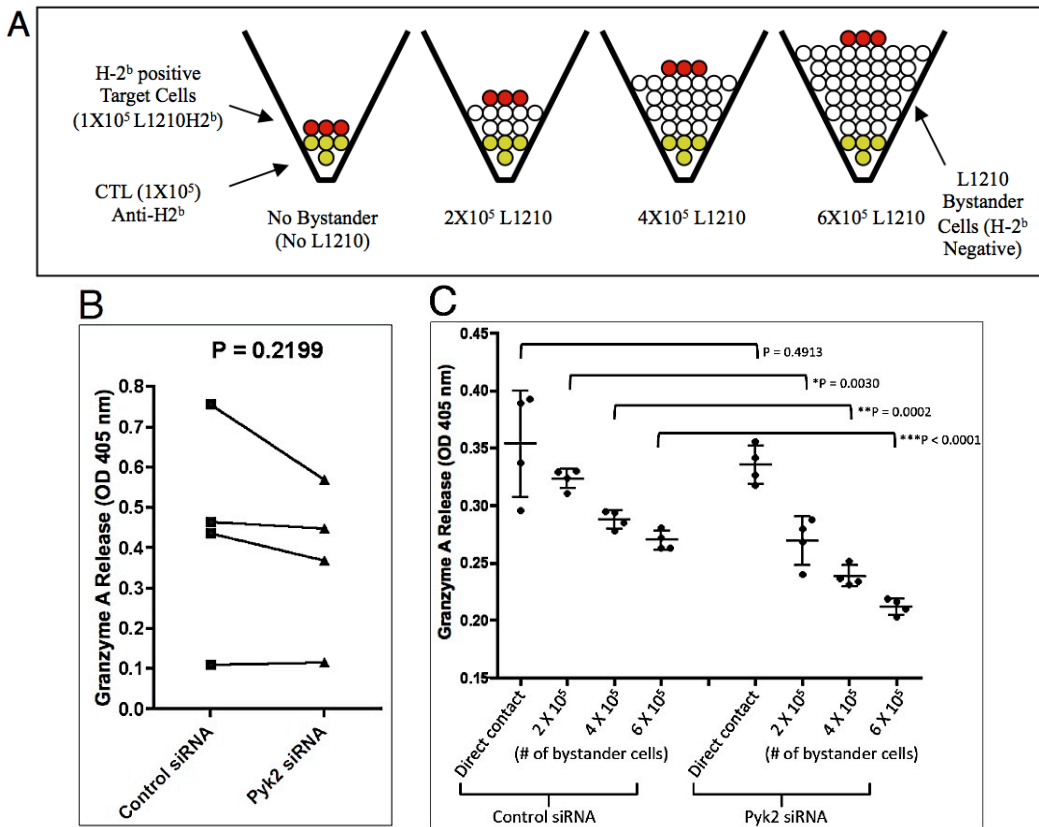
Figure 4-17. Knockdown of Pyk2 delays CTL migration toward target cells as measured by CTL degranulation. (A) Schematic diagram for the general experiment set up for each condition. Details were described in the materials and methods. CTL clone AB.1 were treated with PF431396 or DMSO control followed by centrifugation on a 96 well V-bottom plate. Various amounts of bystander cells (H-2^b negative) were added and centrifuged on top of the CTL. Target cells were added last without centrifugation and incubated at 37°C for 8 hours. Sample supernatants were collected and assayed for granzyme A activity as a measure of CTL degranulation, using an established colorimetric assay. (B) Control siRNA or Pyk2 siRNA transfected CTL were mixed with L1210 target cells (H-2^b positive) at a 1:1 ratio. Four independent experiments are shown. Each dot represents the mean value of several colorimetric measurements. P value was obtained using a paired t test. (C) The extent of degranulation was determined for each CTL group. Four colorimetric measurements were determined for each sample. Error bar represents mean with standard deviation. P values were determined using unpaired t-test for each corresponding condition to evaluate the statistical difference between control siRNA and Pyk2 siRNA transfected CTL groups. The experiment was performed independent three times and the representative data are shown.

C. Discussion

In this chapter I have used three distinct methods to manipulate Pyk2 to determine its role in CTL migration. I found that Pyk2 contributes to the initial adhesion of CTL on an ICAM-1 coated surface (Figure 4-2), but it is not absolutely required for CTL adhesion to an ICAM-1 surface at later time points (Figure 4-3). Analysis of live-cell images revealed that CTL have a significant defect in their ability to de-adhere from ICAM-1 at the trailing edge when Pyk2 function is compromised (Figures 4-4 to 4-8). I found that ectopically expressed Pyk2 localizes to the ICAM-1 contact sites (Figure 4-10) and comparison of CTL expressing different Pyk2 domains suggests that the FAT domain alone was responsible for the de-adhesion defect (Figures 4-4, 4-6 and 4-8). I also found that Pyk2 phosphorylated on different tyrosines have distinct cellular localization in CTL, and tyrosine 881 phosphorylated Pyk2 preferentially localizes to the trailing edge (Figure 4-11). Taken together, these results indicate that the C-terminal FAT domain of Pyk2 is important for regulation of CTL de-adhesion.

My data show that inhibition or knockdown of Pyk2 impairs the ability of CTL to establish early adhesion to ICAM-1 upon initial engagement (Figure 4-2). This is consistent with a study examining adhesion of CD8 T cells from Pyk2 knockout mice where a significant decrease in cell adhesion on plate-bound ICAM-1 was observed (166). Since CTL subsequently restored adhesion to ICAM-1 under Pyk2 inhibition (Figure 4-3), Pyk2 is not required for the tight adhesion that occurs at a later stage of the adhesion

process. How Pyk2 facilitates the establishment of cell adhesion is currently unknown. My data show that Pyk2 is targeted to the site of integrin signaling (Figure 4-10) and it is tyrosine phosphorylated on Y579 and Y580 at the leading edge (Figure 4-11). This suggests that the kinase activity of Pyk2 at the leading edge is important for facilitating the CTL adhesion upon integrin engagement. Evidence to support this is given by the fact that macrophages derived from Pyk2-/- mice exhibit a delay in the leading edge extension in response to chemokine stimulation (164). In my experimental conditions, I did not observe an overt defect or delay in the CTL leading edge formation when Pyk2 is inhibited (Figure 4-4). However, since CTL were not subjected to a chemokine gradient in the migration analysis, whether Pyk2 inhibition could affect CTL leading edge formation upon chemokine stimulation is unknown. Nonetheless, a defect in CTL migration was clearly observed when Pyk2 was inhibited with or without chemokine (Figures 4-4 and 4-9).

Deregulation of Pyk2 impairs CTL de-adhesion on plate-bound ICAM-1 (Figure 4-4) and consequently reduced the net motility of CTL (Figures 4-5 to 4-8). I determined that the reduction in chemotaxis when Pyk2 was inhibited was not due to a defect in cell adhesion (Figure 4-9). The observed de-adhesion defect in Pyk2-inhibited CTL provides a plausible explanation for the reduced chemotactic response reported in both Pyk2-deficient macrophages and CD8 T cells (164, 166). Interestingly, unlike the Pyk2-deficient CD8 T cells that were unable to adhere on ICAM-1, Pyk2-deficient macrophages were able to adhere but the cell polarity was altered (164,

166). I found that the majority of the CTL were able to establish adhesion on plate-bound ICAM-1 within the first 10 to 15 minutes. In the presence of PF431396, CTL require 20 to 30 minutes to establish adhesion on plate-bound ICAM-1. Perhaps adhesion could have been observed in the Pyk2-/- CD8 T cell study if the cells were allowed to incubate for longer on the plate-bound ICAM-1 surface (166). In conditions where CTL were expressing the Pyk2 C-terminal FAT domain, cell motility can be observed after adhesion has been established. However, when these cells were incubated on plate-bound ICAM-1 for longer than 4 hours, the cells became immobile and lost their migration phenotype. The immobile, FAT-domain expressing CTL look strikingly similar to the Pyk2-deficient macrophages, which display altered polarity characterized by multiple lamellipodia extensions toward different directions (164). My detailed kinetic study in CTL provides an explanation to address the difference in phenotypes between Pyk2-/- CD8 T cell and macrophage.

My data show that normal de-adhesion at the trailing edge is disrupted in cells expressing the Pyk2 FAT domain (Figure 4-4). The confocal images also suggest that the FAT domain is sufficient to localize at the contact site and form elongated structures that resemble focal adhesion complexes at the trailing edge (Figure 4-10). Since these elongated structures are not normally observed in the control CTL (Figure 4-4), it is possible that the Pyk2 FAT domain interferes with endogenous Pyk2 Y881 phosphorylation at the trailing edge (Figure 4-11). In support of this idea, it

was shown that expression of the C-terminal domain of FAK (FRNK) reduces Y925 (equivalent to Y881 on Pyk2) phosphorylation (241). Expression of the Pyk2 FAT-domain could potentially block endogenous Pyk2 Y881 phosphorylation, which may serve an important role in trailing edge de-adhesion. Furthermore, knockdown of Pyk2 expression yields a similar defective trailing edge phenotype (Figure 4-3) as that seen in cells expressing Pyk2 FAT domain (Figure 4-4), implying that the FAT domain may compete with endogenous Pyk2 for the substrate or regulatory factors that are important for normal de-adhesion processes.

Inhibition of calpain severely compromises human T cell migration on ICAM-1 (71). I speculated that Pyk2 and calpain operate under the same pathway to regulate integrin-dependent CTL migration (Figure 4-12). However, my data indicate that while calpain inhibition induces LFA-1 shedding, there is no obvious LFA-1 shedding when Pyk2 is inhibited (Figures 4-13 and 4-14). This suggests that LFA-1 remains bound strongly to ICAM-1 under calpain inhibition but manages to detach from ICAM-1 when Pyk2 is inhibited. Intriguingly, I found that inhibition of Pyk2 deregulates the intracellular distribution of LFA-1 (Figure 4-15). The mechanism of integrin trafficking and recycling has only been recently described and there is no direct evidence in the literature to suggest that Pyk2 is involved in the process (222). My data show that Pyk2 can regulate some aspects of LFA-1 turnover in CTL. Whether Pyk2 plays a role in integrin endocytosis at the trailing edge, intracellular integrin trafficking, or exocytosis at the leading

edge is unknown. Nonetheless, Pyk2 appears to be the major signaling effector downstream of LFA-1 since Pyk2-deficient mice have a similar T cell phenotype as αL subunit of LFA-1 deficient mice (166). This study is the first demonstration that Pyk2 can respond to LFA-1 signaling as well as regulate LFA-1 distribution.

My results in this chapter highlight Pyk2 as an important regulator of CTL de-adhesion. Inhibition of Pyk2 activity has been proposed as a potential treatment for cancers that have elevated Pyk2 expression and activation (174, 175). However, deregulation of Pyk2 certainly reduces the ability of CTL to efficiently reach the target cell thus potentially impairing immune surveilance and tumor cell clearance. The influence of any Pyk2 inhibitor on CTL responses in addition to their effects on cancer cells must be considered.

CHAPTER 5

PYK2 REGULATES CTL-MEDIATED CYTOTOXICITY

A. Introduction

CTL recognize target cells through TCR binding specific antigen in the context of MHC. As few as 3 peptide:MHC complexes are sufficient to induce CTL to kill their cognate target (242). Experimentally, CTL are activated by TCR crosslinking using soluble anti-CD3 antibodies in suspension or by stimulation on an immobilized anti-CD3 antibody coated surface. In order to trigger a degranulation response, CTL must be stimulated on an immobilized anti-CD3 coated surface that provides a sustained and directional signal (95).

The MTOC, or centrosome, serves as a command center to direct CTL cytolytic granules toward the target cell synapse for subsequent granule exocytosis (243). The MTOC is characteristically positioned near the trailing edge of migrating CTL, but rapidly re-orientates around the nucleus and translocates to the TCR signaling complex after target cell recognition (76). The kinetic movement and quantity of cytolytic granule exocytosis toward the target cell is governed by the signal strength transduced by the TCR (244). A study showed that a single mutation in the cognate peptide can trigger MTOC translocation toward the target without significant granule movement or exocytosis (94). This highlights the specificity and sensitivity of CTL recognition as well as suggesting that there are differential signaling requirements between MTOC polarization and cytolytic granule movement toward target cells (245).

The signaling mechanism that governs CTL-mediated cytotoxicity is gradually emerging. After TCR is activated, Fyn controls the signals required for MTOC reorientation around the nucleus while Lck mediates MTOC translocation to the membrane at the site of contact with the target cell (92). Further downstream along the TCR signaling pathway, the production of DAG as a result of PLCγ activation is sufficient to drive MTOC polarization toward the plasma membrane in CD4 T cells (246). The accumulation of DAG proximal to TCR signaling complex directs the sequential recruitment of selective novel PKC (nPKC) family members including PKCε and PKCη followed by PKCθ (247). It is speculated that while PKCε and PKCη control the early polarization of MTOC to the immune synapse, PKCθ regulates MTOC positional refinement at the membrane (49). The regulation by nPKC proteins indicate that MTOC polarization does not require Ca^{2+} in CD4 T cells, and this was confirmed experimentally using Ca^{2+} chelating agents (246). In contrast, Ca^{2+} is absolutely required for CTL degranulation to occur (248). The intensity of Ca^{2+} mobilization correlates with the kinetics of cytolytic granule movement toward the immune synapse (244). Although it has not been demonstrated in CTL, the Ca^{2+}-dependent degranulation mechanism may involve Munc13-4, which is required for granule fusion to the plasma membrane (249). Other proteins critical for vesicle fusion, such as Munc18-2 and Syntaxin 11, act downstream of Munc13-4 but are not dependent on Ca^{2+} (97). These studies suggest that Ca^{2+}-dependent effector molecules play a specific role in some aspects of cytolytic granule fusion to the target cell.

The earliest evidence of a role for Pyk2 in killer cell function came from studies of natural killer cells (168, 169). One study showed that the expression of kinase-dead Pyk2, but not the wild-type Pyk2, impaired NK cell lysis of targets (168). Another study showed that either expression of wild-type or kinase-dead Pyk2 significantly reduces NK cell-mediated cytotoxicity (169). The subtle differences between these two studies can likely be attributed to the level of Pyk2 expression. In addition, Pyk2 is required for integrin-mediated neutrophil degranulation (170). These reports collectively indicate that Pyk2 is an important regulator of killer cell-mediated cytotoxicity and degranulation.

It has been established that stimulation with anti-CD3 antibody alone is sufficient to induce MTOC reorientation (160, 250). However, one group demonstrated that anti-CD3 mediated MTOC reorientation does not occur in T cells derived from CD11a (LFA-1 alpha subunit) knockout mice (251). This demonstrates that LFA-1-dependent signaling is required for MTOC reorientation downstream of TCR activation. In addition, tyrosine phosphorylated Pyk2 is found at the CTL immune synapse upon target cell stimulation (161). The fact that Pyk2 is tyrosine phosphorylated in response to both TCR and LFA-1 signaling activation (Figure 3-9A & 4-1A), and its association with the immune synapse, led me to speculate that Pyk2 is important for CTL effector function.

B. Results

Inhibition of Pyk2 suppresses target cell mediated CTL degranulation

To determine whether Pyk2 regulates CTL degranulation, I first established the conditions to measure CTL degranulation induced by target cell stimulation. I performed the experiment using CTL clone 3/4, which is specific for the H-2D^b MHC class I complex bound to the peptide (ASNENMETM) derived from influenza nucleoprotein (NP) (180). The target cells used were an EL4 lymphoma cell line, which expresses the H-2D^b MHC class I haplotype. I stimulated CTL clone 3/4 with EL4 that were incubated with various amounts of NP peptide. I then measured the surface expression of the lysosome-associated membrane protein 1 (LAMP-1 or CD107a) as an indirect measurement of degranulation (252). In the control experiment (Figure 5-1A), there was a successive increase in the percentage of CTL clone 3/4 that express CD107a in response to EL4 treated with increasing amounts of NP peptide. In two other repeated trials, I found that there are variations in the extent of overall CTL clone 3/4 CD107a expression from one experiment to another (maximum 12% and 25% CD107a expression, respectively, of CTL clone 3/4 CD107a expression induced by stimulation with EL4 treated with 10 μM NP peptide). In spite of the variation, maximal CTL clone 3/4 CD107a expression was generally observed when using 10 μM NP peptides. The negative control condition showed that the presence of chelator EGTA, which inhibits CD107a expression (248), thus validating my

assay. In the absence of NP peptide, the background CD107a expression was minimal in CTL clone 3/4.

To determine if Pyk2 is required for CTL degranulation, I treated EL4 target cells with 10 μM of NP-peptide then stimulated CTL clone 3/4 in the presence of various amount of PF431396. As shown in Figure 5-1B, degranulation of CTL clone 3/4 was inhibited by the presence of PF431396 in a dose dependent manner. The number of CTL clone 3/4 that degranulated was reduced by more than half at 5.0 μM PF431396 concentration. I concluded that target cell induced CTL degranulation requires Pyk2 kinase activity.
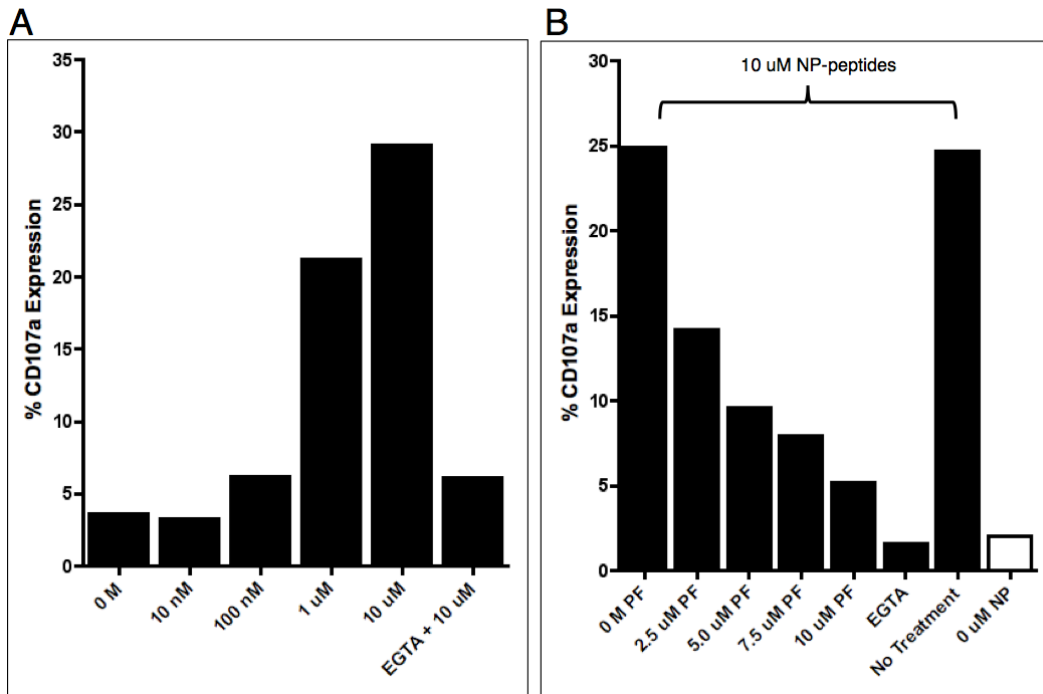
Figure 5-1. Pyk2 inhibition reduces the quantity of NP-specific CTL degranulation in response to target cell stimulation. (A) EL4 target cells were first labeled with Cell Tracker Blue followed by incubation with the NP-peptide (ASNENMETM) at the indicated concentration for 1 hour at 37°C. CTL clone 3/4 CTL were mixed with NP-peptide pulsed EL4 at 1:3 ratios before centrifuging gently at 4°C to induce conjugate formation. CTL:EL4 conjugates were activated for 15 minutes at 37°C in the presence of FITC-labeled anti-CD107a antibody. As a negative control, 4 mM EGTA was added to the sample at room temperature for 20 minutes prior to conjugate formation. After CTL activation, cell conjugates were disrupted by vortexing in the presence of 5 mM EDTA. Samples were analyzed immediately using FACSCanto. The percentage of surface CD107a expressing CTL was determined by gating on the Cell Tracker Blue negative population to exclude EL4 cells. (B) The experiment was performed as described in part (A), with the exception that CTL:EL4 conjugates were mixed in a 1:4 ratio. All of the CTL stimulation was performed using EL4 cells treated with 10 μM NP-peptide except for the open bar, which has no peptide added. The experiment was performed in the presence of the indicated concentration of PF431396 (PF). No treatment means in the absence of DMSO carrier control. The experiments were performed three times independently and representative data are shown.

To further validate that Pyk2 inhibition impairs CTL degranulation, I performed a similar experiment using a different CTL clone. In addition, I used an established colorimetric-based enzymatic assay to detect granzyme A (or serine esterase) release after CTL stimulation (248). As shown in Figure 5-2A, the allo-reactive CTL clone AB.1 was activated by target cells L1210 expressing the $H\text{-}2K^b$ MHC class I haplotype (L1210Kb) and degranulation was assessed by CD107a surface expression. There was no induction of CD107a expression in CTL clone AB.1 stimulated by target cells that lacked $H\text{-}2K^b$ MHC class I expression (L1210) or stimulated with L1210Kb cells in the presence of EGTA. In conditions that were stimulated by L1210Kb, CTL expression of CD107a was strongly inhibited by PF431396. Similar trends were observed in experiments that measured the relative quantity of granzyme A released (Figure 5-2B). My data show that both CD107a expression and granzyme A release assays are comparable for measurement of CTL degranulation. These results further support that inhibition of Pyk2 impairs CTL degranulation induced by target cell stimulation.
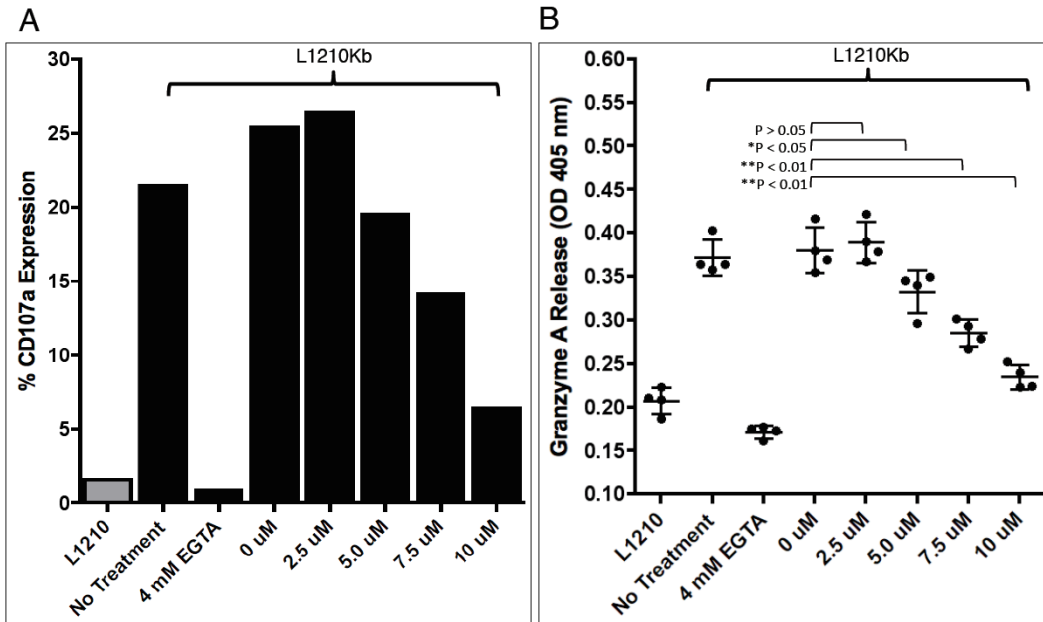
Figure 5-2. Pyk2 inhibition reduced alloreactive-CTL degranulation in response to target cell stimulation. (A) L1210 target cells stably expressing the MHC-I H2-K^b/D^d (L1210Kb) were labeled with Cell Tracker Blue, followed by mixing with CTL clone AB.1 at a 1:1 ratio. Parental L1210 cells, which do not express the MHC-I H2-K^b/D^d, were used as a negative control. Conjugation and analysis was performed as described in Figure 5-1A, with the exception that conjugation was induced and then incubated for 3 hours at 37°C prior to analysis. The experiment was performed in the presence of PF431396 and FITC-conjugated anti-CD107a antibodies throughout. (B) A fraction of samples from each condition described in experiment (A) were incubated separately without CD107a antibody. After incubation at 37°C for 4 hours the supernatants were obtained to assay for granzyme A activity as described in materials and methods. Neither L1210 nor L1210Kb cells were labeled with Cell Tracker Blue. The error bars represent the mean and standard deviation of quadruplicate samples for each condition in a single experiment. All experiments were performed independently at least three times and the representative data are shown. The P value was obtained using one-way ANOVA analysis, which is less than 0.0001, with Dunnett's multiple comparison test result shown.

Pyk2 inhibition impairs conjugate formation between CTL and target cells.

The extent of CTL degranulation is regulated by the duration and strength of TCR:peptide:MHC interactions as well as adhesion between CTL and its target (253, 254). My results from the previous chapter showed that Pyk2 regulates optimal ICAM-1 dependent adhesion (Figure 4-2). Therefore, the quality of conjugation between CTL and its target may have contributed to the results in Figure 5-1 and 5-2. To determine if Pyk2 regulates CTL binding to its target, I performed experiments to determine the level of conjugation in the presence of PF431396. As shown in Figure 5-3, CTL clone AB.1 bound L1210Kb cells, which are antigen-dependent in the context of MHC class I H-2K^b, to a higher degree than to the non-antigen-expressing L1210 cells. In the presence of PF431396, both antigen-specific (L1210Kb) and antigen-independent (L1210) mediated CTL conjugation were reduced. This implies that inhibition of Pyk2 impairs the quality of cell-to-cell contact regardless of antigen. The difference between CTL binding to L1210Kb and L1210 were similar at the 3-minute time point in the absence of PF431396. As the experiment progressed, CTL binding to L1210Kb was sustained while CTL binding to L1210 was gradually reduced. The observed defect in CTL adhesion is consistent with my results in Chapter 4, where I have shown that CTL are defective in binding an ICAM-1 coated substrate under PF431396 treatment (Figure 4-2A).
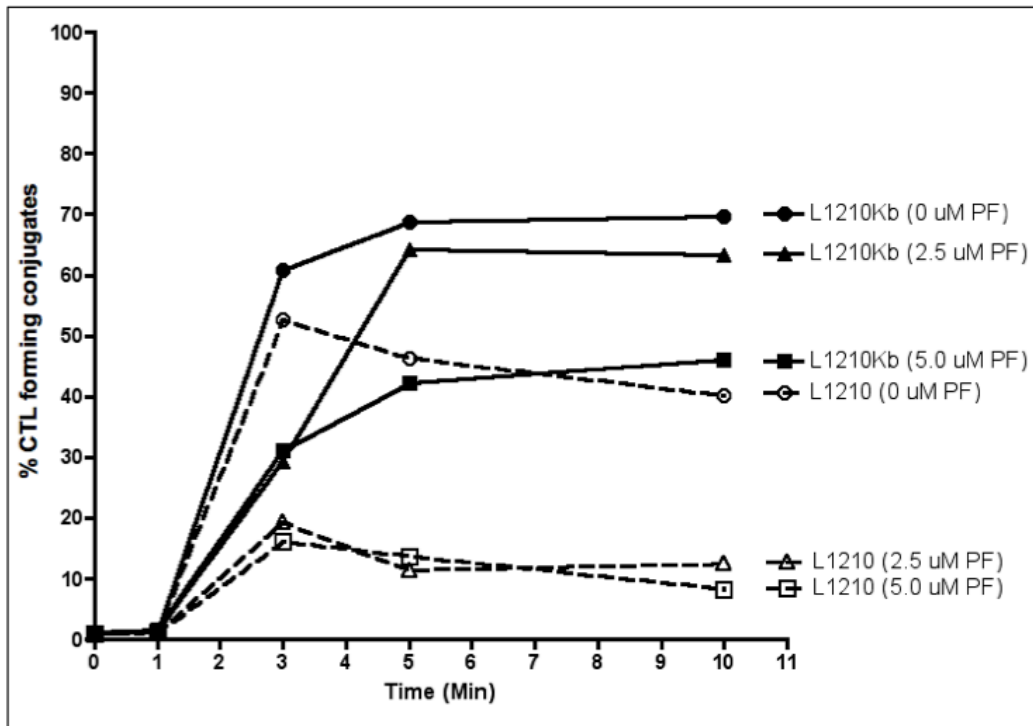
Figure 5-3. Pyk2 is required for optimal CTL adhesion to target cells. CTL clone AB.1 were labeled with Cell Tracker Green, while L1210 and L1210Kb cells were labeled with Cell Tracker Blue as described in Materials and Methods. All cells were treated with either DMSO or PF431396 for 20 minutes at room temperature prior to mixing CTL with target cells at a 1:2 ratio. Conjugates were induced by brief centrifugation at 4°C (as described in methods) followed by incubation at 37°C for the indicated time and then vortexed to disrupt cell pellets. Cells were fixed immediately by adding equal volume of 4% paraformaldehyde after vortexing and analyzed using FACSCanto. The percentage of conjugates was calculated based on the cell proportion that is positive for both Cell Tracker Green and Cell Tracker Blue among the total number of CTL. The experiment was performed twice independently and representative data are shown.

Pyk2 inhibition impairs the intrinsic ability of CTL to degranulate.

It was unknown whether the observed defect in CTL degranulation (Figure 5-2) was a result of an impaired T cell activation due to poor conjugate formation (Figure 5-3) or it was caused by a defect in the intrinsic ability of the CTL to degranulate under Pyk2 inhibition. To address this question, I used a different approach to stimulate CTL degranulation in the absence of target cells under Pyk2 inhibition. We previously demonstrated that CTL degranulation can be elicited by stimulation with anti-CD3 antibodies immobilized on a solid surface, which provides sustained and directional TCR signaling activation (95). I found that CTL degranulation induced by immobilized anti-CD3 antibodies was inhibited by PF431396 in a dose-dependent manner (Figure 5-4A). The inhibitory effect can be seen in three different CTL clones, although there were variations in inhibition among them. The results show that Pyk2 is important for optimal CTL degranulation triggered by TCR signaling, and Pyk2 regulates the intrinsic ability of CTL to degranulate.

CTL degranulation can also be induced by a combined stimulation of PMA and ionomycin (P/I), which mimic DAG response and activates Ca^{2+}-dependent signaling pathways required for degranulation, respectively. This method effectively by-passes the requirement for TCR triggering, thus allowing us to focus on the pathways that control degranulation (255). I performed parallel experiments to compare TCR- and P/I-induced CTL degranulation in the presence of PF431396. As shown in Figure 5-4B, both

immobilized anti-CD3 antibodies and P/I stimulation resulted in similar quantities of granzyme A release after 2 hours of stimulation (Figure 5-4B left). The extent of P/I stimulated degranulation was slightly reduced in contrast to anti-CD3 stimulation at a later time point (Figure 5-4B right). The difference may reflect the duration and effectiveness of the stimulus. In either case, it is clear that PF431396 inhibited CTL degranulation. This further supports the function of Pyk2 in the regulation of CTL degranulation.

In the previous chapter, I showed that knockdown Pyk2 expression has no significant effect on target cell mediated CTL degranulation (Figure 4-17B). Whether reduced Pyk2 protein expression effects anti-CD3 mediated degranulation is unknown. To answer this question, I transfected CTL with control or a combined pool of Pyk2 siRNA for 48 hours, then stimulated CTL on an immobilized anti-CD3 antibodies coated surface. As seen in Figure 5-5, the extent of CTL degranulation was consistently reduced but not significantly inhibited in both trials. The results indicate that optimal Pyk2 protein expression may contribute to, but is not absolutely required for, CTL degranulation.
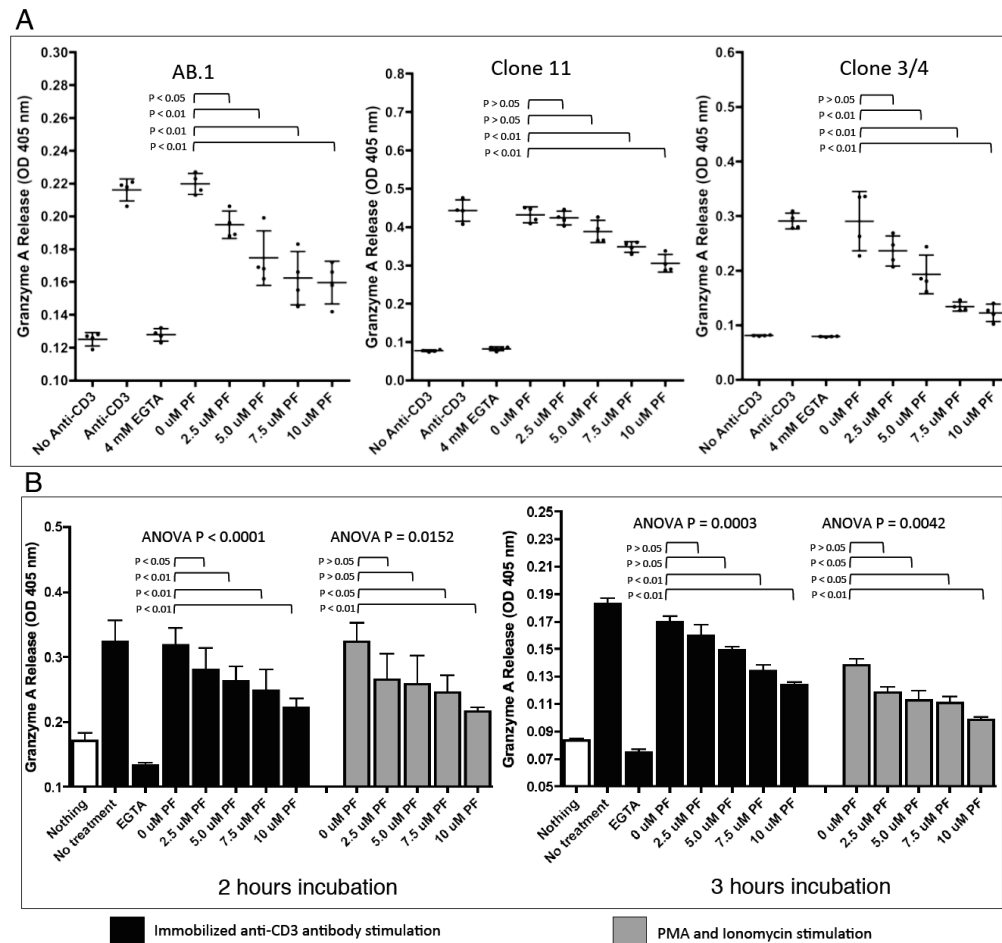
Figure 5-4. Pyk2 is important for optimal CTL degranulation. (A) CTL clones were treated with DMSO control, 4 mM EGTA or the indicated amount of PF431396 at room temperature for at least 30 minutes. For each test condition, 1.5×10^5 CTL were transferred to culture plates coated with 10 μg/ml of 145-2C11 anti-CD3 antibody. Cells incubated on culture plates without anti-CD3 antibody served as a negative control. All conditions were blocked with 2% BSA prior to cell seeding. All cells were incubated at 37°C for 4 hours with or without PF431396 before obtaining the supernatant to assay for granzyme A activity. Experiments using CTL clone AB.1 and CTL clone 11 were performed 3 and 2 times, respectively. Experiments using CTL clone 3/4 were performed once. Each experiment was performed in quadruplicate and the data from a single experiment is shown. All P values obtained from a one-way ANOVA analysis are less than 0.0001. (B) The activation and treatment of CTL clone AB.1 using anti-CD3 antibody (Black box) was described in part (A). In the experiment that used PMA and ionomycin stimulation (Grey box), 100 ng/ml PMA and 2 μM ionomycin were used simultaneously to stimulate the CTL followed by 37°C incubation. This experiment was performed independently 3 times. Representative results from a single experiment are shown. The error bars represent the mean and standard deviation of granzyme A activity measured.
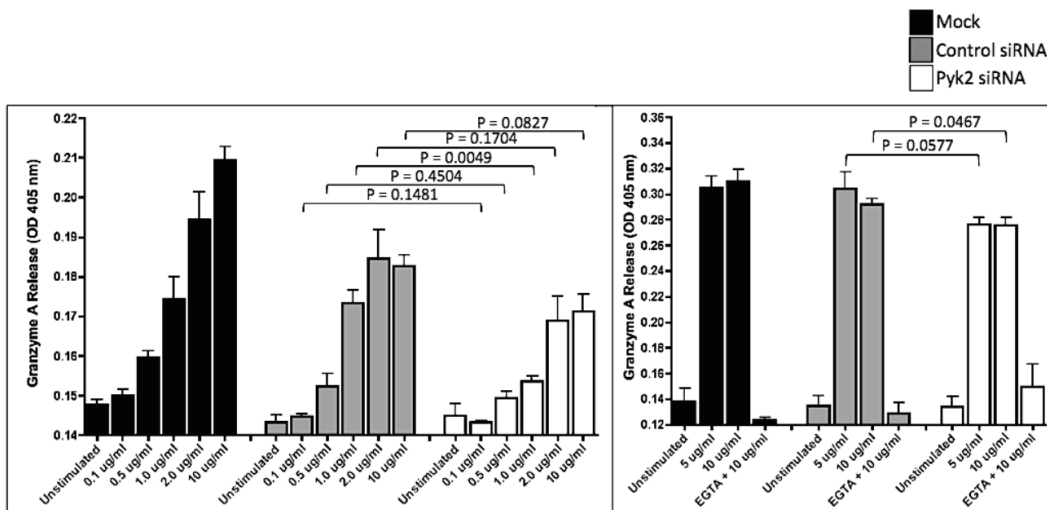
Figure 5-5. **Knockdown of Pyk2 reduces TCR-mediated CTL degranulation.** CTL clone AB.1 cells were transfected with the indicated siRNA for 48 hours, followed by transfer to culture wells coated with the indicated concentration of anti-CD3 antibodies. CTL were incubated for 4 hours at 37°C and the supernatant was collected to assay for granzyme A activity. 4 mM EGTA was added as a negative control for degranulation in one of the experiments. The two experiments were performed independently and both results are shown.

Inhibition of Pyk2 impairs target cell-induced MTOC reorientation

Since Pyk2 regulates microtubule stability (165), I hypothesized that the reduction in degranulation is caused by defective MTOC reorientation in CTL. I performed experiments to determine if defective degranulation is due to impaired MTOC reorientation under Pyk2 inhibition. As mentioned in the introduction MTOC is normally located at the trailing edge of migrating CTL but rapidly reorientates around the nucleus and translocates to the TCR upon target cell recognition (76). I stimulated CTL with the peptide-treated cognate target cells in the presence of PF431396 followed by visual examination of conjugates using confocal microcopy to determine the extent of MTOC reorientation.

As shown in Figure 5-6, both CTL clone 3/4 and OT-1 CTL treated with PF431396 showed a moderate reduction in MTOC reorientation toward the target cells. Despite the reduction in MTOC reorientation with increasing doses of PF431396, approximately 50% of conjugates remained unaffected. This suggests that Pyk2 kinase activity only contributes to optimal MTOC reorientation but is not absolutely necessary. Due to the low image resolution, it is unclear whether the re-orientated MTOC remained attached to the nucleus or if it was docking at the plasma membrane. Further experiments using high-resolution imaging would be required to resolve this issue. My data suggest that MTOC reorientation is impaired, or delayed, in CTL stimulated with target cell under Pyk2 inhibition.
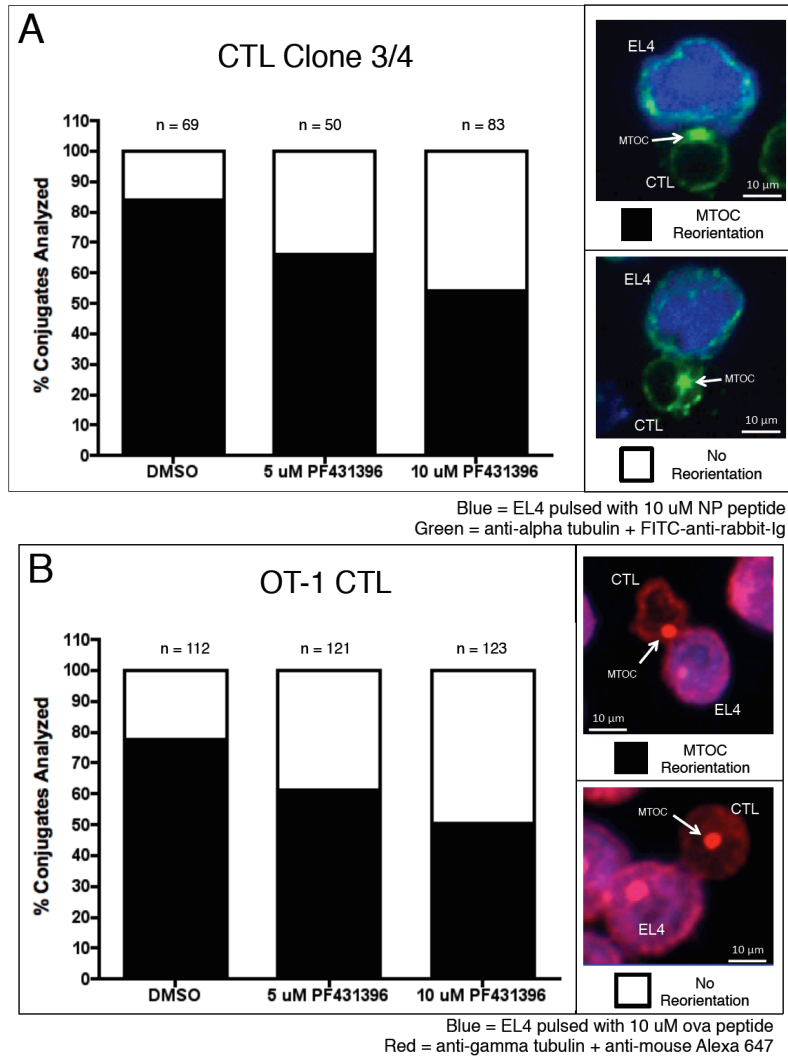
Figure 5-6. Pyk2 contributes to MTOC reorientation. (A) EL4 target cells were labeled with Cell Tracker Blue and then treated with 10 μM NP peptides, followed by incubation with CTL clone 3/4 at a CTL:EL4 ratio of 1:2. CTL were pretreated with the indicated concentration of PF431396 for 1 hour at room temperature. Conjugates were induced by centrifugation and then incubated at 37°C for 10 minutes. After incubation, the conjugates were disrupted then transferred to poly-l-lysine coated imaging slides for another 10 minutes at room temperature. Cells were fixed with paraformaldehyde, then permeabilized and stained with anti-tubulin antibodies followed by the indicated secondary antibodies. This experiment was performed twice and the representative data are shown. (B) The experiment was conducted as described in part A, except that EL4 cells were treated with 10 μM OVA peptides and mixed with *ex-vivo* activated CD8^{+} T cells from OT-1 transgenic mice at a 1:5 effector to target ratio. This experiment was performed once for validation purposes. The images depict the criteria for MTOC reorientation. The number of conjugates analyzed for each condition is shown (n).

168

GFP-coupled Pyk2 is associated with the MTOC

Our research group has recently demonstrated that Pyk2 is localized to the MTOC with paxillin in resting T cells, but after stimulation with target cells Pyk2 is tyrosine phosphorylated and enriched at the contact point (161). In a Pyk2-/- mouse study, Pyk2 is involved in the maintenance of microtubule stability in osteoclasts (165). The localization of Pyk2 with the MTOC and its role in maintenance of microtubule stability suggest that Pyk2 is important for aspects of MTOC function. Since expression of Pyk2 FAT domain has the same inhibitory effect on CTL migration as PF431396 (Figure 4-5 & 4-6), and Pyk2 inhibition impairs MTOC reorientation (Figure 5-6), I transfected the Pyk2 FAT domain or the kinase-dead Pyk2 in CTL to determine if the expression of the specific construct has an inhibitory effect on MTOC reorientation.

First, I have validated that the localization of ectopically expressed Pyk2 to the MTOC is unaffected under my experimental conditions. I co-transfected CTL with individual GFP-coupled Pyk2 constructs and mCherry-tagged tubulin (a known marker for MTOC) for live-cell imaging studies. As shown in Figure 5-7, the MTOC is clearly visible in cells expressing mCherry-tagged tubulin. Each GFP-coupled Pyk2 construct can be seen associated with the MTOC in CTL. This confirmed that the CTL expressing the GFP-coupled Pyk2 construct could be used for the MTOC reorientation study.
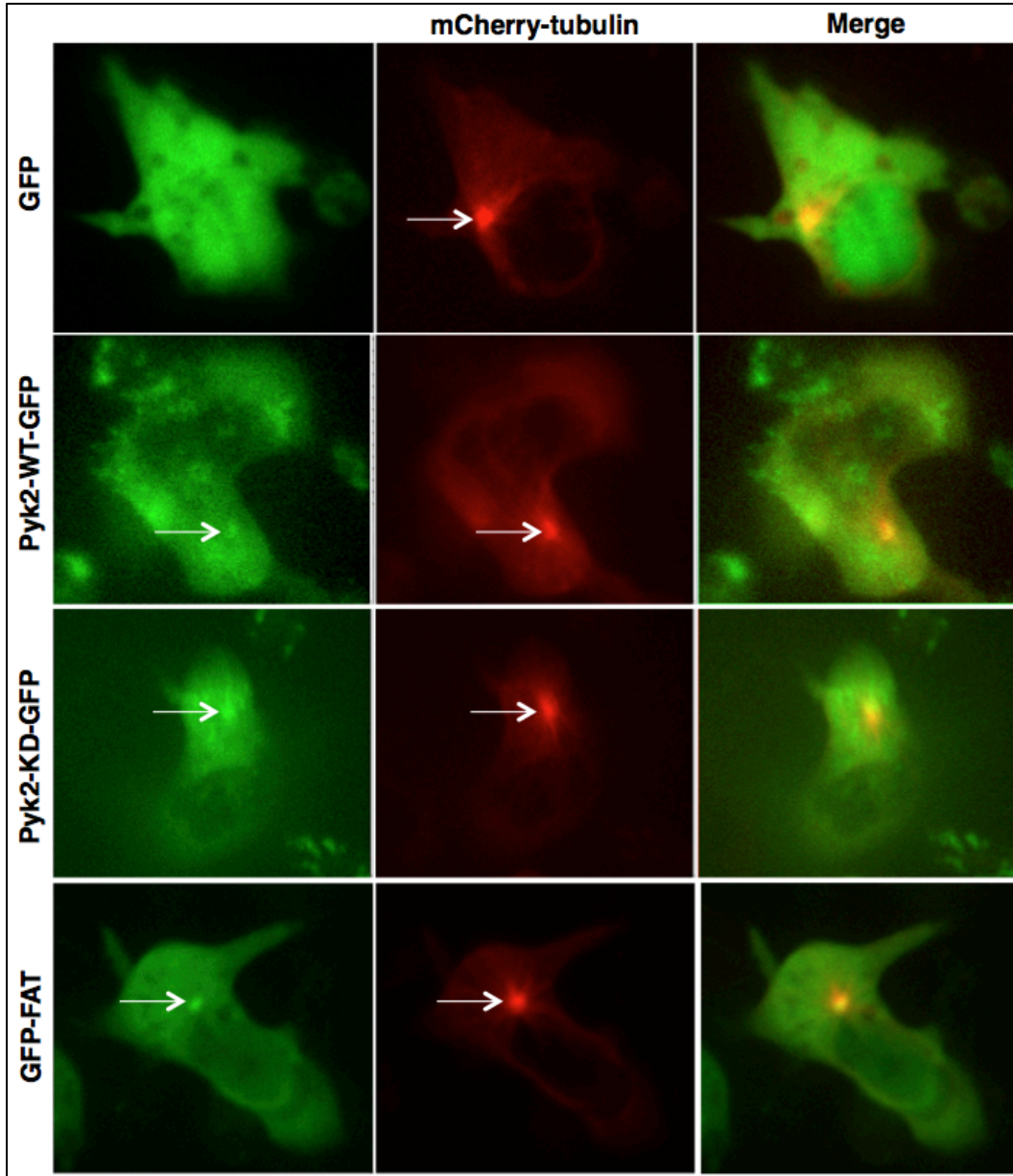
Figure 5-7. GFP-coupled Pyk2 is targeted to the MTOC. CTL clone 11 cells were co-transfected with the indicated GFP-coupled Pyk2 construct and mCherry-coupled alpha tubulin. After 24 hours, cells were transferred to an imaging slide coated with 3 μg/ml ICAM-1. Cells were incubated on the slide for 30 minutes at 37°C to allow for settling and adhesion. Images were acquired using a spinning disk confocal microscope at room temperature. For clarity, the images only show the region focused at the z-stacks, which span the entire MTOC. The images are not a projection of the whole cell. This specific experiment was performed once and at least three cells were examined for each condition. Representative images are shown.

Ectopically expressed Pyk2 in CTL interferes with target cell-induced MTOC reorientation.

The localization of ectopically expressed Pyk2 to the MTOC appeared to be normal under my experimental conditions. This allowed me to examine whether expression of a specific GFP-coupled Pyk2 construct has any inhibitory effect on target cell–induced MTOC reorientation. I transfected CTL with GFP alone, GFP-coupled Pyk2, GFP-coupled kinase-dead Pyk2, or GFP-coupled FAT domain to perform a conjugation experiment followed by evaluation of MTOC reorientation. In this experiment, I focused on analyzing the GFP positive CTL conjugates that correspond to the specific Pyk2 constructs. I found that MTOC reorientation was impaired in both CTL clone 11 and CTL derived from T cells isolated from OT-1 transgenic mice (Figure 5-8). Interestingly, conjugates expressing the kinase-dead Pyk2 exhibit the greatest reduction in MTOC reorientation. This is consistent with my earlier data where inhibition of Pyk2 impaired MTOC reorientation (Figure 5-6). The reduction in MTOC reorientation induced by GFP-tagged wild-type Pyk2 expression is less apparent, whereas the expression of FAT domain was moderate. Although it is unclear if the expression level contributes to the extent of inhibition, my results suggest that Pyk2 is involved in some aspects of MTOC reorientation.
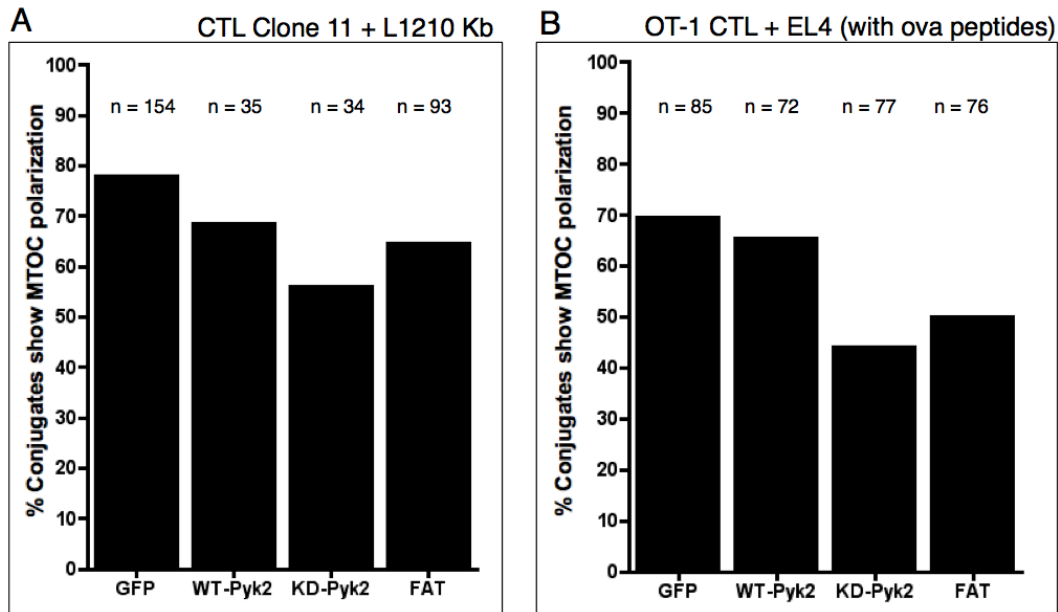
Figure 5-8. Ectopic expression of Pyk2 in CTL interferes with target cell induced MTOC reorientation. (A) CTL clone 11 were transfected with the indicated Pyk2 constructs for 24 hours prior to mixing with the Cell Tracker Blue labeled L1210Kb cells at a 1:5 CTL:L1210Kb ratio. The experiment followed the same protocol as described in Figure 5-6 and in Materials and Methods. Sample acquisition was performed within 24 hours of paraformaldehyde fixation. Only the conjugates with GFP expression were selected for analysis. (B) *Ex-vivo* activated OT-1 CD8$^+$ T cells were transfected with the indicated Pyk2 constructs for 24 hours prior to mixing with Cell Tracker Blue labeled EL4 cells pulsed with 20 μM OVA peptide. Conjugates were mixed in a 1:2 CTL:EL4 ratio followed by centrifuge-induced conjugation. Conjugates were activated at 37°C for 15 minutes. Cells were immunostained for gamma tubulin. Gamma tubulin was visualized using anti-mouse Alexa-647 as the secondary antibody for both experiments. All conjugates were visually scored for the relative position of MTOC to the target cells. This experiment was performed once on CTL clone 11 and once on *ex-vivo* OT-1 CD8$^+$ T cells. The number of conjugates analyzed (n) is indicated above each column.

Expression of paxillin tyrosine mutant in CTL has no effect on MTOC reorientation.

My data indicate that the catalytic function of Pyk2 plays a critical role in CTL degranulation and contributes to optimal MTOC reorientation (Figure 5-4 & 5-6). This suggests that the downstream tyrosine phosphorylation substrates of Pyk2 are responsible for regulating CTL degranulation and MTOC reorientation. Paxillin is a known substrate of Pyk2 (170) and I have demonstrated that treatment with PF431396 strongly inhibits Paxillin tyrosine phosphorylation in CTL (Figure 4-1). In addition, we recently showed that paxillin contributes to MTOC reorientation through its leucine-aspartic acid (LD) domains (160) and it is co-localized with Pyk2 at the MTOC (161). Therefore, paxillin is a likely candidate acting downstream of Pyk2 to regulate MTOC reorientation. To investigate this possibility, I transfected CTL with a GFP-tagged paxillin containing a double tyrosine mutation (Y31F/Y118F) to examine if MTOC reorientation is affected. After analyzing a group of conjugates, I found no difference between the wild-type and Y31F/Y118F paxillin expressing CTL in MTOC reorientation (Figure 5-9). It is possible that the expression of paxillin construct does not act as a dominant negative protein over the endogenous paxillin in CTL. My result here indicates that paxillin double tyrosine mutant Y31F/Y118F has no effect on MTOC reorientation under this particular experimental condition.
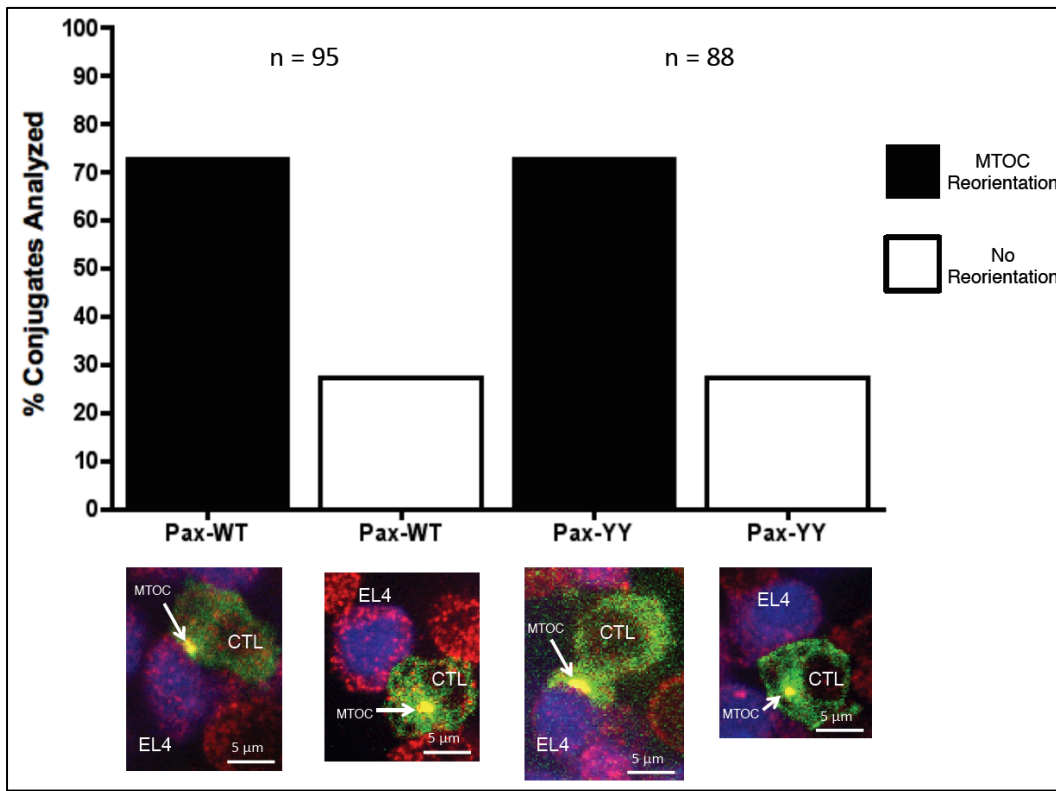
Figure 5-9. Expression of a paxillin tyrosine mutant has no apparent effect on MTOC reorientation. *Ex-vivo* activated OT-1 CD8 T cells were transfected with the indicated paxillin constructs for 24 hours, followed by mixing with Cell Tracker Blue labeled EL4 cells pulsed with 10 μM ova (SIINFEKL) peptide. Cells were mixed together at 1:1 CTL:EL4 ratio and then incubated at 37°C for 15 minutes on a poly-l-lysine coated slide without centrifugation. Cells were fixed with paraformaldehyde and permeabilized then immunostained for gamma tubulin. Gamma tubulin was visualized using anti-mouse Alexa-647 as the secondary antibody. Image acquisition was performed immediately within 24 hours post paraformaldehyde fixation. The images on the bottom show the representative examples of MTOC reorientation for the corresponding group of conjugates. The analysis was focused on CTL that were positive for GFP and the number of conjugates (n) analyzed for each group is indicated. This experiment was performed once as a pilot study.

PF431396 has minimal effect on CTL-mediated target cell lysis.

Pyk2 contributes to CTL intrinsic ability to degranulate (Figure 5-4). It follows that CTL-induced target cell death would be affected by PF431396. To assess the extent of target cell death in the presence of PF431396, I performed a conventional chromium (^{51}Cr) release assay. In order to specifically examine degranulation without potential influence from FasL, I used L1210Kb target cells which have very low level of Fas expression (89). As shown in Figure 5-10, there was a moderate decrease in target cell death over the course of three hours. While the reduction in target cell death was not dramatic, the trend suggests that Pyk2 inhibition affected the quantity of target cell lysis throughout the experiment. According to my data, Pyk2 may contribute to, but is not absolutely required for, CTL-mediated target cell lysis.
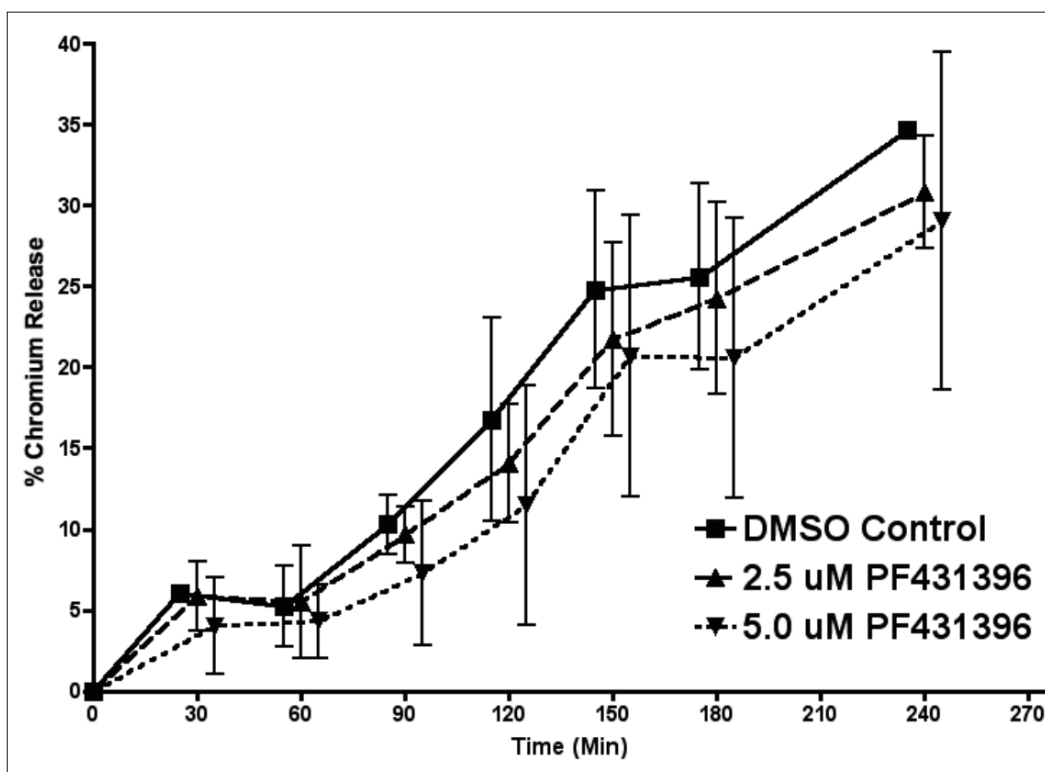
Figure 5-10. PF431396 has minimal effect on CTL-mediated target cell killing. CTL clone AB.1 were pretreated with either DMSO or the indicated PF431396 for 1 hour at room temperature before mixing with ^{51}Cr labeled target cells (L1210Kb) at a 1:1 ratio. CTL and target cells were incubated in the presence of the indicated PF431396 and a small aliquot of the supernatant was obtained at the indicated time points to assay for ^{51}Cr release. Experiments were performed independently three times (by Dong-Er Gong) and the pooled result is shown. Data from each group were deliberately separated by 5 minutes apart for clarity. Each point represents the mean lysis value from three independent experiments and error bars represent the mean and standard error.

C. Discussion

In this chapter I have found that Pyk2 contributes to optimal CTL degranulation and plays a role in MTOC reorientation. Pyk2 might serve a specific role in regulating aspects of CTL degranulation independent of MTOC reposition. A conventional model for CTL degranulation described that MTOC translocation precedes cytolytic granule transport and exocytosis to the target cell (245). However, it has been demonstrated that upon recognition of low avidity antigenic peptide the MTOC is recruited to the immune synapse without subsequent granule polarization and exocytosis (94). This suggests that MTOC reorientation and granule exocytosis are independently regulated. Since Pyk2 is associated with the MTOC and enriched at the contact point between CTL and its target, it is a potential signal modulator to execute optimal CTL degranulation upon target cell recognition.

My data showed that inhibition of Pyk2 results in a substantial reduction, but not a complete block, in CTL degranulation (Figure 5-4). The inhibition of degranulation was more apparent in CTL clone AB.1 and clone 3/4 compared to CTL clone 11. The partial suppression of degranulation was also reported in a study of Pyk2-/- neutrophils (170). It was suggested that Pyk2 regulates a specific subset of neutrophil granules (170). Since CTL cytolytic granules are spatially distinct from the FasL storage compartment (88), it is unknown whether FasL expression is regulated by Pyk2. My results indicate that Pyk2 is important for optimal CTL degranulation.

The observed reduction in CTL degranulation under Pyk2 inhibition may be due to a defect in translocation of cytolytic granules. Whether Pyk2 regulates granule movement along microtubules, granule docking, or membrane fusion is unknown. Currently, there is no direct evidence that Pyk2 is involved in any of these cellular events. My data support a role of Pyk2 in granule trafficking inside CTL since inhibition of Pyk2 leads to deregulation of intracellular LFA-1 distribution (Figure 4-15). This implicates Pyk2 in normal turnover of intracellular trafficking of LFA-1 containing vesicles and perhaps the movement of lysosomal vesicles as well. A recent study showed that siRNA knockdown of paxillin impairs granule polarization in NK cells (256). It is tempting to speculate that Pyk2 phosphorylation of paxillin may be important for polarization of cytolytic granules in CTL.

I found that inhibition of Pyk2 only impaired MTOC reorientation (Figure 5-6), which is required for directed granule exocytosis toward the target cell. It is likely that the reduction in degranulation is merely caused by a fraction of CTL that show no MTOC reorientation. This would explain why the inhibition of degranulation is incomplete. However, we cannot exclude the possibility that inhibition of Pyk2 simply delays CTL degranulation because Pyk2 is a putative signal amplifier downstream of TCR signaling pathways. This is supported by my results in Chapter 4, which suggest that Pyk2 acts as a major effector downstream of LFA-1 signaling and by the fact that integrin signaling is known to augment CTL responses (254).

My data suggest that the kinase activity of Pyk2 is more relevant for CTL degranulation compared to its protein expression (Figures 5-4 & 5-5). The minor effect on CTL degranulation under reduced Pyk2 expression indicates that low levels of Pyk2 is sufficient for a normal CTL response. In experiments where PF431396 was used, the inhibition of CTL degranulation (Figure 5-4) did not correspond to a significant difference in target cell survival (Figure 5-10). There is a possibility that the target cells L1210Kb are insensitive to cytolytic granzymes after extended culturing. Therefore, it may be necessary to increase the effector cell number in the future when performing a similar assay in order to observe a greater difference in target cell lysis. Alternatively, one can use a more sensitive assay to detect early signs of target cell apoptosis before membrane potential is compromised (88).

A potential function of Pyk2 is to stabilize MTOC at the immune synapse (IS). The IS of CTL is a tightly organized junction, which allows direct and regulated delivery of granule contents to the target cell (245). The granule contents are unloaded toward the target cell through a region between the cSMAC (central supramolecular activation complex) and pSMAC (peripheral supramolecular activation complex) that is composed of TCR:peptide:MHC signaling cluster surrounded by LFA-1:ICAM-1 interactions (245). We found that Pyk2 and paxillin are co-localized to the MTOC in resting cells (161). Once CTL recognize a target cell, activated Pyk2 translocates from the MTOC to the IS (161) but paxillin remains associated

with the MTOC (160). Since both Pyk2 and paxillin are targeted to the IS and found at the MTOC, it is possible that the trans-molecular interaction between Pyk2 and paxillin stabilizes MTOC at the IS. This speculation is supported by the crystal structure of Pyk2 in complex with paxillin, which showed that two FAT domains of Pyk2 form a stable crystal with four paxillin LD4 peptides (159). Therefore, the individual Pyk2-paxillin complex at the pSMAC potentially interacts with additional paxillin from the MTOC to stabilize the docking of MTOC at the immune synapse.

In search for a connection between Pyk2 and the regulation of cytolytic granules, one study provided insight on how Pyk2 may be involved in this process. Bonnette et. al. showed that Pyk2 can tyrosine phosphorylate the transmembrane protein E-Syt1 (Extended Synaptotagmin-1) (257). Synaptotagmins are Ca^{2+} sensors and are involved in triggering membrane trafficking (104). E-Syt1 functions upstream of the proteins that are important for granule fusion including Munc, Syntaxin, and VAMP (vesicle associated membrane protein) (104). Since E-Syt1 associates with the membrane of intracellular compartments (258), Pyk2 may be important for the activation of E-Syt1, which is critical for subsequent trafficking and exocytosis of cytolytic granules. However, whether E-Syt1 is expressed in CTL or if it regulates the function of Syntaxin 11 and Munc 18-4 that are known to be important for CTL degranulation awaits further investigation.

CHAPTER 6

GENERAL DISCUSSION

A. Research Highlights

TCR-mediated Ca^{2+}-dependent Pyk2 activation is through production of ROS.

We found that Pyk2 is activated through both Ca^{2+} dependent and independent pathways based on the method of TCR stimulation (190). We observed that Ca^{2+} is important for Pyk2 activation in the signaling pathway induced by soluble crosslinking of TCR, but not for the pathway activated by immobilized anti-CD3 antibodies (190). I found that CTL stimulated with ionomycin or thapsigargin, which increases intracellular Ca^{2+} concentration, results in NADPH oxidase-dependent Pyk2 tyrosine phosphorylation (Figure 3-2 and 3-3A). The product of NADPH oxidase is critical for Ca^{2+}-mediated Pyk2 activation (Figure 3-3B) and I showed that ionomycin and thapsigargin stimulation elicits H_2O_2 production in CTL (Figure 3-4C & 3-4D). H_2O_2 stimulation alone is sufficient to trigger Pyk2 activation (Figure 3-5). Further investigation revealed that Ca^{2+}-induced Pyk2 tyrosine phosphorylation requires Erk, and I demonstrated that H_2O_2 stimulates Erk activation (Figure 3-8). Since Src-family kinase is absolutely required for both TCR and Ca^{2+}-mediated Pyk2 activation (190), and it can be regulated by Erk (208), I established a potential signaling mechanism. My model demonstrates how Ca^{2+} signaling leads to NADPH oxidase-dependent H_2O_2 production, which could activate Erk to regulate Src-family kinase-dependent Pyk2 activation

(Figure 3-10). My experiment results provide evidence for a plausible signaling mechanism that defines how Ca^{2+} mobilization indirectly regulates Pyk2 activation in T cells.

Pyk2 regulates ICAM-1 mediated CTL adhesion and migration.

Pyk2 is required for optimal CTL adhesion during initial contact to ICAM-1 substrates (Figure 4-2), which is consistent with the results reported in a previous study using CD8 T cells from Pyk2-deficient mice (166). The observed defective CTL adhesion on an ICAM-1 surface was eventually restored, but the cells displayed abnormal morphology (Figure 4-3). Live cell imaging analysis revealed that Pyk2 regulates normal CTL de-adhesion during migration on ICAM-1 (Figure 4-4A). De-regulation of Pyk2 leads to a significant reduction in migration distance and velocity in both differentiated CTL and *ex-vivo* activated CD8 T cells (Figure 4-5 to 4-8). My data provided a potential explanation for the chemotaxis defect found in Pyk2-deficient CD8 T cells (166). The migration defect was likely due to an inability of the T cells to de-adhere from ICAM-1 rather than an inability to bind ICAM-1 (Figure 4-9). I found that Pyk2 is targeted to the ICAM-1 contact zone (Figure 4-10). Pyk2 phosphorylated at specific sites preferentially associates with different contact regions in CTL (Figure 4-11). The morphological defect found in CTL trailing edge resulting from Pyk2 deregulation was different compared to the defect induced by calpain inhibition (Figure 4-13 and 4-14). Unexpectedly, inhibition of Pyk2 de-regulates total cellular LFA-1 distribution (Figure 4-

15). A significant difference in cell trafficking was not observed in an *in-vivo* migration assay (Figure 4-16), but knockdown of Pyk2 with siRNA clearly impairs CTL migration through a cell layer (Figure 4-17). My results indicate that Pyk2 is required for optimal cell-contact dependent CTL migration.

Pyk2 is required for optimal CTL degranulation.

In studying the potential contribution of Pyk2 in CTL-mediated cytotoxicity, I found that target cell mediated CTL degranulation is significantly reduced in the presence of a Pyk2 inhibition (Figure 5-1 & 5-2). The reduction in degranulation is possibly attributed to a weakened conjugate formation between the CTL and its target cell (Figure 5-3). Further examination revealed that Pyk2 inhibition impairs CTL degranulation in the absence of target cells (Figure 5-4). This indicates that the kinase activity of Pyk2 regulates the intrinsic ability of CTL to degranulate. In contrast to the data in Chapter 4, where I found that both inhibition and knockdown of Pyk2 led to a similar de-adhesion defect, knockdown of Pyk2 expression has no major effect on CTL degranulation (Figure 5-5). This suggests that CTL degranulation still occurs under conditions of reduced Pyk2 protein expression.

In other experiments, inhibition of Pyk2 kinase activity impairs MTOC reorientation in CTL stimulated by target cells (Figure 5-6). Results from my imaging analysis suggests that CTL expressing the GFP-coupled kinase-dead Pyk2 have a higher frequency of non-reorientated MTOC toward target cell

compared to CTL expressing either the wild-type Pyk2 or Pyk2 FAT-domain (Figure 5-8). These data indicate that deregulation of Pyk2 kinase activity only interferes with MTOC reorientation. Lastly, optimal target cell lysis requires intact Pyk2 function (Figure 5-10). Taken together, my results show that Pyk2 regulates aspects of CTL degranulation.

B. Model for the regulation and function of Pyk2 in CTL.

Potential contribution of Pyk2 in T cell priming

Productive T cell activation requires three signals generated from the antigen-receptor, co-stimulatory molecules, and cytokines (Figure 1-1). Although integrin is not generally considered as one of the three signal requirements, it plays an important role in stabilizing the immune synapse between APC and T cells that is critical for optimal T cell priming (259, 260). CD8 T cells deficient in CD11a (αL subunit of LFA-1) generate a reduced quantity of short-lived effector T cells during lymphocytic choriomeningitis virus (LCMV) infection (166). A similar defect in effector CD8 T cell generation was observed in mice with ICAM-1 deficient APC (259). These studies indicate that the signal stemming from the engagement of LFA-1 to ICAM-1 is crucial for T cell priming (166, 259).

My data in Chapter 4 showed that Pyk2 plays an important role in mediating LFA-1 function in T cells. This could explain why deficiency in either LFA-1 or Pyk2 produces similar defects in the generation of short-lived effector CD8 T cells during viral infection (166). I speculated that the defect

resulted from an ineffective T cell movement inside the secondary lymphoid organs during priming. Pyk2 is important for cell-to-cell contact regardless of antigen (Figure 5-3), once the cell contact has been established the CTL do not efficiently detach from the cell it bound when Pyk2 is deregulated (Figure 4-17). Consequently, Pyk2-deficient T cells are less efficient in finding the APC for activation due to a defect in de-adhesion from the surrounding cells. Since Pyk2 deregulation leads to a reduction rather than a complete inhibition in T cell motility, Pyk2-deficient T cells have less opportunity to encounter APC for activation. Pyk2-deficient T cells are not completely immobile and this explains why we see a reduced quantity instead of a complete absence of effector CD8 T cells generated during viral challenge in Pyk2-deficient mice (166).

Pyk2 contributes to optimal T cell signaling activation

Our early study showed that integrins are important for regulating CTL function under sub-optimal TCR stimulation (254). We found that sub-optimal TCR stimulation using low concentrations of anti-CD3 antibody in addition to ICAM-1 triggers robust degranulation compared to stimulation using anti-CD3 antibody alone (254). This indicated that the T cell secretory machinery is augmented by integrin activation under reduced level of TCR signaling. Along the same line, it was reported that the cytokine production in CD8 T cells under comparable stimulatory conditions is regulated by Pyk2 (166). In conditions where optimal TCR stimulation was provided, the effect

185

of integrin stimulation or the presence of Pyk2 was dispensable in CTL degranulation and cytokine production, respectively (166, 254). These findings support that Pyk2 functions as a major effector downstream of integrin signaling to amplify TCR-mediated responses. The signaling mechanism for Pyk2-mediated amplification of T cell response upon integrin engagement is unknown.

Inhibition of Pyk2 in CTL reduces initial ICAM-1 binding (Figure 4-2) and Pyk2 regulates optimal adhesion to both antigen-bearing and non-antigen-bearing cells (Figure 5-3). This demonstrates that Pyk2 is important for the optimal integrin-mediated adhesion of CTL to target cells regardless of antigen. A current model proposes that ZAP-70 phosphorylation of VAV1 relieves the inhibitory effect of VAV1 on talin, thereby allowing LFA-1 affinity switch to occur (66). Since Pyk2 forms a complex with VAV1, and VAV1 phosphorylation is impaired in the absence of Pyk2 (154, 170), it is possible that Pyk2 regulates translocation and phosphorylation of VAV1 to facilitate talin-dependent integrin activation at the contact site (Figure 6-1). In theory, phosphorylation of VAV1 is mediated by ZAP-70 without Pyk2 (66), and this would explain why CTL are still able to adhere to ICAM-1 at a reduced level when Pyk2 is deregulated (Figure 4-2). In actuality, regardless of the mechanism, Pyk2 does contribute to integrin-dependent adhesion during the initial phase of LFA-1 engagement. Under ideal (or normal) conditions, CTL adhere to the potential target cell in order to efficiently scan the cell surface for antigen. When Pyk2 is inhibited, CTL binds the potential target cell

weakly thereby reducing the probability of recognizing antigen. Therefore, Pyk2 reduces the threshold for TCR activation by enabling the best possible adhesion between CTL and its potential target cell.

Activation and potential function of Pyk2 during CTL migration

Pyk2 is tyrosine phosphorylated at Y579 and Y580 at the leading edge where integrin engagement and activation occurs (Figure 4-11). We do not know whether Pyk2 was targeted to the contact site for tyrosine phosphorylation or if it has been phosphorylated before targeting to the contact site. Tyrosine phosphorylation of Y579 and Y580 is suggested to enhance the catalytic activity of Pyk2 (145). I speculated that activation of Pyk2 at the leading edge phosphorylates the substrates that play an important role in integrin deactivation. A proteomic screen identified docking protein 1 (Dok1) as one of the Pyk2 downstream substrates (257). While the function of Dok1 in integrin activation and T cell migration is unknown, some studies suggest that Dok1 negatively regulates T cell signaling activation (261, 262). In other studies, overexpression of Dok1 promotes cell migration in tumor cell lines (263, 264). Since Dok1 binds activated integrin cytoplasmic domains with a higher affinity than talin (265), it is possible that as the CTL migrate Pyk2 initially phosphorylates Dok1 at the leading edge. Subsequently, Dok1 displaces talin at the trailing edge to negatively regulate integrin activation (Figure 6-1). This could explain why inhibition or knockdown of Pyk2 impairs de-adhesion of CTL on

an ICAM-1 coated surface. However, additional mechanisms must exist since expression of FAT-domain also impairs CTL de-adhesion. Perhaps Pyk2 tyrosine phosphorylation at Y881 at the trailing edge recruits additional proteins that negatively regulate integrin. As a result, overexpression of Pyk2 FAT-domain potentially interferes with integrin deactivation that normally involves endogenous Pyk2 Y881 phosphorylation.
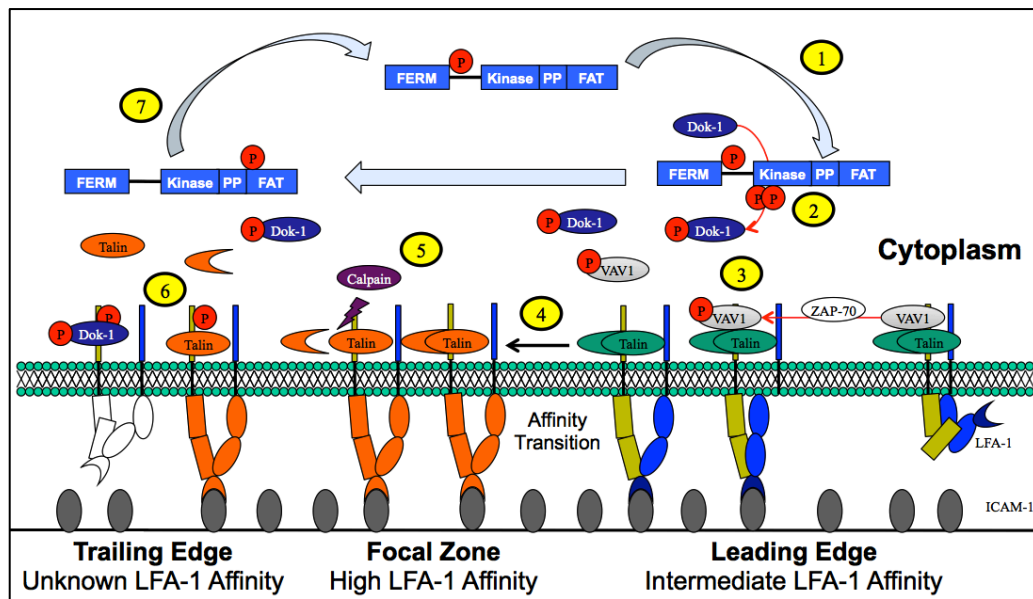
Figure 6-1. Proposed model for Pyk2 regulation of CTL migration. (1) Pyk2 is activated in response to integrin engagement. (2) Pyk2 is targeted to the site of integrin signaling activation and becomes tyrosine phosphorylated at Y579 and Y580. Activated Pyk2 phosphorylates Dok-1 at the leading edge. (3) Integrin-associated ZAP-70 phosphorylates VAV1 to relieve its inhibitory effect on talin. Alternatively, Pyk2 facilitates activation of talin by bringing VAV1 to the integrin. (4) Activated talin triggers integrin conformational change and induces strong integrin binding to ICAM-1. (5) Integrin inactivation requires calpain processing of talin. (6) Phosphorylation of integrin cytoplasmic domain enables Dok-1 to displace calpain-processed talin. Once talin is no longer bound to integrin, integrin becomes deactivated and begins to recycle. Pyk2 tyrosine phosphorylated at Y881 at the trailing edge may serve as a molecular adaptor to facilitate the phosphorylation and inactivation of integrin. (7) Turnover of Pyk2 occurs at the trailing edge to ensure protein recycling for continuous cell migration.

Cellular targets of Pyk2 downstream of the TCR

It seems that Pyk2 can interact with and/or phosphorylate a spectrum of proteins depending on the cell type (138, 257, 266). The identity of substrates regulated by Pyk2 upon TCR activation is not yet completely established. Thus it remains unclear which TCR-mediated signaling pathway is specifically regulated by Pyk2. Paxillin is a well-characterized Pyk2 substrate in CTL. I showed that Pyk2 inhibition selectively inhibits paxillin tyrosine phosphorylation but not serine/threonine phosphorylation (Figure 4-1C). Paxillin is an adaptor protein that constitutively associates with Pyk2 (157). It localizes to the MTOC (267) and we propose that it plays a role in targeting Pyk2 to the MTOC (161). Similar to Pyk2, paxillin also contributes to MTOC reorientation (160) and mediates T cell adhesion and migration (268). The similar molecular functions of Pyk2 and paxillin in CTL places paxillin as a major effector of Pyk2. It is rational to hypothesize that ectopically expressed paxillin tyrosine mutants in CTL should generate similar functional defects as inhibition of Pyk2. The preliminary results from my experiments indicate that expression of a paxillin double tyrosine mutant (Y31F/Y118F) in CTL neither affected target cell-induced MTOC reorientation (Figure 5-9) nor ICAM-1 dependent CTL migration. A list of potential substrates for Pyk2 has been identified (257) but whether these substrates serve as a downstream effector of Pyk2 in CTL remains to be determined.

A common role for Pyk2 in CTL adhesion, migration, and effector function

I have shown that Pyk2 regulates CTL adhesion, migration, and contributes to CTL degranulation as well as MTOC reorientation. How does Pyk2 regulate multiple aspects of T cell function? A common theme is that all of these processes involve the cytoskeleton and some aspects of vesicular trafficking. It is established that integrin recycling is critical for T cell migration (65). Integrin recycling involves endocytosis of unbound LFA-1 at the trailing edge for turnover followed by intracellular vesicular transport to the leading edge for exocytosis (269). My data indicate that inhibition of Pyk2 impairs intracellular LFA-1 distribution (Figure 4-15). This suggests that Pyk2 contributes to some aspects of integrin recycling, but whether Pyk2 regulates integrin endocytosis at the trailing edge, trafficking of integrin-containing vesicle, or exocytosis to the leading edge is unknown.

Endocytosis of integrin is important for focal adhesion disassembly in migrating cells (270). Focal adhesion structures, if they exist in T cells, have never been characterized or defined in the literature. Interestingly, my data show that the accumulation of ectopically expressed Pyk2 at the CTL trailing edge resemble a focal adhesion structure (Figure 4-10). Perhaps the overexpressed Pyk2 in CTL is acting as a dominant negative protein to inhibit the function of endogenous Pyk2. This is supported by the dominant effect reported in an NK cell functional study (169). A defect in cell de-adhesion as a result of deregulation of Pyk2 might lead to defective or delayed integrin

endocytosis. Consequently, imbalances in LFA-1 recycling affect distribution of LFA-1 to the leading edge. The back-to-front imbalance explains why initial ICAM-1 adhesion is reduced.

Pyk2 may regulate other steps of the integrin recycling process such as intracellular trafficking. The evidence for Pyk2 in regulating vesicular transport is apparent in my data, which shows that Pyk2 is required for optimal cytolytic granule secretion in CTL (Figure 5-4). The important role of Pyk2 in regulating degranulation is supported in a Pyk2-deficient neutrophil study (170). Since the cytolytic granules of a migrating CTL are localized near the trailing edge and LFA-1 is highly expressed at the trailing edge, perhaps Pyk2 functions as a regulator for vesicular transport from the back to the front of the CTL. However, it is also possible that Pyk2 is involved at the point of vesicular fusion to the plasma membrane. Future studies should address whether Pyk2 selectively regulates intracellular trafficking or vesicle fusion at the membrane, or both.

Pyk2 is not the only protein known to influence both CTL degranulation and LFA-1 function. Rab27a, a small GTPase, is critical for granule exocytosis and is targeted to the uropod of migrating cells. Rab27a regulates integrin expression and is required for normal neutrophil migration (271, 272). From an evolutionary standpoint, Pyk2 may belong to a group of molecules that adapted to carry out multiple cellular functions that control both integrin-dependent CTL migration and cell-mediated cytotoxicity.

C. Conclusion

We are beginning to understand the molecular factors and regulatory processes that control CTL function. Defining the specific role of Pyk2 in CTL is not straightforward since Pyk2 responds to multiple stimuli and regulates a variety of responses. In addition, the function of Pyk2 appears to be cell-context dependent. My research shows that Pyk2 is a regulator of cytoskeletal-dependent processes that control adhesion, migration, and cytolytic granule secretion. More importantly, my research results indicate that Pyk2 is required for optimal CTL migration and contributes to CTL degranulation. How Pyk2 functions in other cell types is the subject of ongoing research. Although it is logical to target Pyk2 for its prominent role in cancer metastasis and tumor growth, my research indicates that Pyk2 is also important for normal CTL function. When designing a therapeutic intervention, we must understand the consequence of molecular inhibition in both the killer and the target cell because a cancer cell that does not divide still requires a functional CTL for its elimination.

D. Future Directions

The molecular identity of NADPH oxidase that is regulated by calcium in T cells remains unknown. Furthermore, whether ROS is required for CTL activation and degranulation has not been established. As calcium controls multiple aspects of T cell function, it is of great interest to see if ROS follow a similar pattern in regulating CTL function. Since antioxidants have been suggested as a supplement in cancer therapy, knowing whether CTL require ROS for proper function is of significant importance to therapeutic design.

Although I have shown that Pyk2 is important for CTL degranulation, we still do not know whether Pyk2 is required for granule polarization or granule fusion with the membrane. This could be easily addressed by performing confocal analysis to determine the relative position of the CTL granules to the target cell within a conjugate. The results of this experiment could also provide insight into how the MTOC polarization and translocation is achieved relative to granule movement.

I have elucidated the phenotype associated with inhibition or knockdown of Pyk2 in CTL. The consequence by which constitutively active Pyk2 affects CTL function is unknown. Since the constitutively active form of FAK mutants (Y576E/Y577E/K578E/K581E) has been shown to promote cell migration and has an increased kinase activity (273), it is possible to generate a near-identical mutation in Pyk2 (Y579E/Y580E/K581E/V584I) for study of CTL function. I hypothesize that if inhibition of Pyk2 kinase results in a reduced CTL degranulation, then uninhibited Pyk2 activity

theoretically should augment CTL-mediated cytotoxicity. Identifying a molecular target or pathway that can increase the cytolytic activity of CTL is definitely important for the elimination of cancer cells that are commonly resistant to apoptosis.

CHAPTER 7

BIBLIOGRAPHY

1.   Amulic B, Cazalet C, Hayes GL, Metzler KD, Zychlinsky A. 2012. Neutrophil function: from mechanisms to disease. *Annu Rev Immunol* 30: 459-89

2.   Makepeace BL, Martin C, Turner JD, Specht S. 2012. Granulocytes in helminth infection -- who is calling the shots? *Curr Med Chem* 19: 1567-86

3.   Gilfillan AM, Beaven MA. 2011. Regulation of mast cell responses in health and disease. *Crit Rev Immunol* 31: 475-529

4.   Harding CV, Ramachandra L, Wick MJ. 2003. Interaction of bacteria with antigen presenting cells: influences on antigen presentation and antibacterial immunity. *Curr Opin Immunol* 15: 112-9

5.   Vivier E, Tomasello E, Baratin M, Walzer T, Ugolini S. 2008. Functions of natural killer cells. *Nat Immunol* 9: 503-10

6.   Mellman I, Turley SJ, Steinman RM. 1998. Antigen processing for amateurs and professionals. *Trends Cell Biol* 8: 231-7

7.   Thery C, Amigorena S. 2001. The cell biology of antigen presentation in dendritic cells. *Curr Opin Immunol* 13: 45-51

8.   Belz GT. 2008. DC migration: hard-wired for T cell activation. *Immunity* 29: 388-90

9.   Butcher EC, Picker LJ. 1996. Lymphocyte homing and homeostasis. *Science* 272: 60-6

10.   von Andrian UH, Mempel TR. 2003. Homing and cellular traffic in lymph nodes. *Nat Rev Immunol* 3: 867-78

11.   Germain RN, Jenkins MK. 2004. In vivo antigen presentation. *Curr Opin Immunol* 16: 120-5

12.   Davis MM. 2004. The evolutionary and structural 'logic' of antigen receptor diversity. *Semin Immunol* 16: 239-43

13.   Itano AA, Jenkins MK. 2003. Antigen presentation to naive CD4 T cells in the lymph node. *Nat Immunol* 4: 733-9

14.   Zhu J, Yamane H, Paul WE. 2010. Differentiation of effector CD4 T cell populations (*). *Annu Rev Immunol* 28: 445-89

15.   Elgueta R, de Vries VC, Noelle RJ. 2010. The immortality of humoral immunity. *Immunol Rev* 236: 139-50

16.   Batista FD, Harwood NE. 2009. The who, how and where of antigen presentation to B cells. *Nat Rev Immunol* 9: 15-27

17.   Lanzavecchia A. 1985. Antigen-specific interaction between T and B cells. *Nature* 314: 537-9

18.   Allen CD, Okada T, Cyster JG. 2007. Germinal-center organization and cellular dynamics. *Immunity* 27: 190-202

19.   Reinhardt RL, Liang HE, Locksley RM. 2009. Cytokine-secreting follicular T cells shape the antibody repertoire. *Nat Immunol* 10: 385-93

20.   Wong P, Pamer EG. 2003. CD8 T cell responses to infectious pathogens. *Annu Rev Immunol* 21: 29-70

21.   Boyman O, Sprent J. 2012. The role of interleukin-2 during homeostasis and activation of the immune system. *Nat Rev Immunol* 12: 180-90

22.   Gill J, Malin M, Sutherland J, Gray D, Hollander G, Boyd R. 2003. Thymic generation and regeneration. *Immunol Rev* 195: 28-50

23.   von Boehmer H. 2005. Unique features of the pre-T-cell receptor alpha-chain: not just a surrogate. *Nat Rev Immunol* 5: 571-7

24.   Pang SS, Berry R, Chen Z, Kjer-Nielsen L, Perugini MA, King GF, Wang C, Chew SH, La Gruta NL, Williams NK, Beddoe T, Tiganis T, Cowieson NP, Godfrey DI, Purcell AW, Wilce MC, McCluskey J, Rossjohn J. 2010. The structural basis for autonomous dimerization of the pre-T-cell antigen receptor. *Nature* 467: 844-8

25.   Ciofani M, Zuniga-Pflucker JC. 2010. Determining gammadelta versus alphass T cell development. *Nat Rev Immunol* 10: 657-63

26.   Starr TK, Jameson SC, Hogquist KA. 2003. Positive and negative selection of T cells. *Annu Rev Immunol* 21: 139-76

27.   Kappes DJ, He X, He X. 2005. CD4-CD8 lineage commitment: an inside view. *Nat Immunol* 6: 761-6

28.   Felix NJ, Allen PM. 2007. Specificity of T-cell alloreactivity. *Nat Rev Immunol* 7: 942-53

29.   Suchin EJ, Langmuir PB, Palmer E, Sayegh MH, Wells AD, Turka LA. 2001. Quantifying the frequency of alloreactive T cells in vivo: new answers to an old question. *J Immunol* 166: 973-81

30.   Fitch FW. 1984. Alloreactive T cell clones. *Adv Exp Med Biol* 172: 347-63

31.   Rudd CE, Schneider H. 2003. Unifying concepts in CD28, ICOS and CTLA4 co-receptor signalling. *Nat Rev Immunol* 3: 544-56

32.   Mescher MF, Curtsinger JM, Agarwal P, Casey KA, Gerner M, Hammerbeck CD, Popescu F, Xiao Z. 2006. Signals required for programming effector and memory development by CD8+ T cells. *Immunol Rev* 211: 81-92

33.   van der Merwe PA, Dushek O. 2011. Mechanisms for T cell receptor triggering. *Nat Rev Immunol* 11: 47-55

34.   Palacios EH, Weiss A. 2004. Function of the Src-family kinases, Lck and Fyn, in T-cell development and activation. *Oncogene* 23: 7990-8000

35.   Turner JM, Brodsky MH, Irving BA, Levin SD, Perlmutter RM, Littman DR. 1990. Interaction of the unique N-terminal region of tyrosine kinase p56lck with cytoplasmic domains of CD4 and CD8 is mediated by cysteine motifs. *Cell* 60: 755-65

36. Schilham MW, Fung-Leung WP, Rahemtulla A, Kuendig T, Zhang L, Potter J, Miller RG, Hengartner H, Mak TW. 1993. Alloreactive cytotoxic T cells can develop and function in mice lacking both CD4 and CD8. *Eur J Immunol* 23: 1299-304

37. Ostergaard HL, Shackelford DA, Hurley TR, Johnson P, Hyman R, Sefton BM, Trowbridge IS. 1989. Expression of CD45 alters phosphorylation of the lck-encoded tyrosine protein kinase in murine lymphoma T-cell lines. *Proc Natl Acad Sci U S A* 86: 8959-63

38. McNeill L, Salmond RJ, Cooper JC, Carret CK, Cassady-Cain RL, Roche-Molina M, Tandon P, Holmes N, Alexander DR. 2007. The differential regulation of Lck kinase phosphorylation sites by CD45 is critical for T cell receptor signaling responses. *Immunity* 27: 425-37

39. Nika K, Soldani C, Salek M, Paster W, Gray A, Etzensperger R, Fugger L, Polzella P, Cerundolo V, Dushek O, Hofer T, Viola A, Acuto O. 2010. Constitutively active Lck kinase in T cells drives antigen receptor signal transduction. *Immunity* 32: 766-77

40. Wang H, Kadlecek TA, Au-Yeung BB, Goodfellow HE, Hsu LY, Freedman TS, Weiss A. 2010. ZAP-70: an essential kinase in T-cell signaling. *Cold Spring Harb Perspect Biol* 2: a002279

41. Malissen B, Marguet D. 2011. La(s)t but not least. *Nat Immunol* 12: 592-3

42. Williamson DJ, Owen DM, Rossy J, Magenau A, Wehrmann M, Gooding JJ, Gaus K. 2011. Pre-existing clusters of the adaptor Lat do not participate in early T cell signaling events. *Nat Immunol* 12: 655-62

43. Roncagalli R, Mingueneau M, Gregoire C, Malissen M, Malissen B. 2010. LAT signaling pathology: an "autoimmune" condition without T cell self-reactivity. *Trends Immunol* 31: 253-9

44. Weiss A. 2009. TCR signal transduction: opening the black box. *J Immunol* 183: 4821-7

45. Smith-Garvin JE, Koretzky GA, Jordan MS. 2009. T cell activation. *Annu Rev Immunol* 27: 591-619

46. Zhang W, Trible RP, Zhu M, Liu SK, McGlade CJ, Samelson LE. 2000. Association of Grb2, Gads, and phospholipase C-gamma 1 with phosphorylated LAT tyrosine residues. Effect of LAT tyrosine mutations on T cell angigen receptor-mediated signaling. *J Biol Chem* 275: 23355-61

47. Grasis JA, Tsoukas CD. 2011. Itk: the rheostat of the T cell response. *J Signal Transduct* 2011: 297868

48. Roose JP, Mollenauer M, Gupta VA, Stone J, Weiss A. 2005. A diacylglycerol-protein kinase C-RasGRP1 pathway directs Ras activation upon antigen receptor stimulation of T cells. *Mol Cell Biol* 25: 4426-41

49. Huse M. 2012. Microtubule-organizing center polarity and the immunological synapse: protein kinase C and beyond. *Front Immunol* 3: 235

50. Robert V, Triffaux E, Savignac M, Pelletier L. 2011. Calcium signalling in T-lymphocytes. *Biochimie* 93: 2087-94

51. Zhang SL, Yu Y, Roos J, Kozak JA, Deerinck TJ, Ellisman MH, Stauderman KA, Cahalan MD. 2005. STIM1 is a Ca2+ sensor that activates CRAC channels and migrates from the Ca2+ store to the plasma membrane. *Nature* 437: 902-5

52. Feske S. 2007. Calcium signalling in lymphocyte activation and disease. *Nat Rev Immunol* 7: 690-702

53. Toyoshima C, Nomura H, Sugita Y. 2003. Structural basis of ion pumping by Ca(2+)-ATPase of sarcoplasmic reticulum. *FEBS Lett* 555: 106-10

54. Forman HJ, Maiorino M, Ursini F. 2010. Signaling functions of reactive oxygen species. *Biochemistry* 49: 835-42

55. Bedard K, Krause KH. 2007. The NOX family of ROS-generating NADPH oxidases: physiology and pathophysiology. *Physiol Rev* 87: 245-313

56. Lambeth JD, Kawahara T, Diebold B. 2007. Regulation of Nox and Duox enzymatic activity and expression. *Free Radic Biol Med* 43: 319-31

57. Jackson SH, Devadas S, Kwon J, Pinto LA, Williams MS. 2004. T cells express a phagocyte-type NADPH oxidase that is activated after T cell receptor stimulation. *Nat Immunol* 5: 818-27

58. Meng TC, Fukada T, Tonks NK. 2002. Reversible oxidation and inactivation of protein tyrosine phosphatases in vivo. *Mol Cell* 9: 387-99

59. Mahadev K, Zilbering A, Zhu L, Goldstein BJ. 2001. Insulin-stimulated hydrogen peroxide reversibly inhibits protein-tyrosine phosphatase 1b in vivo and enhances the early insulin action cascade. *J Biol Chem* 276: 21938-42

60. Kwon J, Lee SR, Yang KS, Ahn Y, Kim YJ, Stadtman ER, Rhee SG. 2004. Reversible oxidation and inactivation of the tumor suppressor PTEN in cells stimulated with peptide growth factors. *Proc Natl Acad Sci U S A* 101: 16419-24

61. Rhee SG, Kang SW, Jeong W, Chang TS, Yang KS, Woo HA. 2005. Intracellular messenger function of hydrogen peroxide and its regulation by peroxiredoxins. *Curr Opin Cell Biol* 17: 183-9

62. Hogg N, Laschinger M, Giles K, McDowall A. 2003. T-cell integrins: more than just sticking points. *J Cell Sci* 116: 4695-705

63. Scharffetter-Kochanek K, Lu H, Norman K, van Nood N, Munoz F, Grabbe S, McArthur M, Lorenzo I, Kaplan S, Ley K, Smith CW, Montgomery CA, Rich S, Beaudet AL. 1998. Spontaneous skin ulceration and defective T cell function in CD18 null mice. *J Exp Med* 188: 119-31

64. Semmrich M, Smith A, Feterowski C, Beer S, Engelhardt B, Busch DH, Bartsch B, Laschinger M, Hogg N, Pfeffer K, Holzmann B. 2005.

Importance of integrin LFA-1 deactivation for the generation of immune responses. *J Exp Med* 201: 1987-98

65. Smith A, Stanley P, Jones K, Svensson L, McDowall A, Hogg N. 2007. The role of the integrin LFA-1 in T-lymphocyte migration. *Immunol Rev* 218: 135-46

66. Hogg N, Patzak I, Willenbrock F. 2011. The insider's guide to leukocyte integrin signalling and function. *Nat Rev Immunol* 11: 416-26

67. Evans R, Lellouch AC, Svensson L, McDowall A, Hogg N. 2011. The integrin LFA-1 signals through ZAP-70 to regulate expression of high-affinity LFA-1 on T lymphocytes. *Blood* 117: 3331-42

68. Garcia-Bernal D, Parmo-Cabanas M, Dios-Esponera A, Samaniego R, Hernan PdlOD, Teixido J. 2009. Chemokine-induced Zap70 kinase-mediated dissociation of the Vav1-talin complex activates alpha4beta1 integrin for T cell adhesion. *Immunity* 31: 953-64

69. Ye F, Hu G, Taylor D, Ratnikov B, Bobkov AA, McLean MA, Sligar SG, Taylor KA, Ginsberg MH. 2010. Recreation of the terminal events in physiological integrin activation. *J Cell Biol* 188: 157-73

70. Franco SJ, Rodgers MA, Perrin BJ, Han J, Bennin DA, Critchley DR, Huttenlocher A. 2004. Calpain-mediated proteolysis of talin regulates adhesion dynamics. *Nat Cell Biol* 6: 977-83

71. Svensson L, McDowall A, Giles KM, Stanley P, Feske S, Hogg N. 2010. Calpain 2 controls turnover of LFA-1 adhesions on migrating T lymphocytes. *PLoS One* 5: e15090

72. Kinashi T. 2005. Intracellular signalling controlling integrin activation in lymphocytes. *Nat Rev Immunol* 5: 546-59

73. Ghandour H, Cullere X, Alvarez A, Luscinskas FW, Mayadas TN. 2007. Essential role for Rap1 GTPase and its guanine exchange factor CalDAG-GEFI in LFA-1 but not VLA-4 integrin mediated human T-cell adhesion. *Blood* 110: 3682-90

74. Abram CL, Lowell CA. 2009. The ins and outs of leukocyte integrin signaling. *Annu Rev Immunol* 27: 339-62

75. Griffiths GM, Tsun A, Stinchcombe JC. 2010. The immunological synapse: a focal point for endocytosis and exocytosis. *J Cell Biol* 189: 399-406

76. Kupfer A, Dennert G. 1984. Reorientation of the microtubule-organizing center and the Golgi apparatus in cloned cytotoxic lymphocytes triggered by binding to lysable target cells. *J Immunol* 133: 2762-6

77. Stinchcombe JC, Majorovits E, Bossi G, Fuller S, Griffiths GM. 2006. Centrosome polarization delivers secretory granules to the immunological synapse. *Nature* 443: 462-5

78. Smyth MJ, Thia KY, Street SE, MacGregor D, Godfrey DI, Trapani JA. 2000. Perforin-mediated cytotoxicity is critical for surveillance of spontaneous lymphoma. *J Exp Med* 192: 755-60

79. van den Broek ME, Kagi D, Ossendorp F, Toes R, Vamvakas S, Lutz WK, Melief CJ, Zinkernagel RM, Hengartner H. 1996. Decreased tumor surveillance in perforin-deficient mice. *J Exp Med* 184: 1781-90

80. Barry M, Bleackley RC. 2002. Cytotoxic T lymphocytes: all roads lead to death. *Nat Rev Immunol* 2: 401-9

81. Zagury D, Bernard J, Noelle T, Feldman M, Berke G. 1975. Isolation and characterization of individual functionally reactive cytotoxic T lymphocytes: conjugation, killing and recycling at the single cell level. *Eur J Immunol* 5: 818 - 22

82. Young JD, Cohn ZA. 1988. How killer cells kill. *Sci Am* 258: 38-44

83. Shi L, Keefe D, Durand E, Feng H, Zhang D, Lieberman J. 2005. Granzyme B binds to target cells mostly by charge and must be added at the same time as perforin to trigger apoptosis. *J Immunol* 174: 5456-61

84. Kurschus FC, Fellows E, Stegmann E, Jenne DE. 2008. Granzyme B delivery via perforin is restricted by size, but not by heparan sulfate-dependent endocytosis. *Proc Natl Acad Sci U S A* 105: 13799-804

85. Ewen CL, Kane KP, Bleackley RC. 2012. A quarter century of granzymes. *Cell Death Differ* 19: 28-35

86. Nakajima H, Park HL, Henkart PA. 1995. Synergistic roles of granzymes A and B in mediating target cell death by rat basophilic leukemia mast cell tumors also expressing cytolysin/perforin. *J Exp Med* 181: 1037-46

87. Shi L, Mai S, Israels S, Browne K, Trapani JA, Greenberg AH. 1997. Granzyme B (GraB) autonomously crosses the cell membrane and perforin initiates apoptosis and GraB nuclear localization. *J Exp Med* 185: 855-66

88. He JS, Ostergaard HL. 2007. CTLs contain and use intracellular stores of FasL distinct from cytolytic granules. *J Immunol* 179: 2339-48

89. He JS, Gong DE, Ostergaard HL. 2010. Stored Fas ligand, a mediator of rapid CTL-mediated killing, has a lower threshold for response than degranulation or newly synthesized Fas ligand. *J Immunol* 184: 555-63

90. Hidalgo LG, Halloran PF. 2002. Role of IFN-gamma in allograft rejection. *Crit Rev Immunol* 22: 317-49

91. Ratner S, Sherrod WS, Lichlyter D. 1997. Microtubule retraction into the uropod and its role in T cell polarization and motility. *J Immunol* 159: 1063-7

92. Tsun A, Qureshi I, Stinchcombe JC, Jenkins MR, de la Roche M, Kleczkowska J, Zamoyska R, Griffiths GM. 2011. Centrosome docking at the immunological synapse is controlled by Lck signaling. *J Cell Biol* 192: 663-74

93. Lui-Roberts WW, Stinchcombe JC, Ritter AT, Akhmanova A, Karakesisoglou I, Griffiths GM. 2012. Cytotoxic T lymphocyte effector function is independent of nucleus-centrosome dissociation. *Eur J Immunol* 42: 2132-41

94.   Jenkins MR, Tsun A, Stinchcombe JC, Griffiths GM. 2009. The strength of T cell receptor signal controls the polarization of cytotoxic machinery to the immunological synapse. *Immunity* 31: 621-31

95.   Berg NN, Puente LG, Dawicki W, Ostergaard HL. 1998. Sustained TCR signaling is required for mitogen-activated protein kinase activation and degranulation by cytotoxic T lymphocytes. *J Immunol* 161: 2919-24

96.   Ostergaard H, Clark WR. 1987. The role of Ca2+ in activation of mature cytotoxic T lymphocytes for lysis. *J Immunol* 139: 3573-9

97.   Pachlopnik Schmid J, Cote M, Menager MM, Burgess A, Nehme N, Menasche G, Fischer A, de Saint Basile G. 2010. Inherited defects in lymphocyte cytotoxic activity. *Immunol Rev* 235: 10-23

98.   Stinchcombe JC, Barral DC, Mules EH, Booth S, Hume AN, Machesky LM, Seabra MC, Griffiths GM. 2001. Rab27a is required for regulated secretion in cytotoxic T lymphocytes. *J Cell Biol* 152: 825-34

99.   Neeft M, Wieffer M, de Jong AS, Negroiu G, Metz CH, van Loon A, Griffith J, Krijgsveld J, Wulffraat N, Koch H, Heck AJ, Brose N, Kleijmeer M, van der Sluijs P. 2005. Munc13-4 is an effector of rab27a and controls secretion of lysosomes in hematopoietic cells. *Mol Biol Cell* 16: 731-41

100.   Menasche G, Menager MM, Lefebvre JM, Deutsch E, Athman R, Lambert N, Mahlaoui N, Court M, Garin J, Fischer A, de Saint Basile G. 2008. A newly identified isoform of Slp2a associates with Rab27a in cytotoxic T cells and participates to cytotoxic granule secretion. *Blood* 112: 5052-62

101.   Arneson LN, Brickshawana A, Segovis CM, Schoon RA, Dick CJ, Leibson PJ. 2007. Cutting edge: syntaxin 11 regulates lymphocyte-mediated secretion and cytotoxicity. *J Immunol* 179: 3397-401

102.   Bryceson YT, Rudd E, Zheng C, Edner J, Ma D, Wood SM, Bechensteen AG, Boelens JJ, Celkan T, Farah RA, Hultenby K, Winiarski J, Roche PA, Nordenskjold M, Henter JI, Long EO, Ljunggren HG. 2007. Defective cytotoxic lymphocyte degranulation in syntaxin-11 deficient familial hemophagocytic lymphohistiocytosis 4 (FHL4) patients. *Blood* 110: 1906-15

103.   Kogl T, Muller J, Jessen B, Schmitt-Graeff A, Janka G, Ehl S, Zur Stadt U, Aichele P. 2013. Hemophagocytic lymphohistiocytosis in syntaxin-11-deficient mice: T-cell exhaustion limits fatal disease. *Blood* 121: 604-13

104.   Kasai H, Takahashi N, Tokumaru H. 2012. Distinct initial SNARE configurations underlying the diversity of exocytosis. *Physiol Rev* 92: 1915-64

105.   Pores-Fernando AT, Zweifach A. 2009. Calcium influx and signaling in cytotoxic T-lymphocyte lytic granule exocytosis. *Immunol Rev* 231: 160-73

106.   Thiery J, Keefe D, Boulant S, Boucrot E, Walch M, Martinvalet D, Goping IS, Bleackley RC, Kirchhausen T, Lieberman J. 2011. Perforin

pores in the endosomal membrane trigger the release of endocytosed granzyme B into the cytosol of target cells. *Nat Immunol* 12: 770-7

107. Veugelers K, Motyka B, Goping IS, Shostak I, Sawchuk T, Bleackley RC. 2006. Granule-mediated killing by granzyme B and perforin requires a mannose 6-phosphate receptor and is augmented by cell surface heparan sulfate. *Mol Biol Cell* 17: 623-33

108. Kaiserman D, Bird CH, Sun J, Matthews A, Ung K, Whisstock JC, Thompson PE, Trapani JA, Bird PI. 2006. The major human and mouse granzymes are structurally and functionally divergent. *J Cell Biol* 175: 619-30

109. Lieberman J. 2003. The ABCs of granule-mediated cytotoxicity: new weapons in the arsenal. *Nat Rev Immunol* 3: 361-70

110. Cullen SP, Martin SJ. 2008. Mechanisms of granule-dependent killing. *Cell Death Differ* 15: 251-62

111. Trapani JA, Jans DA, Jans PJ, Smyth MJ, Browne KA, Sutton VR. 1998. Efficient nuclear targeting of granzyme B and the nuclear consequences of apoptosis induced by granzyme B and perforin are caspase-dependent, but cell death is caspase-independent. *J Biol Chem* 273: 27934-8

112. Li LY, Luo X, Wang X. 2001. Endonuclease G is an apoptotic DNase when released from mitochondria. *Nature* 412: 95-9

113. Sutton VR, Wowk ME, Cancilla M, Trapani JA. 2003. Caspase activation by granzyme B is indirect, and caspase autoprocessing requires the release of proapoptotic mitochondrial factors. *Immunity* 18: 319-29

114. Anthony DA, Andrews DM, Watt SV, Trapani JA, Smyth MJ. 2010. Functional dissection of the granzyme family: cell death and inflammation. *Immunol Rev* 235: 73-92

115. Thomas DA, Du C, Xu M, Wang X, Ley TJ. 2000. DFF45/ICAD can be directly processed by granzyme B during the induction of apoptosis. *Immunity* 12: 621-32

116. Metkar SS, Menaa C, Pardo J, Wang B, Wallich R, Freudenberg M, Kim S, Raja SM, Shi L, Simon MM, Froelich CJ. 2008. Human and mouse granzyme A induce a proinflammatory cytokine response. *Immunity* 29: 720-33

117. Martinvalet D, Dykxhoorn DM, Ferrini R, Lieberman J. 2008. Granzyme A cleaves a mitochondrial complex I protein to initiate caspase-independent cell death. *Cell* 133: 681-92

118. Lev S, Moreno H, Martinez R, Canoll P, Peles E, Musacchio JM, Plowman GD, Rudy B, Schlessinger J. 1995. Protein tyrosine kinase PYK2 involved in Ca(2+)-induced regulation of ion channel and MAP kinase functions. *Nature* 376: 737-45

119. Sasaki H, Nagura K, Ishino M, Tobioka H, Kotani K, Sasaki T. 1995. Cloning and characterization of cell adhesion kinase beta, a novel protein-tyrosine kinase of the focal adhesion kinase subfamily. *J Biol Chem* 270: 21206-19

120. Avraham S, London R, Fu Y, Ota S, Hiregowdara D, Li J, Jiang S, Pasztor LM, White RA, Groopman JE, et al. 1995. Identification and characterization of a novel related adhesion focal tyrosine kinase (RAFTK) from megakaryocytes and brain. *J Biol Chem* 270: 27742-51

121. Yu H, Li X, Marchetto GS, Dy R, Hunter D, Calvo B, Dawson TL, Wilm M, Anderegg RJ, Graves LM, Earp HS. 1996. Activation of a novel calcium-dependent protein-tyrosine kinase. Correlation with c-Jun N-terminal kinase but not mitogen-activated protein kinase activation. *J Biol Chem* 271: 29993-8

122. Herzog H, Nicholl J, Hort YJ, Sutherland GR, Shine J. 1996. Molecular cloning and assignment of FAK2, a novel human focal adhesion kinase, to 8p11.2-p22 by nonisotopic in situ hybridization. *Genomics* 32: 484-6

123. Dikic I, Dikic I, Schlessinger J. 1998. Identification of a new Pyk2 isoform implicated in chemokine and antigen receptor signaling. *J Biol Chem* 273: 14301-8

124. Li X, Hunter D, Morris J, Haskill JS, Earp HS. 1998. A calcium-dependent tyrosine kinase splice variant in human monocytes. Activation by a two-stage process involving adherence and a subsequent intracellular signal. *J Biol Chem* 273: 9361-4

125. Franklin RA, Atherfold PA, Robinson PJ, Bonner D. 2001. Regulation of Pyk2 expression by p56(Lck) in Jurkat T lymphocytes. *Cell Signal* 13: 65-9

126. Kacena MA, Eleniste PP, Cheng YH, Huang S, Shivanna M, Meijome TE, Mayo LD, Bruzzaniti A. 2012. Megakaryocytes regulate expression of Pyk2 isoforms and caspase-mediated cleavage of actin in osteoblasts. *J Biol Chem* 287: 17257-68

127. Xiong WC, Macklem M, Parsons JT. 1998. Expression and characterization of splice variants of PYK2, a focal adhesion kinase-related protein. *J Cell Sci* 111 (Pt 14): 1981-91

128. Li X, Dy RC, Cance WG, Graves LM, Earp HS. 1999. Interactions between two cytoskeleton-associated tyrosine kinases: calcium-dependent tyrosine kinase and focal adhesion tyrosine kinase. *J Biol Chem* 274: 8917-24

129. Park SY, Li H, Avraham S. 2007. RAFTK/Pyk2 regulates EGF-induced PC12 cell spreading and movement. *Cell Signal* 19: 289-300

130. Lysechko TL. 2007. Examination of the Role and Regulation of the Tyrosine Kinase Pyk2 in Cytotoxic T Lymphocytes.

131. Berg NN, Ostergaard HL. 1997. T cell receptor engagement induces tyrosine phosphorylation of FAK and Pyk2 and their association with Lck. *J Immunol* 159: 1753-7

132. Ganju RK, Hatch WC, Avraham H, Ona MA, Druker B, Avraham S, Groopman JE. 1997. RAFTK, a novel member of the focal adhesion kinase family, is phosphorylated and associates with signaling molecules upon activation of mature T lymphocytes. *J Exp Med* 185: 1055-63

133. Qian D, Lev S, van Oers NS, Dikic I, Schlessinger J, Weiss A. 1997. Tyrosine phosphorylation of Pyk2 is selectively regulated by Fyn during TCR signaling. *J Exp Med* 185: 1253-9

134. Rodriguez-Fernandez JL, Sanchez-Martin L, Rey M, Vicente-Manzanares M, Narumiya S, Teixido J, Sanchez-Madrid F, Cabanas C. 2001. Rho and Rho-associated kinase modulate the tyrosine kinase PYK2 in T-cells through regulation of the activity of the integrin LFA-1. *J Biol Chem* 276: 40518-27

135. Li R, Wong N, Jabali MD, Johnson P. 2001. CD44-initiated cell spreading induces Pyk2 phosphorylation, is mediated by Src family kinases, and is negatively regulated by CD45. *J Biol Chem* 276: 28767-73

136. Davis CB, Dikic I, Unutmaz D, Hill CM, Arthos J, Siani MA, Thompson DA, Schlessinger J, Littman DR. 1997. Signal transduction due to HIV-1 envelope interactions with chemokine receptors CXCR4 or CCR5. *J Exp Med* 186: 1793-8

137. Miyazaki T, Takaoka A, Nogueira L, Dikic I, Fujii H, Tsujino S, Mitani Y, Maeda M, Schlessinger J, Taniguchi T. 1998. Pyk2 is a downstream mediator of the IL-2 receptor-coupled Jak signaling pathway. *Genes Dev* 12: 770-5

138. Ostergaard HL, Lysechko TL. 2005. Focal adhesion kinase-related protein tyrosine kinase Pyk2 in T-cell activation and function. *Immunol Res* 31: 267-82

139. Tsuchida M, Knechtle SJ, Hamawy MM. 1999. CD28 ligation induces tyrosine phosphorylation of Pyk2 but not Fak in Jurkat T cells. *J Biol Chem* 274: 6735-40

140. Avraham H, Park SY, Schinkmann K, Avraham S. 2000. RAFTK/Pyk2-mediated cellular signalling. *Cell Signal* 12: 123-33

141. Lietha D, Cai X, Ceccarelli DF, Li Y, Schaller MD, Eck MJ. 2007. Structural basis for the autoinhibition of focal adhesion kinase. *Cell* 129: 1177-87

142. Kohno T, Matsuda E, Sasaki H, Sasaki T. 2008. Protein-tyrosine kinase CAKbeta/PYK2 is activated by binding Ca2+/calmodulin to FERM F2 alpha2 helix and thus forming its dimer. *Biochem J* 410: 513-23

143. Park SY, Avraham HK, Avraham S. 2004. RAFTK/Pyk2 activation is mediated by trans-acting autophosphorylation in a Src-independent manner. *J Biol Chem* 279: 33315-22

144. Riggs D, Yang Z, Kloss J, Loftus JC. 2011. The Pyk2 FERM regulates Pyk2 complex formation and phosphorylation. *Cell Signal* 23: 288-96

145. Lyons PD, Dunty JM, Schaefer EM, Schaller MD. 2001. Inhibition of the catalytic activity of cell adhesion kinase beta by protein-tyrosine phosphatase-PEST-mediated dephosphorylation. *J Biol Chem* 276: 24422-31

146. Davidson D, Shi X, Zhong MC, Rhee I, Veillette A. 2010. The phosphatase PTP-PEST promotes secondary T cell responses by

dephosphorylating the protein tyrosine kinase Pyk2. *Immunity* 33: 167-80

147. McLeod SJ, Shum AJ, Lee RL, Takei F, Gold MR. 2004. The Rap GTPases regulate integrin-mediated adhesion, cell spreading, actin polymerization, and Pyk2 tyrosine phosphorylation in B lymphocytes. *J Biol Chem* 279: 12009-19

148. Schaller MD. 2010. Cellular functions of FAK kinases: insight into molecular mechanisms and novel functions. *J Cell Sci* 123: 1007-13

149. Zrihan-Licht S, Fu Y, Settleman J, Schinkmann K, Shaw L, Keydar I, Avraham S, Avraham H. 2000. RAFTK/Pyk2 tyrosine kinase mediates the association of p190 RhoGAP with RasGAP and is involved in breast cancer cell invasion. *Oncogene* 19: 1318-28

150. Sun CK, Man K, Ng KT, Ho JW, Lim ZX, Cheng Q, Lo CM, Poon RT, Fan ST. 2008. Proline-rich tyrosine kinase 2 (Pyk2) promotes proliferation and invasiveness of hepatocellular carcinoma cells through c-Src/ERK activation. *Carcinogenesis* 29: 2096-105

151. Ren XR, Du QS, Huang YZ, Ao SZ, Mei L, Xiong WC. 2001. Regulation of CDC42 GTPase by proline-rich tyrosine kinase 2 interacting with PSGAP, a novel pleckstrin homology and Src homology 3 domain containing rhoGAP protein. *J Cell Biol* 152: 971-84

152. Haglund K, Ivankovic-Dikic I, Shimokawa N, Kruh GD, Dikic I. 2004. Recruitment of Pyk2 and Cbl to lipid rafts mediates signals important for actin reorganization in growing neurites. *J Cell Sci* 117: 2557-68

153. Sanjay A, Houghton A, Neff L, DiDomenico E, Bardelay C, Antoine E, Levy J, Gailit J, Bowtell D, Horne WC, Baron R. 2001. Cbl associates with Pyk2 and Src to regulate Src kinase activity, alpha(v)beta(3) integrin-mediated signaling, cell adhesion, and osteoclast motility. *J Cell Biol* 152: 181-95

154. Gao C, Blystone SD. 2009. A Pyk2-Vav1 complex is recruited to beta3-adhesion sites to initiate Rho activation. *Biochem J* 420: 49-56

155. Butler B, Blystone SD. 2005. Tyrosine phosphorylation of beta3 integrin provides a binding site for Pyk2. *J Biol Chem* 280: 14556-62

156. Osada M, Ohmori T, Yatomi Y, Satoh K, Hosogaya S, Ozaki Y. 2001. Involvement of Hic-5 in platelet activation: integrin alphaIIbbeta3-dependent tyrosine phosphorylation and association with proline-rich tyrosine kinase 2. *Biochem J* 355: 691-7

157. Ostergaard HL, Lou O, Arendt CW, Berg NN. 1998. Paxillin phosphorylation and association with Lck and Pyk2 in anti-CD3- or anti-CD45-stimulated T cells. *J Biol Chem* 273: 5692-6

158. Deakin NO, Turner CE. 2008. Paxillin comes of age. *J Cell Sci* 121: 2435-44

159. Lulo J, Yuzawa S, Schlessinger J. 2009. Crystal structures of free and ligand-bound focal adhesion targeting domain of Pyk2. *Biochem Biophys Res Commun* 383: 347-52

160. Robertson LK, Ostergaard HL. 2011. Paxillin associates with the microtubule cytoskeleton and the immunological synapse of CTL

through its leucine-aspartic acid domains and contributes to microtubule organizing center reorientation. *J Immunol* 187: 5824-33

161. St-Pierre J, Lysechko TL, Ostergaard HL. 2011. Hypophosphorylated and inactive Pyk2 associates with paxillin at the microtubule organizing center in hematopoietic cells. *Cell Signal* 23: 718-30

162. Ilic D, Furuta Y, Kanazawa S, Takeda N, Sobue K, Nakatsuji N, Nomura S, Fujimoto J, Okada M, Yamamoto T. 1995. Reduced cell motility and enhanced focal adhesion contact formation in cells from FAK-deficient mice. *Nature* 377: 539-44

163. Guinamard R, Okigaki M, Schlessinger J, Ravetch JV. 2000. Absence of marginal zone B cells in Pyk-2-deficient mice defines their role in the humoral response. *Nat Immunol* 1: 31-6

164. Okigaki M, Davis C, Falasca M, Harroch S, Felsenfeld DP, Sheetz MP, Schlessinger J. 2003. Pyk2 regulates multiple signaling events crucial for macrophage morphology and migration. *Proc Natl Acad Sci U S A* 100: 10740-5

165. Gil-Henn H, Destaing O, Sims NA, Aoki K, Alles N, Neff L, Sanjay A, Bruzzaniti A, De Camilli P, Baron R, Schlessinger J. 2007. Defective microtubule-dependent podosome organization in osteoclasts leads to increased bone density in Pyk2(-/-) mice. *J Cell Biol* 178: 1053-64

166. Beinke S, Phee H, Clingan JM, Schlessinger J, Matloubian M, Weiss A. 2010. Proline-rich tyrosine kinase-2 is critical for CD8 T-cell short-lived effector fate. *Proc Natl Acad Sci U S A*

167. Chavez-Galan L, Arenas-Del Angel MC, Zenteno E, Chavez R, Lascurain R. 2009. Cell death mechanisms induced by cytotoxic lymphocytes. *Cell Mol Immunol* 6: 15-25

168. Gismondi A, Jacobelli J, Mainiero F, Paolini R, Piccoli M, Frati L, Santoni A. 2000. Cutting edge: functional role for proline-rich tyrosine kinase 2 in NK cell-mediated natural cytotoxicity. *J Immunol* 164: 2272-6

169. Sancho D, Nieto M, Llano M, Rodriguez-Fernandez JL, Tejedor R, Avraham S, Cabanas C, Lopez-Botet M, Sanchez-Madrid F. 2000. The tyrosine kinase PYK-2/RAFTK regulates natural killer (NK) cell cytotoxic response, and is translocated and activated upon specific target cell recognition and killing. *J Cell Biol* 149: 1249-62

170. Kamen LA, Schlessinger J, Lowell CA. 2011. Pyk2 is required for neutrophil degranulation and host defense responses to bacterial infection. *J Immunol* 186: 1656-65

171. Sun CK, Ng KT, Sun BS, Ho JW, Lee TK, Ng I, Poon RT, Lo CM, Liu CL, Man K, Fan ST. 2007. The significance of proline-rich tyrosine kinase2 (Pyk2) on hepatocellular carcinoma progression and recurrence. *Br J Cancer* 97: 50-7

172. Zhang S, Qiu X, Gu Y, Wang E. 2008. Up-regulation of proline-rich tyrosine kinase 2 in non-small cell lung cancer. *Lung Cancer* 62: 295-301

173. Sun CK, Ng KT, Lim ZX, Cheng Q, Lo CM, Poon RT, Man K, Wong N, Fan ST. 2011. Proline-rich tyrosine kinase 2 (Pyk2) promotes cell motility

of hepatocellular carcinoma through induction of epithelial to mesenchymal transition. *PLoS One* 6: e18878

174. Felty Q. Redox sensitive Pyk2 as a target for therapeutics in breast cancer. *Front Biosci* 16: 568-77

175. Lipinski CA, Loftus JC. Targeting Pyk2 for therapeutic intervention. *Expert Opin Ther Targets* 14: 95-108

176. Hogquist KA, Jameson SC, Heath WR, Howard JL, Bevan MJ, Carbone FR. 1994. T cell receptor antagonist peptides induce positive selection. *Cell* 76: 17-27

177. Suen AY, Baldwin TA. 2012. Proapoptotic protein Bim is differentially required during thymic clonal deletion to ubiquitous versus tissue-restricted antigens. *Proc Natl Acad Sci U S A* 109: 893-8

178. Blakely A, Gorman K, Ostergaard H, Svoboda K, Liu CC, Young JD, Clark WR. 1987. Resistance of cloned cytotoxic T lymphocytes to cell-mediated cytotoxicity. *J Exp Med* 166: 1070-83

179. Kane KP, Sherman LA, Mescher MF. 1989. Molecular interactions required for triggering alloantigen-specific cytolytic T lymphocytes. *J Immunol* 142: 4153-60

180. Kane KP, Mescher MF. 1993. Activation of CD8-dependent cytotoxic T lymphocyte adhesion and degranulation by peptide class I antigen complexes. *J Immunol* 150: 4788-97

181. Zheng L, Baumann U, Reymond JL. 2004. An efficient one-step site-directed and site-saturation mutagenesis protocol. *Nucleic Acids Res* 32: e115

182. Hiregowdara D, Avraham H, Fu Y, London R, Avraham S. 1997. Tyrosine phosphorylation of the related adhesion focal tyrosine kinase in megakaryocytes upon stem cell factor and phorbol myristate acetate stimulation and its association with paxillin. *J Biol Chem* 272: 10804-10

183. Raja S, Avraham S, Avraham H. 1997. Tyrosine phosphorylation of the novel protein-tyrosine kinase RAFTK during an early phase of platelet activation by an integrin glycoprotein IIb-IIIa-independent mechanism. *J Biol Chem* 272: 10941-7

184. Brinson AE, Harding T, Diliberto PA, He Y, Li X, Hunter D, Herman B, Earp HS, Graves LM. 1998. Regulation of a calcium-dependent tyrosine kinase in vascular smooth muscle cells by angiotensin II and platelet-derived growth factor. Dependence on calcium and the actin cytoskeleton. *J Biol Chem* 273: 1711-8

185. Hirotani S, Higuchi Y, Nishida K, Nakayama H, Yamaguchi O, Hikoso S, Takeda T, Kashiwase K, Watanabe T, Asahi M, Taniike M, Tsujimoto I, Matsumura Y, Sasaki T, Hori M, Otsu K. 2004. Ca(2+)-sensitive tyrosine kinase Pyk2/CAK beta-dependent signaling is essential for G-protein-coupled receptor agonist-induced hypertrophy. *J Mol Cell Cardiol* 36: 799-807

186. Ginnan R, Singer HA. 2002. CaM kinase II-dependent activation of tyrosine kinases and ERK1/2 in vascular smooth muscle. *Am J Physiol Cell Physiol* 282: C754-61

187. Guo J, Meng F, Fu X, Song B, Yan X, Zhang G. 2004. N-methyl-D-aspartate receptor and L-type voltage-gated Ca2+ channel activation mediate proline-rich tyrosine kinase 2 phosphorylation during cerebral ischemia in rats. *Neurosci Lett* 355: 177-80

188. Xu J, Gao XP, Ramchandran R, Zhao YY, Vogel SM, Malik AB. 2008. Nonmuscle myosin light-chain kinase mediates neutrophil transmigration in sepsis-induced lung inflammation by activating beta2 integrins. *Nat Immunol* 9: 880-6

189. Collins M, Tremblay M, Chapman N, Curtiss M, Rothman PB, Houtman JC. 2010. The T cell receptor-mediated phosphorylation of Pyk2 tyrosines 402 and 580 occurs via a distinct mechanism than other receptor systems. *J Leukoc Biol* 87: 691-701

190. Lysechko TL, Cheung SM, Ostergaard HL. 2010. Regulation of the tyrosine kinase Pyk2 by calcium is through production of reactive oxygen species in cytotoxic T lymphocytes. *J Biol Chem* 285: 31174-84

191. Tanaka T, Ohmura T, Hidaka H. 1983. Calmodulin antagonists' binding sites on calmodulin. *Pharmacology* 26: 249-57

192. Jan CR, Yu CC, Huang JK. 2000. N-(6-aminohexyl)-5-chloro-1-naphthalenesulfonamide hydrochloride) (W-7) causes increases in intracellular free Ca2+ levels in bladder female transitional carcinoma (BFTC) cells. *Anticancer Res* 20: 4355-9

193. Waheed A, Koopmann I, Ammon HP. 1995. Calmodulin antagonist W7 increases inositol phosphates in insulin secreting RINm5F cells. *Exp Clin Endocrinol Diabetes* 103: 280-4

194. Singh DK, Kumar D, Siddiqui Z, Basu SK, Kumar V, Rao KV. 2005. The strength of receptor signaling is centrally controlled through a cooperative loop between Ca2+ and an oxidant signal. *Cell* 121: 281-93

195. Fulton DJ. 2009. Nox5 and the regulation of cellular function. *Antioxid Redox Signal* 11: 2443-52

196. Zhao R, Masayasu H, Holmgren A. 2002. Ebselen: a substrate for human thioredoxin reductase strongly stimulating its hydroperoxide reductase activity and a superfast thioredoxin oxidant. *Proc Natl Acad Sci U S A* 99: 8579-84

197. Crow JP. 1997. Dichlorodihydrofluorescein and dihydrorhodamine 123 are sensitive indicators of peroxynitrite in vitro: implications for intracellular measurement of reactive nitrogen and oxygen species. *Nitric Oxide* 1: 145-57

198. Devadas S, Zaritskaya L, Rhee SG, Oberley L, Williams MS. 2002. Discrete generation of superoxide and hydrogen peroxide by T cell receptor stimulation: selective regulation of mitogen-activated protein kinase activation and fas ligand expression. *J Exp Med* 195: 59-70

199. Frank GD, Motley ED, Inagami T, Eguchi S. 2000. PYK2/CAKbeta represents a redox-sensitive tyrosine kinase in vascular smooth muscle cells. *Biochem Biophys Res Commun* 270: 761-5

200. Banno Y, Ohguchi K, Matsumoto N, Koda M, Ueda M, Hara A, Dikic I, Nozawa Y. 2005. Implication of phospholipase D2 in oxidant-induced phosphoinositide 3-kinase signaling via Pyk2 activation in PC12 cells. *J Biol Chem* 280: 16319-24

201. Loot AE, Schreiber JG, Fisslthaler B, Fleming I. 2009. Angiotensin II impairs endothelial function via tyrosine phosphorylation of the endothelial nitric oxide synthase. *J Exp Med* 206: 2889-96

202. Hanke JH, Gardner JP, Dow RL, Changelian PS, Brissette WH, Weringer EJ, Pollok BA, Connelly PA. 1996. Discovery of a novel, potent, and Src family-selective tyrosine kinase inhibitor. Study of Lck- and FynT-dependent T cell activation. *J Biol Chem* 271: 695-701

203. Salmond RJ, Filby A, Qureshi I, Caserta S, Zamoyska R. 2009. T-cell receptor proximal signaling via the Src-family kinases, Lck and Fyn, influences T-cell activation, differentiation, and tolerance. *Immunol Rev* 228: 9-22

204. Lee K, Esselman WJ. 2002. Inhibition of PTPs by H(2)O(2) regulates the activation of distinct MAPK pathways. *Free Radic Biol Med* 33: 1121-32

205. Kishihara K, Penninger J, Wallace VA, Kundig TM, Kawai K, Wakeham A, Timms E, Pfeffer K, Ohashi PS, Thomas ML, et al. 1993. Normal B lymphocyte development but impaired T cell maturation in CD45-exon6 protein tyrosine phosphatase-deficient mice. *Cell* 74: 143-56

206. Byth KF, Conroy LA, Howlett S, Smith AJ, May J, Alexander DR, Holmes N. 1996. CD45-null transgenic mice reveal a positive regulatory role for CD45 in early thymocyte development, in the selection of CD4+CD8+ thymocytes, and B cell maturation. *J Exp Med* 183: 1707-18

207. Hardwick JS, Sefton BM. 1997. The activated form of the Lck tyrosine protein kinase in cells exposed to hydrogen peroxide is phosphorylated at both Tyr-394 and Tyr-505. *J Biol Chem* 272: 25429-32

208. Watts JD, Sanghera JS, Pelech SL, Aebersold R. 1993. Phosphorylation of serine 59 of p56lck in activated T cells. *J Biol Chem* 268: 23275-82

209. Joung I, Kim T, Stolz LA, Payne G, Winkler DG, Walsh CT, Strominger JL, Shin J. 1995. Modification of Ser59 in the unique N-terminal region of tyrosine kinase p56lck regulates specificity of its Src homology 2 domain. *Proc Natl Acad Sci U S A* 92: 5778-82

210. Atherfold PA, Norris MS, Robinson PJ, Gelfand EW, Franklin RA. 1999. Calcium-induced ERK activation in human T lymphocytes. *Mol Immunol* 36: 543-9

211. DeSilva DR, Jones EA, Favata MF, Jaffee BD, Magolda RL, Trzaskos JM, Scherle PA. 1998. Inhibition of mitogen-activated protein kinase kinase blocks T cell proliferation but does not induce or prevent anergy. *J Immunol* 160: 4175-81

212. Shatynski KE, Chen H, Kwon J, Williams MS. 2012. Decreased STAT5 phosphorylation and GATA-3 expression in NOX2-deficient T cells: role in T helper development. *Eur J Immunol* 42: 3202-11

213. Kwon J, Shatynski KE, Chen H, Morand S, de Deken X, Miot F, Leto TL, Williams MS. 2010. The nonphagocytic NADPH oxidase Duox1 mediates a positive feedback loop during T cell receptor signaling. *Sci Signal* 3: ra59

214. Rigutto S, Hoste C, Grasberger H, Milenkovic M, Communi D, Dumont JE, Corvilain B, Miot F, De Deken X. 2009. Activation of dual oxidases Duox1 and Duox2: differential regulation mediated by camp-dependent protein kinase and protein kinase C-dependent phosphorylation. *J Biol Chem* 284: 6725-34

215. Harper RW, Xu C, Eiserich JP, Chen Y, Kao CY, Thai P, Setiadi H, Wu R. 2005. Differential regulation of dual NADPH oxidases/peroxidases, Duox1 and Duox2, by Th1 and Th2 cytokines in respiratory tract epithelium. *FEBS Lett* 579: 4911-7

216. Leto TL, Morand S, Hurt D, Ueyama T. 2009. Targeting and regulation of reactive oxygen species generation by Nox family NADPH oxidases. *Antioxid Redox Signal* 11: 2607-19

217. Cheng JJ, Chao YJ, Wang DL. 2002. Cyclic strain activates redox-sensitive proline-rich tyrosine kinase 2 (PYK2) in endothelial cells. *J Biol Chem* 277: 48152-7

218. Yamamoto S, Shimizu S, Kiyonaka S, Takahashi N, Wajima T, Hara Y, Negoro T, Hiroi T, Kiuchi Y, Okada T, Kaneko S, Lange I, Fleig A, Penner R, Nishi M, Takeshima H, Mori Y. 2008. TRPM2-mediated Ca2+influx induces chemokine production in monocytes that aggravates inflammatory neutrophil infiltration. *Nat Med* 14: 738-47

219. Son Y, Cheong YK, Kim NH, Chung HT, Kang DG, Pae HO. 2011. Mitogen-Activated Protein Kinases and Reactive Oxygen Species: How Can ROS Activate MAPK Pathways? *J Signal Transduct* 2011: 792639

220. Mehdi MZ, Azar ZM, Srivastava AK. 2007. Role of receptor and nonreceptor protein tyrosine kinases in H2O2-induced PKB and ERK1/2 signaling. *Cell Biochem Biophys* 47: 1-10

221. Eleniste PP, Bruzzaniti A. 2012. Focal adhesion kinases in adhesion structures and disease. *J Signal Transduct* 2012: 296450

222. Margadant C, Monsuur HN, Norman JC, Sonnenberg A. 2011. Mechanisms of integrin activation and trafficking. *Curr Opin Cell Biol* 23: 607-14

223. Rodriguez-Fernandez JL, Sanchez-Martin L, de Frutos CA, Sancho D, Robinson M, Sanchez-Madrid F, Cabanas C. 2002. LFA-1 integrin and the microtubular cytoskeleton are involved in the Ca(2)(+)-mediated regulation of the activity of the tyrosine kinase PYK2 in T cells. *J Leukoc Biol* 71: 520-30

224. Ma EA, Lou O, Berg NN, Ostergaard HL. 1997. Cytotoxic T lymphocytes express a beta3 integrin which can induce the phosphorylation of focal adhesion kinase and the related PYK-2. *Eur J Immunol* 27: 329-35

225. Rodriguez-Fernandez JL, Gomez M, Luque A, Hogg N, Sanchez-Madrid F, Cabanas C. 1999. The interaction of activated integrin lymphocyte function-associated antigen 1 with ligand intercellular adhesion molecule 1 induces activation and redistribution of focal adhesion kinase and proline-rich tyrosine kinase 2 in T lymphocytes. *Mol Biol Cell* 10: 1891-907

226. Mace EM, Monkley SJ, Critchley DR, Takei F. 2009. A dual role for talin in NK cell cytotoxicity: activation of LFA-1-mediated cell adhesion and polarization of NK cells. *J Immunol* 182: 948-56

227. Buckbinder L, Crawford DT, Qi H, Ke HZ, Olson LM, Long KR, Bonnette PC, Baumann AP, Hambor JE, Grasser WA, 3rd, Pan LC, Owen TA, Luzzio MJ, Hulford CA, Gebhard DF, Paralkar VM, Simmons HA, Kath JC, Roberts WG, Smock SL, Guzman-Perez A, Brown TA, Li M. 2007. Proline-rich tyrosine kinase 2 regulates osteoprogenitor cells and bone formation, and offers an anabolic treatment approach for osteoporosis. *Proc Natl Acad Sci U S A* 104: 10619-24

228. Walker DP, Bi FC, Kalgutkar AS, Bauman JN, Zhao SX, Soglia JR, Aspnes GE, Kung DW, Klug-McLeod J, Zawistoski MP, McGlynn MA, Oliver R, Dunn M, Li JC, Richter DT, Cooper BA, Kath JC, Hulford CA, Autry CL, Luzzio MJ, Ung EJ, Roberts WG, Bonnette PC, Buckbinder L, Mistry A, Griffor MC, Han S, Guzman-Perez A. 2008. Trifluoromethylpyrimidine-based inhibitors of proline-rich tyrosine kinase 2 (PYK2): structure-activity relationships and strategies for the elimination of reactive metabolite formation. *Bioorg Med Chem Lett* 18: 6071-7

229. Han S, Mistry A, Chang JS, Cunningham D, Griffor M, Bonnette PC, Wang H, Chrunyk BA, Aspnes GE, Walker DP, Brosius AD, Buckbinder L. 2009. Structural characterization of proline-rich tyrosine kinase 2 (PYK2) reveals a unique (DFG-out) conformation and enables inhibitor design. *J Biol Chem* 284: 13193-201

230. Puente LG, Ostergaard HL. 2003. Beta 1/beta 3 integrin ligation is uncoupled from ERK1/ERK2 activation in cytotoxic T lymphocytes. *J Leukoc Biol* 73: 391-8

231. Brown MC, Turner CE. 2004. Paxillin: adapting to change. *Physiol Rev* 84: 1315-39

232. Schaller MD, Sasaki T. 1997. Differential signaling by the focal adhesion kinase and cell adhesion kinase beta. *J Biol Chem* 272: 25319-25

233. Ganju RK, Brubaker SA, Chernock RD, Avraham S, Groopman JE. 2000. Beta-chemokine receptor CCR5 signals through SHP1, SHP2, and Syk. *J Biol Chem* 275: 17263-8

234. Groom JR, Luster AD. 2011. CXCR3 in T cell function. *Exp Cell Res* 317: 620-31

235. Chan KT, Bennin DA, Huttenlocher A. 2010. Regulation of adhesion dynamics by calpain-mediated proteolysis of focal adhesion kinase (FAK). *J Biol Chem* 285: 11418-26

236. Franco SJ, Huttenlocher A. 2005. Regulating cell migration: calpains make the cut. *J Cell Sci* 118: 3829-38

237. Randriamboavonjy V, Isaak J, Elgheznawy A, Pistrosch F, Fromel T, Yin X, Badenhoop K, Heide H, Mayr M, Fleming I. 2012. Calpain inhibition stabilizes the platelet proteome and reactivity in diabetes. *Blood* 120: 415-23

238. Carragher NO, Westhoff MA, Fincham VJ, Schaller MD, Frame MC. 2003. A novel role for FAK as a protease-targeting adaptor protein: regulation by p42 ERK and Src. *Curr Biol* 13: 1442-50

239. Bridgewater RE, Norman JC, Caswell PT. 2012. Integrin trafficking at a glance. *J Cell Sci* 125: 3695-701

240. Smith A, Carrasco YR, Stanley P, Kieffer N, Batista FD, Hogg N. 2005. A talin-dependent LFA-1 focal zone is formed by rapidly migrating T lymphocytes. *J Cell Biol* 170: 141-51

241. Mitra SK, Mikolon D, Molina JE, Hsia DA, Hanson DA, Chi A, Lim ST, Bernard-Trifilo JA, Ilic D, Stupack DG, Cheresh DA, Schlaepfer DD. 2006. Intrinsic FAK activity and Y925 phosphorylation facilitate an angiogenic switch in tumors. *Oncogene* 25: 5969-84

242. Purbhoo MA, Irvine DJ, Huppa JB, Davis MM. 2004. T cell killing does not require the formation of a stable mature immunological synapse. *Nat Immunol* 5: 524-30

243. Stinchcombe JC, Griffiths GM. 2007. Secretory mechanisms in cell-mediated cytotoxicity. *Annu Rev Cell Dev Biol* 23: 495-517

244. Beal AM, Anikeeva N, Varma R, Cameron TO, Vasiliver-Shamis G, Norris PJ, Dustin ML, Sykulev Y. 2009. Kinetics of early T cell receptor signaling regulate the pathway of lytic granule delivery to the secretory domain. *Immunity* 31: 632-42

245. Jenkins MR, Griffiths GM. 2010. The synapse and cytolytic machinery of cytotoxic T cells. *Curr Opin Immunol* 22: 308-13

246. Quann EJ, Merino E, Furuta T, Huse M. 2009. Localized diacylglycerol drives the polarization of the microtubule-organizing center in T cells. *Nat Immunol* 10: 627-35

247. Quann EJ, Liu X, Altan-Bonnet G, Huse M. 2011. A cascade of protein kinase C isozymes promotes cytoskeletal polarization in T cells. *Nat Immunol* 12: 647-54

248. Ostergaard HL, Kane KP, Mescher MF, Clark WR. 1987. Cytotoxic T lymphocyte mediated lysis without release of serine esterase. *Nature* 330: 71-2

249. Boswell KL, James DJ, Esquibel JM, Bruinsma S, Shirakawa R, Horiuchi H, Martin TF. 2012. Munc13-4 reconstitutes calcium-dependent SNARE-mediated membrane fusion. *J Cell Biol* 197: 301-12

250. Lowin-Kropf B, Shapiro VS, Weiss A. 1998. Cytoskeletal polarization of T cells is regulated by an immunoreceptor tyrosine-based activation motif-dependent mechanism. *J Cell Biol* 140: 861-71

251. Li D, Molldrem JJ, Ma Q. 2009. LFA-1 regulates CD8+ T cell activation via T cell receptor-mediated and LFA-1-mediated Erk1/2 signal pathways. *J Biol Chem* 284: 21001-10

252. Wolint P, Betts MR, Koup RA, Oxenius A. 2004. Immediate cytotoxicity but not degranulation distinguishes effector and memory subsets of CD8+ T cells. *J Exp Med* 199: 925-36

253. Riquelme E, Carreno LJ, Gonzalez PA, Kalergis AM. 2009. The duration of TCR/pMHC interactions regulates CTL effector function and tumor-killing capacity. *Eur J Immunol* 39: 2259-69

254. Berg NN, Ostergaard HL. 1995. Characterization of intercellular adhesion molecule-1 (ICAM-1)-augmented degranulation by cytotoxic T cells. ICAM-1 and anti-CD3 must be co-localized for optimal adhesion and stimulation. *J Immunol* 155: 1694-702

255. Berrebi G, Takayama H, Sitkovsky MV. 1987. Antigen-receptor interaction requirement for conjugate formation and lethal-hit triggering by cytotoxic T lymphocytes can be bypassed by protein kinase C activators and Ca2+ ionophores. *Proc Natl Acad Sci U S A* 84: 1364-8

256. March ME, Long EO. 2011. beta2 integrin induces TCRzeta-Syk-phospholipase C-gamma phosphorylation and paxillin-dependent granule polarization in human NK cells. *J Immunol* 186: 2998-3005

257. Bonnette PC, Robinson BS, Silva JC, Stokes MP, Brosius AD, Baumann A, Buckbinder L. 2010. Phosphoproteomic characterization of PYK2 signaling pathways involved in osteogenesis. *J Proteomics* 73: 1306-20

258. Min SW, Chang WP, Sudhof TC. 2007. E-Syts, a family of membranous Ca2+-sensor proteins with multiple C2 domains. *Proc Natl Acad Sci U S A* 104: 3823-8

259. Scholer A, Hugues S, Boissonnas A, Fetler L, Amigorena S. 2008. Intercellular adhesion molecule-1-dependent stable interactions between T cells and dendritic cells determine CD8+ T cell memory. *Immunity* 28: 258-70

260. Fooksman DR, Vardhana S, Vasiliver-Shamis G, Liese J, Blair DA, Waite J, Sacristan C, Victora GD, Zanin-Zhorov A, Dustin ML. 2010. Functional anatomy of T cell activation and synapse formation. *Annu Rev Immunol* 28: 79-105

261. Yasuda T, Bundo K, Hino A, Honda K, Inoue A, Shirakata M, Osawa M, Tamura T, Nariuchi H, Oda H, Yamamoto T, Yamanashi Y. 2007. Dok-1 and Dok-2 are negative regulators of T cell receptor signaling. *Int Immunol* 19: 487-95

262. Wu L, Bijian K, Shen SH. 2009. CD45 recruits adapter protein DOK-1 and negatively regulates JAK-STAT signaling in hematopoietic cells. *Mol Immunol* 46: 2167-77

263. Niu Y, Roy F, Saltel F, Andrieu-Soler C, Dong W, Chantegrel AL, Accardi R, Thepot A, Foiselle N, Tommasino M, Jurdic P, Sylla BS. 2006. A nuclear export signal and phosphorylation regulate Dok1 subcellular localization and functions. *Mol Cell Biol* 26: 4288-301

264. Mercier PL, Bachvarova M, Plante M, Gregoire J, Renaud MC, Ghani K, Tetu B, Bairati I, Bachvarov D. 2011. Characterization of DOK1, a candidate tumor suppressor gene, in epithelial ovarian cancer. *Mol Oncol* 5: 438-53

265. Anthis NJ, Haling JR, Oxley CL, Memo M, Wegener KL, Lim CJ, Ginsberg MH, Campbell ID. 2009. Beta integrin tyrosine phosphorylation is a conserved mechanism for regulating talin-induced integrin activation. *J Biol Chem* 284: 36700-10

266. Lipinski CA, Loftus JC. 2010. Targeting Pyk2 for therapeutic intervention. *Expert Opin Ther Targets* 14: 95-108

267. Herreros L, Rodriguez-Fernandez JL, Brown MC, Alonso-Lebrero JL, Cabanas C, Sanchez-Madrid F, Longo N, Turner CE, Sanchez-Mateos P. 2000. Paxillin localizes to the lymphocyte microtubule organizing center and associates with the microtubule cytoskeleton. *J Biol Chem* 275: 26436-40

268. Lee YC, Chang AY, Lin-Feng MH, Tsou WI, Chiang IH, Lai MZ. 2012. Paxillin phosphorylation by JNK and p38 is required for NFAT activation. *Eur J Immunol* 42: 2165-75

269. Fabbri M, Di Meglio S, Gagliani MC, Consonni E, Molteni R, Bender JR, Tacchetti C, Pardi R. 2005. Dynamic partitioning into lipid rafts controls the endo-exocytic cycle of the alphaL/beta2 integrin, LFA-1, during leukocyte chemotaxis. *Mol Biol Cell* 16: 5793-803

270. Ezratty EJ, Bertaux C, Marcantonio EE, Gundersen GG. 2009. Clathrin mediates integrin endocytosis for focal adhesion disassembly in migrating cells. *J Cell Biol* 187: 733-47

271. Haddad EK, Wu X, Hammer JA, 3rd, Henkart PA. 2001. Defective granule exocytosis in Rab27a-deficient lymphocytes from Ashen mice. *J Cell Biol* 152: 835-42

272. Singh RK, Liao W, Tracey-White D, Recchi C, Tolmachova T, Rankin SM, Hume AN, Seabra MC. 2012. Rab27a-mediated protease release regulates neutrophil recruitment by allowing uropod detachment. *J Cell Sci* 125: 1652-6

273. Gabarra-Niecko V, Keely PJ, Schaller MD. 2002. Characterization of an activated mutant of focal adhesion kinase: 'SuperFAK'. *Biochem J* 365: 591-603